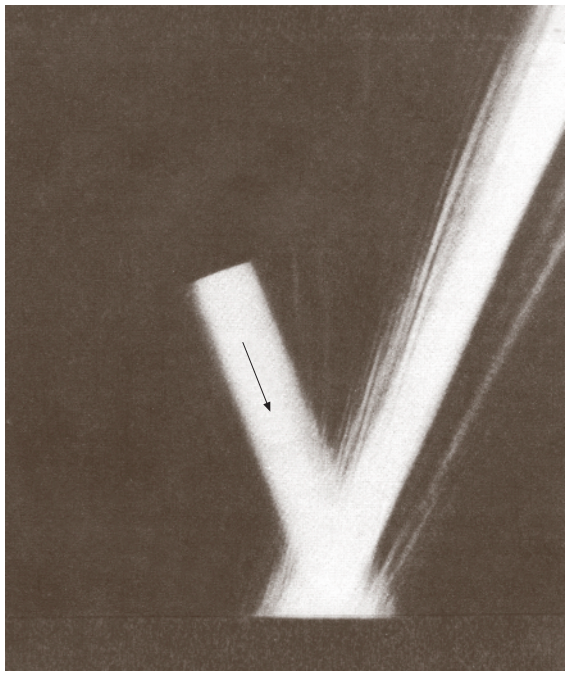


Fig. 6.28 Schlieren photograph showing backward displacement of a 6 MHz ultrasonic beam at a corrugated water–brass interface

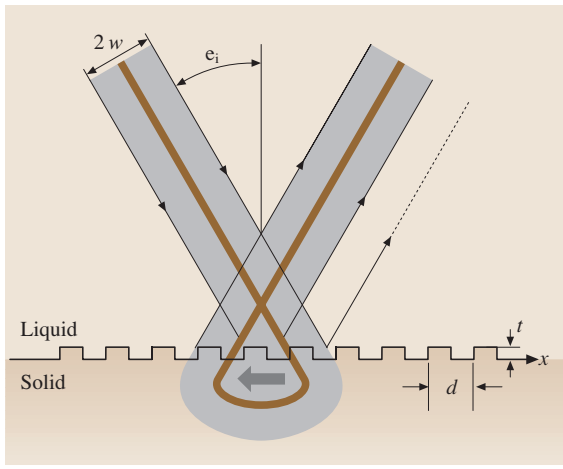


Fig. 6.29 Diagram of incident beam coupling to a backward-directed leaky wave to produce backward displacement of the reflected beam

At a corrugated interface it is possible that the incident beam couples to a negatively directed surface wave so that the reflected beam is displaced in the negative direction. This phenomenon was predicted for optical waves by *Tamir* and *Bertoni* [6.32]. They determined that the optimum angle for this to occur is given by

$$\sin\theta_\mathrm{i} = V_\mathrm{liq}\left(\frac{1}{fd} - \frac{1}{V_\mathrm{R}}\right) \tag{6.69}$$

where d is the period, f is the frequency, V_liq is the wave propagation velocity in the liquid, and V_R is the propagation velocity of the leaky surface wave. Figure 6.28 is a Schlieren photograph which shows what happens in this case [6.33]. Figure 6.29 is a diagram of the phenomenon [6.33]. The incident beam couples to a backward-directed surface wave to produce backward displacement of the reflected beam.

6.5 Nonlinear Acoustics

There are several sources of nonlinearity whether the propagating medium be a gas, liquid, or solid. They are described in more detail in Chap. 8. Even in an ideal medium in which one considers only interatomic forces, there is still a source of nonlinear behavior since compression requires a slightly different force from dilatation. With Hooke's law (strain is proportional to stress) one assumes that they are equal. This is seldom true. The subject of nonlinear acoustics has been developed to the point that it is now possible to go beyond the linear approximation with many substances.

6.5.1 Nonlinearity of Fluids

If one assumes an ideal gas and keeps the first set of nonlinear terms, *Beyer* has shown that the equation of motion in one dimension becomes [6.34]

$$\frac{\partial^2\xi}{\partial t^2} = \frac{c_o^2}{\left(1+\frac{\partial\xi}{\partial a}\right)^{\gamma+1}}\frac{\partial^2\xi}{\partial a^2}\,. \tag{6.70}$$

This form of the nondissipative wave equation in one dimension in Lagrangian coordinates includes nonlinear

Amazon
EX1010 Page 251

terms. In this equation γ is the ratio of specific heats and

$$c_o^2 = \frac{\gamma p_o}{\rho_o} \frac{1}{\left(1+\frac{\partial \xi}{\partial a}\right)^{\gamma-1}} . \tag{6.71}$$

One can also generalize this equation in a form which applies to all fluids. By expanding the equation of state $p = p_o \left(\frac{\rho}{\rho_o}\right)^{\gamma}$ in powers of the condensation $s = \frac{\rho-\rho_o}{\rho_o}$, one obtains

$$p = p_o + As + \frac{B}{2!}s^2 + \ldots \quad \text{and}$$
$$c^2 = c_o^2 \left[1 + \left(\frac{B}{A}\right) s + \ldots\right] . \tag{6.72}$$

This makes it possible to obtain the nonlinear wave equation in the form [6.24]:

$$\frac{\partial^2 \xi}{\partial t^2} = \frac{c_o^2}{\left(1+\frac{\partial \xi}{\partial a}\right)^{2+\frac{B}{A}}} \frac{\partial^2 \xi}{\partial a^2} . \tag{6.73}$$

In this form one can recognize that the quantity $2 + B/A$ for fluids plays the same role as $\gamma + 1$ for ideal gases. Values of B/A for fluids given in Table 6.3 indicate that nonlinearity of fluids, even in the absence of bubbles of air, cannot always be ignored. The nonlinearity of fluids is discussed in greater detail in Chap. 8.

Table 6.3 Values of B/A

Substance	T (°C)	B/A
Distilled water	0	4.2
	20	5.0
	40	5.4
	60	5.7
	80	6.1
	100	6.1
Sea water (3.5%)	20	5.25
Methanol	20	9.6
Ethanol	0	10.4
	20	10.5
	40	10.6
N-propanol	20	10.7
N-butanol	20	10.7
Acetone	20	9.2
Beneze	20	9/0
Chlorobenzene	30	9.3
Liquid nitrogen	b.p.	6.6
Benzyl alcohol	30	10.2
Diethylamine	30	10.3
Ethylene glycol	30	9.7
Ethyl formate	30	9.8
Heptane	30	10.0
Hexane	30	9.9
Methyl acetate	30	9.7
Mercury	30	7.8
Sodium	110	2.7
Potassium	100	2.9
Tin	240	4.4
Monatomic gas	20	0.67
Diatomic gas	20	0.40

6.5.2 Nonlinearity of Solids

The propagation of a wave in a nonlinear solid is described by first introducing third-order elastic constants. When extending the stress–strain relationship (which essentially is a force-based approach) it becomes difficult to keep a consistent approximation among the various nonlinear terms. However, If one instead uses an energy approach, a consistent approximation is automatically maintained for all the terms of higher order.

Beginning with the elastic potential energy, one can define both the second-order constants (those determining the wave velocity in the linear approximation) and the third-order elastic constants simultaneously. The elastic potential energy is

$$\phi(\eta) = \frac{1}{2!}\sum_{ijkl} C_{ijkl}\eta_{ij}\eta_{kl} + \frac{1}{3!}\sum_{ijklmn} C_{ijklmn}\eta_{ij}\eta_{kl}\eta_{mn} + \ldots , \tag{6.74}$$

Table 6.4 K_2 and K_3 for the principal directions in a cubic crystal

Direction	K_2	K_3
[100]	C_{11}	C_{111}
[110]	$\frac{C_{11}+C_{12}+2C_{44}}{2}$	$\frac{C_{111}+3C_{112}+12C_{166}}{4}$
[111]	$\frac{C_{11}+2C_{12}+4C_{44}}{3}$	$\frac{1}{9}(C_{111}+6C_{112}+12C_{144}+24C_{166}+2C_{123}+16C_{456})$

Amazon
EX1010 Page 252

Table 6.5 Comparison of room-temperature values of the ultrasonic nonlinearity parameters of solids. BCC = body-centered cubic; FCC = face-centered cubic

Material or structure	Bonding	β_{avg}
Zincblende	Covalent	2.2
Flourite	Ionic	3.8
FCC	Metallic	5.6
FCC (inert gas)	van der Waals	6.4
BCC	Metallic	8.2
NaCl	Ionic	14.6
Fused silica	Isotropic	−3.4
$YBa_2Cu_3O_{7-\delta}$ (ceramic)	Isotropic	14.3

where the η are the strains, C_{ijkl} are the second-order elastic constants, and C_{ijklmn} are the third-order elastic constants. For cubic crystals there are only three second-order elastic constants: C_{11}, C_{12} and C_{44}, and only six third-order elastic constants: C_{111}, C_{112}, C_{144}, C_{166}, C_{123} and C_{456}. This makes the investigation of cubic crystals relatively straightforward [6.35]. By using the appropriate form of Lagrange's equations, specializing to a specific orientation of the coordinates with respect to the ultrasonic wave propagation direction, and neglecting attenuation and higher-order terms, one can write the nonlinear wave equation for propagation in the directions that allow the propagation of purely longitudinal waves (with no excitation of transverse waves). In a cubic crystalline lattice there are three of these *pure mode* directions for longitudinal waves and the nonlinear wave equation has the form [6.35]

$$\rho_o \frac{\partial^2 u}{\partial t^2} = K_2 \frac{\partial^2 u}{\partial a^2} + (3K_2 + K_3) \frac{\partial u}{\partial a} \frac{\partial^2 u}{\partial a^2} + \dots , \tag{6.75}$$

where both K_2 and K_3 depend on the orientation considered. The quantity K_2 determines the wave velocity: $K_2 = c_o^2 \rho_o$. The quantity K_3 contains only third-order elastic constants. The quantities K_2 and K_3 are given for the three pure-mode directions in a cubic lattice in Table 6.4. The ratio of the coefficient of the nonlinear term to that of the linear term has a special significance. It is often called the *nonlinearity parameter* β and its magnitude is $\beta = 3 + \frac{K_3}{K_2}$. Since K_3 is an inherently negative quantity and is usually greater in magnitude than $3K_2$, a minus sign is often included in the definition:

$$\beta = -\left(3 + \frac{K_3}{K_2}\right) . \tag{6.76}$$

Table 6.6 Parameters entering into the description of finite-amplitude waves in gases, liquids and solids

Parameter	Ideal gas	Liquid	Solid
c_0^2	$\frac{\gamma P_0}{\rho_0}$	$\frac{A}{\rho_0}$	$\frac{K_2}{\rho_0}$
Nonlinearity parameter β	$\gamma + 1$	$\frac{B}{A} + 2$	$-\left(\frac{K_3}{K_2} + 3\right)$

The nonlinearity parameters of many cubic solids have been measured. As might be expected, there is a difference between the quantities measured in the three pure-mode directions (usually labeled as the [100], [110] and [111] directions). These differences, however, are not great. If one averages them, one gets the results shown in Table 6.5. The nonlinearity parameters cover the range 2–15. This means that for cubic crystals the coefficient of the nonlinear term in the nonlinear wave equation is 2–15 times as large as the coefficient of the linear term. This gives an impression of the approximation involved when one ignores nonlinear acoustics.

There is also a source of nonlinearity of solids that appears to come from the presence of domains in lithium niobate; this has been called *acoustic memory* [6.36].

It is possible to measure all six third-order elastic constants of cubic crystals. To do so, however, it is necessary to make additional measurements. The procedure that minimizes errors in the evaluation of third-order elastic constants from combination of nonlinearity parameters with the results of hydrostatic-pressure measurements has been considered by *Breazeale* et al. [6.37] and applied to the evaluation of the third-order elastic constants of two perovskite crystals.

6.5.3 Comparison of Fluids and Solids

To facilitate comparison between fluids and solids, it is necessary to use a binomial expansion of the denominator of (6.73)

$$\left(1 + \frac{\partial \xi}{\partial a}\right)^{-\left(\frac{B}{A}+2\right)} = 1 + \left(\frac{B}{A} + 2\right) \frac{\partial \xi}{\partial a} + \dots \tag{6.77}$$

Using this expression, (6.73) becomes

$$\frac{\partial^2 \xi}{\partial t^2} = c_o^2 \frac{\partial^2 \xi}{\partial a^2} + c_o^2 \left(\frac{B}{A} + 2\right) \frac{\partial \xi}{\partial a} \frac{\partial^2 \xi}{\partial a^2} + \dots \tag{6.78}$$

This form of the equation can be compared directly with (6.74) for solids. The ratio of the coefficient of the nonlinear term to that of the linear term can be evaluated

Amazon
EX1010 Page 253

directly. The nonlinearity parameters of the various substances are listed in Table 6.6. Use of Table 6.6 allows one to make a comparison between the nonlinearity of fluids as listed in Table 6.3 and the nonlinearity parameters of solids listed in Table 6.5. Nominally, they are of the same order of magnitude. This means that solids exhibit intrinsic nonlinearity that is comparable to that exhibited by fluids. Thus, the approximation made by assuming that Hooke's law (strain is proportional to stress) is valid for solids is comparable to the approximation made in the derivation of the linear wave equation for fluids.

References

6.1 R.N. Thurston, A.D. Pierce (Eds.): *Physical Acoustics*, Vol. XXV (Academic, San Diego 1999)

6.2 W.P. Mason (Ed.): *Physical Acoustics*, Vol. I A,B (Academic, New York 1964)

6.3 R.N. Thurston: Wave propagation in fluids and normal solids. In: *In: Physical Acoustics*, Vol. I A, ed. by P.W. Mason (Academic, New York 1964)

6.4 A. Migliori, T.W. Darling, J.P. Baiardo, F. Freibert: Resonant ultrasound spectroscopy (RUS). In: *Handbook of Elastic Properties of Solids, Liquids, and Gases*, Vol. I, ed. by M. Levy, H. Bass, R. Stern (Academic, New York 2001) p. 10, Cha

6.5 R. Truell, C. Elbaum, B. Chick: *Ultrasonic Methods in Solid State Physics* (Academic, New York 1969)

6.6 C. Allen, I. Rudnick: A powerful high-frequency siren, J. Acoust. Soc. Am. **19**, 857–865 (1947)

6.7 D.F. Gaitan, L.A. Crum, C.C. Church, R.A. Roy: Sonoluminescence and bubble dynamics for a single, stable, cavitation bubble, J. Acoust. Soc. Am. **91**, 3166–3183 (1992)

6.8 J. Wu: Acoustical tweezers, J. Acoust. Soc. Am. **89**, 2140–2143 (1991)

6.9 N. Marinesco, J.J. Trillat: Action des ultrasons sur les plaques photographiques, C. R. Acad. Sci. Paris **196**, 858 (1933)

6.10 H. Frenzel, H. Schultes: Luminiszenz im ultraschallbeschickten Wasse, Z. Phys. Chem. **27**, 421 (1934)

6.11 I.V. Ostrovskii, P. Das: Observation of a new class of crystal sonoluminescence at piezoelectric crystal surface, Appl. Phys. Lett. **70**, 167–169 (1979)

6.12 I. Miyake, H. Futama: Sonoluminescence in X-rayed KCl crystals, J. Phys. Soc. Jpn. **51**, 3985–3989 (1982)

6.13 B.P. Barber, R. Hiller, K. Arisaka, H. Fetterman, S.J. Putterman: Resolving the picosecond characteristics of synchronous sonoluminescence, J. Acoust. Soc. Am. **91**, 3061 (1992)

6.14 J.T. Carlson, S.D. Lewia, A.A. Atchley, D.F. Gaitan, X.K. Maruyama, M.E. Lowry, M.J. Moran, D.R. Sweider: Spectra of picosecond sonoluminescence. In: *Advances in Nonlinear Acoustics*, ed. by H. Hobaek (World Scientific, Singapore 1993)

6.15 R. Hiller, S.J. Putterman, B.P. Barber: Spectrum of synchronous picosecond sonoluminescence, Phys. Rev. Lett. **69**, 1182–1184 (1992)

6.16 G.W. Swift: Thermoacoustic engines, J. Acoust. Soc. Am. **84**, 1145–1180 (1988)

6.17 L. J. House, D. B. Pape: Method and Apparatus for Acoustic Energy – Identification of Objects Buried in Soil, US Patent 5357063 (1993)

6.18 C.G. Don, A.J. Rogers: Using acoustic impulses to identify a buried non-metallic objects, J. Acoust. Soc. Am. **95**, 2837–2838 (1994)

6.19 D. D. Caulfield: Acoustic Detection Apparatus, US Patent 4922467 (1989)

6.20 D.M. Donskoy: Nonlinear vibro-acoustic technique for land mine detection, SPIE Proc. **3392**, 211–217 (1998)

6.21 D.M. Donskoy: Detection and discrimination of nonmetallic mines, SPIE Proc. **3710**, 239–246 (1999)

6.22 D.M. Donskoy, N. Sedunov, A. Ekimov, M. Tsionskiy: Optimization of seismo-acoustic land mine detection using dynamic impedances of mines and soil, SPIE Proc. **4394**, 575–582 (2001)

6.23 J.M. Sabatier, N. Xiang: Laser-doppler based acoustic-to-seismic detection of buried mines, Proc. SPIE **3710**, 215–222 (1999)

6.24 N. Xiang, J.M. Sabatier: Detection and Remediation Technologies for Mines and Minelike Targets VI, Proc. SPIE **4394**, 535–541 (2001)

6.25 F.D. Martin, M.A. Breazeale: A simple way to eliminate diffraction lobes emitted by ultrasonic transducers, J. Acoust. Soc. Am. **49**, 1668–1669 (1971)

6.26 G. Du, M.A. Breazeale: The ultrasonic field of a Gaussian transducer, J. Acoust. Soc. Am. **78**, 2083–2086 (1985)

6.27 R.D. Peters, M.A. Breazeale: Third harmonic of an initially sinusoidal ultrasonic wave in copper, Appl. Phys. Lett. **12**, 106–108 (1968)

6.28 F. Goos, H. Hänchen: Ein neuer und fundamentaler Versuch zur Totalreflexion, Ann. Phys. **1**, 333–346 (1947), 6. Folge

6.29 K. Ergin: Energy ratio of seismic waves reflected and refracted at a rock-water boundary, Bull. Seismol. Soc. Am. **42**, 349–372 (1952)

6.30 L.M. Brekhovskikh: *Waves in Layered Media* (Academic, New York 1960)

6.31 W.G. Neubauer: Ultrasonic reflection of a bounded beam at Rayleigh and critical angles for a plane liquid-solid interface, J. Appl. Phys. **44**, 48–55 (1973)

Amazon
EX1010 Page 254

6.32 T. Tamir, H.L. Bertoni: Lateral displacement of optical beams at multilayered and periodic structures, J. Opt. Soc. Am. **61**, 1397–1413 (1971)
6.33 M.A. Breazeale, M.A. Torbett: Backward displacement of waves reflected from an interface having superimposed periodicity, Appl. Phys. Lett. **29**, 456–458 (1976)
6.34 R.T. Beyer: *Nonlinear Acoustics* (Naval Ships Systems Command, Washington 1974)
6.35 M.A. Breazeale: Third-order elastic constants of cubic crystals. In: *Handbook of Elastic Properties of Solids, Liquids and Gases*, Vol. I, ed. by M. Levy, H. Bass, R. Stern (Academic, New York 2001) pp. 489–510, Chap. 21
6.36 M.S. McPherson, I. Ostrovskii, M.A. Breazeale: Observation of acoustical memory in $LiNbO_3$, Phys. Rev. Lett. **89**, 115506 (2002)
6.37 M.A. Breazeale, J. Philip, A. Zarembowitch, M. Fischer, Y. Gesland: Acoustical measurement of solid state nonlinearity: Aplication to $CsCdF_3$ and $KZnF_3$, J. Sound Vib. **88**, 138–140 (1983)

Amazon
EX1010 Page 255

7. Thermoacoustics

Thermodynamic and fluid-dynamic processes in sound waves in gases can convert energy from one form to another. In these *thermoacoustic* processes [7.1, 2], high-temperature heat or chemical energy can be partially converted to acoustic power, acoustic power can produce heat, acoustic power can pump heat from a low temperature or to a high temperature, and acoustic power can be partially converted to chemical potential in the separation of gas mixtures. In some cases, the thermoacoustic perspective brings new insights to decades-old technologies. Well-engineered thermoacoustic devices using extremely intense sound approach the power conversion per unit volume and the efficiency of mature energy-conversion equipment such as internal combustion engines, and the simplicity of few or no moving parts drives the development of practical applications.

This chapter surveys thermoacoustic energy conversion, so the reader can understand how thermoacoustic devices work and can estimate some relevant numbers. After a brief history, an initial section defines vocabulary and establishes preliminary concepts, and subsequent sections explain engines, dissipation, refrigeration, and mixture separation. Combustion thermoacoustics is mentioned only briefly. Transduction and measurement systems that use heat-generated surface and bulk acoustic waves in solids are not discussed.

7.1 **History** 239

7.2 **Shared Concepts** 240
7.2.1 Pressure and Velocity 240
7.2.2 Power 243

7.3 **Engines** 244
7.3.1 Standing-Wave Engines 244
7.3.2 Traveling-Wave Engines 246
7.3.3 Combustion 248

7.4 **Dissipation** 249

7.5 **Refrigeration** 250
7.5.1 Standing-Wave Refrigeration 250
7.5.2 Traveling-Wave Refrigeration 251

7.6 **Mixture Separation** 253

References 254

7.1 History

The history of thermoacoustic energy conversion has many interwoven roots, branches, and trunks. It is a complicated history because invention and technology development outside of the discipline of acoustics have sometimes preceded fundamental understanding; at other times, fundamental science has come first.

Rott [7.3, 4] developed the mathematics describing acoustic oscillations in a gas in a channel with an axial temperature gradient, with lateral channel dimensions of the order of the gas thermal penetration depth (typically ≈ 1 mm), this being much shorter than the wavelength (typically ≈ 1 m). The problem had been investigated by Rayleigh and by Kirchhoff, but without quantitative success. In Rott's time, the motivation to understand the problem arose largely from the cryogenic phenomenon known as Taconis oscillations – when a gas-filled tube is cooled from ambient temperature to a cryogenic temperature, the gas sometimes oscillates spontaneously, with large heat transport from ambient to the cryogenic environment. *Yazaki* [7.5] demonstrated convincingly that Rott's analysis of Taconis oscillations was quantitatively accurate.

A century earlier, *Rayleigh* [7.6] understood the qualitative features of such heat-driven oscillations: "If heat be given to the air at the moment of greatest condensation (i.e., greatest density) or be taken from it at the moment of greatest rarefaction, the vibration is encouraged." He had studied Sondhauss oscillations [7.7], the glassblowers' precursor to Taconis oscillations.

Amazon
EX1010 Page 256

Applying Rott's mathematics to a situation where the temperature gradient along the channel was too weak to satisfy Rayleigh's criterion for spontaneous oscillations, *Hofler* [7.8] invented a standing-wave thermoacoustic refrigerator, and demonstrated [7.9] again that Rott's approach to acoustics in small channels was quantitatively accurate. In this type of refrigerator, the coupled oscillations of gas motion, temperature, and heat transfer in the sound wave are phased in time so that heat is absorbed from a load at a low temperature and waste heat is rejected to a sink at a higher temperature.

Meanwhile, completely independently, pulse-tube refrigeration was becoming the most actively investigated area of cryogenic refrigeration. This development began with *Gifford*'s [7.10] accidental discovery and subsequent investigation of the cooling associated with square-wave pulses of pressure applied to one end of a pipe that was closed at the other end. Although the relationship was not recognized at the time, this phenomenon shared much physics with Hofler's refrigerator. *Mikulin*'s [7.11] attempt at improvement in heat transfer in one part of this basic pulse-tube refrigerator led unexpectedly to a dramatic improvement of performance, and *Radebaugh* [7.12] realized that the resulting *orifice* pulse-tube refrigerator was in fact a variant of the Stirling cryocooler.

Development of Stirling engines and refrigerators started in the 19th century, the engines at first as an alternative to steam engines [7.13]. Crankshafts, multiple pistons, and other moving parts seemed at first to be essential. An important modern chapter in their development began in the 1970s with the invention of *free-piston* Stirling engines and refrigerators, in which each piston's motion is determined by interactions between the piston's dynamics and the gas's dynamics rather than by a crankshaft and connecting rod. Analysis of such complex, coupled phenomena is complicated, because the oscillating motion causes oscillating pressure differences while simultaneously the oscillating pressure differences cause oscillating motion. *Ceperley* [7.14,15] added an explicitly acoustic perspective to Stirling engines and refrigerators when he realized that the time phasing between pressure and motion oscillations in the heart of their regenerators is that of a traveling acoustic wave. Many years later, acoustic versions of such engines were demonstrated by *Yazaki* [7.16], *de-Blok* [7.17], and *Backhaus* [7.18], the last achieving a heat-to-acoustic energy efficiency comparable to that of other mature energy-conversion technologies.

7.2 Shared Concepts

7.2.1 Pressure and Velocity

For a monofrequency wave, oscillating variables can be represented with complex notation, such as

$$p(x,t) = p_\mathrm{m} + \mathrm{Re}\left[p_1(x)\mathrm{e}^{\mathrm{i}\omega t}\right] \tag{7.1}$$

for the pressure p, where p_m is the mean pressure, Re (z) indicates the real part of z, $\omega = 2\pi f$ is the angular frequency, f is the frequency, and the complex number p_1 specifies both the amplitude and the time phase of the oscillating part of the pressure. For propagation in the x direction through a cross-sectional area A in a duct, p_1 is a function of x. In the simple lossless, uniform-area situation the sinusoidal x dependence can be found from the wave equation, which can be written with $i\omega$ substituted for time derivatives as

$$\omega^2 p_1 + c^2 \frac{\mathrm{d}^2 p_1}{\mathrm{d}x^2} = 0\,, \tag{7.2}$$

where $c^2 = (\partial p/\partial\rho)_s$ is the square of the adiabatic sound speed, with ρ the density and s the entropy. In thermoacoustics, intuition is well served by thinking of (7.2) as two first-order differential equations coupling two variables, pressure p_1 and the x component of volume velocity, U_1:

$$\frac{\mathrm{d}p_1}{\mathrm{d}x} = -\frac{\mathrm{i}\omega\rho_\mathrm{m}}{A} U_1\,, \tag{7.3}$$

$$\frac{\mathrm{d}U_1}{\mathrm{d}x} = -\frac{\mathrm{i}\omega A}{\rho_\mathrm{m} c^2} p_1\,. \tag{7.4}$$

For a reasonably short length of duct Δx, these can be written approximately as

$$\Delta p_1 = -\mathrm{i}\omega L\, U_1\,, \tag{7.5}$$

$$p_1 = -\frac{1}{\mathrm{i}\omega C}\Delta U_1\,, \tag{7.6}$$

where

$$L = \frac{\rho_\mathrm{m}\Delta x}{A}\,, \tag{7.7}$$

$$C = \frac{A\Delta x}{\rho_\mathrm{m} c^2}\,. \tag{7.8}$$

Amazon
EX1010 Page 257

Table 7.1 The acoustic–electric analog. The basic building blocks of thermoacoustic energy-conversion devices are inertances L, compliances C, viscous and thermal resistances R_{visc} and R_{therm}, gains (or losses) G, and power transducers

Acoustic variables	Electric variables
Pressure p_1	Voltage
Volume velocity U_1	Current
Inertance L	Series inductance
Viscous resistance R_{visc}	Series resistance
Compliance C	Capacitance to ground
Thermal-hysteresis resistance R_{therm}	Resistance to ground
Gain/loss along temperature gradient, G	Proportionally controlled current injector
Stroke-controlled transducer	Current source
Force-controlled transducer	Voltage source

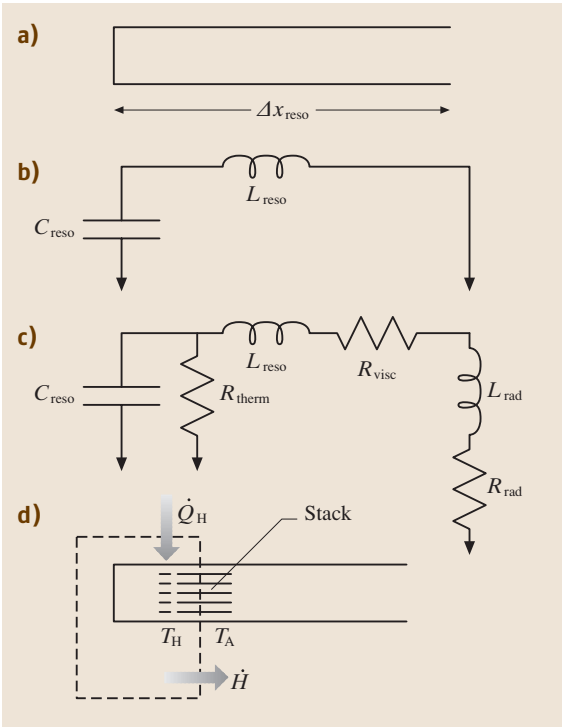


Fig. 7.1a–d Quarter-wavelength resonator. **(a)** A quarter-wavelength resonator: a tube closed at one end and open at the other. **(b)** A simple lossless lumped-element model of the resonator as a compliance C_{reso} in series with an inertance L_{reso}. **(c)** A more complicated lumped-element model, including thermal-hysteresis resistance R_{therm} in the compliance, viscous resistance R_{visc} in the inertance, and radiation impedance $R_{rad} + i\omega L_{rad}$. **(d)** An illustration of the first law of thermodynamics for a control volume, shown enclosed by the dashed line, which intersects the stack of a well-insulated standing-wave engine. In steady state, the thermal power $\dot{Q}_H$ that flows into the system at the hot heat exchanger must equal the total power $\dot{H}$ that flows along the stack

As introduced in Chap. 6 (Physical Acoustics) (7.3) is the acoustic Euler equation, the inviscid form of the momentum equation. It describes the force that the pressure gradient must exert to overcome the gas's inertia. In the lumped-element form (7.5), the geometrical and gas-property aspects of the inertia of the gas in the duct are represented by the duct's inertance L. Similarly introduced in Chap. 6, (7.4) and (7.6) are, respectively, the differential and lumped-element versions of the continuity equation combined with the gas's adiabatic equation of state. These describe the compressibility of the gas in response to being squeezed along the x-direction. In the lumped-element form (7.6), the geometrical and gas-property aspects of the compressibility of the gas in the duct are represented by the duct's compliance C.

Accurate calculation of the wave in a long duct or a long series of ducts requires analytical or numerical integration of differential equations [7.1], but for the purposes of this chapter we will consider lumped-element approximations, because they are satisfactorily accurate for many estimates, they allow a *circuit model* representation of devices, and they facilitate intuition based on experience with alternating-current (AC) electrical circuits. Table 7.1 shows the analogy between acoustic devices and electrical circuits.

For example, the closed–open resonator shown in Fig. 7.1a has a resonance frequency that can be calculated by setting its length Δx_{reso} equal to a quarter wavelength of sound; the result is $f_{reso} = c/4\Delta x_{reso}$. The simplest lumped-element approximation of the quarter-wavelength resonator is shown in Fig. 7.1b. We assign compliance C_{reso} to the left half of the resonator, because the compressibility of the gas is more important than its inertia in the left half, where $|p_1|$ is high and $|U_1|$ is low. Similarly, we assign inertance L_{reso} to the right half of the resonator, because the inertia is more important in the right half where $|U_1|$ is high. Setting $\Delta x = \Delta x_{reso}/2$ in (7.7) and (7.8), and recalling that the resonance frequency of an electrical LC circuit is given by $\omega^2 = 1/LC$, we find $f_{reso} = c/\pi\Delta x_{reso}$, differing from the exact result only by a factor of $4/\pi$. Such accuracy will be acceptable for estimation and understanding in this chapter.

Amazon
EX1010 Page 258

Circuit models can include as much detail as is necessary to convey the essential physics [7.1]. When the viscosity is included in the momentum equation, the lumped-element form becomes

$$\Delta p_1 = -\left(\mathrm{i}\omega L + R_{\mathrm{visc}}\right) U_1 \,, \tag{7.9}$$

and when the thermal conductivity and a temperature gradient in the x direction are included in the continuity equation, the lumped-element form becomes

$$\Delta U_1 = -\left(\mathrm{i}\omega C + \frac{1}{R_{\mathrm{therm}}}\right) p_1 + G U_{\mathrm{in},1} \,. \tag{7.10}$$

Figure 7.1c is a better model than Fig. 7.1b for the closed–open resonator of Fig. 7.1a, because it includes thermal-hysteresis resistance in the compliance, viscous resistance in the inertance, and the inertial and resistive radiation impedance at the open end. This model would yield reasonably accurate estimates for the free-decay time and quality factor of the resonator as well as its resonance frequency.

Ducts filled with porous media and having temperature gradients in the x-direction play a central role in thermoacoustic energy conversion [7.1]. The pore size is characterized by the hydraulic radius r_{h}, defined as the ratio of gas volume to gas–solid contact area. In a circular pore, r_{h} is half the circle's radius; in the gap between parallel plates, r_{h} is half the gap. The term *stack* is used for a porous medium whose r_{h} is comparable to the gas thermal penetration depth

$$\delta_{\mathrm{therm}} = \sqrt{2k/\omega\rho_{\mathrm{m}} c_{\mathrm{p}}} \,, \tag{7.11}$$

where k is the gas thermal conductivity and c_{p} is its isobaric heat capacity per unit mass, while a porous medium with $r_{\mathrm{h}} \ll \delta_{\mathrm{therm}}$ is known as a *regenerator*. The viscous penetration depth

$$\delta_{\mathrm{visc}} = \sqrt{2\mu/\omega\rho_{\mathrm{m}}} \,, \tag{7.12}$$

where μ is the viscosity, is typically comparable to, but smaller than, the thermal penetration depth. If the distance between a particular mass of gas and the nearest solid wall is much greater than the penetration depths, thermal and viscous interactions with the wall do not affect that gas.

In such porous media with axial temperature gradients, the gain/loss term $G U_{\mathrm{in},1}$ in (7.10) is responsible for the creation of acoustic power by engines and for the thermodynamically required consumption of acoustic power by refrigerators. This term represents cyclic thermal expansion and contraction of the gas as it moves along and experiences the temperature gradient in the solid. In regenerators, the gain G is nearly real, and ΔU_1 caused by the motion along the temperature gradient is in phase with U_1 itself, because of the excellent thermal contact between the gas in small pores and the

Table 7.2 Expressions for the lumped-element building blocks L, R_{visc}, C, R_{therm}, and $G U_1$, and for the total power $\dot{H}$, in the boundary-layer limit $r_{\mathrm{h}} \gg \delta$ and in the small-pore limit $r_{\mathrm{h}} \ll \delta$. The symbol "$\sim$" in the small-pore limit indicates that the numerical prefactor depends on the shape of the pore

	Boundary-layer limit	Small-pore limit
L	$\dfrac{\rho_{\mathrm{m}}\Delta x}{A}$	$\sim \dfrac{\rho_{\mathrm{m}}\Delta x}{A}$
R_{visc}	$\dfrac{\mu\Delta x}{A r_{\mathrm{h}}\delta_{\mathrm{visc}}}$	$\sim \dfrac{2\mu\Delta x}{A r_{\mathrm{h}}^2}$
C	$\dfrac{A\Delta x}{\rho_{\mathrm{m}} c^2} = \dfrac{A\Delta x}{\gamma p_{\mathrm{m}}}$	$\dfrac{\gamma A\Delta x}{\rho_{\mathrm{m}} c^2} = \dfrac{A\Delta x}{p_{\mathrm{m}}}$
R_{therm}	$\dfrac{\rho_{\mathrm{m}}^2 c_{\mathrm{p}}^2 T_{\mathrm{m}} r_{\mathrm{h}}\delta_{\mathrm{therm}}}{kA\Delta x}$	$\sim \dfrac{3kT_{\mathrm{m}}}{4\omega^2 r_{\mathrm{h}}^2 A\Delta x}$
$G U_1$	$\dfrac{1-\mathrm{i}}{2}\dfrac{1}{1+\sqrt{\sigma}}\dfrac{\delta_{\mathrm{therm}}}{r_{\mathrm{h}}}\dfrac{\Delta T_{\mathrm{m}}}{T_{\mathrm{m}}} U_1$	$\dfrac{\Delta T_{\mathrm{m}}}{T_{\mathrm{in,m}}} U_{\mathrm{in},1}$
$\dot{H}$	$\dfrac{\delta_{\mathrm{therm}}}{4r_{\mathrm{h}}(1+\sigma)} \mathrm{Re}\left\{\tilde{p}_1 U_1 \left[\mathrm{i}\left(1+\sqrt{\sigma}\right)+\left(1-\sqrt{\sigma}\right)\right]\right\}$ $-\dfrac{\delta_{\mathrm{therm}}\rho_{\mathrm{m}} c_{\mathrm{p}}\left(1-\sigma\sqrt{\sigma}\right)\lvert U_1\rvert^2}{4r_{\mathrm{h}} A\omega\left(1-\sigma^2\right)}\dfrac{\Delta T}{\Delta x}$ $+\dot{E} - \left(Ak + A_{\mathrm{solid}} k_{\mathrm{solid}}\right)\dfrac{\Delta T}{\Delta x}$	$-A_{\mathrm{solid}} k_{\mathrm{solid}}\dfrac{\Delta T}{\Delta x}$

Amazon
EX1010 Page 259

walls of the pores. (Positive G indicates gain; negative G indicates loss.) In stacks, a nonzero imaginary part of G reflects imperfect thermal contact in the pores and the resultant time delay between the gas's cyclic motion along the solid's temperature gradient and the gas's thermal expansion and contraction.

Table 7.2 gives expressions for the impedances in the boundary-layer limit, $r_h \gg \delta_{therm}$ and $r_h \gg \delta_{visc}$, which is appropriate for large ducts, and in the small-pore limit appropriate for regenerators. Boundary-layer-limit entries are usefully accurate in stacks, in which $r_h \sim \delta$. General expressions for arbitrary r_h and many common pore shapes are given in [7.1].

The lumped-element approach summarized in Table 7.1 and the limiting expressions given in Table 7.2 are sufficient for most of this overview, but quantitatively accurate thermoacoustic analysis requires slightly more sophisticated techniques and includes more phenomena [7.1]. Every differential length dx of duct has dL, dC, dR_{visc}, and $d(1/R_{therm})$, and if $dT_m/dx \neq 0$ it also has dG, so a finite-length element is more analogous to an electrical transmission line than to a few lumped impedances. In addition to smoothly varying x dependencies for all variables, important phenomena include turbulence, which increases R_{visc} above the values given in Table 7.2; pore sizes which are in neither of the limits given in Table 7.2; nonlinear terms in the momentum and continuity equations, which cause frequency doubling, tripling, etc., so that the steady-state wave is a superposition of waves of many frequencies; and streaming flows caused by the wave itself. Many of these subjects are introduced in Chap. 8 (Nonlinear Acoustics). Thermoacoustics software that includes most or all of these phenomena and has the properties of several commonly used gases is available [7.19, 20].

For estimating the behavior of thermoacoustic devices, it is useful to remember some properties of common ideal gases [7.21]. The equation of state is

$$p = \frac{\rho R_{univ} T}{M} , \tag{7.13}$$

where $R_{univ} = 8.3\,\mathrm{J/(mole\,K)}$ is the universal gas constant and M is the molar mass. The ratio of isobaric to isochoric specific heats, γ, is 5/3 for monatomic gases such as helium and 7/5 for diatomic gases such as nitrogen and air near ambient temperature, and appears in both the adiabatic sound speed

$$c = \sqrt{\frac{\gamma R_{univ} T}{M}} \tag{7.14}$$

and the isobaric heat capacity per unit mass

$$c_p = \frac{\gamma R_{univ}}{(\gamma - 1)\, M} . \tag{7.15}$$

The viscosity of many common gases (e.g., air, helium, and argon) is about

$$\mu \simeq (2 \times 10^{-5}\,\mathrm{kg/m\,s}) \left(\frac{T}{300\,\mathrm{K}} \right)^{0.7} , \tag{7.16}$$

and the thermal conductivity k can be estimated by remembering that the Prandtl number

$$\sigma = \frac{\mu c_p}{k} \tag{7.17}$$

is about 2/3 for pure gases, but somewhat lower for gas mixtures [7.22].

7.2.2 Power

In addition to ordinary acoustic power $\dot{E}$, the time-averaged thermal power $\dot{Q}$, total power $\dot{H}$, and exergy flux $\dot{X}$ are important in thermoacoustic energy conversion. These thermoacoustic powers are related to the simpler concepts of work, heat, enthalpy, and exergy that are encountered in introductory [7.21] and advanced [7.23] thermodynamics.

Just as acoustic intensity is the time-averaged product of pressure and velocity, acoustic power $\dot{E}$ is the time-averaged product of pressure and volume velocity. In complex notation,

$$\dot{E} = \frac{1}{2} \mathrm{Re}\,(\tilde{p}_1 U_1) , \tag{7.18}$$

where the tilde denotes complex conjugation. At transducers, it is apparent that acoustic power is closely related to thermodynamic work, because a moving piston working against gas in an open space with volume V transforms mechanical power to acoustic power (or vice versa) at a rate $f \oint p\, dV$, which is equal to (7.18) for sinusoidal pressure and motion. Resistances R dissipate acoustic power; the gain/loss term GU_1 in components with temperature gradients can either consume or produce acoustic power, and inertances L and compliances C neither dissipate nor produce acoustic power, but simply pass it along while changing p_1 or U_1.

Time-averaged thermal power $\dot{Q}$ (i.e., time-averaged heat per unit time) is added to or removed from the gas at heat exchangers, which are typically arrays of tubes, high-conductivity fins, or both, spanning a duct. Thermal power can be supplied to an engine by high-temperature combustion products flowing through such

Amazon
EX1010 Page 260

tubes or by circulation of a high-temperature heat-transfer fluid through such tubes and a source of heat elsewhere. Thermal power is often removed from engines and refrigerators by ambient-temperature water flowing through such tubes.

Of greatest importance is the total time-averaged power

$$\dot{H} = \int \left[\frac{1}{2} \rho_m \mathrm{Re}\left(\widetilde{h}_1 u_1 \right) - k \frac{\mathrm{d}T_m}{\mathrm{d}x} \right] \mathrm{d}A \,, \qquad (7.19)$$

based on the x component u of velocity and the enthalpy h per unit mass, which is the energy of most utility in fluid mechanics. Fig. 7.1d uses a simple standing-wave engine (discussed more fully below) to illustrate the centrality of $\dot{H}$ to the first law of thermodynamics in thermoacoustics. The figure shows a heat exchanger and stack in a quarter-wavelength resonator. When heat is applied to the hot heat exchanger, the resonance is driven by processes (described below) in the stack. The dashed line in Fig. 7.1d encloses a volume whose energy must be constant when the engine is running in steady state. If the side walls of the engine are well insulated and rigid within that volume, then the only energy flows per unit time into and out of the volume are $\dot{Q}_H$ and whatever power flows to the right through the stack. We define the total power flow through the stack to be $\dot{H}$, and the first law of thermodynamics ensures that $\dot{H} = \dot{Q}_H$ in this simple engine.

As shown in (7.19), the total power $\dot{H}$ is the sum of ordinary steady-state heat conduction (most importantly in the solid parts of the stack or regenerator and the surrounding duct walls) and the total power carried convectively by the gas itself. Analysis of the gas contribution requires spatial and temporal averaging of the enthalpy transport in the gas [7.4], and shows that the most important contributions are acoustic power flowing through the pores of the stack and a shuttling of energy by the gas that occurs because entropy oscillations in the gas are nonzero and have a component in phase with velocity. Remarkably, these two phenomena nearly cancel in the small pores of a regenerator.

Finally, the exergy flux $\dot{X}$ represents the rate at which thermodynamic work can be done, in principle, with unrestricted access to a thermal bath at ambient temperature [7.1,23]. Exergy flux is sometimes used in complex systems to analyze sources of inefficiency according to location or process.

7.3 Engines

Implicit in Rayleigh's criterion [7.6] for spontaneous oscillations, "If heat be given to the air at the moment of greatest (density) or be taken from it at the moment of greatest rarefaction, the vibration is encouraged," is the existence of a vibration in need of encouragement, typically a resonance with a high quality factor. Today, we would express Rayleigh's criterion in either of two ways, depending on whether we adopt a Lagrangian perspective, focusing on discrete masses of gas as they move, or an Eulerian perspective, focusing on fixed locations in space as the gas moves past them. In the Lagrangian perspective, some of the gas in a thermoacoustic engine must experience $\oint p \, \mathrm{d}V > 0$, where V is the volume of an identified mass of gas. In the Eulerian perspective, part of the device must have $\mathrm{d}\dot{E}/\mathrm{d}x > 0$, arising from $\mathrm{Re}\,(\tilde{p}_1 \, \mathrm{d}U_1/\mathrm{d}x) > 0$ and the G term in (7.10).

By *engine* we mean a prime mover, i.e., something that converts heat to work or acoustic power. We describe three varieties: standing-wave engines, traveling-wave engines, and pulse combustors.

7.3.1 Standing-Wave Engines

Continuing the quarter-wavelength example introduced in Fig. 7.1, Fig. 7.2 shows a simple standing-wave engine, of a type that is available as a classroom demonstration [7.24]. A stack and hot heat exchanger are near the left end of the resonator, and its right end is open to the air. When heat $\dot{Q}_H$ is first applied to the hot heat exchanger, the heat exchanger and the adjacent end of the stack warm up, establishing an axial temperature gradient from hot to ambient in the stack. When the gradient is steep enough (as explained below), the acoustic oscillations start spontaneously, and grow in intensity as more heat is added and a steady state is approached. In the steady state, total power $\dot{H}$ equal to $\dot{Q}_H$ (minus any heat leak to the room) flows through the stack, creating acoustic power, some of which is dissipated elsewhere in the resonator and some of which is radiated into the room. To the right of the stack, where an ambient-temperature heat exchanger would often be located, the heat is carried rightward and out of this resonator by streaming-driven

Amazon
EX1010 Page 261

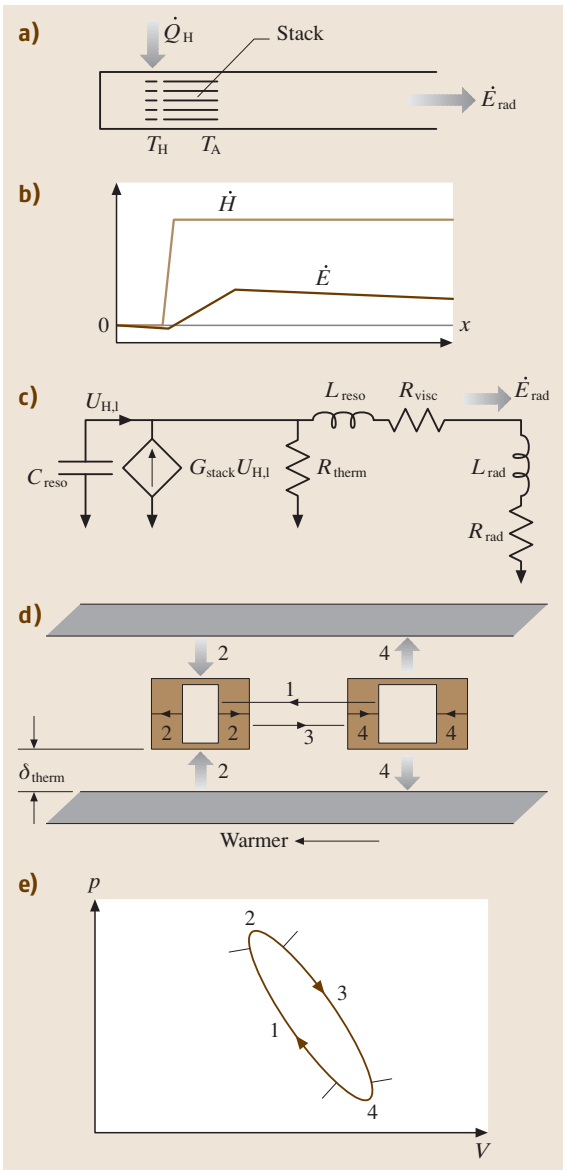


Fig. 7.2a–e A standing-wave engine. **(a)** A hot heat exchanger and a stack in a quarter-wavelength resonator. Heat $\dot{Q}_H$ is injected at the hot heat exchanger, and the device radiates acoustic power $\dot{E}_{rad}$ into the surroundings. **(b)** Total power flow $\dot{H}$ and acoustic power $\dot{E}$ as functions of position x in the device. Positive power flows in the positive-x direction. **(c)** Lumped-element model of the device. **(d)** Close-up view of part of one pore in the stack of **(a)**, showing a small mass of gas going through one full cycle, imagined as four discrete steps. *Thin arrows* represent motion, and *wide, open arrows* represent heat flow. **(e)** Plot showing how the pressure p and volume V of that small mass of gas evolve with time in a clockwise elliptical trajectory. *Tick marks* show approximate boundaries between the four numbered steps of the cycle shown in **(d)**

convection in the resonator, while fresh air at ambient temperature T_A streams inwards.

The most important process in the standing-wave engine is illustrated in Fig. 7.2d and Fig. 7.2e from a Lagrangian perspective. Figure 7.2d shows a greatly magnified view of a mass of gas inside one pore of the stack. The sinusoidal thermodynamic cycle of that mass of gas in pressure p and volume V is shown in Fig. 7.2e; the mass's temperature, entropy, density, and other properties also vary sinusoidally in time. However, for qualitative understanding of the processes, we describe the cycle as if it were a time series of four discrete steps, numbered 1–4 in Fig. 7.2d and Fig. 7.2e. In step 1, the gas is simultaneously compressed to a smaller volume and moved leftward by the wave a distance $2\,|\xi_1|$, which is much smaller than the length Δx of the stack. While the gas is moving leftwards, the pressure changes by $2\,|p_1|$ and the temperature would change by $2\,|T_1| = 2T_m(\gamma-1)\,|p_1|\,/\gamma p_m$ if the process were adiabatic. This suggests the definition of a critical temperature gradient

$$\nabla T_{crit} = |T_1| \,/\, |\xi_1| \ . \tag{7.20}$$

Thermal contact in the stack's large pores is imperfect, so step 1 is actually not too far from adiabatic. However, the temperature gradient imposed on the stack is greater than ∇T_{crit}, so the gas arrives at its new location less warm than the adjacent pore walls. Thus, in step 2, heat flows from the solid into the gas, warming the gas and causing thermal expansion of the gas to a larger volume. In step 3, the gas is simultaneously expanded to a larger volume and moved rightward by the wave. It arrives at its new location warmer than the adjacent solid, so in step 4 heat flows from the gas to the solid, cooling the gas and causing thermal contraction of the gas to a smaller volume. This brings it back to the start of the cycle, ready to repeat step 1.

Although the mass of gas under consideration returns to its starting conditions each cycle, its net effect on its surroundings is nonzero. First, its thermal expansion occurs at a higher pressure than its thermal contraction, so $\oint p\ \mathrm{d}V > 0$: the gas does work on its surroundings, satisfying Rayleigh's criterion. This work is responsible for the positive slope of $\dot{E}$ versus x in the stack in Fig. 7.2b and is represented by the gain element $G_{stack}U_{H,1}$ in

Amazon
EX1010 Page 262

Fig. 7.2c. All masses of gas within the stack contribute to this production of acoustic power; one can think of the steady-state operation as due to all masses of gas within the stack adding energy to the oscillation every cycle, to make up for energy lost from the oscillation elsewhere, e.g., in viscous drag in the resonator and acoustic radiation to the surroundings. Second, the gas absorbs heat from the solid at the left extreme of its motion, at a relatively warm temperature, and delivers heat to the solid farther to the right at a lower temperature. In this way, all masses of gas within the stack pass heat along the solid, down the temperature gradient from left to right; within a single pore, the gas masses are like members of a bucket brigade (a line of people fighting a fire by passing buckets of water from a source of water to the fire while passing empty buckets back to the source). This transport of heat is responsible for most of $\dot{H}$ inside the stack, shown in Fig. 7.2b.

This style of engine is called *standing wave* because the time phasing between pressure and motion is close to that of a standing wave. (If it were *exactly* that of a standing wave, $\dot{E}$ would have to be exactly zero at all x.) To achieve the time phasing between pressure and volume changes that is necessary for $\oint p\ \mathrm{d}V > 0$, imperfect thermal contact between the gas and the solid in the stack is required, so that the gas can be somewhat thermally isolated from the solid during the motion in steps 1 and 3 but still exchange significant heat with the solid during steps 2 and 4. This imperfect thermal contact occurs because the distance between the gas and the nearest solid surface is of the order of δ_{therm}, and it causes R_{therm} to be significant, so standing-wave engines are inherently inefficient. Nevertheless, standing-wave engines are exceptionally simple. They include milliwatt classroom demonstrations like the illustration in Fig. 7.2, similar demonstrations with the addition of a water- or air-cooled heat exchanger at the ambient end of the stack, research engines [7.25, 26] up to several kW, and the Taconis and Sondhauss oscillations [7.5, 7]. Variants based on the same physics of intrinsically irreversible heat transfer include the *no-stack* standing-wave engine [7.27], which has two heat exchangers but no stack, and the Rijke tube [7.28], which has only a single, hot heat exchanger and uses a superposition of steady and oscillating flow of air through that heat exchanger to create $\oint p\ \mathrm{d}V > 0$.

7.3.2 Traveling-Wave Engines

One variety of what acousticians call traveling-wave engines has been known for almost two centuries as a Stirling engine [7.13, 29, 30], and is illustrated in Fig. 7.3a, Fig. 7.3b, Fig. 7.3f, and Fig. 7.3g. A regenerator bridges the gap between two heat exchangers, one at ambient temperature T_{A} and the other at hot temperature T_{H}; this assembly lies between two pistons, whose oscillations take the gas through a sinusoidal cycle that can be approximated as four discrete steps: compression, displacement rightward toward higher temperature, expansion, and displacement leftward toward lower temperature. For a small mass of gas in a single pore in the heart of the regenerator, the four steps of the cycle are illustrated in Fig. 7.3f. In step 1, the gas is compressed by rising pressure, rejecting heat to the nearby solid. In step 2, it is moved to the right, toward higher temperature, absorbing heat from the solid and experiencing thermal expansion as it moves. In step 3, the gas is expanded by falling pressure, and absorbs heat from the nearby solid. In step 4, the gas is moved leftward, toward lower temperature, rejecting heat to the solid and experiencing thermal contraction as it moves. The Stirling engine accomplishes $\oint p\ \mathrm{d}V > 0$ in Fig. 7.3g for each mass of gas in the regenerator, and this work production allows the hot piston to extract more work from the gas in each cycle than the ambient piston delivers to the gas.

The similarities and differences between this process and the standing-wave process of Fig. 7.2 are instructive. Here, the pore size is $\ll \delta_{\mathrm{therm}}$, so the thermal contact between the gas and the solid in the regenerator is excellent and the gas is always at the temperature of the part of the solid to which it is adjacent. Thus, the thermal expansion and contraction occur during the motion parts of the cycle, instead of during the stationary parts of the cycle in the standing-wave engine, and the pressure must be high during the rightward motion and low during the leftward motion to accomplish $\oint p\ \mathrm{d}V > 0$. This is the time phasing between motion and pressure that occurs in a traveling wave [7.14, 15], here traveling from left to right. The small pore size maintains thermodynamically reversible heat transfer, so R_{therm} is negligible, and traveling-wave engines have inherently higher efficiency than standing-wave engines. One remaining source of inefficiency is the viscous resistance R_{visc} in the regenerator, which can be significant because the small pores necessary for thermal efficiency cause R_{visc} to be large. To minimize the impact of R_{visc}, traveling-wave engines have $|p_1| > \rho_{\mathrm{m}} c\,|U_1|/A$, so the magnitude of the specific acoustic impedance $|z_{\mathrm{ac}}| = |p_1|\,A/|U_1|$ is greater than that of a traveling wave.

The gain G listed in Table 7.2 takes on a particularly simple form in the tight-pore limit: $G_{\mathrm{reg}} = \Delta T_{\mathrm{m}}/T_{\mathrm{in,m}}$.

Amazon
EX1010 Page 263

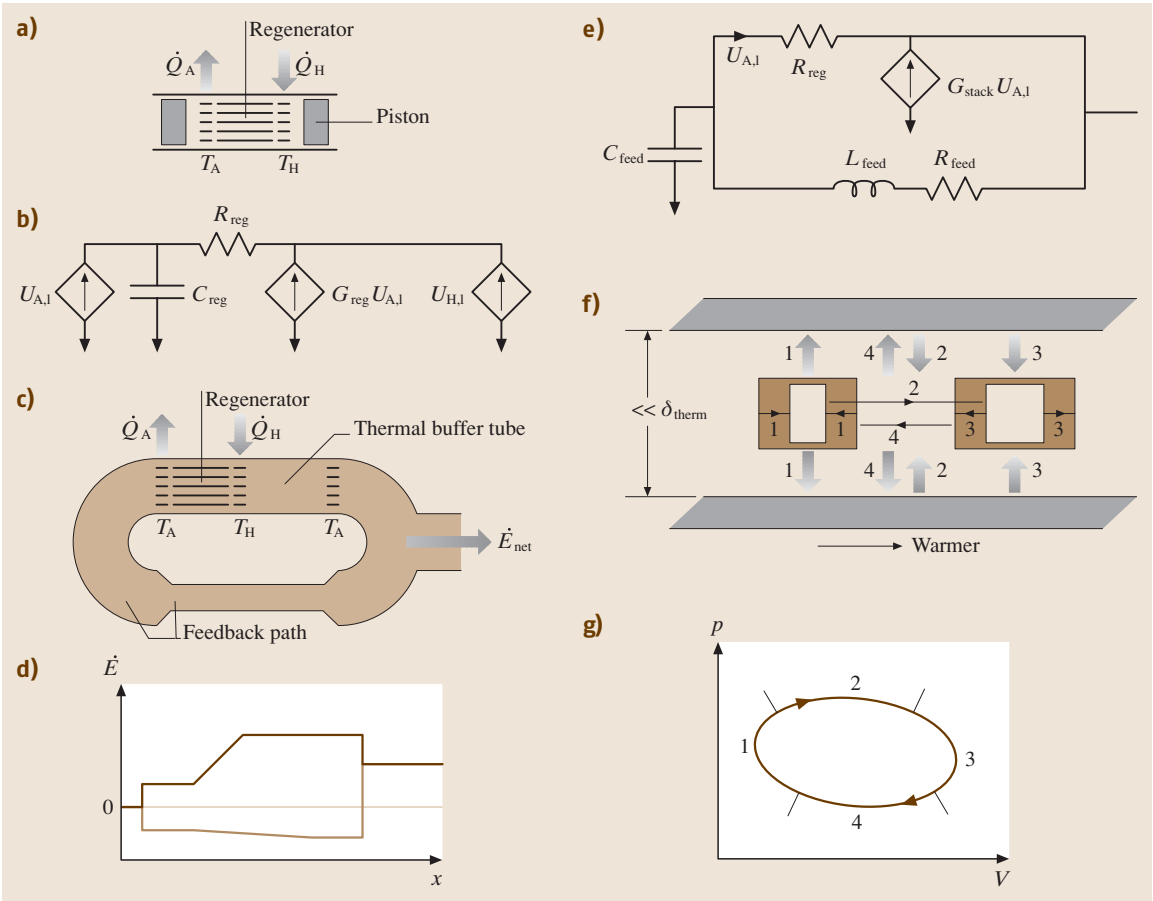


Fig. 7.3a–g Traveling-wave engines. **(a)** A Stirling engine. From *left to right*, the ambient piston, the ambient heat exchanger, the regenerator, the hot heat exchanger, and the hot piston. Time-averaged thermal power $\dot{Q}_H$ is injected into the gas at hot temperature T_H, waste thermal power $\dot{Q}_A$ is removed at ambient temperature T_A, and net mechanical power is extracted by the two pistons. **(b)** Lumped-element model of the engine in **(a)**. **(c)** Acoustic–Stirling hybrid engine, with the same processes as **(a)** in the regenerator and its two adjacent heat exchangers, but with additional acoustic components replacing the two pistons. **(d)** Acoustic power $\dot{E}$ as a function of position x in the device shown in **(c)**. Positive power flows in the positive-x direction, so the bottom branch of the curve represents power flowing leftward through the feedback path. Total power $\dot{H}$ is not shown, because it is essentially zero in the regenerator and essentially identical to $\dot{E}$ in the open parts of the device. **(e)** Lumped-element model of the engine in **(c)**. **(f)** Close-up view of part of one pore in the regenerator of **(a)** or **(c)**, showing a small mass of gas going through one full cycle, imagined as four discrete steps. **(g)** Plot showing how the pressure p and volume V of that small mass of gas evolve with time in a clockwise elliptical trajectory. *Tick marks* show approximate boundaries between the four steps of the cycle shown in **(f)**

In the engine of Fig. 7.3a, the initial temperature is T_A, and $\Delta T_m = T_H - T_A$, so the extra volume velocity that the lumped-element model injects at the right end of the regenerator is $U_{A,1}\,(T_H - T_A)\,/T_A$ and the total volume velocity at the right end of the regenerator is $U_{A,1}\,T_H/T_A$. Thus, the regenerator acts like an amplifier of volume velocity, with amplification T_H/T_A. If R_{reg} is small so that p_1 is nearly the same on both sides of the regenerator, then the regenerator amplifies $\dot{E}$ by nearly T_H/T_A.

Figure 7.3c-e illustrates a thermoacoustic–Stirling hybrid engine [7.16–18], in which the processes in the regenerator and its adjacent heat exchangers are the same

Amazon
EX1010 Page 264

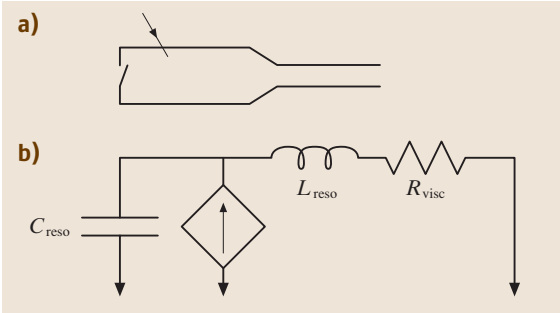


Fig. 7.4a,b Pulsed combustor. **(a)** From *left to right*, check valve for admitting fresh air, fuel injection, combustion cavity, neck. **(b)** Lumped-element model of the combustor

as in the Stirling engine and in Fig. 7.3f and Fig. 7.3g, but with acoustic elements replacing the Stirling engine's pistons. The toroidal topology of the thermoacoustic–Stirling hybrid allows some of the acoustic power that leaves the hot end of the regenerator to be fed back to the ambient end of the regenerator, eliminating the need for the Stirling engine's ambient piston. The feedback path has an inertance L_{feed} (with an unavoidable but small viscous resistance R_{feed}) and a compliance C_{feed}, with $1/L_{feed}C_{feed} \gg \omega^2$ and with ωL_{feed} significantly smaller than the regenerator viscous resistance R_{reg}. These choices let the $L_{feed}C_{feed}$ feedback path boost p_1 as acoustic power flows through it, providing the extra p_1 needed to drive U_1 into the regenerator at its ambient end.

The Stirling engine in Fig. 7.3a has a hot piston, which extracts acoustic power from the gas. From the hot piston's face, mechanical power flows from T_H to T_A along a temperature gradient in a moving part, either the piston itself or a connecting rod. In the thermoacoustic–Stirling hybrid engine of Fig. 7.3c, this thermal isolation function is accomplished by the thermal buffer tube, a thermally stratified column of moving gas. A well-designed thermal buffer tube passes acoustic power with little attenuation and has $\dot{H} \simeq \dot{E}$, so almost no thermal power flows from hot to ambient along the tube and little thermal power need be removed at the auxiliary heat exchanger at the thermal buffer tube's ambient end. Minimizing streaming and attendant heat convection in thermal buffer tubes, which otherwise causes $\dot{H} \neq \dot{E}$, is a topic of current research in thermoacoustics.

Traditional Stirling engines are used for propulsion in some submarines [7.31] and for auxiliary power in boats [7.32], and are under development for residential cogeneration of electricity and space heating [7.33], concentrated solar electricity generation, and nuclear generation of electricity for spacecraft [7.34]. In most of these applications, piston motion is converted to electricity via relative motion of wires and permanent magnets, either with a rotary alternator for crankshaft-coupled pistons or a linear alternator (reminiscent of a loudspeaker) for resonant *free-piston* configurations. Thermoacoustic-Stirling hybrid engines are under consideration for small-scale natural-gas liquefaction [7.25, 35] and for spacecraft power [7.36]. In the former case, acoustic power is fed directly from the engine to cryogenic acoustic refrigerators, without transduction to electrical power.

7.3.3 Combustion

In the standing-wave and traveling-wave engines, Rayleigh's criterion $\oint p \, dV > 0$ is met with volume changes that arise from temperature changes; those temperature changes, in turn, arise from thermal contact between the gas and nearby solid surfaces. In pulsed combustion, the volume changes needed to meet Rayleigh's criterion arise from both temperature and mole-number changes, which in turn are due to time-dependent chemical reactions whose rate is controlled by the time-dependent pressure or time-dependent velocity [7.37, 38].

Figure 7.4 illustrates one configuration in which pulsed combustion can occur. At the closed end of a closed–open resonator, a check valve periodically lets fresh air into the resonator and a fuel injector adds fuel, either steadily or periodically. If the rate of the exothermic chemical reaction increases with pressure (e.g., via the temperature's adiabatic dependence on pressure), positive dV occurs when p is high, meeting Rayleigh's criterion. A four-step diagram of the process, resembling Fig. 7.2d and Fig. 7.3f, is not included in Fig. 7.4 because the process is fundamentally not cyclic: a given mass of gas does not return to its starting conditions, but rather each mass of fresh-air–fuel mixture burns and expands only once.

Combustion instabilities can occur in rockets, jet engines, and gas turbines, with potentially devastating consequences if the pressure oscillations are high enough to cause structural damage. Much of the literature on thermoacoustic combustion is devoted to understanding such oscillations and using active or passive means to prevent them. However, some devices such as high-efficiency residential gas-fired furnaces deliberately use pulsed combustion as illustrated in Fig. 7.4 to pump fresh air in and exhaust gases out of the combus-

Amazon
EX1010 Page 265

tor. This eliminates the need to leave the exhaust gases hot enough for strong chimney convection, so a larger fraction of the heat of combustion can be delivered to the home.

7.4 Dissipation

The dissipative processes represented above by R_{visc} and R_{therm} occur whenever gas-borne sound interacts with solid surfaces. Figure 7.5 illustrates this in the case of a short length dx of a large-radius duct with no axial temperature gradient. The origin of the viscous dissipation of acoustic power is viscous shear within the viscous penetration depth δ_{visc}, as shown in Fig. 7.5c. Most people find viscous dissipation intuitively plausible, imagining the frictional dissipation of mechanical energy when one surface rubs on another. More subtle is the thermal relaxation of acoustic power, illustrated in Fig. 7.5d and Fig. 7.5e. Gas is pressurized nearly adiabatically in step 1, then shrinks during thermal equilibration with the surface in step 2. It is depressurized nearly adiabatically in step 3, and then thermally expands during thermal equilibration with the surface during step 4. As shown in Fig. 7.5e, the net effect is $\oint p\ dV < 0$: the gas absorbs acoustic power from the wave, because the contraction occurs at high pressure and the expansion at low pressure. To avoid a hopelessly cluttered illustration, Fig. 7.5d shows the thermal-hysteresis process superimposed on the left–right oscillating motion in steps 1 and 3, but the thermal-hysteresis process occurs even in the absence of such motion.

Differentiating (7.18) with respect to x shows that the dissipation of acoustic power in the duct in length

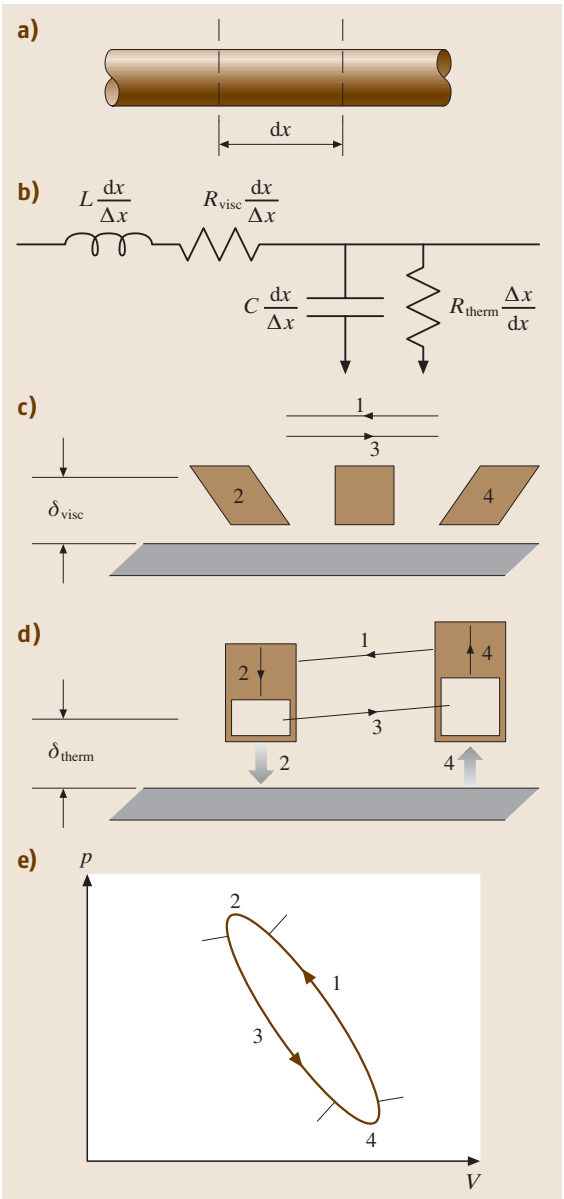


Fig. 7.5a–e Boundary dissipation in acoustic waves. **(a)** A duct with no temperature gradient, with one short length dx identified. **(b)** Each length dx has inertance, viscous resistance, compliance, and thermal hysteresis resistance. **(c)** The dissipation of acoustic power by viscous resistance is due to shear in the gas within roughly δ_{visc} of the boundary, here occurring during steps 1 and 3 of the cycle. **(d)** and **(e)** The dissipation of acoustic power by thermal relaxation hysteresis occurs within roughly δ_{therm} of the boundary. Gas is pressurized nearly adiabatically in step 1, then shrinks during thermal equilibration with the surface in step 2. It is depressurized nearly adiabatically in step 3, and then thermally expands during thermal equilibration with the surface during step 4. The net effect is that the gas absorbs acoustic power from the wave

Amazon
EX1013 Page 266
EX1010 Page 266

$\mathrm{d}x$ is given by

$$\mathrm{d}\dot{E} = \frac{1}{2}\,\mathrm{Re}\left(\frac{\mathrm{d}\tilde{p}_1}{\mathrm{d}x}U_1 + \tilde{p}_1\frac{\mathrm{d}U_1}{\mathrm{d}x}\right)\,\mathrm{d}x\,, \tag{7.21}$$

and examination of (7.10) and (7.9) associates R_{visc} with the first term and R_{therm} with the second term. Expressions for R_{visc} and R_{therm} in the boundary-layer approximation are given in Table 7.2, and allow the expression of (7.21) in terms of the dissipation of acoustic power per unit of surface area S:

$$\mathrm{d}\dot{E} = \frac{1}{4}\rho_{\mathrm{m}}\,|u_1|^2\,\omega\delta_{\mathrm{visc}}\,\mathrm{d}S + \frac{1}{4}\,(\gamma-1)\,\frac{|p_1|^2}{\rho_{\mathrm{m}}c^2}\omega\delta_{\mathrm{therm}}\,\mathrm{d}S\,, \tag{7.22}$$

where $u_1 = U_1/A$ is the velocity outside the boundary layer, parallel to the surface. Each term in this result expresses a dissipation as the product of a stored energy per unit volume $\rho_{\mathrm{m}}\,|u_1|^2\,/4$ or $(\gamma-1)\,|p_1|^2\,/4\rho_{\mathrm{m}}c^2$, a volume $\delta_{\mathrm{visc}}\,\mathrm{d}S$ or $\delta_{\mathrm{therm}}\,\mathrm{d}S$, and a rate ω.

7.5 Refrigeration

7.5.1 Standing-Wave Refrigeration

The thermal-hysteresis process described in Sect. 7.4 consumes acoustic power without doing anything thermodynamically useful. Standing-wave refrigeration consumes acoustic power via a similar process, but achieves a thermodynamic purpose: pumping heat up a temperature gradient, either to remove heat from a temperature below ambient or (less commonly) to deliver heat to a temperature above ambient. Figure 7.6a–c shows a standing-wave refrigerator of the style pioneered by *Hofler* [7.8, 9] and recently studied by *Tijani* [7.39]. At the left end, a driver such as a loudspeaker injects acoustic power $\dot{E}$, which flows rightward through the stack, causing a leftward flow of total energy $\dot{H}$.

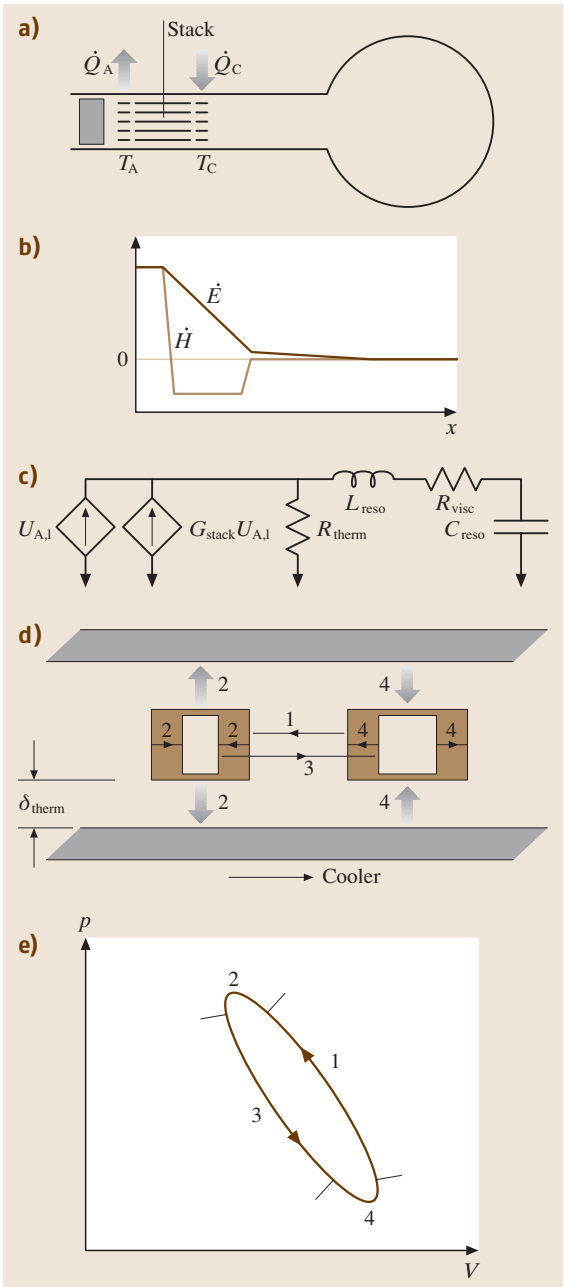
The most important process in a standing-wave refrigerator is illustrated in Fig. 7.6d and Fig. 7.6e from a Lagrangian perspective. Fig. 7.6d shows a greatly magnified view of a small mass of gas inside one pore of the stack. The sinusoidal thermodynamic cycle of that mass of gas in pressure p and volume V is shown in Fig. 7.6e; the mass's temperature, entropy, density, and other properties also vary sinusoidally in time. However, for qualitative understanding of the processes, we describe them as if they are a time series of four discrete steps, numbered 1–4 in Fig. 7.6d and Fig. 7.6e. In step 1, the gas is simultaneously compressed to a smaller volume and moved leftward by the wave. Thermal contact is imperfect in the pores of a stack, so during step 1 the gas experiences a nearly adiabatic temperature increase due to the pressure increase that causes the compression. It arrives at its new location warmer than the adjacent solid because the temperature gradient in the solid is less than the critical temperature gradient ∇T_{crit} defined in (7.20). Thus, in step 2, heat flows from the gas into the solid, cooling the gas and causing thermal contraction of the gas to a smaller volume. In step 3, the gas is simultaneously expanded to a larger volume and moved rightward by the wave. It arrives at its new location cooler than the adjacent solid, so in step 4 heat flows from the solid to the gas, warming the gas and causing thermal expansion of the gas to a larger volume. This brings it back to the start of the cycle, ready to repeat step 1.

The mass of gas shown in Fig. 7.6d has two time-averaged effects on its surroundings. First, the gas absorbs heat from the solid at the right extreme of its motion, at a relatively cool temperature, and delivers heat to the solid farther to the left at a higher temperature. In this way, all masses of gas within the stack pass heat along the solid, up the temperature gradient from right to left—within a single pore, the gas masses are like members of a bucket brigade passing water. This provides the desired refrigeration or heat-pumping effect. If the left heat exchanger is held at ambient temperature, as shown in Fig. 7.6a, then the system is a refrigerator, absorbing thermal power $\dot{Q}_{\mathrm{C}}$ from an external load at the right heat exchanger at one end of the bucket brigade at T_{C}, as waste thermal power is rejected to an external ambient heat sink at the other end of the bucket brigade at T_{A}. (The system functions as a heat pump if the right heat exchanger is held at ambient temperature; then the left heat exchanger is above ambient temperature.) Second, the gas's thermal expansion occurs at a lower pressure than its thermal contraction, so $\oint p\ \mathrm{d}V < 0$: the gas absorbs work from its surroundings. This work is responsible for the negative slope of $\dot{E}$ versus x in the stack in Fig. 7.6b and is represented by the gain element $G_{\mathrm{stack}}U_{\mathrm{A},1}$ in Fig. 7.6c. All masses of gas within the stack contribute

Amazon
EX1010 Page 267

to this consumption of acoustic power, which must be supplied by the driver.

As in the standing-wave engine, the time phasing between pressure and motion in the standing-wave refrigerator is close to that of a standing wave. Imperfect thermal contact between the gas and the solid in the stack is required to keep the gas rather isolated from the solid during the motion in steps 1 and 3 but still able to exchange significant heat with the solid during steps 2 and 4. This imperfect thermal contact occurs because the distance between the gas and the nearest solid surface is of the order of δ_{therm}, and it causes R_{therm} to be significant, so standing-wave refrigerators are inherently inefficient.



7.5.2 Traveling-Wave Refrigeration

Several varieties of traveling-wave refrigerator are commercially available or under development. At their core is a regenerator, in which the process shown in Fig. 7.7a,b operates. In step 1 of the process, the gas is compressed by rising pressure, rejecting heat to the nearby solid. In step 2, it is moved to the right, toward lower temperature, rejecting heat to the solid and experiencing thermal contraction as it moves. In step 3, the gas is expanded by falling pressure, and absorbs heat from the nearby solid. In step 4, the gas is moved leftward, toward higher temperature, absorbing heat from the solid and experiencing thermal expansion as it moves. The heat transfers between gas and solid in steps 2 and 4 are equal and opposite, so the net thermal effect of each mass of gas on the solid is due to steps 1 and 3, and is to move heat from right to left, up the temperature gradient. As before, the motion of any particular mass of gas is less than the length of the regenerator, so the heat is passed bucket-brigade fashion from the cold end of the regenerator to the ambient end. Each mass of gas absorbs $\oint p\, \mathrm{d}V$ of acoustic power from the wave as shown in Fig. 7.7b, because the thermal contraction in step 2 occurs at high pres-

Fig. 7.6a–e A standing-wave refrigerator. **(a)** From *left to right*, a piston, ambient heat exchanger, stack, cold heat exchanger, tube, and tank. Acoustic power is supplied to the gas by the piston to maintain the standing wave, and results in thermal power $\dot{Q}_C$ being absorbed by the gas from a load at cold temperature T_C while waste thermal power $\dot{Q}_A$ is rejected by the gas to an external heat sink at ambient temperature T_A. **(b)** Total power flow $\dot{H}$ and acoustic power $\dot{E}$ as functions of position x in the device. Positive power flows in the positive-x direction. **(c)** Lumped-element model of the device. **(d)** Close-up view of part of one pore in the stack of **(a)**, showing a small mass of gas going through one full cycle, imagined as four discrete steps. **(e)** Plot showing how the pressure p and volume V of that small mass of gas evolve with time in a counter-clockwise elliptical trajectory. *Tick marks* show approximate boundaries between the four steps of the cycle shown in **(d)**

Amazon
EX1010 Page 268

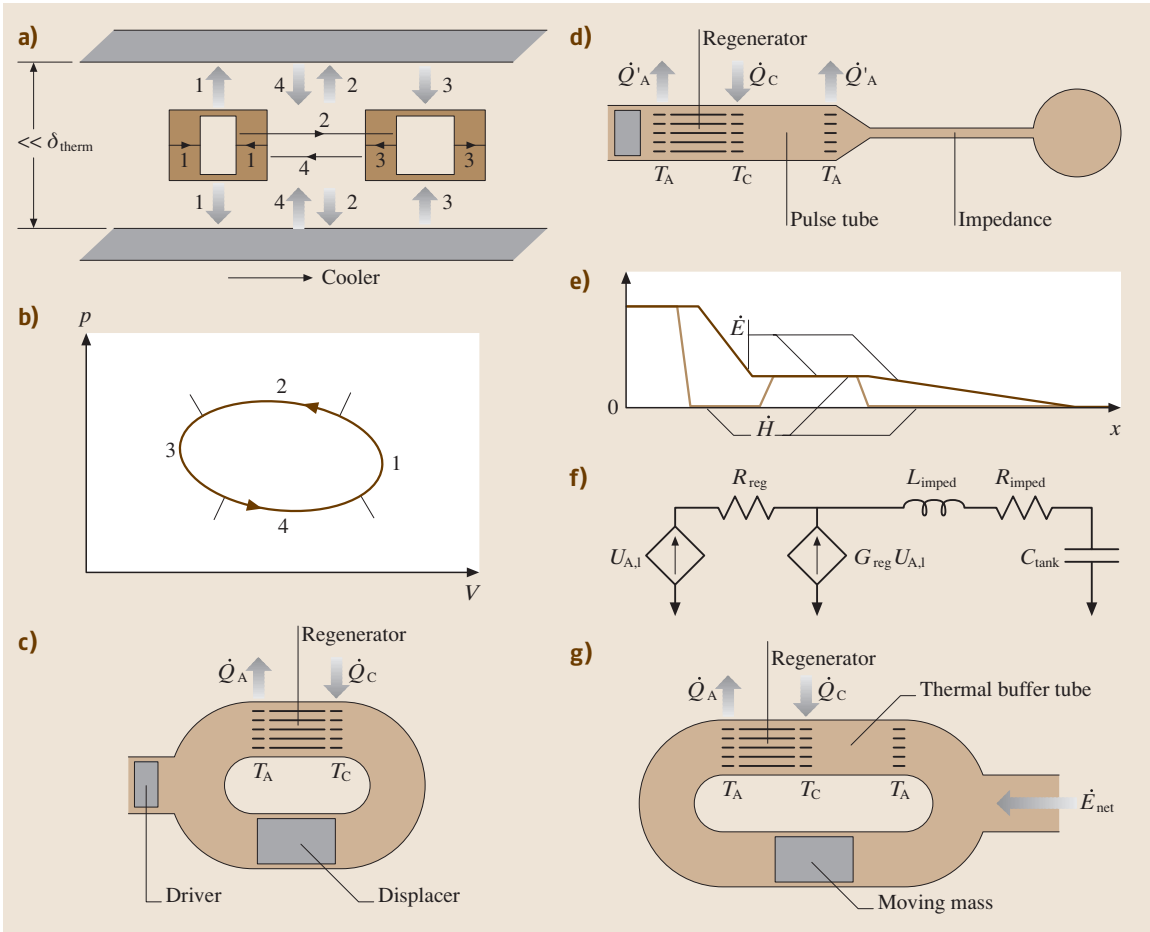


Fig. 7.7a–g Traveling-wave refrigerators. **(a)** Close-up view of part of one pore in the regenerator of a traveling-wave refrigerator, showing a small mass of gas going through one full cycle, imagined as four discrete steps. **(b)** Plot showing how the pressure p and volume V of that small mass of gas evolve with time in a counterclockwise elliptical trajectory. Tick marks show approximate boundaries between the four steps of the cycle shown in **(a)**. **(c)** A traditional Stirling refrigerator. From *left to right*, the ambient driver piston; the ambient heat exchanger, the regenerator, and the cold heat exchanger are across the top; the displacer is below. Time-averaged thermal power $\dot{Q}_C$ is removed by the gas from an external heat load at cold temperature T_C, while waste thermal power $\dot{Q}_A$ is rejected by the gas to an external heat sink at ambient temperature T_A and net acoustic power is supplied to the gas by the driver. **(d)** Pulse-tube refrigerator, with the same processes as **(c)** in the regenerator and its two adjacent heat exchangers, but with the displacer replaced by acoustic components. **(e)** Acoustic power $\dot{E}$ and total power $\dot{H}$ as functions of position x in the device shown in **(d)**. Positive power flows in the positive-x direction. **(f)** Lumped-element model of the pulse-tube refrigerator in **(d)**. **(g)** A refrigerator in which the thermal-buffer function and moving-mass function of **(c)**'s displacer are in two separate components

sure and the thermal expansion in step 4 occurs at low pressure. The small pore size, $r_h \ll \delta_{\text{therm}}$, maintains thermodynamically reversible heat transfer, so R_{therm} is negligible, and traveling-wave refrigerators have an inherently high efficiency. Acoustically, the process shown in Fig. 7.7a represents acoustic power traveling from left to right through the regenerator, and being partly consumed as it goes. Different varieties of traveling-wave refrigerator use different methods to create the necessary amplitudes and relative time phasing of motion and pressure to achieve this acoustic power flow through the regenerator.

Amazon
EX1010 Page 269

The traditional Stirling refrigerator [7.40] uses two moving pistons, which can be either crankshaft-coupled in a configuration like that of the engine in Fig. 7.3a or of the *free-displacer* variety shown in Fig. 7.7c. In the free-displacer Stirling refrigerator (often called *free piston*), the solid displacer moves in response to the gas-pressure forces on it, without linkage to any external motor. Its area and mass are selected to give its motion the desired amplitude and time phase [7.29]. Acoustic power is transmitted through it, from right to left, so that the acoustic power that flows out of the right end of the regenerator is fed through the displacer to the left, added to the acoustic power supplied by the driver, and injected into the left end of the regenerator. The displacer must be a thermal insulator, because its right end is at T_C and its left end at T_A. Crankshaft-coupled Stirling refrigerators were used in the 19th century to keep beef cold on the long sea voyage from South America to Britain. Free-piston Stirling cryocoolers are in common use today for cooling infrared sensors in military night-vision goggles and surveillance satellites, and a free-piston Stirling refrigerator built into a small, portable *ice chest* is commercially available at low cost for picnics [7.41].

The pulse-tube refrigerator [7.12], illustrated in Fig. 7.7d–f, uses only one piston. The acoustic power flowing out of the right end of the regenerator is absorbed in an acoustic impedance, instead of being fed back to the left end of the regenerator. This gives the pulse-tube refrigerator a lower efficiency than the Stirling refrigerator, but for cryogenic applications the reduced efficiency is a small price to pay for the elimination of the Stirling's cold moving part. The lumped-element model of the impedance and adjacent tank shown in Fig. 7.7f correctly suggests that proper design of L_{imped}, R_{imped}, and C_{tank} can create almost any desired ratio of $|U_1|$ to $|p_1|$ and time phasing between U_1 and p_1 at the right end of the regenerator. The desired impedance is often achieved by choosing $R_{\text{visc}} \sim \omega L_{\text{imped}} \gg 1/\omega C_{\text{imped}}$. The so-called pulse tube, and the ambient heat exchanger to its right, thermally isolate the cold heat exchanger from the dissipation of acoustic power in the impedance, just as the thermal buffer tube performs that function in Fig. 7.3c. Pulse-tube refrigerators are in common use today in satellites [7.42] and are under development for many other applications such as small-scale oxygen liquefaction and cooling superconducting equipment.

Another variation of the theme is shown in Fig. 7.7g, where the thermal buffer tube and the moving mass perform the thermal-insulation and inertial functions of the free displacer of Fig. 7.7c in two separate locations [7.43,44]. This variety is under development for commercial food refrigeration [7.45]. Yet another variety [7.46] replaces the inertial moving mass of Fig. 7.7g with inertial moving gas, similar to the thermoacoustic–Stirling hybrid engine of Fig. 7.3c.

7.6 Mixture Separation

In thermoacoustic mixture separation, acoustic power causes the components of a gas mixture to separate [7.47, 48]. The process is loosely analogous to the pumping of heat through the stack in a standing-wave refrigerator. The expenditure of acoustic power results in an increase in the Gibbs free energy of the mixture's components, and the efficiency of the process is comparable to that of some other practical separation processes [7.49].

Figure 7.8 illustrates the process for a binary gas mixture of heavy and light molecules, whose motions are indicated by filled and open arrows, respectively. The motion of the molecules in steps 1 and 3 of the process is bulk motion of the gas, and the motion during steps 2 and 4 is thermal diffusion, in which light molecules diffuse toward higher temperature and heavy molecules diffuse toward lower temperature. In step 1, the gas in the center of the pore moves leftward and its pressure rises, so its temperature rises nearly adiabatically. Trapped by the viscous boundary layer near the wall of the tube is some other gas that does not move and whose thermal contact with the pore wall keeps its temperature from rising. During step 2, the temperature difference between the central gas and the peripheral gas causes light atoms to diffuse into the center and heavy atoms to diffuse out of the center, enriching the center in light atoms. Bulk motion rightward in step 3 carries this central light-enriched gas to the right. Simultaneously, the pressure drops in step 3, and hence the central temperature drops nearly adiabatically. Thus thermal diffusion in step 4 pulls heavy molecules into the center and drives light molecules out of the center, leaving the center enriched in heavy molecules so that the leftward motion during step 1 carries heavy-enriched gas leftward. The net effect of steps 1 and 3 is to move heavy molecules leftward and light molecules rightward. The process

Amazon
EX1010 Page 270

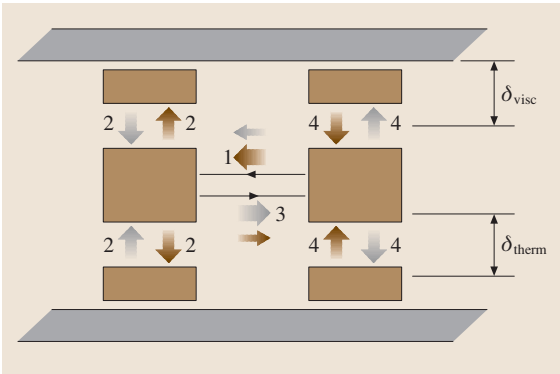


Fig. 7.8 Close-up view of part of one pore in a thermoacoustic mixture separator, showing a small body of gas in the center of the pore going through one full cycle, imagined as four discrete steps, and exchanging mass with neighboring, immobile gas. The *gray* and *brown arrows* in steps 2 and 4 signify thermally driven diffusion of light and heavy molecules between the central gas and the peripheral gas close to the wall of the pore. In steps 1 and 3, the *gray* and *brown arrows* signify bulk motion of the gas, without diffusion

takes place when the mole-fraction gradient is less than a critical gradient, analogous to the critical temperature gradient below which standing-wave refrigeration occurs.

As is evident from Fig. 7.8, the process works best for tubes with r_h somewhat larger than δ_{therm} and δ_{visc}. However, unlike the description above, the process actually works best near traveling-wave phasing, because two 45° phase shifts were ignored in that description. High separation purities require long tubes, and high mole fluxes will require many passages in parallel, perhaps in structures similar to the stacks of standing-wave engines and refrigerators.

In a 2 m-long tube, a 50–50 helium–argon mixture has been separated to yield 70% helium, 30% argon at one end and 30% helium, 70% argon at the other end; and a measurable enrichment of ^{22}Ne from natural neon has been achieved [7.50].

References

7.1 G.W. Swift: *Thermoacoustics: A Unifying Perspective for some Engines and Refrigerators* (Acoustical Society of America Publications, Sewickley PA 2002)

7.2 S.L. Garrett: Resource letter TA-1, Thermoacoustic engines and refrigerators, Am. J. Phys. **72**, 11–17 (2004)

7.3 N. Rott: Damped and thermally driven acoustic oscillations in wide and narrow tubes, Z. Angew. Math. Phys. **20**, 230–243 (1969)

7.4 N. Rott: Thermally driven acoustic oscillations, Part III: Second-order heat flux, Z. Angew. Math. Phys. **26**, 43–49 (1975)

7.5 T. Yazaki, A. Tominaga, Y. Narahara: Experiments on thermally driven acoustic oscillations of gaseous helium, J. Low Temp. Phys. **41**, 45–60 (1980)

7.6 J.W. Strutt (Baron Rayleigh): The explanation of certain acoustical phenomena, Nature **18**, 319–321 (1878)

7.7 K.T. Feldman: Review of the literature on Sondhauss thermoacoustic phenomena, J. Sound Vibrat. **7**, 71–82 (1968)

7.8 T. Hofler, J.C. Wheatley, G.W. Swift, A. Migliori: Acoustic cooling engine, US Patent No. 4,722,201. (1988)

7.9 T.J. Hofler: *Thermoacoustic refrigerator design and performance. Ph.D. thesis, Physics Department* (University of California, San Diego 1986)

7.10 W.E. Gifford, R.C. Longsworth: Pulse tube refrigeration progress, Adv. Cryogenic Eng. B **10**, 69–79 (1965)

7.11 E.L. Mikulin, A.A. Tarasov, M.P. Shkrebyonock: Low-temperature expansion pulse tubes, Adv. Cryogenic Eng. **29**, 629–637 (1984)

7.12 R. Radebaugh: *Development of the pulse tube refrigerator as an efficient and reliable cryocooler* (Proc. Inst. Refrigeration, London 2000) pp. 11–29

7.13 G. Walker: *Stirling Engines* (Clarendon, Oxford 1960)

7.14 P.H. Ceperley: A pistonless Stirling engine – The traveling wave heat engine, J. Acoust. Soc. Am. **66**, 1508–1513 (1979)

7.15 P.H. Ceperley: Gain and efficiency of a short traveling wave heat engine, J. Acoust. Soc. Am. **77**, 1239–1244 (1985)

7.16 T. Yazaki, A. Iwata, T. Maekawa, A. Tominaga: Traveling wave thermoacoustic engine in a looped tube, Phys. Rev. Lett. **81**, 3128–3131 (1998)

7.17 C.M. de Blok: Thermoacoustic system, 1998. Dutch Patent: International Application Number PCT/NL98/00515. US Patent 6,314,740, November 13 (2001)

7.18 S. Backhaus, G.W. Swift: A thermoacoustic-Stirling heat engine, Nature **399**, 335–338 (1999)

7.19 D. Gedeon: *A globally implicit Stirling cycle simulation, Proceedings of the 21st Intersociety Energy Conversion Engineering Conference* (Am. Chem. Soc.,

Amazon
EX1010 Page 271

Washington 1986) pp. 550–554, Software available from Gedeon Associates, Athens, Ohio
7.20 W.C. Ward, G.W. Swift: Design environment for low amplitude thermoacoustic engines (DeltaE), J. Acoust. Soc. Am. **95**, 3671–3672 (1994), Software and user's guide available either from the Los Alamos thermoacoustics web site www.lanl.gov/thermoacoustics/ or from the Energy Science and Technology Software Center, US Department of Energy, Oak Ridge, Tennessee
7.21 R.E. Sonntag, C. Borgnakke, G.J. Van Wylen: *Fundamentals of Thermodynamics* (Wiley, New York 2003)
7.22 F.W. Giacobbe: Estimation of Prandtl numbers in binary mixtures of helium and other noble gases, J. Acoust. Soc. Am. **96**, 3568–3580 (1994)
7.23 A. Bejan: *Advanced Engineering Thermodynamics*, 2nd edn. (Wiley, New York 1997)
7.24 Acoustic Laser Kit, Graduate Program in Acoustics, P. O. Box 30, State College, PA 16804-0030 (www.acs.psu.edu/thermoacoustics/refrigeration/laserdemo.htm)
7.25 G.W. Swift, J.J. Wollan: Thermoacoustics for liquefaction of natural gas, GasTIPS **8**(4), 21–26 (2002), Also available at www.lanl.gov/thermoacoustics/Pubs/GasTIPS.pdf
7.26 D.L. Gardner, G.W. Swift: A cascade thermoacoustic engine, J. Acoust. Soc. Am. **114**, 1905–1919 (2003)
7.27 R.S. Wakeland, R.M. Keolian: Thermoacoustics with idealized heat exchangers and no stack, J. Acoust. Soc. Am. **111**, 2654–2664 (2002)
7.28 K.T. Feldman: Review of the literature on Rijke thermoacoustic phenomena, J. Sound Vibrat. **7**, 83–89 (1968)
7.29 I. Urieli, D.M. Berchowitz: *Stirling Cycle Engine Analysis* (Adam Hilger, Bristol 1984)
7.30 A.J. Organ: *Thermodynamics and Gas Dynamics of the Stirling Cycle Machine* (Cambridge Univ. Press, Cambridge 1992)
7.31 H. Nilsson, C. Bratt: Test results from a 15 kW air-independent Stirling power generator. In: *Proc. 6th International Symposium on Unmanned Untethered Submersible Technology* (IEEE, 1989) pp. 123–128
7.32 WhisperGen Limited, Christchurch, New Zealand
7.33 S. Qiu, D.L. Redinger, J.E. Augenblick: The next generation infinia free-piston Stirling engine for micro-CHP applications. In: *Proc. 12th International Stirling Engine Conference* (Durham University, 2005) pp. 156–165
7.34 M.A. White: A new paradigm for high-power Stirling applications, Proc. Space Nuclear Conference, Stirling Technology Company, Kennewick WA (2005)
7.35 B. Arman, J. Wollan, V. Kotsubo, S. Backhaus, G. Swift: Operation of thermoacoustic Stirling heat engine driven large multiple pulse tube refrigerators. In: *Cryocoolers 13*, ed. by R.G. Ross (Springer, Berlin, New York 2005) pp. 181–188
7.36 S. Backhaus, E. Tward, M. Petach: Traveling-wave thermoacoustic electric generator, Appl. Phys. Lett. **85**, 1085–1087 (2004)
7.37 B. Zinn: Pulsating combustion. In: *Advanced Combustion Methods*, ed. by F.J. Weinberg (Academic, London 1986) pp. 113–181
7.38 F.E.C. Culick: Combustion instabilities and Rayleigh's criterion. In: *Modern Research Topics in Aerospace Propulsion*, ed. by C. Casci, G. Angelino, L. DeLuca, W.A. Sirignano (Springer, Berlin, New York 1991) pp. 508–517, (in honor of Corrado Casci)
7.39 M.E.H. Tijani, J.C.H. Zeegers, A.T.A.M. deWaele: The optimal stack spacing for thermoacoustic refrigeration, J. Acoust. Soc. Am. **112**, 128–133 (2002)
7.40 G. Walker: *Cryocoolers* (Plenum, New York 1983)
7.41 N.W. Lane: Commercialization status of free-piston Stirling machines. In: *Proc. 12th International Stirling Engine Conference* (Durham University, 2005) pp. 30–37
7.42 E. Tward, C.K. Chan, C. Jaco, J. Godden, J. Chapsky, P. Clancy: Miniature space pulse tube cryocoolers, Cryogenics **39**, 717–720 (1999)
7.43 R.W.M. Smith, M.E. Poese, S.L. Garrett, R.S. Wakeland: Thermoacoustic device, US Patent No. 6,725,670.(2004)
7.44 M. E. Poese, R. W. M. Smith, R. S. Wakeland, S. L. Garrett: Bellows bounce thermoacoustic device, US Patent No. 6,792,764.(2004)
7.45 S.L. Garret: Pennsylvania State University, private communication
7.46 G.W. Swift, D.L. Gardner, S. Backhaus: Acoustic recovery of lost power in pulse tube refrigerators, J. Acoust. Soc. Am. **105**, 711–724 (1999)
7.47 D.A. Geller, G.W. Swift: Saturation of thermoacoustic mixture separation, J. Acoust. Soc. Am. **111**, 1675–1684 (2002)
7.48 P.S. Spoor, G.W. Swift: Thermoacoustic separation of a He-Ar mixture, Phys. Rev. Lett. **85**, 1646–1649 (2000)
7.49 D.A. Geller, G.W. Swift: Thermodynamic efficiency of thermoacoustic mixture separation, J. Acoust. Soc. Am. **112**, 504–510 (2002)
7.50 D.A. Geller, G.W. Swift: Thermoacoustic enrichment of the isotopes of neon, J. Acoust. Soc. Am. **115**, 2059–2070 (2004),

Amazon
EX1010 Page 272

8. Nonlinear Acoustics in Fluids

At high sound intensities or long propagation distances at sufficiently low damping acoustic phenomena become nonlinear. This chapter focuses on nonlinear acoustic wave properties in gases and liquids. The origin of nonlinearity, equations of state, simple nonlinear waves, nonlinear acoustic wave equations, shock-wave formation, and interaction of waves are presented and discussed. Tables are given for the nonlinearity parameter *B/A* for water and a range of organic liquids, liquid metals and gases. Acoustic cavitation with its nonlinear bubble oscillations, pattern formation and sonoluminescence (light from sound) are modern examples of nonlinear acoustics. The language of nonlinear dynamics needed for understanding chaotic dynamics and acoustic chaotic systems is introduced.

8.1 **Origin of Nonlinearity** 258
8.2 **Equation of State** 259
8.3 **The Nonlinearity Parameter** *B/A* 260
8.4 **The Coefficient of Nonlinearity** β 262
8.5 **Simple Nonlinear Waves** 263
8.6 **Lossless Finite-Amplitude Acoustic Waves** 264
8.7 **Thermoviscous Finite-Amplitude Acoustic Waves** 268
8.8 **Shock Waves** 271
8.9 **Interaction of Nonlinear Waves** 273
8.10 **Bubbly Liquids** 275
8.10.1 Incompressible Liquids 276
8.10.2 Compressible Liquids 278
8.10.3 Low-Frequency Waves: The Korteweg–de Vries Equation 279
8.10.4 Envelopes of Wave Trains: The Nonlinear Schrödinger Equation 282
8.10.5 Interaction of Nonlinear Waves. Sound–Ultrasound Interaction 284
8.11 **Sonoluminescence** 286
8.12 **Acoustic Chaos** 289
8.12.1 Methods of Chaos Physics 289
8.12.2 Chaotic Sound Waves 291
References 293

Acoustics belongs to those areas of physics, where nonlinear phenomena were observed first [8.1–4]. All musical instruments including the human voice belong to nonlinear acoustics as they produce sound waves and these, moreover, are not simple sinusoidal waves. Generation processes are necessarily nonlinear as new phenomena appear that are not proportional to already existing ones. Propagation, on the other hand, is normally linear for propagation distances that are not too long and only starts to show nonlinear effects at high intensities. As mankind started to speak early in its history and also is supposed to have made music early on, nonlinear acoustics belongs to the oldest parts of science. Sorge in 1745 and Tartini in 1754 report that, when two tones of frequency f_1 and $f_2 > f_1$ are presented to the ear at high intensities, the difference frequency $f_2 - f_1$ is additionally heard. For a long time there was a debate of whether these tones were generated in the ear or were already present in the propagating medium. Today we know that in this case the ear generates the difference frequency. But we also know that a difference frequency can be generated in a nonlinear medium during the propagation of a sound wave [8.5]. This fact is used in the parametric acoustic array to transmit and receive highly directed low-frequency sound beams. Under suitable circumstances generally a series of combination frequencies $f_{mn} = m f_1 + n f_2$ with $m, n = 0, \pm 1, \pm 2, \ldots$ can be generated.

A special case is a single harmonic wave of frequency f propagating in a nonlinear medium. It generates the higher harmonics $f_m = m f$. This leads to a steepening of the wave and often to the formation of shock waves. Further nonlinear effects are subsumed under the heading of self-action, as changes in the medium are produced by the sound wave that act back on the wave. Examples are self-focusing and self-transparency.

Amazon
EX1010 Page 273

Also forces may be transmitted to the medium setting it into motion, as exemplified by the phenomenon of acoustic streaming. Acoustic radiation forces may be used to levitate objects and keep them in traps. In other areas of science this is accomplished by electrical or electromagnetical forces (ion traps, optical tweezers). Nonlinear acoustics is the subject of many books, congress proceedings and survey articles [8.1–4, 6–19].

In liquids a special phenomenon occurs, the rupture of the medium by sound waves, called acoustic cavitation [8.20–27]. This gives rise to a plethora of special effects bringing acoustics in contact with almost any other of the natural sciences. Via the dynamics of the cavities, or the cavitation bubbles produced, dirt can be removed from surfaces (ultrasonic cleaning), light emission may occur upon bubble collapse (sonoluminescence [8.28]) and chemical reactions are initiated (sonochemistry [8.29, 30]).

Recently, the general theory of nonlinear dynamics lead to the interesting finding that nonlinear dynamical systems may not just show this simple scenario of combination tones and self-actions, but complicated dynamics resembling stochastic behavior. This is known as deterministic chaos or, in the context of acoustics, *acoustic chaos* [8.31, 32].

Nonlinear acoustics also appears in wave propagation in solids. In this case, further, entirely different, nonlinear phenomena appear, because not only longitudinal but also transverse waves are supported. A separate chapter of this Handbook is devoted to this topic.

8.1 Origin of Nonlinearity

All acoustic phenomena necessarily become nonlinear at high intensities. This can be demonstrated when looking at the propagation of a harmonic sound wave in air. In Fig. 8.1 a harmonic sound wave is represented graphically. In the upper diagram the sound pressure p is plotted versus location x. The static pressure p_{stat} serves as a reference line around which the sound pressure oscillates. This pressure p_{stat} is normally about 1 bar. In the lower diagram the density distribution is given schematically in a grey scale from black to white for the pressure range of the sound wave.

Assuming that the sound pressure amplitude is increased steadily, a point is reached where the sound pressure amplitude attains p_{stat} giving a pressure of zero in the sound pressure minimum. It is impossible to go below this point as there cannot be less than zero air molecules in the minimum. However, air can be compressed above the pressure p_{stat} just by increasing the force. Therefore, beyond a sound pressure amplitude $p = p_{\mathrm{stat}}$ no harmonic wave can exist in a gas; it must become nonlinear and contain harmonics. The obvious reason for the nonlinearity in this case (a gas)

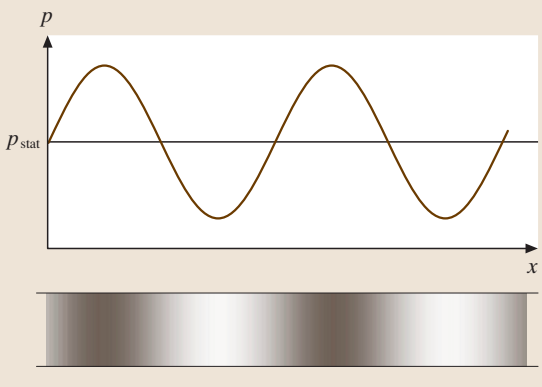


Fig. 8.1 Graphical representation of a harmonic sound wave

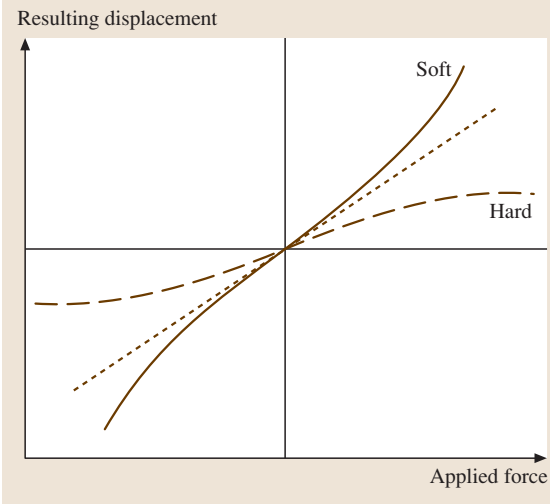


Fig. 8.2 Symmetric nonlinear expansion and compression laws compared to a linear law (*straight dotted line*) with soft spring behavior (*solid line*) and hard spring behavior (*dashed line*)

Amazon
EX1010 Page 274

is the asymmetry in density between compression and expansion.

However, symmetric expansion and compression also lead to nonlinear effects when they are not proportional to an applied force or stress. Figure 8.2 shows two types of symmetric nonlinearities: hard and soft spring behavior upon expansion and compression with reference to a linear law represented by a straight (dotted) line. An example of hard spring behavior is a string on a violin, because the average string tension increases with increasing wave amplitude. It is intrinsically symmetric, as positive and negative elongation are equivalent. An example of soft spring behavior is the pendulum, also having a symmetric force–displacement law in a homogeneous gravitational field. An example of an asymmetric mixed type, but with overall soft spring behavior, is a bubble in water oscillating in a sound field. Upon compression a bubble shows hard spring behavior, upon expansion soft spring behavior in such a way that soft spring behavior dominates.

Acoustic waves also show nonlinear behavior in propagation, even without any nonlinearity of the medium. This is due to the cumulative effect of distortion of the wave profile by convection, introduced by the particle velocity that itself constitutes the sound wave. Larger particle velocities propagate faster than slower ones, leading to distortion of an acoustic wave upon propagation. This property can be considered an intrinsic self-action of the wave, leading to an intrinsic nonlinearity in acoustics. This aspect of nonlinearity is discussed below in the context of the coefficient of nonlinearity β.

8.2 Equation of State

The compression and expansion of a medium is described by the equation of state, for which an interrelation between three quantities is needed, usually the pressure p, density ϱ and specific entropy s (entropy per unit mass). Often the variation of entropy can be neglected in acoustic phenomena and the calculations can be carried out at constant entropy; the equations are then called isentropic. A basic quantity in acoustics, the velocity of sound or sound speed c of a medium, is related to these quantities:

$$c^2 = \left(\frac{\partial p}{\partial \varrho}\right)_s \,. \tag{8.1}$$

The subscript index s indicates that the entropy is to be held constant to give the isentropic velocity of sound.

Even an ideal gas is nonlinear, because it obeys the isentropic equation of state

$$p = p_0 \left(\frac{\varrho}{\varrho_0}\right)^{\gamma} \,, \tag{8.2}$$

where p_0 and ϱ_0 are the reference (ambient) pressure and density, respectively, and

$$\gamma = \frac{c_\mathrm{p}}{c_\mathrm{v}} \,, \tag{8.3}$$

where γ is the quotient of the specific heat c_p at constant pressure and c_v that at constant volume.

An empirical formula, the Tait equation, is often used for liquids, obviously constructed similarly to the equation of state of the ideal gas:

$$p = P \left(\frac{\varrho}{\varrho_0}\right)^{\gamma_\mathrm{L}} - Q \tag{8.4}$$

or

$$\frac{p+Q}{p_\infty+Q} = \left(\frac{\varrho}{\varrho_0}\right)^{\gamma_\mathrm{L}} \,. \tag{8.5}$$

The two quantities Q and γ_L have to be fitted to the experimental pressure–density curve. For water $\gamma_\mathrm{L} = 7$, $P = p_\infty + Q = 3001$ bar and $Q = 3000$ bar are used. (Note that γ_L in the Tait equation is not the quotient of the specific heats.)

There is another way of writing the equation of state where the pressure is developed as a Taylor series as a function of density and entropy [8.17]. In the isentropic case it reads [8.33–35]

$$p - p_0 = \left(\frac{\partial p}{\partial \varrho}\right)_{s,\varrho=\varrho_0} (\varrho - \varrho_0) + \frac{1}{2}\left(\frac{\partial^2 p}{\partial \varrho^2}\right)_{s,\varrho=\varrho_0} (\varrho - \varrho_0)^2 + \ldots \tag{8.6}$$

or

$$p - p_0 = A\frac{\varrho - \varrho_0}{\varrho_0} + \frac{B}{2}\left(\frac{\varrho - \varrho_0}{\varrho_0}\right)^2 + \frac{C}{6}\left(\frac{\varrho - \varrho_0}{\varrho_0}\right)^3 + \ldots \tag{8.7}$$

Amazon
EX1010 Page 275

with

$$A = \varrho_0 \left(\frac{\partial p}{\partial \varrho}\right)_{s,\varrho=\varrho_0} = \varrho_0 c_0^2 \ , \tag{8.8}$$

$$B = \varrho_0^2 \left(\frac{\partial^2 p}{\partial \varrho^2}\right)_{s,\varrho=\varrho_0} \ , \tag{8.9}$$

$$C = \varrho_0^3 \left(\frac{\partial^3 p}{\partial \varrho^3}\right)_{s,\varrho=\varrho_0} \ . \tag{8.10}$$

Here, c_0 is the velocity of sound under the reference conditions. The higher-order terms of the Taylor series can normally be neglected.

8.3 The Nonlinearity Parameter *B/A*

To characterize the strength of the nonlinearity of a medium properly the relation of B to the linear coefficient A is important [8.43, 44]. Therefore A and B are combined as B/A, the *nonlinearity parameter*, a pure number.

Table 8.1 B/A values for pure water at atmospheric pressure

T(°C)	B/A	Year	Ref.
0	4.2	1974	[8.36]
20	5	1974	[8.36]
20	4.985 ± 0.063	1989	[8.37]
25	5.11 ± 0.20	1983	[8.38]
26	5.1	1989	[8.39]
30	5.31	1985	[8.40]
30	5.18 ± 0.033	1991	[8.41]
30	5.280 ± 0.021	1989	[8.37]
30	5.38 ± 0.12	2001	[8.42]
40	5.4	1974	[8.36]
40	5.54 ± 0.12	2001	[8.42]
50	5.69 ± 0.13	2001	[8.42]
60	5.7	1974	[8.36]
60	5.82 ± 0.13	2001	[8.42]
70	5.98 ± 0.13	2001	[8.42]
80	6.1	1974	[8.36]
80	6.06 ± 0.13	2001	[8.42]
100	6.1	1974	[8.36]

It is easy to show that for an ideal gas we get from (8.2) together with (8.8) and (8.9)

$$\frac{B}{A} = \gamma - 1 \ , \tag{8.11}$$

so that $B/A = 0.67$ for a monatomic gas (for example noble gases) and $B/A = 0.40$ for a diatomic gas (for example air). Moreover, it can be shown that

$$\frac{C}{A} = (\gamma - 1)(\gamma - 2) \tag{8.12}$$

for an ideal gas, leading to negative values.

When there is no analytic expression for the equation of state recourse must be made to the direct definitions of A and B and appropriate measurements. From the expressions for A (8.8) and B (8.9) a formula for the nonlinearity parameter B/A is readily found:

$$\frac{B}{A} = \frac{\varrho_0}{c_0^2} \left(\frac{\partial^2 p}{\partial \varrho^2}\right)_{s,\varrho=\varrho_0} \ . \tag{8.13}$$

To determine B/A from this formula, as well as the density and sound velocity the variation in pressure effected by an isentropic (adiabatic) variation in density has to be measured. Due to the small density variations with pressure in liquids and the error-increasing second derivative this approach is not feasible.

Fortunately, equivalent expressions for B/A have been found in terms of more easily measurable

Table 8.2 Pressure and temperature dependence of the B/A values for water [8.42]

T(K) / P(MPa)	303.15	313.15	323.15	333.15	343.15	353.15	363.15	373.15
0.1	5.38 ± 0.12	5.54 ± 0.12	5.69 ± 0.13	5.82 ± 0.13	5.98 ± 0.13	6.06 ± 0.13	–	–
5	5.46 ± 0.12	5.59 ± 0.12	5.76 ± 0.13	5.87 ± 0.13	6.04 ± 0.13	6.07 ± 0.13	6.03 ± 0.13	6.05 ± 0.13
10	5.55 ± 0.12	5.62 ± 0.12	5.78 ± 0.13	5.94 ± 0.13	6.03 ± 0.13	6.11 ± 0.13	6.06 ± 0.13	6.01 ± 0.13
15	5.57 ± 0.12	5.66 ± 0.12	5.83 ± 0.13	5.96 ± 0.13	6.07 ± 0.13	6.09 ± 0.13	6.11 ± 0.13	6.08 ± 0.13
20	5.61 ± 0.12	5.68 ± 0.13	5.81 ± 0.13	5.98 ± 0.13	6.10 ± 0.13	6.14 ± 0.14	6.12 ± 0.13	6.06 ± 0.13
30	5.63 ± 0.12	5.70 ± 0.13	5.84 ± 0.13	5.95 ± 0.13	6.07 ± 0.13	6.16 ± 0.14	6.09 ± 0.13	6.08 ± 0.13
40	5.73 ± 0.13	5.77 ± 0.13	5.86 ± 0.13	6.02 ± 0.13	6.11 ± 0.13	6.14 ± 0.14	6.16 ± 0.14	6.14 ± 0.14
50	5.82 ± 0.13	5.84 ± 0.13	5.93 ± 0.13	6.04 ± 0.13	6.13 ± 0.13	6.16 ± 0.14	6.12 ± 0.13	6.09 ± 0.13

Amazon
EX1010 Page 276

Table 8.3 B/A values for organic liquids at atmospheric pressure

Substance	T(°C)	B/A	Ref.
1,2-DHCP	30	11.8	[8.36]
1-Propanol	20	9.5	[8.45]
1-Butanol	20	9.8	[8.45]
1-Pentanol	20	10	[8.45]
1-Pentanol	20	10	[8.45]
1-Hexanol	20	10.2	[8.45]
1-Heptanol	20	10.6	[8.45]
1-Octanol	20	10.7	[8.45]
1-Nonanol	20	10.8	[8.45]
1-Decanol	20	10.7	[8.45]
Acetone	20	9.23	[8.46]
	20	8.0	[8.45]
	40	9.51	[8.46]
Benzene	20	9	[8.36]
	20	8.4	[8.47]
	25	6.5	[8.48]
	40	8.5	[8.48]
Benzyl alcohol	30	10.19	[8.46]
	50	9.97	[8.46]
Carbon bisulfide	10	6.4	[8.48]
	25	6.2	[8.48]
	40	6.1	[8.48]
Carbon tetrachloride	10	8.1	[8.48]
	25	8.7	[8.48]
	25	7.85 ± 0.31	[8.38]
	40	9.3	[8.48]
Chlorobenzene	30	9.33	[8.46]
Chloroform	25	8.2	[8.48]
Cyclohexane	30	10.1	[8.36]
Diethylamine	30	10.3	[8.46]
Ethanol	0	10.42	[8.46]
	20	10.52	[8.46]
	20	9.3	[8.45]
	40	10.6	[8.46]
Ethylene glycol	25	9.88 ± 0.4	[8.38]
	26	9.6	[8.39]
	30	9.7	[8.36]
	30	9.93	[8.40]
	30	9.88 ± 0.035	[8.41]
Ethyl formate	30	9.8	[8.36]
Heptane	30	10	[8.36]
	40	10.05	[8.49]
Hexane	25	9.81 ± 0.39	[8.38]
	30	9.9	[8.36]
	40	10.39	[8.49]

Table 8.3 (cont.)

Substance	T(°C)	B/A	Ref.
Methanol	20	8.6	[8.45]
	20	9.42	[8.46]
	30	9.64	[8.46]
Methyl acetate	30	9.7	[8.36]
Methyl iodide	30	8.2	[8.36]
Nitrobenzene	30	9.9	[8.36]
n-Butanol	0	10.71	[8.46]
	20	10.69	[8.46]
	40	10.75	[8.46]
n-Propanol	0	10.47	[8.46]
	20	10.69	[8.46]
	40	10.73	[8.46]
Octane	40	9.75	[8.49]
Pentane	30	9.87	[8.49]
Toluene	20	5.6	[8.48]
	25	7.9	[8.48]
	30	8.929	[8.50]

Table 8.4 B/A values for liquid metals and gases at atmospheric pressure

Substance	T(°C)	B/A	Ref.
Liquid metals			
Bismuth	318	7.1	[8.36]
Indium	160	4.6	[8.36]
Mercury	30	7.8	[8.36]
Potassium	100	2.9	[8.36]
Sodium	110	2.7	[8.36]
Tin	240	4.4	[8.36]
Liquid gases			
Argon	-187.15	5.01	[8.51]
	-183.15	5.67	[8.51]
Helium	-271.38	4.5	[8.52]
Hydrogen	-259.15	5.59	[8.51]
	-257.15	6.87	[8.51]
	-255.15	7.64	[8.51]
	-253.15	7.79	[8.51]
Methane	-163.15	17.95	[8.51]
	-153.15	10.31	[8.51]
	-143.15	6.54	[8.51]
	-138.15	5.41	[8.51]
Nitrogen	-203.15	7.7	[8.51]
	-195.76	6.6	[8.52]
	-193.15	8.03	[8.51]
	-183.15	9.00	[8.51]
Other substances			
Sea water (3.5% NaCl)	20	5.25	[8.36]
Sulfur	121	9.5	[8.36]

Amazon
EX1010 Page 277

quantities, namely the variation of sound velocity with pressure and temperature. Introducing the definition of the sound velocity the following formulation chain holds: $(\partial^2 p/\partial \varrho^2)_{s,\varrho=\varrho_0} = (\partial c^2/\partial \varrho)_{s,\varrho=\varrho_0} = 2c_0(\partial c/\partial \varrho)_{s,\varrho=\varrho_0} = 2c_0(\partial c/\partial p)_{s,p=p_0}(\partial p/\partial \varrho)_{s,\varrho=\varrho_0} = 2c_0^3(\partial c/\partial p)_{s,p=p_0}$. Insertion of this result into (8.9) yields

$$B = \varrho_0^2 \left(\frac{\partial^2 p}{\partial \varrho^2}\right)_{s,\varrho=\varrho_0} = 2\varrho_0^2 c_0^3 \left(\frac{\partial c}{\partial p}\right)_{s,p=p_0} \quad (8.14)$$

and into (8.13) results in

$$\frac{B}{A} = 2\varrho_0 c_0 \left(\frac{\partial c}{\partial p}\right)_{s,p=p_0} . \quad (8.15)$$

Here B/A is essentially given by the variation of sound velocity c with pressure p at constant entropy s. This quantity can be measured with sound waves when the pressure is varied sufficiently rapidly but still smoothly (no shocks) to maintain isentropic conditions.

Equation (8.15) can be transformed further [8.44,53] using standard thermodynamic manipulations and definitions. Starting from $c = c(p, t, s = \text{const.})$ it follows that $\mathrm{d}c = (\partial c/\partial p)_{T,p=p_0}\mathrm{d}p + (\partial c/\partial p)_{p,T=T_0}\mathrm{d}T$ or

$$\left(\frac{\partial c}{\partial p}\right)_{s,p=p_0} = \left(\frac{\partial c}{\partial p}\right)_{T,p=p_0} + \left(\frac{\partial c}{\partial T}\right)_{p,T=T_0}\left(\frac{\partial T}{\partial p}\right)_{s,p=p_0} . \quad (8.16)$$

From the general thermodynamic relation $T\mathrm{d}s = c_\mathrm{p}\mathrm{d}T - (\alpha_T/\varrho)T\mathrm{d}p = 0$ for the isentropic case the relation

$$\left(\frac{\partial T}{\partial p}\right)_{s,p=p_0} = \frac{T_0\alpha_T}{\varrho_0 c_\mathrm{p}} . \quad (8.17)$$

follows, where

$$\alpha_T = \frac{1}{V}\left(\frac{\partial V}{\partial T}\right)_{p,T=T_0} = -\frac{1}{\varrho_0}\left(\frac{\partial \varrho}{\partial T}\right)_{p,T=T_0} \quad (8.18)$$

is the isobaric volume coefficient of the thermal expansion and c_p is the specific heat at constant pressure of the liquid. Insertion of (8.17) into (8.16) together with (8.15) yields

$$\frac{B}{A} = 2\varrho_0 c_0 \left(\frac{\partial c}{\partial p}\right)_{T,p=p_0} + 2\frac{c_0 T_0 \alpha_\mathrm{T}}{\varrho_0 c_\mathrm{p}}\left(\frac{\partial c}{\partial T}\right)_{p,T=T_0} . \quad (8.19)$$

This form of B/A divides its value into an isothermal (first) and isobaric (second) part. It has been found that the isothermal part dominates.

For liquids, B/A mostly varies between 2 and 12. For water under normal conditions it is about 5. Gases (with B/A smaller than one, see before) are much less nonlinear than liquids. Water with gas bubbles, however, may have a very large value of B/A, strongly depending on the volume fraction, bubble sizes and frequency of the sound wave. Extremely high values on the order of 1000 to 10 000 have been reported [8.54, 55]. Tables with values of B/A for a large number of materials can be found in [8.43,44].

As water is the most common fluid two tables (Table 8.1, 2) of B/A for water as a function of temperature and pressure are given (see also [8.56]). Two more tables (Table 8.3, 4) list B/A values for organic liquids and for liquid metals and gases, both at atmospheric pressure.

8.4 The Coefficient of Nonlinearity β

In a sound wave the propagation velocity $\mathrm{d}x/\mathrm{d}t$ of a quantity (pressure, density) as observed by an outside stationary observer changes along the wave. As shown by *Riemann* [8.57] and *Earnshaw* [8.58], for a forward-traveling plane wave it is given by

$$\frac{\mathrm{d}x}{\mathrm{d}t} = c + u , \quad (8.20)$$

c being the sound velocity in the medium without the particle velocity u introduced by the sound wave. The sound velocity c is given by (8.1), $c^2 = (\partial p/\partial \varrho)_s$, and contains the nonlinear properties of the medium. It is customary to incorporate this nonlinearity in (8.20) in a second-order approximation as [8.59, 60]

$$\frac{\mathrm{d}x}{\mathrm{d}t} = c_0 + \beta u , \quad (8.21)$$

introducing a *coefficient of nonlinearity* β. Here c_0 is the sound velocity in the limit of vanishing sound pressure amplitude. The coefficient of nonlinearity β is related to the parameter of nonlinearity B/A as derived from the Taylor expansion of the isentropic equation of state [8.7] via

$$\beta = 1 + \frac{B}{2A} . \quad (8.22)$$

Amazon
EX1010 Page 278

The number 1 in this equation comes from the u in [8.22]. For an ideal gas [8.2] $B/A = \gamma - 1$ (8.11) and thus

$$\beta = 1 + \frac{\gamma - 1}{2} = \frac{\gamma + 1}{2} \,. \tag{8.23}$$

The quantity β is made up of two terms. They can be interpreted as coming from the nonlinearity of the medium (second term) and from convection (first term). This convective part is inevitably connected with the sound wave and is an inherent (kinematic) nonlinearity that is also present when there is no nonlinearity in the medium (thermodynamic nonlinearity) [8.60].

The introduction of β besides B/A is justified because it not only incorporates the nonlinearity of the medium, as does B/A, but also the inherent nonlinearity of acoustic propagation. The deformation of a wave as it propagates is described by β.

8.5 Simple Nonlinear Waves

In the linear case the wave equation is obtained for the quantities pressure $p - p_0$, density $\varrho - \varrho_0$ and each component of the particle velocity $\boldsymbol{u} - \boldsymbol{u}_0$ (p_0 ambient pressure, ρ_0 ambient density, $\boldsymbol{u}_0$ constant (mean) velocity, often $\boldsymbol{u}_0 = 0$) from the equations for a compressible fluid. In the spatially one-dimensional case, when φ denotes one of the perturbational quantities, one gets

$$\varphi_{tt} - c_0^2 \varphi_{xx} = 0 \,, \tag{8.24}$$

where c_0 is the propagation velocity of the perturbation, given by $c_0^2 = (\partial p/\partial \varrho)_{s,\varrho=\varrho_0}$, and the subscripts t and x denote partial differentiation with respect to time and space, respectively. A simple way to incorporate the influence of nonlinearities of the medium without much mathematical effort consists in considering the propagation velocity no longer as constant. One proceeds as follows. As nonlinear waves do not superpose interaction-free, and because waves running in opposite directions (*compound waves*) would cause problems, the wave equation above is written as

$$\left(\frac{\partial}{\partial t} - c_0 \frac{\partial}{\partial x}\right)\left(\frac{\partial}{\partial t} + c_0 \frac{\partial}{\partial x}\right)\varphi = 0 \tag{8.25}$$

and only one part, i. e. a wave running in one direction only, called a *progressive* or *traveling wave*, is taken, for instance:

$$\varphi_t + c_0 \varphi_x = 0 \,, \tag{8.26}$$

a forward, i. e. in the $+x$-direction, traveling wave. The general solution of this equation is

$$\varphi(x, t) = f(x - c_0 t) \,. \tag{8.27}$$

The function f can be a quite general function of the argument $x - c_0 t$. A nonlinear extension can then be written as

$$\varphi_t + v(\varphi)\varphi_x = 0 \,, \tag{8.28}$$

whereby now the propagation velocity $v(\varphi)$ is a function of the perturbation φ. In this way the simplest propagation equation for nonlinear waves is obtained; it already leads to the problem of breaking waves and the occurrence of shock waves.

A solution to the nonlinear propagation equation (8.28) can be given in an implicit way:

$$\varphi(x, t) = f[x - v(\varphi)t] \,, \tag{8.29}$$

as can be proven immediately by insertion. This seems of little use for real calculations of the propagation of the perturbation profile. However, the equation allows for a simple physical interpretation, that is, that the quantity φ propagates with the velocity $v(\varphi)$. This leads to a simple geometric construction for the propagation of a perturbation (Fig. 8.3).

To this end the *initial-value problem* (restricted to progressive waves in one direction only and cutting out one wavelength traveling undisturbed) is considered:

$$\varphi(x, t = 0) = f(\xi) \,. \tag{8.30}$$

To each ξ value belongs a value $f(\xi)$ that propagates with the velocity $v[f(\xi)]$:

$$\left.\frac{\mathrm{d}x}{\mathrm{d}t}\right|_f = v[f(\xi)] \tag{8.31}$$

or

$$x = \xi + v[f(\xi)]t \,. \tag{8.32}$$

This is the equation of a straight line in the (x, t)-plane that crosses $x(t = 0) = \xi$ with the derivative $v(f(\xi))$. Along this straight line φ stays constant. These lines are called *characteristics* and were introduced by *Riemann* [8.57]. In this way the solution of (hyperbolic) partial differential equations can be transformed to the solution of ordinary differential equations, which is of great advantage numerically.

Amazon
EX1010 Page 279

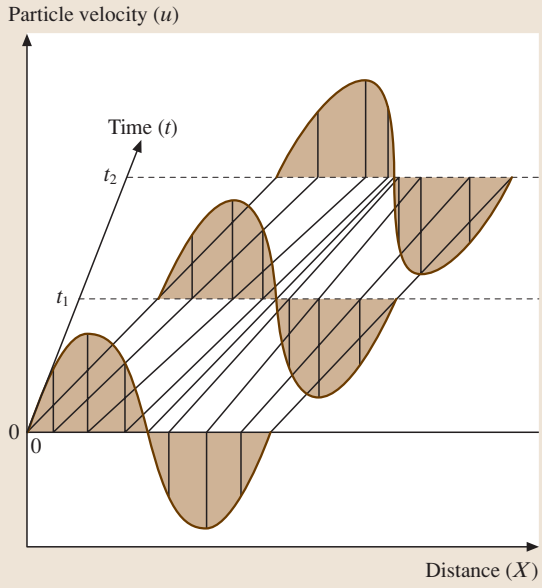


Fig. 8.3 Characteristics and the construction of the waveform for nonlinear progressive wave propagation (after Beyer [8.3])

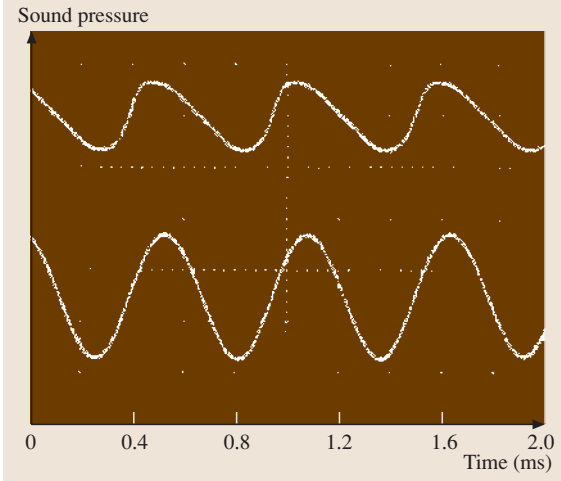


Fig. 8.4 Form of the sound wave at the launch site (lower) and after three meters of propagation (upper) in a tube filled with air. Measurement done at the Drittes Physikalisches Institut, Göttingen

The initial-value problem (8.30) is difficult to realize experimentally. Normally a sound wave is launched by a loudspeaker or transducer vibrating at some location. For one-dimensional problems a piston in a tube is a good approximation to a *boundary condition* $\varphi(x=0,t)=g(t)$, when the finite amplitude of the piston can be neglected. (The piston cannot vibrate and stay stationary at $x=0$.) Also, simple waves are produced from the outset without the complications of compound waves and their mixed flow being produced by an initial condition in which the perturbation values are given in space at a fixed time ($t=0$) [8.61].

The steepening of a wavefront has been measured this way by sending a strong sound wave through a nonlinear medium and monitoring the wave with a microphone. Figure 8.4 shows the steepening of a sound wave in air after three meters of propagation. The wave at a frequency of 2 kHz was guided inside a plastic tube. As the horizontal axis denotes time, the steepening is on the left flank, the flank of the propagation direction that passes the microphone first.

8.6 Lossless Finite-Amplitude Acoustic Waves

How elastic waves propagate through a medium is a main topic in acoustics and has been treated to various degrees of accuracy. The starting point is a set of equations from fluid mechanics. For plane acoustic waves in nondissipative fluids this set is given by three equations: the equation of continuity, the Euler equation and the equation of state:

$$\frac{\partial\varrho}{\partial t}+u\frac{\partial\varrho}{\partial x}+\varrho\frac{\partial u}{\partial x}=0\,, \tag{8.33}$$

$$\frac{\partial u}{\partial t}+u\frac{\partial u}{\partial x}+\frac{1}{\varrho}\frac{\partial p}{\partial x}=0\,, \tag{8.34}$$

$$p=p(\varrho)\,. \tag{8.35}$$

The quantities ϱ, u and p are the density of the fluid, the particle velocity and the pressure, respectively. The three equations can be condensed into two in view of the unique relation between p and ϱ. From (8.35) it follows that $\partial p/\partial x=c^2\partial\varrho/\partial x$ and with (8.34) we obtain

$$\frac{\partial u}{\partial t}+u\frac{\partial u}{\partial x}+\frac{c^2}{\varrho}\frac{\partial\varrho}{\partial x}=0\,, \tag{8.36}$$

where c is the sound velocity of the medium. The following relation between u and ϱ holds for forward-traveling

Amazon
EX1010 Page 280

waves [8.57, 58] (see also [8.1]):

$$\frac{\partial u}{\partial x} = \frac{c}{\varrho}\frac{\partial \varrho}{\partial x} \tag{8.37}$$

giving the propagation equation

$$\frac{\partial u}{\partial t} + (u + c)\frac{\partial u}{\partial x} = 0 \tag{8.38}$$

for a plane progressive wave without dissipation. The propagation velocity c (here for the particle velocity we use u) due to the nonlinearity of the medium to a second-order approximation follows from $u + c = c_0 + \beta u$ (see (8.21) and (8.22)) as

$$c = c_0 + \frac{B}{2A}u \,. \tag{8.39}$$

The corresponding relation for an ideal gas,

$$c = c_0 + \frac{\gamma - 1}{2}u \,, \tag{8.40}$$

is exact.

Comparing the propagation equation (8.38) with (8.28) where a general function $v(\varphi)$ was introduced for the nonlinear propagation velocity with φ a disturbance of the medium, for instance u, the function can now be specified as

$$v(u) = u + c(u) \,. \tag{8.41}$$

This finding gives rise to the following degrees of approximation.

The linear approximation

$$v(u) = c_0 \,, \tag{8.42}$$

the kinematic approximation, where the medium is still treated as linear,

$$v(u) = u + c_0 \,, \tag{8.43}$$

the quadratic approximation

$$v(u) = u + c_0 + \frac{B}{2A}u = c_0 + \beta u \,, \tag{8.44}$$

and so forth, as further approximations are included. From these equations it follows that $v(u = 0) = c_0$ regardless of the degree of approximation. This means that the wave as a whole propagates with the linear velocity c_0; its form, however, changes. This holds true as long as the form of the wave stays continuous. Also, there is no truly linear case. Even if the medium is considered linear the kinematic approximation reveals that there is a distortion of the wave. Only in the limit of infinitely small amplitude of the particle velocity u (implying also an infinitely small amplitude of acoustic pressure $p - p_0$) does a disturbance propagate linearly. There is no finite amplitude that propagates linearly. This is different from the transverse waves that appear in solids, for instance, and in electromagnetic wave propagation. In these cases, linear waves of finite amplitude exist, because they do not experience distortion due to a kinematic term u.

A solution to the propagation equation (8.38) to a second-order approximation,

$$\frac{\partial u}{\partial t} + (c_0 + \beta u)\frac{\partial u}{\partial x} = 0 \,, \tag{8.45}$$

can be given in implicit form as for (8.28):

$$u(x, t) = f[x - (c_0 + \beta u)t] \,. \tag{8.46}$$

For the boundary condition (source or signaling problem)

$$u(x = 0, t) = u_\mathrm{a} \sin \omega t \tag{8.47}$$

the implicit solution reads with the function $f = u_\mathrm{a} \sin(\omega t - kx)$ and $k = \omega / v(u)$:

$$u(x, t) = u_\mathrm{a} \sin\left(\omega t - \frac{\omega}{c_0 + \beta u}x\right) \,, \tag{8.48}$$

or, when expanding and truncating the denominator in the argument of the sine wave:

$$u(x, t) = u_\mathrm{a} \sin\left[\omega t - \frac{\omega}{c_0}\left(1 - \beta\frac{u}{c_0}\right)x\right] \,. \tag{8.49}$$

With the wave number

$$k_0 = \frac{\omega}{c_0} \,, \tag{8.50}$$

$\omega = 2\pi f$, where f is the frequency of the sound wave, and

$$M_\mathrm{a} = \frac{u_\mathrm{a}}{c_0} \,, \tag{8.51}$$

is the initial (peak) acoustic Mach number, the solution reads:

$$\frac{u(x, t)}{u_\mathrm{a}} = \sin\left[\omega t - k_0 x\left(1 + \beta M_\mathrm{a}\frac{u(x, t)}{u_\mathrm{a}}\right)\right] \,. \tag{8.52}$$

This implicit solution can be turned into an explicit one, as shown by Fubini in 1935 [8.62] (see also [8.59, 63]), when the solution is expanded in a Fourier series ($\varphi = \omega t - k_0 x$):

$$\frac{u}{u_\mathrm{a}} = \sum_{n=1}^{\infty} B_n \sin(n\varphi) \tag{8.53}$$

Amazon
EX1010 Page 281

with

$$B_n = \frac{1}{\pi}\int_0^{2\pi} \frac{u}{u_a}\sin(n\varphi)\mathrm{d}\varphi\,. \tag{8.54}$$

After insertion of (8.52) into (8.54) and some mathematical operations the Bessel functions J_n of the first kind of order n yield

$$B_n = \frac{2}{\beta M_a k_0 n x} J_n(\beta M_a k_0 n x)\,. \tag{8.55}$$

The explicit solution then reads

$$\frac{u(x,t)}{u_a} = \frac{2}{\beta M_a k_0}\sum_{n=1}^{\infty}\frac{J_n(\beta M_a k_0 n x)}{n x}\sin n(\omega t - k_0 x)\,. \tag{8.56}$$

The region of application of this solution is determined by $\beta M_a k_0$. The inverse has the dimensions of a length:

$$x_\perp = \frac{1}{\beta M_a k_0}\,, \tag{8.57}$$

and is called the *shock distance*, because at this distance the wave develops a vertical tangent, the beginning of becoming a shock wave. The solution is valid only up to this distance $x = x_\perp$.

To simplify the notation the dimensionless normalized distance σ may be introduced:

$$\sigma = \frac{x}{x_\perp}\,. \tag{8.58}$$

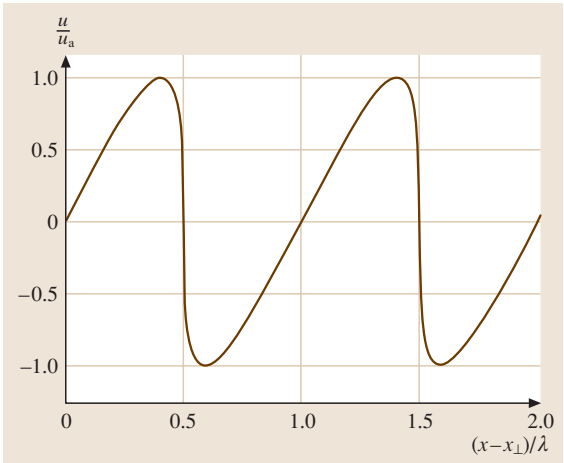


Fig. 8.5 Waveform of the Fubini solution (8.66) at the shock formation time $t_\perp$ ($\sigma_t = 1$) for the initial-value problem. λ is the wavelength of the sound wave

The Fubini solution then reads

$$\frac{u}{u_a} = 2\sum_{n=1}^{\infty}\frac{J_n(n\sigma)}{n\sigma}\sin n(\omega t - k_0 x)\,. \tag{8.59}$$

When a pure spatial sinusoidal wave is taken as the initial condition [8.64]:

$$u(x, t=0) = u_a \sin k_0 x\,, \tag{8.60}$$

the implicit solution reads

$$u(x,t) = u_a \sin k_0[x - (c_0 + \beta u)t]\,, \tag{8.61}$$

or, with the acoustic Mach number $M_a = u_a/c_0$ as before:

$$\frac{u(x,t)}{u_a} = \sin k_0\left[x - c_0 t\left(1 + \beta M_a \frac{u(x,t)}{u_a}\right)\right]\,. \tag{8.62}$$

When again doing a Fourier expansion the explicit solution emerges:

$$\frac{u(x,t)}{u_a} = \frac{2}{\beta M_a k_0 c_0}\sum_{n=1}^{\infty}(-1)^{n+1} \times \frac{J_n(\beta M_a k_0 c_0 n t)}{n t}\sin n k_0(x - c_0 t)\,. \tag{8.63}$$

The region of application is determined by $\beta M_a k_0 c_0$. The inverse has the dimension of time:

$$t_\perp = \frac{1}{\beta M_a k_0 c_0}\,. \tag{8.64}$$

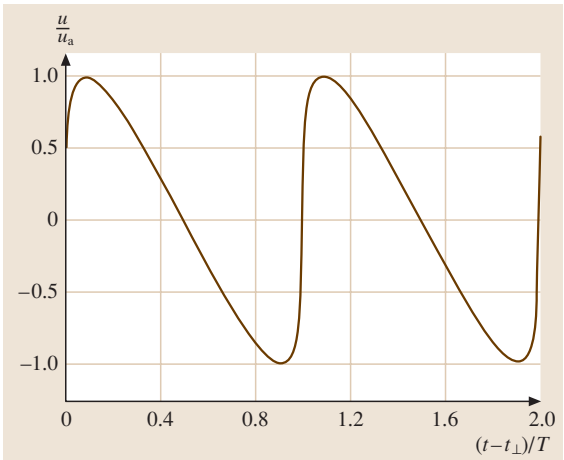


Fig. 8.6 Waveform of the Fubini solution (8.59) at the shock distance $x_\perp$ ($\sigma = 1$) for the source problem. T is the period of the sound wave. Compare the experiment in Fig. 8.4

Amazon
EX1010 Page 282

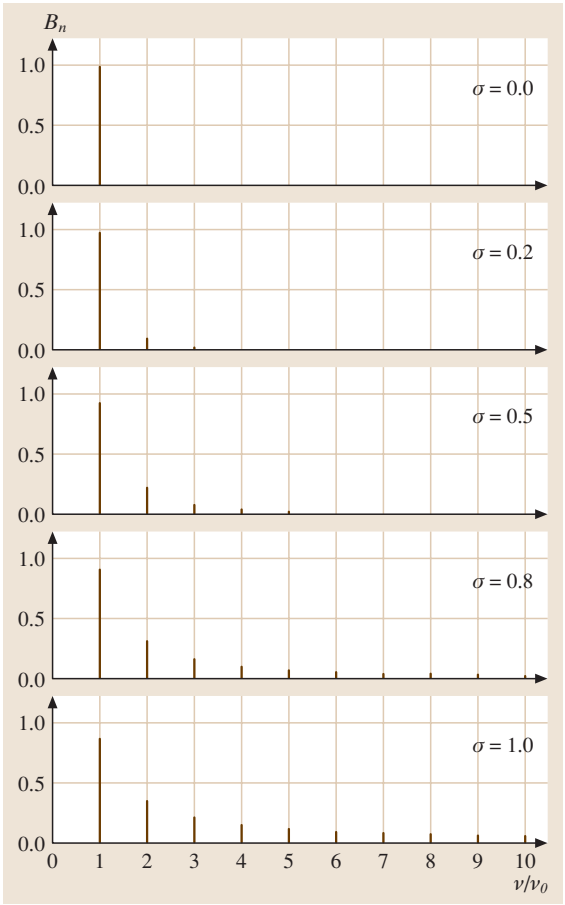


Fig. 8.7 Growth of the harmonics upon propagation for the Fubini solution (8.59) (source problem) at different normalized distances σ up to the shock distance. [8.38]

The quantity $t_\perp$ is called the *shock formation time*, because at this time the wave develops a vertical tangent. The solution is valid only up to this time $t = t_\perp$. To simplify the notation the dimensionless normalized time σ_t may be introduced

$$\sigma_t = \frac{t}{t_\perp} . \tag{8.65}$$

The Fubini solution then reads:

$$\frac{u(x,t)}{u_a} = 2\sum_{n=1}^{\infty}(-1)^{n+1}\frac{J_n(n\sigma_t)}{n\sigma_t}\sin nk_0(x - c_0 t) . \tag{8.66}$$

When comparing $t_\perp$ with $x_\perp$, the relation

$$c_0 t_\perp = x_\perp \tag{8.67}$$

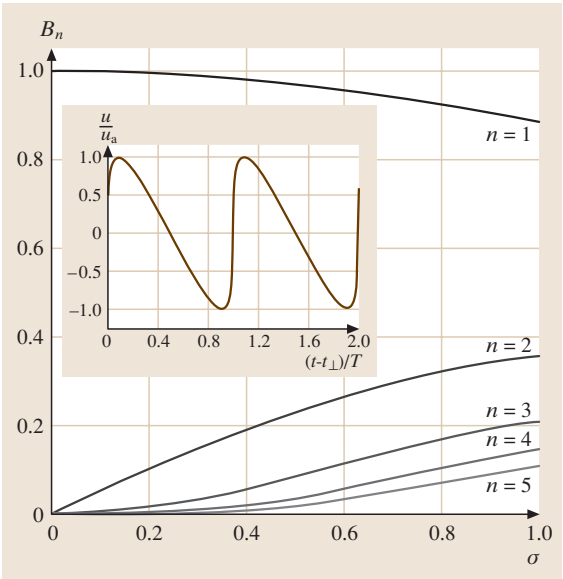


Fig. 8.8 Growth of the first five spectral components B_n of a plane wave as a function of the normalized distance σ for the Fubini solution. The *inset* gives the waveform at $\sigma = 1$ for the source problem, T being the period of the sound wave. [8.64]

is noted. This means that the shock distance is reached in the shock formation time when the wave travels at the linear sound speed c_0. This is in agreement with the earlier observation that the wave travels at the linear sound speed regardless of the nonlinearity as long as the wave stays continuous. In the case of the quadratic approximation the range in space and time for which this property holds can be quantified explicitly.

To give an impression of what the wave looks like when having propagated the shock distance $x_\perp$ in the shock formation time $t_\perp$, Fig. 8.5 shows two wavelengths at the shock formation time $t_\perp$ and Fig. 8.6 shows two periods at the shock distance $x_\perp$.

A set of spectra of the waveform for different normalized distances σ is plotted in Fig. 8.7 for the source problem, where all harmonics have positive value. The growth of the harmonics B_n (8.55) in the spectrum on the way to the shock distance is visualized. Similar plots have been given by *Fubini Ghiron* [8.65]. A plot of the first five Fourier coefficients B_n as a function of σ is given in Fig. 8.8. In the inset the waveform at the shock distance $x_\perp$ is plotted for two periods of the wave.

The solutions (8.59) and (8.66) are given for the particle velocity u. This quantity is difficult to measure. Instead, in experiments, pressure is the variable of

Amazon
EX1013 Page 283

choice. When combining the equation of state for an ideal gas with the definition of sound velocity (see (8.2) and (8.1)) a relation between pressure and sound velocity is obtained:

$$\frac{p}{p_0} = \left(\frac{c}{c_0}\right)^{2\gamma/(\gamma-1)} . \tag{8.68}$$

Insertion of the expression $c = c_0 + [(\gamma-1)/2]u$ (8.40) yields:

$$p = p_0 \left(1 + \frac{\gamma-1}{2}\frac{u}{c_0}\right)^{2\gamma/(\gamma-1)} . \tag{8.69}$$

Inserting the solution for the particle velocity u into this equation will give the pressure p and the acoustic pressure $p - p_0$. This operation is easy to perform numerically but not analytically. However, the approximation scheme for moderate-strength finite-amplitude waves, $|u/c_0| \ll 1$, is only consistent when expanding (8.69) and taking only the linear part. This leads to the *linear* relation between acoustic pressure $p - p_0$ and acoustic particle velocity u (local linearity property for weak nonlinearity) [8.61, 66]:

$$p - p_0 = \varrho_0 c_0 u , \tag{8.70}$$

where the expression $\varrho_0 c_0$ is known as the impedance. When the boundary condition (8.47) is rewritten as

$$\begin{aligned}(p - p_0)(x = 0, t) &= \varrho_0 c_0 u_a \sin \omega t \\ &= (p_a - p_0) \sin \omega t\end{aligned} \tag{8.71}$$

with $p_a - p_0 = \varrho_0 c_0 u_a$, the relation

$$\frac{p - p_0}{p_a - p_0} = \frac{u}{u_a} \tag{8.72}$$

is obtained. The normalized Fubini solution then reads in terms of the acoustic pressure for the boundary-value or source problem

$$\frac{p - p_0}{p_a - p_0} = 2\sum_{n=1}^{\infty} \frac{J_n(n\sigma)}{n\sigma} \sin n(\omega t - k_0 x) , \tag{8.73}$$

and for the initial-value problem:

$$\frac{p - p_0}{p_a - p_0} = 2\sum_{n=1}^{\infty} (-1)^{n+1} \frac{J_n(n\sigma_t)}{n\sigma_t} \sin nk_0(x - c_0 t) . \tag{8.74}$$

The steepening of acoustic waves upon propagation may occur in musical wind instruments, e.g., the trombone [8.67]. It has been shown that depending on the playing level the emitted sound waves steepen when going from piano to fortissimo, even up to shock waves. Indeed, the brightness (the *metallic* sound) of loudly played brass instruments (in particular the trumpet and the trombone as opposed to the saxhorns) is attributed to the increasing harmonic content connected with wave steepening, as exemplified in Fig. 8.7.

8.7 Thermoviscous Finite-Amplitude Acoustic Waves

Because of the inherently nonlinear nature of acoustic wave propagation steep gradients of physical quantities (pressure, density, temperature, ...) inevitably appear after some time of traveling, after which losses can no longer be neglected. In the steep gradients brought about by nonlinearity, linear phenomena that could be neglected before become important [8.68]. These are losses by *diffusive* mechanisms, in particular viscosity and heat conduction, and spreading phenomena by *dispersive* mechanisms as in frequency dispersion. When losses balance nonlinearity, the characteristic waveforms of *shock waves* appear, when frequency dispersion balances nonlinearity the characteristic form of *solitons* appear. Both are given about equal space in this treatment. The inclusion of thermoviscous losses is treated in this chapter, the inclusion of frequency dispersion, small in pure air and water, but large in water with bubbles, is treated in Chap. 8.10 on liquids containing bubbles.

The extension of (8.45) when thermoviscous losses are included as a small effect leads to the Burgers equation

$$\frac{\partial u}{\partial t} + (c_0 + \beta u)\frac{\partial u}{\partial x} = \frac{1}{2}\delta \frac{\partial^2 u}{\partial x^2} . \tag{8.75}$$

Here δ, comprising the losses, has been called the diffusivity of sound by Lighthill [8.69]:

$$\begin{aligned}\delta &= \frac{1}{\rho_0}\left(\frac{4}{3}\mu + \mu_B\right) + \frac{\kappa}{\rho_0}\left(\frac{1}{c_v} - \frac{1}{c_p}\right) \\ &= \nu\left(\frac{4}{3} + \frac{\mu_B}{\mu} + \frac{\gamma-1}{Pr}\right)\end{aligned} \tag{8.76}$$

where μ is the shear viscosity, μ_B the bulk viscosity, $\nu = \mu/\varrho_0$ the kinematic viscosity, κ the thermal conductivity, c_v and c_p the specific heats at constant volume and constant pressure, respectively, and Pr being the Prandtl

Amazon
EX1010 Page 284

number, $Pr = \mu c_p/\kappa$. The equation is an approximation to a more exact second-order equation that, however, does not lend itself to an exact solution as does the Burgers equation above. In the context of acoustics this relation was first derived by *Mendousse*, although for viscous losses only [8.70]. The derivations make use of a careful comparison of the order of magnitude of derivatives retaining the leading terms. The above form of the Burgers equation is best suited to initial-value problems. Source problems are best described when transforming (8.75) to new coordinates (x, τ) with the retarded time $\tau = t - x/c_0$:

$$\frac{\partial u}{\partial x} - \frac{\beta}{c_0^2} u \frac{\partial u}{\partial \tau} = \frac{\delta}{2c_0^3} \frac{\partial^2 u}{\partial \tau^2} \,. \tag{8.77}$$

The equation can be normalized to a form with only one parameter:

$$\frac{\partial W}{\partial \sigma} - W \frac{\partial W}{\partial \varphi} = \frac{1}{\Gamma} \frac{\partial^2 W}{\partial \varphi^2} \,, \tag{8.78}$$

where $W = u/u_0$, $\sigma = x/x_\perp$, $\varphi = \omega\tau = \omega t - k_0 x$, $\Gamma = \beta M_0 k_0/\alpha = 2\pi\beta M_0/\alpha\lambda$, with α being the damping constant for linear waves:

$$\alpha = \frac{\delta k_0^2}{2c_0} \,. \tag{8.79}$$

Γ is called the Gol'dberg number after *Gol'dberg* [8.71] who introduced this normalization (*Blackstock* [8.72]). It can be written as

$$\Gamma = \frac{1/x_\perp}{\alpha} \tag{8.80}$$

where $1/x_\perp = \beta M_0 k_0$ is the strength of the nonlinearity and α is the strength of the damping. The Gol'dberg number is therefore a measure of the importance of nonlinearity in relation to damping. For $\Gamma > 1$ nonlinearity takes over and for $\Gamma < 1$ damping takes over. For $\Gamma \gg 1$ nonlinearity has time to accumulate its effects, for $\Gamma \ll 1$ damping does not allow nonlinear effects to develop.

The Burgers equation is exactly integrable by the Hopf–Cole transformation [8.73, 74]:

$$W = \frac{2}{\Gamma} \frac{1}{\zeta} \frac{\partial \zeta}{\partial \varphi} = \frac{2}{\Gamma} \frac{\partial \ln \zeta}{\partial \varphi} \tag{8.81}$$

that is best done in two steps [8.10]

$$W = \frac{\partial \psi}{\partial \varphi} \,, \tag{8.82}$$

$$\psi = \frac{2}{\Gamma} \ln \zeta \,. \tag{8.83}$$

By this transformation the nonlinear Burgers equation is reduced to the linear heat conduction or diffusion equation

$$\frac{\partial \zeta}{\partial \sigma} = \frac{1}{\Gamma} \frac{\partial^2 \zeta}{\partial \varphi^2} \,. \tag{8.84}$$

For this equation a general explicit solution is available:

$$\zeta(\sigma, \varphi) = \sqrt{\frac{\Gamma}{4\pi\sigma}} \int_{-\infty}^{+\infty} \zeta(0, \varphi') \exp\left(-\Gamma \frac{(\varphi' - \varphi)^2}{4\sigma}\right) \mathrm{d}\varphi' \,. \tag{8.85}$$

For a specific solution the initial or boundary conditions must be specified. A common problem is the piston that starts to vibrate sinusoidally at time $t = 0$. This problem has been treated by *Blackstock* [8.72] whose derivation is closely followed here. The boundary condition is given by

$$\begin{aligned} u(0, t) &= 0 \qquad \text{for} \quad t \le 0 \,, \\ u(0, t) &= u_a \sin \omega t \quad \text{for} \quad t > 0 \,, \end{aligned} \tag{8.86}$$

or in terms of the variable $W(\sigma, \varphi)$

$$\begin{aligned} W(0, \varphi) &= 0 \qquad \text{for} \quad \varphi \le 0 \,, \\ W(0, \varphi) &= \sin \varphi \quad \text{for} \quad \varphi > 0 \,. \end{aligned} \tag{8.87}$$

To solve the heat conduction equation the boundary condition is needed for $\zeta(\sigma, \varphi)$. To this end the Hopf–Cole transformation (8.81) is reversed:

$$\zeta(\sigma, \varphi) = \exp\left(\frac{\Gamma}{2} \int_{-\infty}^{\varphi} W(\sigma, \varphi') \mathrm{d}\varphi'\right) . \tag{8.88}$$

Insertion of $W(0, \varphi)$ yields as the boundary condition for ζ:

$$\begin{aligned} \zeta(0, \varphi) &= 1 \qquad\qquad\quad \text{for} \quad \varphi \le 0 \\ \zeta(0, \varphi) &= \mathrm{e}^{\frac{1}{2}\Gamma(1 - \cos\varphi)} \quad \text{for} \quad \varphi > 0 \end{aligned} \tag{8.89}$$

and insertion into (8.85) yields the solution in terms of ζ. Using $\bar\sigma = \sqrt{4\sigma/\Gamma}$ and $q = (\varphi' - \varphi)/\bar\sigma$ the solution for the vibrating piston in terms of ζ reads

$$\begin{aligned} \zeta(\sigma, \varphi) = {} & \frac{1}{\sqrt{\pi}} \int_{-\infty}^{-\varphi/\bar\sigma} \mathrm{e}^{-q^2} \, \mathrm{d}q \\ & + \frac{1}{\sqrt{\pi}} \mathrm{e}^{\frac{1}{2}\Gamma} \int_{-\varphi/\bar\sigma}^{\infty} \mathrm{e}^{-\frac{1}{2}\Gamma\cos(\bar\sigma q + \varphi)} \, \mathrm{e}^{-q^2} \, \mathrm{d}q \,. \end{aligned} \tag{8.90}$$

Amazon
EX1010 Page 285

This solution is involved and also contains the transients after starting the oscillation. When $\varphi \to \infty$ these transients decay and the steady-state solution is obtained:

$$\zeta(\sigma, \varphi \,|\, \varphi \to \infty) = \frac{1}{\sqrt{\pi}} \, \mathrm{e}^{\frac{1}{2}\Gamma} \int_{-\infty}^{\infty} \mathrm{e}^{-\frac{1}{2}\Gamma \cos(\bar{\sigma} q + \varphi)} \, \mathrm{e}^{-q^2} \, \mathrm{d}q \, . \tag{8.91}$$

With the help of the modified Bessel functions of order n, $I_n(z) = \mathrm{i}^{-n} J_n(\mathrm{i}z)$, and the relation [8.75]

$$\mathrm{e}^{z \cos\theta} = I_0(z) + 2 \sum_{n=1}^{\infty} I_n(z) \cos n\theta \tag{8.92}$$

the expression

$$\begin{aligned} &\mathrm{e}^{-\frac{1}{2}\Gamma \cos(\bar{\sigma} q + \varphi)} \\ &= I_0\left(-\tfrac{1}{2}\Gamma\right) + 2 \sum_{n=1}^{\infty} I_n\left(-\tfrac{1}{2}\Gamma\right) \cos n(\bar{\sigma} q + \varphi) \\ &= I_0\left(\tfrac{1}{2}\Gamma\right) + 2 \sum_{n=1}^{\infty} (-1)^n I_n\left(\tfrac{1}{2}\Gamma\right) \cos n(\bar{\sigma} q + \varphi) \end{aligned} \tag{8.93}$$

is valid. Inserting this into (8.91) and integrating yields, observing that $\int_{-\infty}^{+\infty} \exp(-q^2 x^2) \cos[p(x + \lambda)] \mathrm{d}x = (\sqrt{\pi}/q) \exp[-p^2/(4q^2)] \cos p\lambda$ [8.76]:

$$\zeta(\sigma, \varphi | \varphi \to \infty) = \mathrm{e}^{\frac{1}{2}\Gamma} \left[I_0\left(\tfrac{1}{2}\Gamma\right) + 2 \sum_{n=1}^{\infty} (-1)^n I_n\left(\tfrac{1}{2}\Gamma\right) \mathrm{e}^{-n^2 \sigma/\Gamma} \cos n\varphi \right] . \tag{8.94}$$

This is the exact steady-state solution for the oscillating piston problem given for ζ as a Fourier series. Transforming to $W(\sigma, \varphi)$ via (8.81) gives

$$W(\sigma, \varphi) = \frac{4\Gamma^{-1} \sum_{n=1}^{\infty} (-1)^{n+1} n I_n\left(\frac{1}{2}\Gamma\right) \mathrm{e}^{-n^2 \sigma/\Gamma} \sin n\varphi}{I_0\left(\frac{1}{2}\Gamma\right) + 2 \sum_{n=1}^{\infty} (-1)^n I_n\left(\frac{1}{2}\Gamma\right) \mathrm{e}^{-n^2 \sigma/\Gamma} \cos n\varphi} . \tag{8.95}$$

Finally, for $u(x, t)$ the solution reads

$$\frac{u(x,t)}{u_\mathrm{a}} = \frac{4\Gamma^{-1} \sum_{n=1}^{\infty} (-1)^{n+1} n I_n\left(\frac{1}{2}\Gamma\right) \mathrm{e}^{-n^2 \alpha x} \sin n(\omega t - k_0 x)}{I_0\left(\frac{1}{2}\Gamma\right) + 2 \sum_{n=1}^{\infty} (-1)^n I_n\left(\frac{1}{2}\Gamma\right) \mathrm{e}^{-n^2 \alpha x} \cos n(\omega t - k_0 x)} . \tag{8.96}$$

The equation for the acoustic pressure $p - p_0$ again can be obtained via the approximation (8.72) as before in the lossless case: $(p - p_0)/(p_\mathrm{a} - p_0) = u/u_\mathrm{a}$ gives the identical equation.

There are regions of the parameter Γ and the independent variables x and t where the solution is difficult to calculate numerically. However, in these cases approximations can often be formulated.

For $\Gamma \to \infty$ and $\sigma = x/x_\perp \ll 1$ the Fubini solution is recovered.

For $\sigma \gg \Gamma$, i. e. far away from the source, the first terms in the numerator and the denominator in (8.96) dominate, leading to

$$\frac{u(x,t)}{u_\mathrm{a}} = \frac{4}{\Gamma} \frac{I_1(\Gamma/2)}{I_0(\Gamma/2)} \, \mathrm{e}^{-\alpha x} \sin(\omega t - k_0 x) \, . \tag{8.97}$$

When additionally $\Gamma \gg 1$, i. e. nonlinearity dominates over attenuation, $I_0(\Gamma/2) \approx I_1(\Gamma/2)$ and therefore

$$\begin{aligned} u(x,t) &= u_\mathrm{a} \frac{4}{\Gamma} \, \mathrm{e}^{-\alpha x} \sin(\omega t - k_0 x) \\ &= 4 u_\mathrm{a} \alpha x_\perp \, \mathrm{e}^{-\alpha x} \sin(\omega t - k_0 x) \\ &= \frac{4\alpha c_0^2}{\beta\omega} \, \mathrm{e}^{-\alpha x} \sin(\omega t - k_0 x) \qquad (8.98) \\ &= \frac{2\delta\omega}{\beta c_0} \, \mathrm{e}^{-\alpha x} \sin(\omega t - k_0 x) \, . \qquad (8.99) \end{aligned}$$

This series of equations for the amplitude of the sinusoidal wave radiated from a piston in the far field lends itself to several interpretations. As it is known that for $\Gamma \gg 1$ harmonics grow fast at first, these must later decay leaving the fundamental to a first approximation. The amplitude of the fundamental in the far field is independent of the amplitude u_a of the source, as can be seen from the third row (8.98). This means that there is a saturation effect. Nonlinearity together with attenuation does not allow the amplitude in the far field to increase in proportion to u_a because of the extra damping introduced by the generation of harmonics that are damped more strongly than the fundamental. This even works asymptotically because otherwise u_a would finally appear. The damping constant is frequency dependent (8.79), leading to the last row (8.99). It is seen that the asymptotic amplitude of the fundamental grows with the frequency $f = \omega/2\pi$. This continues until other effects come into play, for instance relaxation effects in the medium. Equations (8.98) and (8.99) for u are different from the equations for the acoustic pressure, as they cannot be normalized with u_a or $p_\mathrm{a} - p_0$, respectively.

Amazon
EX1010 Page 286

They are related via the impedance $\varrho_0 c_0$ (8.70):

$$(p-p_0)(x,t) = \frac{4\alpha\varrho_0 c_0^3}{\beta\omega}\,\mathrm{e}^{-\alpha x}\sin(\omega t - k_0 x) \quad (8.100)$$

$$= \frac{2\delta\varrho_0\omega}{\beta}\,\mathrm{e}^{-\alpha x}\sin(\omega t - k_0 x)\,. \quad (8.101)$$

Good approximations for $\Gamma \gg 1$ have been given by *Fay* [8.78]:

$$\frac{u(x,t)}{u_\mathrm{a}} = \sum_{n=1}^{\infty} \frac{2/\Gamma}{\sinh[n(1+x/x_\perp)/\Gamma]}\sin n(\omega t - k_0 x)\,, \quad (8.102)$$

and *Blackstock* [8.72]:

$$\frac{u(x,t)}{u_\mathrm{a}} = \frac{2}{\Gamma}\sum_{n=1}^{\infty}\frac{1-(n/\Gamma^2)\coth[n(1+x/x_\perp)/\Gamma]}{\sinh[n(1+x/x_\perp)/\Gamma]} \times \sin n(\omega t - k_0 x)\,. \quad (8.103)$$

With an error of less than 1% at $\Gamma = 50$ Fay's solution is valid for $\sigma > 3.3$ and Blackstock's solution for $\sigma > 2.8$, rapidly improving with σ. The gap in σ from about one to three between the Fubini and Fay solution has been closed by Blackstock. He connected both solutions using weak shock theory giving the Fubini–Blackstock–Fay solution ([8.77], see also [8.1]). Figure 8.9 shows the first three harmonic components of the Fubini–Blackstock–Fay solution from [8.79]. Similar curves have been given by *Cook* [8.80]. He developed a numerical scheme for calculating the harmonic content of a wave as it propagates by including the losses in small spatial steps linearly for each harmonic component. As there are occurring only harmonic waves that do not break the growth in each small step is given by the Fubini solution.

In the limit $\Gamma \to \infty$ the Fay solution reduces to

$$\frac{u(x,t)}{u_\mathrm{a}} = \sum_{n=1}^{\infty}\frac{2}{1+x/x_\perp}\sin n(\omega t - k_0 x)\,, \quad (8.104)$$

a solution that is also obtained by weak shock theory.

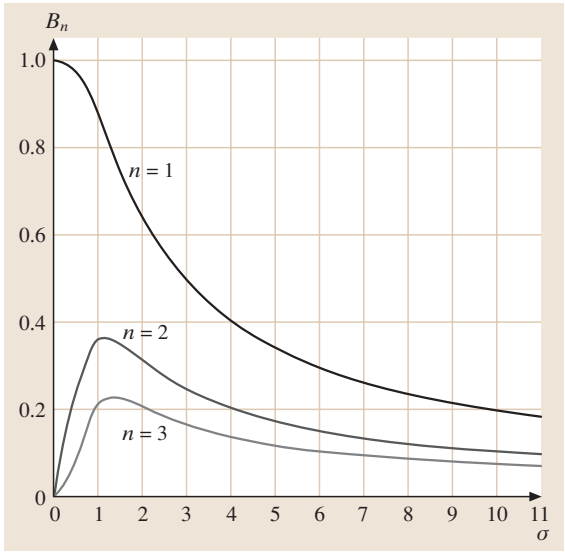


Fig. 8.9 Growth and decay of the first three harmonic components B_n of a plane wave as a function of the normalized distance σ according to the Fubini–Blackstock–Fay solution (after Blackstock [8.77])

When Fay's solution (8.102) is taken and $\sigma \gg \Gamma$ (farfield), the old-age region of the wave is reached. Then $\sinh[n(1+x/x_\perp)/\Gamma] \simeq \frac{1}{2}(\mathrm{e}^{nx/x_\perp\Gamma} - \mathrm{e}^{-nx/x_\perp\Gamma}) \simeq \frac{1}{2}\mathrm{e}^{nx/x_\perp\Gamma} = \frac{1}{2}\mathrm{e}^{n\alpha x}$ and

$$u(x,t) = \frac{4\alpha c_0^2}{\beta\omega}\,,\sum_{n=1}^{\infty}\mathrm{e}^{-n\alpha x}\sin n(\omega t - k_0 x) \quad (8.105)$$

is obtained similarly as for the fundamental (8.98). Additionally all harmonics that behave like the fundamental, i. e. that are not dependent on the initial peak particle velocity u_a, are obtained . Moreover, they do not decay (as linear waves do) proportionally to $\mathrm{e}^{-n^2\alpha x}$ but only proportionally to $\mathrm{e}^{-n\alpha x}$.

In the range $\sigma > 1$ shock waves may develop. These are discussed in the next section.

8.8 Shock Waves

The characteristics of Fig. 8.3 must cross. According to the geometrical construction the profile of the wave then becomes multivalued. This is easily envisaged with water surface waves. With pressure or density waves, however, there is only one pressure or one density at one place. The theory is therefore oversimplified and must be expanded with the help of physical arguments and the corresponding mathematical formulation. Shortly before overturning, the gradients of pressure and density become very large, and it is known that damping

Amazon
EX1010 Page 287

effects brought about by viscosity and heat conduction can no longer be neglected. When these effects are taken into account, the waves no longer turn over. Instead, a thin zone is formed, a *shock wave*, in which the values of pressure, density, temperature, etc. vary rapidly. A theoretical formulation has been given in the preceding section for thermoviscous sound waves based on the Burgers equation.

It has been found that damping effects do not necessarily have to be included in the theory, but that an extended damping free theory can be developed by introducing certain shock conditions that connect the variables across a discontinuity. A description of this theory can be found in the book by *Whitham* [8.10]. The result can be described in a simple construction. In Fig. 8.10 the profile of the wave has been determined according to the methods of characteristics for a time where the characteristics have already crossed. The shock wave then has to be inserted in such a way that the areas between the shock wave and the wave profile to the left and the right are equal (the equal area rule). Moreover, it can be shown that the velocity of the shock wave is approximately given by

$$v_s = \frac{1}{2}(v_1 + v_2)\,, \qquad (8.106)$$

where v_1 and v_2 are the propagation velocities of the wave before and behind the shock, respectively.

Shock waves are inherently difficult to describe by Fourier analysis as a large number of harmonics are needed to approximate a jump-like behavior. A time-domain description is often more favorable here. Such solutions have been developed for the propagation of sound waves in the shock regime. For $\Gamma > \sigma > 3$, *Khokhlov* and *Soluyan* [8.80] have given the following solution

$$\frac{u(x,t)}{u_a} = \frac{1}{1+x/x_\perp}\left(-\varphi + \pi \tanh\frac{\pi\Gamma\varphi}{2(1+x/x_\perp)}\right) \qquad (8.107)$$

for $-\pi < \varphi = \omega t - k_0 x < \pi$, covering a full cycle of the wave.

Figure 8.11 shows the waveforms for $\Gamma = 10$ and $\Gamma = 100$ for different $\sigma = x/x_\perp$. When the wave is followed at fixed Γ for increasing σ (i. e. increasing x), the decay and change of the waveform upon propagation can be observed.

The solution and the waveforms are remarkable as they are exact solutions of the Burgers equation, but

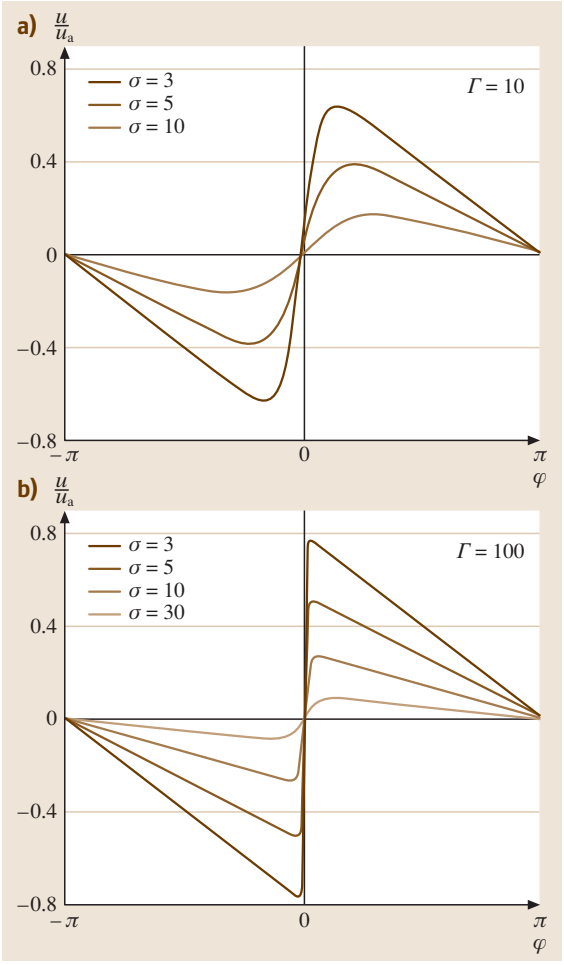


Fig. 8.11a,b Waveforms of the Khokhlov–Soluyan solution for Gol'dberg numbers $\Gamma = 10$ **(a)** and $\Gamma = 100$ **(b)** for different σ (the *age* of the wave)

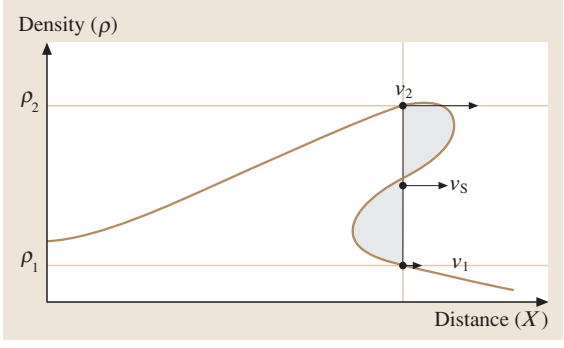


Fig. 8.10 Condition for the location of the shock wave for an overturning wave, the equal area rule

Amazon
EX1010 Page 288

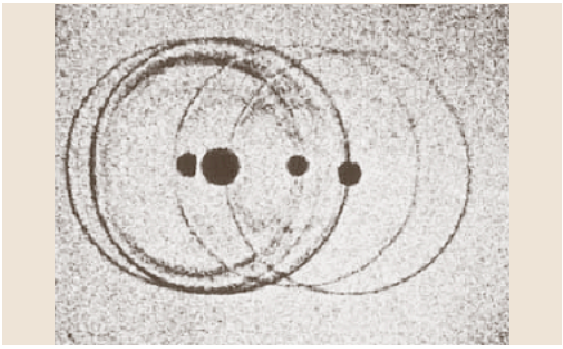


Fig. 8.12 Shock waves (*dark circles*) and bubbles (*dark spheres*) from laser-induced breakdown in water. Reconstructed image from a hologram 1.75 µs after breakdown. The size of the picture is 1.1 × 1.6 mm

approximate solutions with respect to the boundary condition.

When the wave gets very steep, i. e., in the case $\Gamma \to \infty$, it attains the shape of a sawtooth ($\sigma > 3$):

$$\frac{u(x,t)}{u_a} = \begin{cases} \dfrac{1}{1+x/x_\perp}[-\varphi+\pi] & 0 < \varphi \leq \pi \,, \\ \dfrac{1}{1+x/x_\perp}[-\varphi-\pi] & -\pi \leq \varphi < 0 \,, \end{cases} \tag{8.108}$$

where $\varphi = \omega t - k_0 x$. The amplitude of the jump is

$$\frac{u(x,t)}{u_a} = \frac{\pi}{1+x/x_\perp} \,, \tag{8.109}$$

the actual jump height from peak to peak being two times this value and falling off rapidly with x. This solution, too, is an exact solution of the Burgers equation, albeit for $1/\Gamma \equiv 0$, i. e., with the diffusion term missing in the Burgers equation.

The Fourier form solution of the sawtooth wave (8.108) is given by

$$\frac{u(x,t)}{u_a} = \frac{2}{1+x/x_\perp} \sum_{n=1}^{\infty} \frac{1}{n} \sin n(\omega t - k_0 x) \,. \tag{8.110}$$

This form can also be derived as approximation from the Fay solution (see (8.104)). This can be considered a consistency proof in the approximation approaches, one proceeding in the time domain, the other in the frequency domain.

An example of the occurrence of shock waves, albeit spherical ones, is given in Fig. 8.12. A laser pulse has been focused into water, leading to four spots of breakdown, the emission of four shock waves and the growth of four bubbles. Laser-produced bubbles are used in cavitation research to investigate bubble dynamics in liquids and their effects [8.81]. Focused shock waves are used in lithotripsy to fragment kidney stones to small enough pieces to fit through the urinary tract [8.82].

8.9 Interaction of Nonlinear Waves

Linear waves do not interact, in the sense that upon superposition they propagate independently, each according to their own parameters. This makes Fourier theory a powerful technique for linear systems. In nonlinear systems, however, the harmonic components of which an initial perturbation is composed interact and produce new components that again interact, etc. Even a single harmonic oscillation creates higher harmonics, as set out in the preceding sections.

For the description of strong nonlinear acoustic wave interaction it is very fortunate that the Burgers equation (8.78) allows for a linearizing transformation. The superposition can then be evaluated in the linear variables, giving the result of the nonlinear interaction when transforming back.

Of special interest is the interaction of two (primary) waves in the course of which the sum and, in particular, the difference frequency can be generated. A highly directional high-frequency source can be transformed into a highly directed low-frequency source (the parametric array). As the low-frequency beam generated has lower damping than the high-frequency beams it propagates to longer distances. Applications are sound navigation and ranging (SONAR) and surface and subsurface scanning of the ocean bottom.

Taking two waves with amplitudes $u_{1,2}$ and frequencies $\omega_{1,2}$, starting at $t = 0$, the boundary condition becomes

$$u(x=0,t) = \begin{cases} 0 & t < 0 \,, \\ u_1 \sin(\omega_1 t) + u_2 \sin(\omega_2 t) & t \geq 0 \,, \end{cases} \tag{8.111}$$

or with the normalized variables $W = u/u_0$, $\varphi = \omega\tau = \omega(t - x/c_0)$, $\sigma = x/x_\perp$,

Amazon
EX1010 Page 289

$$W(\sigma=0,\varphi) = \begin{cases} 0 & \varphi<0\,, \\ W_1\sin(\Omega_1\varphi)+W_2\sin(\Omega_2\varphi)\,, & \varphi\geq 0\,. \end{cases} \tag{8.112}$$

Here, $\Omega_{1,2}=\omega_{1,2}/\omega$ denote the input frequencies normalized to the reference frequency ω and $W_{1,2}=u_{1,2}/u_0$ the amplitudes normalized to the reference amplitude u_0. The inverse Hopf–Cole transformation (8.88) gives the initial condition for the linearized problem in the variable ζ. For $\varphi<0$ we obtain $\zeta(\sigma=0,\varphi)=1$, while for $\varphi\geq 0$:

$$\begin{aligned}\zeta(\sigma=0,\varphi) &= \exp\left[\frac{\Gamma}{2}\int_0^{\varphi} W(\sigma=0,\varphi')\,\mathrm{d}\varphi'\right] \\ &= \exp\left\{-\frac{\Gamma}{2}\left[\frac{W_1}{\Omega_1}\cos(\Omega_1\varphi')+\frac{W_2}{\Omega_2}\cos(\Omega_2\varphi')\right]_0^{\varphi}\right\}.\end{aligned} \tag{8.113}$$

To simplify notation, introduce the Gol'dberg numbers $\Gamma_{1,2}=\Gamma W_{1,2}/\Omega_{1,2}$ which agree with the definition (8.80) applied to the two input waves, respectively. Then

$$\zeta(\sigma=0,\varphi\geq 0) = \underbrace{\exp\left(\frac{\Gamma_1}{2}+\frac{\Gamma_2}{2}\right)}_{=:C} \times\exp\left[-\frac{\Gamma_1}{2}\cos(\Omega_1\varphi)-\frac{\Gamma_2}{2}\cos(\Omega_2\varphi)\right]. \tag{8.114}$$

With this initial condition, the solution (8.85) of the diffusion equation (8.84) reads:

$$\begin{aligned}\zeta(\sigma,\varphi) &= \sqrt{\frac{\Gamma}{4\pi\sigma}}\int_{-\infty}^{0}\exp\left(-\Gamma\frac{(\varphi'-\varphi)^2}{4\sigma}\right)\mathrm{d}\varphi' \\ &\quad + C\sqrt{\frac{\Gamma}{4\pi\sigma}}\int_0^{+\infty}\exp\left[-\frac{\Gamma_1}{2}\cos(\Omega_1\varphi')\right. \\ &\quad \left.-\frac{\Gamma_2}{2}\cos(\Omega_2\varphi')-\Gamma\frac{(\varphi'-\varphi)^2}{4\sigma}\right]\mathrm{d}\varphi' \\ &= \sqrt{\frac{\Gamma}{4\pi\sigma}}\int_{-\infty}^{-\varphi}\exp\left(-\Gamma\frac{\varphi'^2}{4\sigma}\right)\mathrm{d}\varphi' \\ &\quad + C\sqrt{\frac{\Gamma}{4\pi\sigma}}\int_{-\varphi}^{+\infty}\exp\left\{-\frac{\Gamma_1}{2}\cos[\Omega_1(\varphi'+\varphi)]\right. \\ &\quad \left.-\frac{\Gamma_2}{2}\cos[\Omega_2(\varphi'+\varphi)]-\Gamma\frac{\varphi'^2}{4\sigma}\right\}\mathrm{d}\varphi'\,.\end{aligned}$$

This general solution is quite complicated as the integration limits depend on the phase φ. To dismiss the transients caused by the starting of the waves at $\varphi=0$, again the limit $\varphi\to\infty$ is considered. This means that at a certain position $x=\sigma x_\perp$ in the medium the wave is examined a long time after the passage of the initial perturbation that started at $x=0$, $t=0$. Then, the first integral of (8.115) vanishes, and the second integral can be evaluated from $-\infty$ to $+\infty$ by using the expansion (8.92), written in the following form:

$$\begin{aligned}\exp(z\cos\theta) &= I_0(z)+2\sum_{n=1}^{\infty}I_n(z)\cos(n\theta) \\ &=: \sum_{n=0}^{\infty}b_n I_n(z)\cos(n\theta)\,,\end{aligned} \tag{8.115}$$

where the numerical factors $b_0=1$, $b_n=2$ for $n>0$ have been introduced for convenient notation. Substituting this series in (8.115) and noting that I_n is an even (odd) function for even (odd) n, we get

$$\begin{aligned}\zeta(\sigma,\varphi) &= C\sqrt{\frac{\Gamma}{4\pi\sigma}}\sum_{m=0}^{\infty}\sum_{n=0}^{\infty}(-1)^{m+n}b_m b_n I_m\left(\frac{\Gamma_1}{2}\right)I_n\left(\frac{\Gamma_2}{2}\right) \\ &\quad\times\int_{-\infty}^{+\infty}\cos[m\Omega_1(\varphi'+\varphi)]\cos[n\Omega_2(\varphi'+\varphi)] \\ &\quad\times\exp\left(-\Gamma\frac{\varphi'^2}{4\sigma}\right)\mathrm{d}\varphi'\,.\end{aligned} \tag{8.116}$$

Using $\cos(\alpha)\cos(\beta)=(1/2)\,[\cos(\alpha+\beta)+\cos(\alpha-\beta)]$, and proceeding as in the derivation of (8.94) we get

$$\begin{aligned}\zeta(\sigma,\varphi) &= \frac{C}{2}\sum_{m=0}^{\infty}\sum_{n=0}^{\infty}(-1)^{m+n}b_m b_n I_m\left(\frac{\Gamma_1}{2}\right)I_n\left(\frac{\Gamma_2}{2}\right) \\ &\quad\times\left[\exp\left(-\frac{\left(\Omega_{mn}^{+}\right)^2}{\Gamma}\sigma\right)\cos\left(\Omega_{mn}^{+}\varphi\right)\right. \\ &\quad\left.+\exp\left(-\frac{\left(\Omega_{mn}^{-}\right)^2}{\Gamma}\sigma\right)\cos\left(\Omega_{mn}^{-}\varphi\right)\right].\end{aligned}$$

Here, a short-hand notation for the combination frequencies has been introduced: $\Omega_{mn}^{\pm}=m\Omega_1\pm n\Omega_2$. Transforming back to the original variable yields

Amazon
EX1010 Page 290

$$W(\sigma,\varphi) = \frac{2}{\Gamma}\frac{1}{\zeta(\sigma,\varphi)}\frac{\partial\zeta(\sigma,\varphi)}{\partial\varphi} = \frac{\sum_{m=0}^{\infty}\sum_{n=0}^{\infty}(-w_{mn})\left[\Omega_{mn}^{+}\,\mathrm{e}_{mn}^{+}\sin(\Omega_{mn}^{+}\varphi)+\Omega_{mn}^{-}\,\mathrm{e}_{mn}^{-}\sin(\Omega_{mn}^{-}\varphi)\right]}{(\Gamma/2)\sum_{m=0}^{\infty}\sum_{n=0}^{\infty}w_{mn}\left[\mathrm{e}_{mn}^{+}\cos(\Omega_{mn}^{+}\varphi)+\mathrm{e}_{mn}^{-}\cos(\Omega_{mn}^{-}\varphi)\right]}\,, \tag{8.117}$$

where

$$w_{mn} = (-1)^{m+n}b_m b_n I_m\left(\frac{\Gamma_1}{2}\right)I_n\left(\frac{\Gamma_2}{2}\right)\,,$$

$$\mathrm{e}_{mn}^{+} = \exp\left(-\frac{(\Omega_{mn}^{+})^2}{\Gamma}\sigma\right)\,,$$

$$\mathrm{e}_{mn}^{-} = \exp\left(-\frac{(\Omega_{mn}^{-})^2}{\Gamma}\sigma\right)\,.$$

It is seen that for $\sigma > 0$ the solution in φ contains all combination frequencies $m\Omega_1 \pm n\Omega_2$ of the two input frequencies due to the nonlinear interaction. Note also that for $\Omega_1 = 1$, $\Gamma_1 = \Gamma$, $\Omega_2 = 0$, $\Gamma_2 = 0$ the solution (8.96) is recovered. In its full generality, the expression is rather cumbersome to analyze. However, as higher frequencies are more strongly damped for $\sigma \to \infty$ only a few frequencies remain with sufficient amplitude. In particular, if Ω_1 and $\Omega_2 < \Omega_1$ are close, the difference frequency $\Delta\Omega = \Omega_1 - \Omega_2$ $(m = n = 1)$ will be small and give a strong component with

$$W_{-}(\sigma,\varphi) = -\frac{4\Delta\Omega}{\Gamma}\frac{I_1\left(\frac{\Gamma_1}{2}\right)I_1\left(\frac{\Gamma_2}{2}\right)}{I_0\left(\frac{\Gamma_1}{2}\right)I_0\left(\frac{\Gamma_2}{2}\right)} \times\exp\left(-\frac{(\Delta\Omega)^2}{\Gamma}\sigma\right)\sin(\Delta\Omega\varphi)\,, \tag{8.118}$$

or, returning to physical coordinates and constants,

$$\begin{aligned} u_{-}(x,t) &= -\frac{2\Delta\omega\,\delta}{c_0\beta}\frac{I_1\left(\frac{\Gamma_1}{2}\right)I_1\left(\frac{\Gamma_2}{2}\right)}{I_0\left(\frac{\Gamma_1}{2}\right)I_0\left(\frac{\Gamma_2}{2}\right)} \\ &\quad\times\exp\left(-\frac{\delta(\Delta\omega)^2}{2c_0^3}x\right)\sin[\Delta\omega(t-x/c_0)] \\ &= u_{-}^{(0)}\exp\left(-\frac{\delta(\Delta\omega)^2}{2c_0^3}x\right)\sin[\Delta\omega(t-x/c_0)]\,. \end{aligned} \tag{8.119}$$

The Gol'dberg numbers of the interacting waves determine the quantity $u_{-}^{(0)}$ of the resulting difference-frequency wave. For $\Gamma_{1,2} \ll 1$, i. e., for low-power waves, $I_0(\Gamma/2) \approx 1$ and $I_1(\Gamma/2) \approx \Gamma/4$, thus the value

$$u_{-}^{(0)} = -\frac{2\Delta\omega\,\delta}{c_0\beta}\frac{\Gamma_1\Gamma_2}{16} = -\frac{\Delta\omega\beta c_0}{2\delta}\frac{u_{01}u_{02}}{\omega_1\omega_2} \tag{8.120}$$

is proportional to the product of the amplitudes of the interacting waves. For very intense waves, $\Gamma_{1,2} \gg 1$, as $\lim_{\xi\to\infty} I_1(\xi)/I_0(\xi) = 1$, the quantity $u_{-}^{(0)}$ of the difference-frequency wave becomes independent of u_{01} and u_{02},

$$u_{-}^{(0)} = -\frac{2\Delta\omega\,\delta}{c_0\beta}\,. \tag{8.121}$$

The difference-frequency wave (8.121) has been given for the far field where the two incoming waves have essentially ceased to interact. There, the wave propagates linearly and is exponentially damped by thermoviscous dissipation.

8.10 Bubbly Liquids

Liquids with bubbles have strongly pronounced nonlinear acoustic properties mainly due to the nonlinear oscillations of the bubbles and the high compressibility of the gas inside. Within recent decades theoretical and experimental investigations have detected many kinds of nonlinear wave phenomena in bubbly fluids. To mention just a few of these: ultrasound self-focusing [8.83, 84], acoustic chaos [8.31], sound self-transparency [8.85], wavefront conjugation [8.85], the acoustic phase echo [8.86] intensification of sound waves in nonuniform bubbly fluids [8.87, 88], subharmonic wave generation [8.89], structure formation in acoustic cavitation [8.90, 91], difference-frequency sound generation [8.92, 93]. These phenomena are discussed in several books and review papers [8.2, 9, 81, 94–97].

In this section we are going to discuss some phenomena related to nonlinear acoustic wave propagation in liquids with bubbles. First, the mathematical model for pressure-wave propagation in bubbly liquids will be presented. Second, this model will be used to investigate long nonlinear pressure waves, short pressure wave trains, and some nonlinear interactions between them.

Amazon
EX1010 Page 291

Let α_l and α_g be the volume fractions and ρ_l and ρ_g the densities of the liquid and the gas (vapor), respectively. Then the density of the two-phase mixture, ρ, in the bubbly liquid mixture is given by

$$\rho = \alpha_l \rho_l + \alpha_g \rho_g \,, \tag{8.122}$$

where $\alpha_l + \alpha_g = 1$. Note that the gas (vapor) volume fraction depends on the instantaneous bubble radius R,

$$\alpha_g = \frac{4}{3}\pi R^3 n \,, \tag{8.123}$$

where n is the number density of bubbles in the mixture. Equation (8.123) is true in general and applicable to the case in which bubbles oscillate in an acoustic field, as considered in the following.

8.10.1 Incompressible Liquids

First, we consider the case when the liquid can be treated as incompressible. The bubbly fluid model in this case is based on the *bubble-in-cell* technique [8.94], which divides the bubbly liquid mixture into cells, with each cell consisting of a liquid sphere of radius R_c with a bubble of radius R at its center. A similar approach has been used recently to model wet foam drop dynamics in an acoustic field [8.98] and the acoustics of bubble clusters in a spherical resonator [8.80].

It should be mentioned here that the bubble-in-cell technique may be treated as a first-order correction to a bubbly fluid dynamics model due to a small bubble volume fraction. This technique is not capable of capturing the entire bubbly fluid dynamics for high concentration of bubbles when bubbles lose their spherical shape.

According to the bubble-in-cell technique, the radius, R_c, of the liquid sphere comprising each cell and the embedded bubble, are related to the local void fraction at any instant by

$$\frac{R}{R_c} = \alpha_g^{1/3} \,. \tag{8.124}$$

We note that R_c, R, and α_g are variable in time.

The liquid conservation of mass equation and the assumed liquid incompressibility imply that the radial velocity around a single bubble depends on the radial coordinate:

$$v' = \frac{R^2 \dot{R}}{r'^2}, \quad R \le r' \le R_c \,, \tag{8.125}$$

where $R(t)$ is the instantaneous radius of the bubble, primed quantities denote local (single-cell) variables, namely, r' is the radial coordinate with origin at the bubble's center, v' is the radial velocity of the liquid at radial location r', and the dot denotes a time derivative (i. e., $R = \mathrm{d}R/\mathrm{d}t$).

The dynamics of the surrounding liquid is analyzed by writing the momentum equation for an incompressible, inviscid liquid as

$$\frac{\partial v'}{\partial t} + v' \frac{\partial v'}{\partial r'} + \frac{1}{\rho_l}\frac{\partial p'}{\partial r'} = 0 \,. \tag{8.126}$$

Integrating this equation over $r' \le R_c$ from R to some arbitrary r' and using (8.125) yields

$$p' = p_R - \rho_l \Bigg[R\ddot{R} + \frac{3}{2}\dot{R}^2 - \left(R\ddot{R} + 2\dot{R}^2\right)\frac{R}{r'} + \frac{1}{2}\dot{R}^2 \left(\frac{R}{r'}\right)^4 \Bigg] \,, \tag{8.127}$$

where p' is the liquid pressure at location r' around a bubble, and p_R is the liquid pressure at the bubble interface. Evaluating (8.127) at the outer radius of the cell, $r' = R_c$, and using (8.124), results in

$$\frac{p_R - p_c}{\rho_l} = \left(1 - \alpha_g^{1/3}\right) R\ddot{R} + \frac{3}{2}\left(1 - \frac{4}{3}\alpha_{g^{1/3}} + \frac{1}{3}\alpha_{g^{4/3}}\right)\dot{R}^2 \,. \tag{8.128}$$

This equation bears a resemblance to the well-known Rayleigh–Plesset equation that governs the motion of a single bubble in an infinite liquid. Indeed, in the limit of vanishing void fraction, $\alpha_g \to 0$, the pressure at the outer radius of the cell (p_c) becomes the liquid pressure far from the bubble ($p_c \to p_\infty$), and (8.128) reduces to the Rayleigh–Plesset equation

$$\frac{p_R - p_\infty}{\rho_l} = R\ddot{R} + \frac{3}{2}\dot{R}^2 \,. \tag{8.129}$$

Let us assume that the gas pressure inside the bubble p_g is spatially uniform. The momentum jump condition requires that the gas pressure differs from the liquid pressure at the bubble wall due to surface tension and viscous terms according to

$$p_R = p_g - \frac{2\sigma}{R} - \frac{4\mu_l \dot{R}}{R} \,, \tag{8.130}$$

where σ is the surface tension and μ_l is the liquid viscosity. Furthermore, the gas pressure may be assumed to be governed by a polytropic gas law of the form

$$p_g = \left(p_0 + \frac{2\sigma}{R_0}\right)\left(\frac{R}{R_0}\right)^{-3\kappa} \,, \tag{8.131}$$

Amazon
EX1010 Page 292

where R_0 is the equilibrium radius of the bubble (i. e., the bubble radius at ambient pressure) and κ is a polytropic exponent. Combining (8.128)–(8.131) gives the following relationship between the liquid pressure at the edge of the cell (p_c) and the radius of the bubble (R):

$$p_c = \left(p_0 + \frac{2\sigma}{R}\right)\left(\frac{R}{R_0}\right)^{-3\kappa} - \frac{2\sigma}{R} - \frac{4\mu_l \dot{R}}{R} - \rho_l\left[\left(1-\alpha_g^{1/3}\right)R\ddot{R} + \frac{3}{2}\left(1-\frac{4}{3}\alpha_g^{1/3}+\frac{1}{3}\alpha_g^{4/3}\right)\dot{R}^2\right]. \tag{8.132}$$

Equation (8.132) can be integrated to find the bubble radius, $R(t)$, given the time-dependent pressure at $r' = R_c$ and the initial conditions.

Next, we connect the various cells at points on their outer radii and replace the configuration with an equivalent fluid whose dynamics approximate those of the bubbly liquid. We assume that the velocity of the translational motion of the bubbles in such a fluid is equal to the velocity of the bubbly fluid $\boldsymbol{v}$. The fluid is required to conserve mass, thus

$$\frac{\partial \rho}{\partial t} + \nabla\cdot(\rho \boldsymbol{v}) = 0\,, \tag{8.133}$$

where ρ is given by (8.122). The fluid also satisfies Euler's equation,

$$\rho\frac{\mathrm{d}\boldsymbol{v}}{\mathrm{d}t} + \nabla p = 0\,, \tag{8.134}$$

where $\mathrm{d}/\mathrm{d}t = \partial/\partial t + \boldsymbol{v}\cdot\nabla$ is the material derivative, and p is the mean fluid pressure, which is approximately the pressure at the outer radius of a cell, p_c.

The mass and bubble densities are related by requiring that the total mass of each cell does not change in time. The initial volume of one cell is $V_0 = 1/n_0$, so the initial mass of the cell is $M_0 = \rho_0/n_0$, where $\rho_0 = \alpha_{l0}\rho_{l0} + \alpha_{g0}\rho_{g0}$. Requiring that the mass of each cell remains constant gives

$$\frac{\rho}{n} = \frac{\rho_0}{n_0}\,. \tag{8.135}$$

This set of equations describes the nonlinear dynamics of a bubbly liquid mixture over a wide range of pressures and temperatures.

We can now linearize these equations by assuming that the time-dependent quantities only vary slightly from their equilibrium values. Specifically, we write $\rho = \rho_0 + \tilde{\rho}$, $n = n_0 + \tilde{n}$, $p = p_0 + \tilde{p}$, $\mathbf{v} = \tilde{\mathbf{v}}$, $\alpha_g = \alpha_{g0} + \tilde{\alpha_g}$, and $R = R_0 + \tilde{R}$. The perturbed quantities are assumed to be small, so that any product of the perturbations may be neglected. When these assumptions are introduced into (8.132), we arrive at the following linearized equation:

$$\tilde{p} = -\left[\left(p_0 + \frac{2\sigma}{R_0}\right)\frac{3\kappa}{R_0} - \frac{2\sigma}{R_0^2}\right]\tilde{R} - \frac{4\mu_l}{R_0}\frac{\partial \tilde{R}}{\partial t} - \rho_l\left(1-\alpha_{g0}^{1/3}\right)R_0\frac{\partial^2\tilde{R}}{\partial t^2}\,. \tag{8.136}$$

Linearizing (8.135) gives

$$\tilde{n} = \frac{n_0}{\rho_0}\tilde{\rho}\,. \tag{8.137}$$

Similarly, linearizing the density in (8.122) taking into account that $\rho_g/\rho_l \ll 1$ and using (8.137) yields

$$\tilde{\rho} = -4\pi R_0^2\rho_0 n_0 \tilde{R}, \tag{8.138}$$

where $\rho_0 \approx \rho_l\left(1-\alpha_{g0}\right)$. By combining (8.136) and (8.138) we obtain a pressure–density relationship for the bubbly fluid:

$$\tilde{p} = \frac{C_b^2}{\omega_b^2}\left(\omega_b^2\tilde{\rho} + 2\delta_b\frac{\partial\tilde{\rho}}{\partial t} + \frac{\partial^2\tilde{\rho}}{\partial t^2}\right)\,, \tag{8.139}$$

where C_b represents the low-frequency sound speed in the bubbly liquid

$$C_b^2 = \frac{3\kappa p_0 + (3\kappa-1)\dfrac{2\sigma}{R_0}}{3\alpha_{g0}(1-\alpha_{g0})\rho_l}\,, \tag{8.140}$$

and ω_b is the natural frequency of a bubble in the cell

$$\omega_b^2 = \frac{\omega_M^2}{1-\alpha_{g0}^{1/3}}\,. \tag{8.141}$$

We note that ω_M is the natural frequency of a single bubble in an infinite liquid (i. e. the so-called Minnaert frequency),

$$\omega_M^2 = \frac{3\kappa p_0 + (3\kappa-1)\dfrac{2\sigma}{R_0}}{\rho_l R_0^2}\,. \tag{8.142}$$

In (8.139) the parameter δ_b represents the dissipation coefficient due to the liquid viscosity,

$$\delta_b = \frac{2\mu_l}{\rho_l R_0^2\left(1-\alpha_{g0}^{1/3}\right)}\,. \tag{8.143}$$

Actually acoustic wave damping in bubbly liquids occurs due to several different physical mechanisms:

Amazon
EX1010 Page 293

liquid viscosity, gas/vapor thermal diffusivity, acoustic radiation, etc. The contribution of each of these dissipation mechanisms to the total dissipation during bubble oscillations depends on frequency, bubble size, the type of gas in a bubble and liquid compressibility [8.94]. For convenience one can use an effective dissipation coefficient in the form of a viscous dissipation:

$$\delta_{\text{eff}} = \frac{2\mu_{\text{eff}}}{\rho_{\text{l}} R_0^2 \left(1-\alpha_{\text{g0}}^{1/3}\right)} , \tag{8.144}$$

where μ_{eff} denotes an effective viscosity (instead of just the liquid viscosity), which implicitly includes all the aforementioned dissipation mechanisms in a bubbly liquid. The value for μ_{eff} should be chosen to fit experimental observations and the theoretical data of amplitude versus frequency for a single bubble.

We can also linearize (8.133) and (8.134) to obtain

$$\frac{\partial \tilde{\rho}}{\partial t} + \rho_0 \nabla \cdot \mathbf{v} = 0 , \tag{8.145}$$

$$\rho_0 \frac{\partial \mathbf{v}}{\partial t} + \nabla \tilde{p} = 0 . \tag{8.146}$$

Combining the time derivative of (8.145) with the divergence of (8.146) results in

$$\frac{\partial^2 \tilde{\rho}}{\partial t^2} = \nabla^2 \tilde{p} . \tag{8.147}$$

Combining this result with (8.139) gives a wave equation for the bubbly liquid of the form

$$\frac{\partial^2 \tilde{p}}{\partial t^2} - C_{\text{b}}^2 \left(1 + \frac{2\delta_{\text{eff}}}{\omega_{\text{b}}^2}\frac{\partial}{\partial t} + \frac{1}{\omega_{\text{b}}^2}\frac{\partial^2}{\partial t^2}\right) \nabla^2 \tilde{p} = 0 . \tag{8.148}$$

Equation (8.148) describes the propagation of a linear acoustical pressure perturbations in a liquid with bubbles when the liquid can be treated as incompressible. It also accounts for the effect of a small but finite void fraction on wave propagation [8.9, 94, 95].

8.10.2 Compressible Liquids

When the pressure waves are very intense, and the void fraction is small ($\alpha_{\text{g}} \ll 1$), one should take into account liquid compressibility, which may lead to acoustic radiation by the oscillating bubbles. In this case, correction terms of $\alpha_{\text{g}}^{1/3}$, $\alpha_{\text{g}}^{4/3}$ in (8.128) may be neglected, and in order to account for acoustic radiation (8.128) should be rewritten as follows [8.99, 100]:

$$R\ddot{R} + \frac{3}{2}\dot{R}^2 = \frac{p_{\text{R}} - p}{\rho_{\text{l0}}} + \frac{R}{\rho_{\text{l0}} C_{\text{l}}}\frac{\text{d}}{\text{d}t}\left(p_{\text{R}} - p\right) , \tag{8.149}$$

where C_{l} is the speed of sound in the liquid. In (8.149) the liquid density, ρ_{l}, is taken as a constant ρ_{l0} although the equation of state of the liquid can be approximated as

$$p = p_0 + C_{\text{l}}^2 \left(\rho_{\text{l}} - \rho_{\text{l0}}\right) . \tag{8.150}$$

After linearization (8.149) becomes [compare with (8.136)]:

$$\tilde{p} = -\left[\left(p_0 + \frac{2\sigma}{R_0}\right)\frac{3\kappa}{R_0} - \frac{2\sigma}{R_0^2}\right]\tilde{R} - \frac{4\mu_{\text{l}}}{R_0}\frac{\partial \tilde{R}}{\partial t} - \rho_{\text{l0}} R_0 \left(1 + \frac{R_0}{C_{\text{l}}}\frac{\partial}{\partial t}\right)^{-1} \frac{\partial^2 \tilde{R}}{\partial t^2} . \tag{8.151}$$

In order to evaluate the last term in (8.151) and to incorporate acoustic radiation losses into an *effective* viscosity scheme we use the following approximation for the differential operator:

$$\left(1 + \frac{R_0}{C_{\text{l}}}\frac{\partial}{\partial t}\right)^{-1} \approx 1 - \frac{R_0}{C_{\text{l}}}\frac{\partial}{\partial t} . \tag{8.152}$$

Then (8.151) becomes

$$\tilde{p} \approx -\left[\left(p_0 + \frac{2\sigma}{R_0}\right)\frac{3\kappa}{R_0} - \frac{2\sigma}{R_0^2}\right]\tilde{R} - \frac{4\mu_{\text{l}}}{R_0}\frac{\partial \tilde{R}}{\partial t} - \rho_{\text{l0}} R_0 \frac{\partial^2 \tilde{R}}{\partial t^2} + \frac{\rho_{\text{l0}} R_0^2}{C_{\text{l}}}\frac{\partial^3 \tilde{R}}{\partial t^3} . \tag{8.153}$$

The third derivative in (8.153) can be estimated using the approximation of a freely oscillating bubble

$$\frac{\partial^2 \tilde{R}}{\partial t^2} \approx -\frac{\left(p_0 + \frac{2\sigma}{R_0}\right)\frac{3\kappa}{R_0} - \frac{2\sigma}{R_0^2}}{\rho_{\text{l0}} R_0}\tilde{R} . \tag{8.154}$$

Substituting (8.154) in the third-derivative term of (8.153) we get

$$\tilde{p} = -\left[\left(p_0 + \frac{2\sigma}{R_0}\right)\frac{3\kappa}{R_0} - \frac{2\sigma}{R_0^2}\right]\tilde{R} - \frac{4\mu_{\text{eff}}}{R_0}\frac{\partial \tilde{R}}{\partial t} - \rho_{\text{l0}} R_0 \frac{\partial^2 \tilde{R}}{\partial t^2} , \tag{8.155}$$

where

$$\mu_{\text{eff}} = \mu_{\text{l}} + \mu_{\text{r}}, \quad \mu_{\text{r}} = \frac{(3\kappa - 1)\sigma}{2C_{\text{l}}} + \frac{3\kappa p_0}{4C_{\text{l}}} R_0 . \tag{8.156}$$

It is easy to see from (8.156) that acoustic radiation may lead to a very large dissipation. For example, for

Amazon
EX1010 Page 294

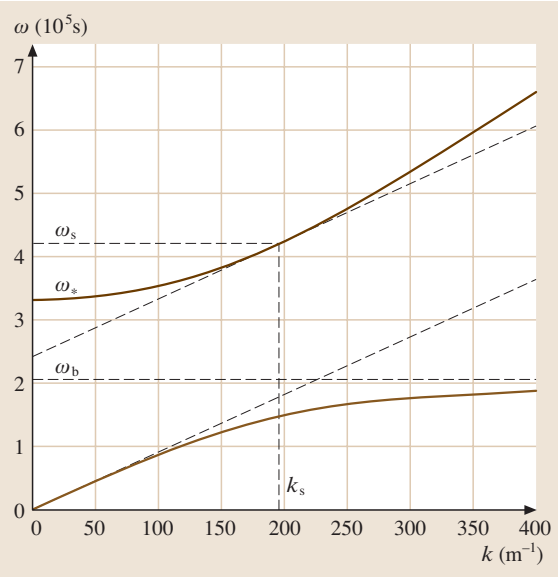


Fig. 8.13 The dispersion relation for water with air bubbles (the liquid is treated as compressible, dissipation is ignored): $C_l = 1500\,\mathrm{m/s}$, $p_0 = 10^5\,\mathrm{Pa}$, $\kappa = 1.4$, $\sigma = 0.0725\,\mathrm{N/m}$, $\rho_{l0} = 10^3\,\mathrm{kg/m}$, $\alpha_{g0} = 10^{-4}$, $R_0 = 10^{-4}\,\mathrm{m}$

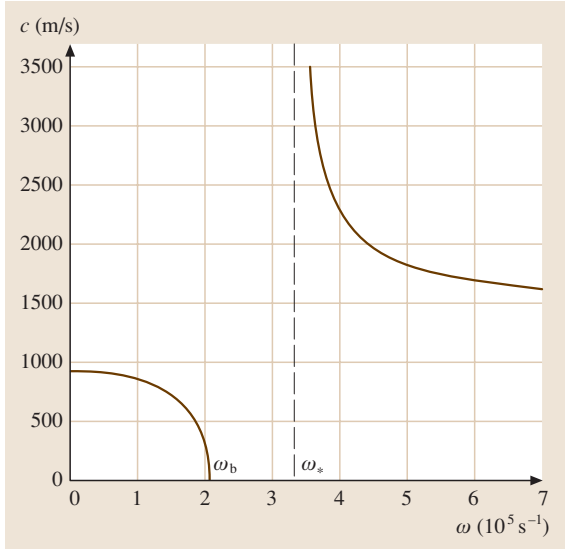


Fig. 8.14 The phase velocity for water with air bubbles (the liquid is treated as compressible, dissipation is ignored): $C_l = 1500\,\mathrm{m/s}$, $p_0 = 10^5\,\mathrm{Pa}$, $\kappa = 1.4$, $\sigma = 0.0725\,\mathrm{N/m}$, $\rho_{l0} = 10^3\,\mathrm{kg/m}$, $\alpha_{g0} = 10^{-4}$, $R_0 = 10^{-4}\,\mathrm{m}$

air bubbles of $R_0 = 10^{-4}$ m in water, effective viscosity due to acoustic radiation μ_r may be about seven times larger than the viscosity of water, μ_l.

Equation (8.135), and eventually its linearized form (8.137), are valid in the case of a compressible liquid. However, the linearized form of (8.122) changes. Now instead of (8.138) we have

$$\tilde{\rho} = \tilde{\rho}_l - 4\pi R_0^2 \rho_0 n_0 \tilde{R} \tag{8.157}$$

or, accounting for the liquid equation of state (8.150),

$$\tilde{\rho} = C_l^{-2}\tilde{p} - 4\pi R_0^2 \rho_0 n_0 \tilde{R}\,. \tag{8.158}$$

Substituting (8.158) into (8.147) we have

$$C_l^{-2}\frac{\partial^2 \tilde{p}}{\partial t^2} - \nabla^2 \tilde{p} = 4\pi R_0^2 n_0 \rho_0 \frac{\partial^2 \tilde{R}}{\partial t^2}\,. \tag{8.159}$$

Equation (8.159) together with (8.155) leads to the following wave equation for a bubbly fluid in the case of a compressible liquid:

$$\frac{\partial^2 \tilde{p}}{\partial t^2} - C_b^2\left(1 + \frac{2\delta_{\mathrm{eff}}}{\omega_b^2}\frac{\partial}{\partial t} + \frac{1}{\omega_b^2}\frac{\partial^2}{\partial t^2}\right)\times \left(\nabla^2 - C_l^{-2}\frac{\partial^2}{\partial t^2}\right)\tilde{p} = 0\,. \tag{8.160}$$

Here ω_b and δ_{eff} are calculated according to (8.141) and (8.144) in which α_{g0} is taken to be zero, and C_b is calculated according to (8.140). It is easy to see that (8.160) reduces to (8.148) in the case when $C_l \to \infty$.

The linear wave equation (8.160) admits the harmonic wave-train solution

$$\tilde{p} = p_a \exp\left[\mathrm{i}(kx - \omega t)\right]\,, \tag{8.161}$$

in which the frequency ω and wave number k are related through the following dispersion relation

$$k^2 = \omega^2\left(\frac{1}{C_l^2} + \frac{1}{C_b^2\left(1 + \mathrm{i}\dfrac{2\omega\delta_{\mathrm{eff}}}{\omega_b^2} - \dfrac{\omega^2}{\omega_b^2}\right)}\right)\,. \tag{8.162}$$

The graph of this dispersion relation is shown in Fig. 8.13. The corresponding phase velocity is given in Fig. 8.14.

8.10.3 Low-Frequency Waves: The Korteweg–de Vries Equation

In order to analyze the low-frequency nonlinear acoustics of a bubbly liquid the low-frequency limit of the

Amazon
EX1010 Page 295

dispersion relation (8.162) is first considered:

$$\omega = Ck + \mathrm{i}\alpha_1 k^2 - \alpha_2 k^3 \,, \tag{8.163}$$

where

$$\frac{1}{C^2} = \frac{1}{C_1^2} + \frac{1}{C_\mathrm{b}^2}, \quad \alpha_1 = \frac{\delta_\mathrm{eff} C^4}{\omega_\mathrm{b}^2 C_\mathrm{b}^2}, \quad \alpha_2 = \frac{C^5}{2C_\mathrm{b}^2 \omega_\mathrm{b}^2} \,. \tag{8.164}$$

Noting that

$$\omega = -\mathrm{i}\frac{\partial}{\partial t}, \quad k = \mathrm{i}\frac{\partial}{\partial x} \,, \tag{8.165}$$

(8.163) can be treated as the Fourier-space equivalent of an operator equation which when operating on $\tilde{p}$, yields

$$\frac{\partial \tilde{p}}{\partial t} + C\frac{\partial \tilde{p}}{\partial x} - \alpha_1 \frac{\partial^2 \tilde{p}}{\partial x^2} + \alpha_2 \frac{\partial^3 \tilde{p}}{\partial x^3} = 0 \,. \tag{8.166}$$

Equation (8.166) should be corrected to account for weak nonlinearity. A systematic derivation is normally based on the *multiple-scales* technique [8.101]. Here we show how this derivation can be done less rigorously, but more simply. We assume that the nonlinearity in bubbly liquids comes only from bubble dynamics. Then (8.155) for weakly nonlinear bubble oscillations has an additional nonlinear term and becomes:

$$\tilde{p} = -B_1 \tilde{R} + B_2 \tilde{R}^2 - \frac{4\mu_\mathrm{eff}}{R_0}\frac{\partial \tilde{R}}{\partial t} - \rho_{l0} R_0 \frac{\partial^2 \tilde{R}}{\partial t^2} \,. \tag{8.167}$$

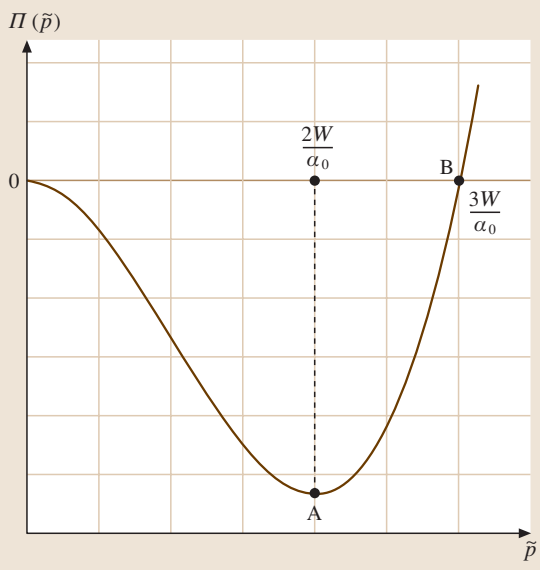


Fig. 8.15 The potential well used to illustrate the "soliton" solution for the KdV equation

$$B_1 = \left(p_0 + \frac{2\sigma}{R_0}\right)\frac{3\kappa}{R_0} - \frac{2\sigma}{R_0^2},$$
$$B_2 = \left(p_0 + \frac{2\sigma}{R_0}\right)\frac{3\kappa(3\kappa+1)}{2R_0^2} - \frac{2\sigma}{R_0^3} \,. \tag{8.168}$$

Equation (8.167) has to be combined with the linear wave equation (8.159), which in the case of plane waves can be written:

$$C_1^{-2}\frac{\partial^2 \tilde{p}}{\partial t^2} - \frac{\partial^2 \tilde{p}}{\partial x^2} = 4\pi R_0^2 n_0 \rho_0 \frac{\partial^2 \tilde{R}}{\partial t^2} \,. \tag{8.169}$$

Taking into account that all the terms except the first one on the right-hand side of (8.167) are small, i. e., of the second order of magnitude, one can derive the following nonlinear wave equation for pressure perturbations in a bubbly liquid:

$$C^{-2}\frac{\partial^2 \tilde{p}}{\partial t^2} - \frac{\partial^2 \tilde{p}}{\partial x^2} = 4\pi R_0^2 n_0 \rho_0 \times \left(\frac{B_2}{B_1^3}\frac{\partial^2 \tilde{p}^2}{\partial t^2} + \frac{4\mu_\mathrm{eff}}{R_0 B_1^2}\frac{\partial^3 \tilde{p}}{\partial t^3} + \frac{\rho_{l0} R_0}{B_1^2}\frac{\partial^4 \tilde{p}}{\partial t^4}\right) \,. \tag{8.170}$$

Equation (8.170) is derived for plane weakly nonlinear pressure waves traveling in a bubbly liquid in both directions. Namely, the left part of this equation contains a classic wave operator when applied to a pressure perturbation function describes waves traveling left to right and right to left. The right part of this equation contain terms of second order of smallness and is therefore responsible for a slight change of these waves. Thus, (8.170) may be structured as follows:

$$\left(C^{-1}\frac{\partial}{\partial t} + \frac{\partial}{\partial x}\right)\left(C^{-1}\frac{\partial}{\partial t} - \frac{\partial}{\partial x}\right)\tilde{p} = O\left(\varepsilon^2\right) \,. \tag{8.171}$$

If one considers only waves traveling left to right then

$$C^{-1}\frac{\partial}{\partial t} + \frac{\partial}{\partial x} = O\left(\varepsilon\right) \,, \tag{8.172}$$

and we can use the following derivative substitution (see [8.10])

$$\frac{\partial}{\partial t} \approx -C\frac{\partial}{\partial x} \,. \tag{8.173}$$

Then, after one time integration over space, and translation to the frame moving left to right with

Amazon
EX1013 Page 296

a speed of sound C, (8.170) leads to the Burgers–Korteweg–de Vries (BKdV) equation for a pressure wave [8.94–96, 102]:

$$\frac{\partial \tilde{p}}{\partial t} + \alpha_0 \tilde{p} \frac{\partial \tilde{p}}{\partial \xi} - \alpha_1 \frac{\partial^2 \tilde{p}}{\partial \xi^2} + \alpha_2 \frac{\partial^3 \tilde{p}}{\partial \xi^3} = 0, \quad \xi = x - Ct\,, \tag{8.174}$$

where

$$\alpha_0 = \frac{C^3}{C_b^2} \cdot \frac{B_2}{B_1^2} \tag{8.175}$$

and the parameters α_1, α_2, and C are presented in (8.164).

Let us first discuss a nondissipative case, $\alpha_1 = 0$. Then (8.174) is called the Korteweg–de Vries (KdV) equation. The low-frequency dispersion relation (8.163) shows that every Fourier component of initial arbitrary pressure perturbation propagates with its own speed, and the shape of the acoustic signal changes. Since $\alpha_2 > 0$, the long-wavelength waves propagate with higher speed than lower-wavelength waves. This means that dispersion may begin to compete with nonlinearity, which stops shock-wave formation. The competition between dispersion and nonlinearity leads to the formation of a so-called *soliton*.

In order to derive the shape of soliton, here we consider a steady solution of (8.174) in the moving frame

$$\eta = \xi - Wt\,. \tag{8.176}$$

Then, assuming that there is no pressure perturbation at infinity, (8.174) can be reduced as follows:

$$\alpha_2 \frac{d^2 \tilde{p}}{d\eta^2} = -\frac{\partial \Pi}{\partial \tilde{p}}, \quad \Pi(\tilde{p}) = -\frac{W\tilde{p}^2}{2} + \frac{\alpha_0 \tilde{p}^3}{6}\,. \tag{8.177}$$

It is instructive to use the analogy that (8.177) is similar to the equation of a point-like particle in a potential well shown schematically in Fig. 8.15. The structure of the pressure *solitary* wave can be viewed as follows: initially the particle is at point O, which corresponds to the fact that far away the pressure perturbation is equal to zero; then the particle slides down to the bottom of the potential well, point A, and due to a conservation law climbs up to point B; at point B it stops and moves all the way back to point O. The solution of (8.177) represents the shape of the soliton, which in the immovable frame is

$$\tilde{p} = \frac{3W}{\alpha_0} \cosh^{-2}\left\{\sqrt{\frac{W}{4\alpha_2}}\,[x - (C + W)t]\right\}\,. \tag{8.178}$$

It was mentioned above that a soliton may be interpreted as a result of the balance between two competitors: nonlinearity and dispersion. To consider this competition in more detail the KdV equation is considered in the frame moving with the speed of sound in a bubbly liquid

$$\frac{\partial \tilde{p}}{\partial t} + \alpha_0 \tilde{p} \frac{\partial \tilde{p}}{\partial \xi} + \alpha_2 \frac{\partial^3 \tilde{p}}{\partial \xi^3} = 0, \quad \xi = x - Ct\,. \tag{8.179}$$

Then the solitary wave has the following shape:

$$\tilde{p} = \frac{3W}{\alpha_0} \cosh^{-2}\left\{\sqrt{\frac{W}{4\alpha_2}}\,(\xi - Wt)\right\} \tag{8.180}$$

with a pressure amplitude equal to $3W/\alpha_0$ and a thickness of about $\sqrt{\alpha_2/W}$.

In order to evaluate the effect of nonlinearity let us consider the simple nonlinear equation

$$\frac{\partial \tilde{p}}{\partial t} + \alpha_0 \tilde{p} \frac{\partial \tilde{p}}{\partial \xi} = 0\,. \tag{8.181}$$

The factor $\alpha_0 \tilde{p}$ stands for the velocity of transportation of pressure perturbations. Thus, part of the pressure profile which has higher pressure will be translated faster than the part which has lower pressure. According to the solitary solution (8.180) the maximum translation velocity is equal to $3W$. The time needed for the pressure peak to be translated the distance of about the thickness of the pressure wave can be estimated as $t_{nl} \sim \alpha_2^{1/2} W^{-3/2}$. This amount of time would be needed to transform the smooth solitary shape to a shock wave.

In order to evaluate the effect of dispersion let us consider the simple dispersive equation

$$\frac{\partial \tilde{p}}{\partial t} + \alpha_2 \frac{\partial^3 \tilde{p}}{\partial \xi^3} = 0\,. \tag{8.182}$$

This equation admits harmonic wave-train solutions of the form $\exp(ik\xi + i\alpha_2 k^3 t)$. The characteristic wave numbers contributing to the wave shape of thickness $\sqrt{\alpha_2/W}$ are $k \sim \sqrt{W/\alpha_2}$. Such wave numbers will gradually change the wave phase on π and thus lead to a substantial deformation of the wave shape. The time interval needed for this, t_d, is calculated as follows: $\alpha_2 \left(\sqrt{W/\alpha_2}\right)^3 t_d = \pi$, thus, $t_d \sim \alpha_2^{1/2} W^{-3/2}$, which is $\sim t_{nl}$. So, the time that is needed for nonlinearity to transform the solitary wave into a shock wave is equal to the time taken for dispersion to smooth out this wave.

One of the most important results obtained from the BKdV equation is the prediction of an oscillatory shock wave. In order to derive the shape of an oscillatory shock wave we again consider the steady-state solution

Amazon
EX1010 Page 297

of (8.174) in the moving frame (8.176). Then, assuming that there is no pressure perturbation at infinity, (8.174) can be reduced to

$$\alpha_2 \frac{\mathrm{d}^2\tilde{p}}{\mathrm{d}\eta^2} - \alpha_1 \frac{\mathrm{d}\tilde{p}}{\mathrm{d}\eta} = -\frac{\partial \Pi}{\partial \tilde{p}} ,$$
$$\Pi(\tilde{p}) = -\frac{W\tilde{p}^2}{2} + \frac{\alpha_0 \tilde{p}^3}{6} . \qquad (8.183)$$

Equation (8.183) represents the equation of a point-like particle in a potential well shown schematically in Fig. 8.15 with friction. Here $\tilde{p}$ stands for the coordinate of the particle, minus ξ stands for the time (time passes from $-\infty$ to $+\infty$), α_2 is the mass of the particle, and α_1 is the friction coefficient. An oscillatory shock wave corresponds to motion of the particle from point O to the bottom of potential well (point A) with some decaying oscillations around the bottom. Thus, the amplitude of the shock wave is equal to $2W/\alpha_0$. Eventually oscillations take place only for relatively small values of the friction coefficient α_1. To derive a criterion for an oscillatory shock wave one should investigate a solution of (8.183) in close vicinity to point A. Assuming that

$$\tilde{p} = \frac{2W}{\alpha_0} + \psi(\xi) , \qquad (8.184)$$

where ψ is small, and linearizing (8.183) we get

$$\alpha_2 \frac{\mathrm{d}^2\psi}{\mathrm{d}\xi^2} - \alpha_1 \frac{\mathrm{d}\psi}{\mathrm{d}\xi} + W\psi = 0 . \qquad (8.185)$$

Equation (8.185) has a solution

$$\psi = A_1 \exp(-\lambda\xi) + A_2 \exp(\lambda\xi),$$
$$\lambda = \frac{\alpha_1}{2\alpha_2} \pm \sqrt{\frac{\alpha_1^2}{4\alpha_2^2} - \frac{W}{\alpha_1}} . \qquad (8.186)$$

It is easy to see that the shock wave has an oscillatory structure if

$$\alpha_1 < \sqrt{4\alpha_2 W} . \qquad (8.187)$$

In terms of the bubbly fluid parameters, (8.187) gives a critical effective viscosity

$$\mu_{\mathrm{eff}} < \mu_{\mathrm{crit}} = \rho_1 R_0^2 \omega_{\mathrm{b}} \frac{C_{\mathrm{b}}}{C} \sqrt{\frac{1}{2}\frac{W}{C}} . \qquad (8.188)$$

The KdV equation for describing the evolution of long-wavelength disturbances in an ideal liquid with adiabatic gas bubbles was first proposed in [8.102]. The solitons and shock waves in bubbly liquids were systematically investigated in [8.95] in the framework of the BKdV equation. Good correlation with experimental data was obtained. In [8.94] wave-propagation phenomena in bubbly liquids were analyzed using a more advanced and complete mathematical model that is valid for higher intensities of pressure waves. In [8.103] the effect of polydispersivity on long small-amplitude nonlinear waves in bubbly liquids was considered. It was shown that evolution equations of BKdV type can be applied for modeling of such waves. In particular, it was shown that for polydisperse bubbly liquids an effective monodisperse liquid model can be used with the bubble sizes found as ratios of some bubble size-distribution moments and corrections to the equation coefficients.

8.10.4 Envelopes of Wave Trains: The Nonlinear Schrödinger Equation

When the amplitude of an acoustic wave in a fluid is small enough the respective linearized system of equations will admit the harmonic wave-train solution

$$u = a \exp\{\mathrm{i}[kx - \omega(k)t]\} . \qquad (8.189)$$

If the amplitude is not small enough the nonlinearity cannot be neglected. The nonlinear terms produce higher harmonics, which react back on the original wave. Thus, the effect of nonlinearity on this sinusoidal oscillation is to cause a variation in its amplitude and phase in both space and time. This variation can be considered as small (in space) and slow (in time) for off-resonant situations. To account for a variation of amplitude and phase it is convenient to consider the amplitude as a complex function of space and time A.

Here we follow [8.104] to show what kind of equation arises as the evolution equation for a carrier-wave envelope in a general dispersive system. A linear system has a dispersion relation which is independent of the wave amplitude

$$\omega = \omega(k) . \qquad (8.190)$$

However, it is instructive to assume that the development of a harmonic wave in a weakly nonlinear system can be represented by a dispersion relation which is amplitude dependent

$$\omega = \omega(k, |A|^2) . \qquad (8.191)$$

Such a situation was initially uncovered in nonlinear optics and plasma where the refractive index or dielectric constant of a medium may be dependent on the electric field. That same situation occurs in bubbly liquids as well.

Amazon
EX1010 Page 298

Let us consider a carrier wave of wave number k_0 and frequency $\omega_0 = \omega(k_0)$. A Taylor expansion of the dispersion relation (8.191) around k_0 gives

$$\Omega = \left(\frac{\partial\omega}{\partial k}\right)_0 K + \frac{1}{2}\left(\frac{\partial^2\omega}{\partial k^2}\right)_0 K^2 + \left(\frac{\partial\omega}{\partial(|A|^2)}\right)_0 |A|^2 , \tag{8.192}$$

where $\Omega = \omega - \omega_0$ and $K = k - k_0$ are the frequency and wave number of the variation of the wave-train amplitude. Equation (8.192) represents a dispersion relation for the complex amplitude modulation. Noting that

$$\Omega = -\mathrm{i}\frac{\partial}{\partial t}, \quad K = \mathrm{i}\frac{\partial}{\partial x} , \tag{8.193}$$

(8.192) can be treated as the Fourier-space equivalent of an operator equation that when operating on A yields

$$\mathrm{i}\left[\frac{\partial}{\partial t} + \left(\frac{\partial\omega}{\partial k}\right)_0 \frac{\partial}{\partial x}\right] A + \frac{1}{2}\left(\frac{\partial^2\omega}{\partial k^2}\right)_0 \frac{\partial^2 A}{\partial x^2} - \left(\frac{\partial\omega}{\partial(|A|^2)}\right)_0 |A|^2 A = 0 . \tag{8.194}$$

In the frame moving with group velocity

$$\xi = x - C_\mathrm{g} t, \quad C_\mathrm{g} = (\partial\omega/\partial k)_0 , \tag{8.195}$$

(8.194) represent the classical nonlinear Schrödinger (NLS) equation

$$\mathrm{i}\frac{\partial A}{\partial t} = \beta_\mathrm{d}\frac{\partial^2 A}{\partial\xi^2} + \gamma_\mathrm{n}|A|^2 A , \tag{8.196}$$

$$\beta_\mathrm{d} = -\frac{1}{2}\left(\frac{\partial^2\omega}{\partial k^2}\right)_0 , \quad \gamma_\mathrm{n} = \left(\frac{\partial\omega}{\partial(|A|^2)}\right)_0 , \tag{8.197}$$

which describes the evolution of wave-train envelopes.

Here A is a complex amplitude that can be represented as follows:

$$A(t,\xi) = a(t,\xi)\exp[\mathrm{i}\varphi(t,\xi)] , \tag{8.198}$$

where a and φ are the (real) amplitude and phase of the wave train. A spatially uniform solution of (8.196) corresponds to an unperturbed wave train. To analyze the stability of this uniform solution let us represent (8.196) as a set of two scalar equations:

$$-a\frac{\partial\varphi}{\partial t} = \beta_\mathrm{d}\left[\frac{\partial^2 a}{\partial\xi^2} - a\left(\frac{\partial\varphi}{\partial\xi}\right)^2\right] + \gamma_\mathrm{n} a^3 , \tag{8.199}$$

$$\frac{\partial a}{\partial t} = \beta_\mathrm{d}\left(2\frac{\partial a}{\partial\xi}\frac{\partial\varphi}{\partial\xi} + a\frac{\partial^2\varphi}{\partial\xi^2}\right) . \tag{8.200}$$

It is easy to verify that a spatially uniform solution ($\partial/\partial\xi \equiv 0$) of (8.199) and (8.200) is:

$$a = a_0, \quad \varphi = -\gamma_\mathrm{n} a_0^2 t . \tag{8.201}$$

The evolution of a small perturbation of this uniform solution

$$a = a_0 + \tilde{a}, \quad \varphi = -\gamma_\mathrm{n} a_0^2 t + \tilde{\varphi} , \tag{8.202}$$

is given by the following linearized equations:

$$a_0\frac{\partial\tilde{\varphi}}{\partial t} + \beta_\mathrm{d}\frac{\partial^2\tilde{a}}{\partial\xi^2} + 2\gamma_\mathrm{n} a_0^2\tilde{a} = 0 . \tag{8.203}$$

$$\frac{\partial\tilde{a}}{\partial t} - \beta_\mathrm{d} a_0\frac{\partial^2\tilde{\varphi}}{\partial\xi^2} = 0 . \tag{8.204}$$

Now let us consider the evolution of a periodic perturbation with wavelength $L = 2\pi/K$ that can be written as

$$\begin{pmatrix}\tilde{a}\\ \tilde{\varphi}\end{pmatrix} = \begin{pmatrix}a_1\\ \varphi_1\end{pmatrix}\exp(\sigma t + \mathrm{i}K\xi) . \tag{8.205}$$

The stability of the uniform solution depends on the sign of the real part of the growth-rate coefficient σ. To compute σ we substitute the perturbation (8.205) into the linearized equations (8.203) and (8.204) and obtain the following formula for σ

$$\sigma^2 = \beta_\mathrm{d}^2 K^2\left(\frac{2\gamma_\mathrm{n}}{\beta_\mathrm{d}} a_0^2 - K^2\right) . \tag{8.206}$$

This shows that the sign of the $\beta_\mathrm{d}\gamma_\mathrm{n}$ product is crucial for wave-train stability. If $\beta_\mathrm{d}\gamma_\mathrm{n} < 0$ then σ is always an imaginary number, and a uniform wave train is stable to small perturbations of any wavelength; if $\beta_\mathrm{d}\gamma_\mathrm{n} > 0$ then in the case that

$$K < K_\mathrm{cr} = \sqrt{\frac{2\gamma_\mathrm{n}}{\beta_\mathrm{d}}}\, a_0 \tag{8.207}$$

σ is real, and a long-wavelength instability occurs.

This heuristic derivation shows how the equation for the evolution of the wave-train envelope arises. The NLS equation has two parameters: β_d, γ_n. Eventually, the parameter β_d can be calculated from the linear dispersion relation discussed in detail earlier. However, the parameter γ_n has to be calculated from more-systematic, nonlinear arguments.

The general method of derivation is often given the name of the *method of multiple scales* [8.101]. A specific multiscale technique for weakly nonlinear oscillations of bubbles was developed in [8.105, 106]. This technique has been applied to analyze pressure-wave propagation in bubbly liquids.

In [8.107] the NLS equation describing the propagation of weakly nonlinear modulation waves in bubbly liquids was obtained for the first time. It was derived

Amazon
EX1010 Page 299

using the multiple asymptotic technique from the governing continuum equations for bubbly liquids presented in detail in this chapter. The NLS equation was applied for determination of the regions of modulation stability/instability in the parametric plane for mono- and polydisperse bubbly liquids.

To understand the behavior of the coefficients of the NLS equation one can consider the simplified model of a monodisperse system presented before. For this we note that the dispersion relation for bubbly liquids with compressible carrier liquid has two branches (Fig. 8.13). The low-frequency branch is responsible for bubble compressibility, and the high-frequency branch is due to liquid compressibility.

The first (low-frequency) branch corresponds to frequencies from zero to ω_b, which is the resonance frequency for bubbles of given size, the second (high-frequency) branch corresponds to frequencies from some $\omega_\star$ to infinity. There are no solutions in the form of spatially oscillating waves for frequencies between ω_b and $\omega_\star$; in this range there are exponentially decaying solutions only. This region is known as the *window of acoustic non-transparency*.

The coefficient β_d is calculated as shown in (8.197). For bubbly liquids this quantity is always positive for the low-frequency branch and always negative for the high-frequency branch.

The coefficient γ_n (see (8.197)) represents the nonlinearity of the system and is a complicated function of frequency ω. If it is positive, then long-wavelength modulation instability occurs. An important region of instability appears near the frequency ω_s, where $C_g(\omega_s) = C_e$, with C_e being the equilibrium speed of sound ($C_e = \omega/k$ for $\omega \to 0$).

For such frequencies the coefficient γ_n has a singularity and changes sign when the frequency is changing around this point. Physically this corresponds to the Benjamin–Feir instability, and can be explained by transfer of energy from mode 0 (DC mode, or mode of zero frequency, for which perturbations propagate with velocity C_e) to the principal mode of the wave train, which moves with the group velocity C_g.

Accounting for a small dissipation in bubbly liquids leads to the Landau–Ginzburg equation, which describes how the wave amplitude should decay due to dissipation. This part includes the dissipation effect due to viscosity and due to internal bubble heat transfer. The difference between the viscous and thermal effects for bubbles is that for an oscillating bubble there is a $\pi/2$ shift in phase between the bubble volume and the heat flux, while the loss of energy due to viscous dissipation occurs in phase with bubble oscillation. This phase shift results in the effect that the pressure in the mixture has some additional shift in phase relative to the mixture density (determined mainly by the bubble volume). This, in fact, can be treated as a weak dispersive effect and included to the dispersion relation in the third-order approximation.

It is interesting to note that the system of governing equations presented can be also obtained as Euler equations for some Lagrangian [8.108, 109]. The variation formulation might be very useful for the analysis of nonlinear acoustics phenomena in bubbly liquids.

8.10.5 Interaction of Nonlinear Waves. Sound–Ultrasound Interaction

The nature of the interactions among individual wave components is quite simple and can be explained by considering the nature of dispersive waves in general.

Suppose u represents some property of the fluid motion, for example the fluid velocity. Then infinitesimal (linear) plane one-dimensional sound waves in a pure liquid are governed by the classical linear wave equation

$$\frac{\partial^2 u}{\partial t^2} - c^2 \frac{\partial^2 u}{\partial x^2} = 0 \,, \tag{8.208}$$

where c is the speed of sound. This equation has elementary solutions of the type

$$u = A \exp[\mathrm{i}(kx \pm \omega t)], \quad \omega = ck \,, \tag{8.209}$$

describing the propagation of a sinusoidal wave with a definite speed c independent of the wavelength ($\lambda = 2\pi/k$, k is the wavenumber). These waves are called nondispersive.

However, many of the waves encountered in fluids do not obey the classical wave equation, and their phase velocity may not be independent of the wavenumber. An example is wave propagation in bubbly liquids.

More generally, for an infinitesimal disturbance, the governing equation is of the type

$$\mathrm{L}(u) = 0 \,, \tag{8.210}$$

where L is a linear operator involving derivatives with respect to position and time. The form of this operator depends upon the fluid system and the particular type of wave motion considered. Again, this linear equation admits solutions of the form

$$u = A \exp[\mathrm{i}(kx \pm \omega t)] \,, \tag{8.211}$$

provided that ω and k satisfy a so-called dispersion relation

$$D(\omega, k) = 0 \tag{8.212}$$

Amazon
EX1010 Page 300

that is characteristic for the fluid system and of the type of wave motion considered.

These infinitesimal wave solutions are useful since in many circumstances the nonlinear effects are weak. Thus, the infinitesimal amplitude solution in many cases represents a very useful first approximation to the motion. The interaction effects can be accounted for by considering an equation of the form

$$\mathrm{L}(u) = \epsilon \mathrm{N}(u) \,, \tag{8.213}$$

where N is some nonlinear operator whose precise nature again depends upon the particular fluid system considered, and ϵ is a small parameter characterizing the amplitude of the motion. Solutions to this equation can be built by successive approximation.

Let us consider two interacting wave trains, given to a first approximation by solutions to the linear equation (8.210):

$$\begin{aligned} u_1 &= A_1 \exp[\mathrm{i}(k_1 x - \omega_1 t)] \,, \\ u_2 &= A_2 \exp[\mathrm{i}(k_2 x - \omega_2 t)] \,, \end{aligned} \tag{8.214}$$

where the individual wave numbers and frequencies are related by the dispersion relation (8.212): $D(\omega_i, k_i) = 0$; $i = 1, 2$. These expressions are to be substituted into the small nonlinear term $\epsilon \mathrm{N}(u)$ of (8.213).

If the lowest-order nonlinearity is quadratic, this substitution leads to expressions of the type

$$\sim \exp \mathrm{i}[(k_1 \pm k_2)x - (\omega_1 \pm \omega_2)t] \,. \tag{8.215}$$

These terms act as a small-amplitude forcing function to the linear system and provide an excitation at the wave numbers ($k_3 = k_1 \pm k_2$) and frequencies ($\omega_3 = \omega_1 \pm \omega_2$). In general, the response of the linear system to this forcing is expected to be small ($\sim \epsilon$). However, if the wavelength and frequency of the forcing are related by the dispersion relation (8.212) as well: $D(\omega_3, k_3) = 0$, then we have a case which normally is referred to as nonlinear resonance wave interaction. Similarly to a well-known resonance behavior of a linear oscillator, the amplitude of the third component

$$u_3 = A_3 \exp[\mathrm{i}(k_3 x - \omega_3 t)] \tag{8.216}$$

grows linearly at the beginning. Later the energy drain from the first two components begins to reduce their amplitudes and consequently the amplitude of the forcing function.

Let us now consider a set of three wave trains undergoing resonant interactions. The solutions representing these wave trains would be expected to look like the solutions of the linear problem, although the amplitudes $A_i (i = 1, 2, 3)$ may possibly vary slowly with time:

$$\begin{aligned} u = \sum_{i=1}^{3} \big\{ & A_i(\epsilon t) \exp[\mathrm{i}(k_i x - \omega_i t)] \\ & + A_i^*(\epsilon t) \exp[-\mathrm{i}(k_i x - \omega_i t)] \big\} \,. \end{aligned} \tag{8.217}$$

Here it is used that u is necessarily real. Substitution of this set into (8.213) with subsequent averaging over a few wavelengths leads to a system of equations for the amplitudes of the interacting wave trains. This system basically describes the energy balance between these wave components.

Thus, the existence of energy transfer of this kind clearly depends upon the existence of these resonance conditions. The classic example of dispersion relations which allow for such resonance conditions are capillary gravity waves on the surface of deep water [8.110]. This example, however, is far from the scope of the present section.

In this section the nonlinear acoustics of liquids with bubbles is discussed as an example of a multiphase fluids with complicated and pronounced nonlinearity and dispersion. The dispersion encountered there may also lead to a special nonlinear wave interaction called *long-wave–short-wave resonance* in this context.

In [8.111] it was suggested a new form of triad resonance between three waves of wave numbers k_1, k_2, and k_3 and frequencies ω_1, ω_2, and ω_3, respectively, such that

$$k_1 = k_2 + k_3, \quad \omega_1 = \omega_2 + \omega_3 \,. \tag{8.218}$$

It was suggested to consider k_1 and k_2 to be very close: $k_1 = k + \varepsilon$, $k_2 = k - \varepsilon$ and $k_3 = 2\varepsilon$ ($\varepsilon \ll k$). The resonance conditions (8.218) are automatically achieved if

$$\omega(k + \varepsilon) - \omega(k - \varepsilon) = \omega_3 \tag{8.219}$$

or

$$2\varepsilon \frac{\mathrm{d}\omega}{\mathrm{d}k} = \omega_3 \,. \tag{8.220}$$

That means the group velocity of the short wave (wave number k) equals the phase velocity of the long wave (wave number 2ε). It is called the long-wave–short-wave resonance. At first sight this resonance would appear hard to achieve but it is clearly possible from Fig. 8.13.

Let us identify the lower (or low-frequency) and upper (or high-frequency) branches of the dispersion relation with subscripts "−" and "+", respectively. The

Amazon
EX1010 Page 301

long-wave asymptotics of the low-frequency branch, $\omega_l(k_l) = \omega_- \,|_{k\to 0}$, and the short-wave asymptotics of the high-frequency branch, $\omega_s(k_s) = \omega_+ \,|_{k\to\infty}$, can be written as follows:

$$\omega_l = c_e k_l + O(k_l^3), \quad \omega_s = c_f k_s + O(k_s^{-1}) \,, \quad (8.221)$$

where

$$c_e = \frac{\omega_l}{k_l}\,|_{k_l\to 0}, \quad c_f = \frac{d\omega_s}{dk_s}\,|_{k_s\to\infty} \,, \quad (8.222)$$

are the *equilibrium* and the *frozen* speeds of sound in the bubbly mixture.

It is easy to see that dispersion relation (8.162) allows the existence of the long-wave–short-wave resonance. Since $c_f > c_e$, there is always some wave number k_s and frequency ω_s (Fig. 8.13) such that its group velocity is equal to the equilibrium velocity of the mixture.

It should be noted that the long-wave–short-wave resonance in bubbly liquids has nothing to do with the resonance of bubble oscillations. Suppose we consider water with air bubbles of radius $R_0 = 0.1$ mm under normal conditions ($p_0 = 0.1$ MPa, $\rho_{l0} = 10^3$ kg/m^3) and with a volume gas content $\alpha_{g0} = 2.22\times 10^{-4}$. The wavelengths of the short and long waves are then $\lambda_s \approx 0.67$ cm and $\lambda_l \approx 6.7$ m, respectively. The equilibrium speed of sound is $c_e \approx 730$ m/s. Thus, the frequency of the long wave is $f_l = c_e/\lambda_l \approx 110$ Hz (audible sound). Obviously, the short-wave frequency $f_s \geq 35.6$ kHz lies in the ultrasound region. Moreover, a decrease in the bubble radius R_0 leads to increasing the short-wave frequency f_s. Hence, the long-wave–short-wave interaction in a bubbly fluid can be considered as the interaction of ultrasound and audible sound propagating in this medium.

The long-wave–short-wave resonance interaction for pressure waves in bubbly liquids was investigated in [8.112–115] using the method of multiple scales. In particular, it was shown that in a nondissipative bubbly medium this type of resonance interaction is described by the following equations [8.116]

$$\frac{\partial L}{\partial \tau} + \frac{\alpha}{2c_e}\frac{\partial |S|^2}{\partial \xi} = 0, \quad i\frac{\partial S}{\partial \tau} + \beta\frac{\partial^2 S}{\partial \xi^2} = \delta L S, \quad (8.223)$$

where L and S are normalized amplitudes of the long- and short-wave pressure perturbations, τ is the (slow) time and ξ is the space coordinate in the frame moving with the group velocity; α and β are parameters of interaction.

It turns out that in bubbly fluids, parameters of interaction can vanish simultaneously at some specific ultrasound frequency [8.115]. The interaction between sound and ultrasound is then *degenerate*, i. e., the equations for interaction are separated. However, such a degeneracy does not mean the absence of interaction. The quasi-monochromatic ultrasonic signal will still generate sound but of much smaller intensity than in the nondegenerate case.

8.11 Sonoluminescence

Sound waves not only give rise to self-steepening and shock waves but may even become the driving agent to the emission of light, a phenomenon called sonoluminescence that is mediated by bubbles in the liquid that are driven to strong oscillations and collapse [8.20–30]. The detection of the conditions where a single bubble can be trapped in the pressure antinode of a standing sound wave [8.117] has furthered this field considerably. In Fig. 8.16 a basic arrangement for single-bubble sonoluminescence (SBSL) can be seen where a bubble is trapped in a rectangular container filled with water.

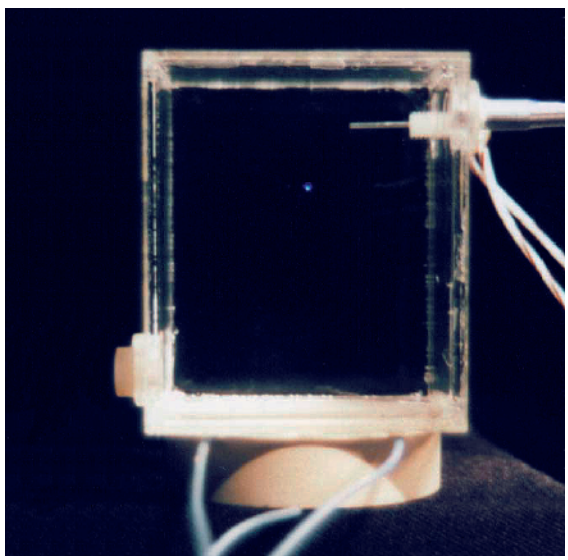


Fig. 8.16 Photograph of a rectangular container with light-emitting bubble. There is only one transducer glued to the bottom plate of the container (dimensions: 50 mm × 50 mm × 60 mm). The piezoelectric transducer (dimensions: height 12 mm, diameter 47 mm) sets up a sound field of high pressure (approx. 1.3 bar) at a frequency of approx. 21 kHz. (Courtesy of R. Geisler)

Amazon
EX1010 Page 302

The sound field is produced by a circular disc of piezoelectric material glued to the bottom of the container. The bright spot in the upper part of the container is the light from the bubble. It is of blueish white color. The needle sticking out into the container in the upper left part of the figure is a platinum wire for producing a bubble via a current pulse. The bubble is then driven via acoustic radiation forces into its position where it is trapped almost forever. The bubble exerts large oscillations that can be photographed [8.118]. Figure 8.17 shows a sequence of the bubble oscillation of a light-emitting bubble. A full cycle is shown after which the oscillation repeats. Indeed, this repetition has been used to sample the series of photographs by shifting the instant of exposure by 500 ns from frame to frame with respect to the phase of the sound wave. The camera is looking directly into the illuminating light source (back illumination). The bubble then appears dark on a bright background because the light is deflected off its surface. The white spot in the middle of the bubble results from the light passing the spherical bubble undeflected.

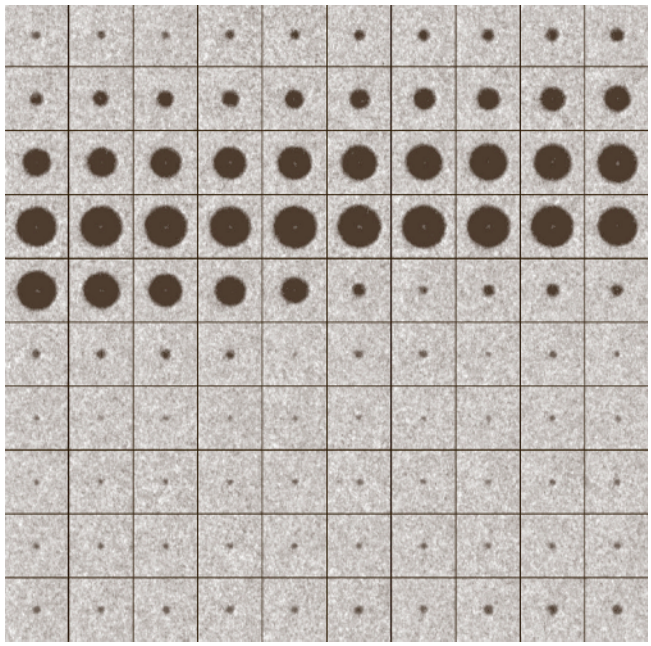


Fig. 8.17 Photographic series of a trapped, sonoluminescing bubble driven at 21.4 kHz and a pressure amplitude of 132 kPa. The interframe time is 500 ns. Picture size is 160 × 160 µm. (Courtesy of R. Geisler)

Upon the first large collapse a shock wave is radiated (Fig. 8.18). At the 30 ns interframe time the 12 frames given cover 330 ns, less than one interframe time Fig. 8.17. The shock wave becomes visible via deflection of the illuminating light. The bubble expands on a much slower time scale than the speed of the shock wave and is seen as a tiny black spot growing in the middle of the ring of the shock wave. Measurements of the shock velocity near the bubble at collapse (average from 6 to 73 µm) leads to about 2000 m/s, giving a shock pressure of about 5500 bar [8.119]. Higher-resolution measurements have increased these values to about 4000 m/s and 60 kbar [8.120].

The bubble oscillation as measured photographically can be compared with theoretical models for the motion of a bubble in a liquid. A comparison is shown in Fig. 8.19. The overall curve is reproduced well, although the steep collapse is not resolved experimentally. For details the reader is referred to [8.81].

There is the question whether shock waves are also emitted into the interior of the bubble [8.121–124]. Theoretically, shock waves occur in certain models, when the collapse is of sufficient intensity. Recently, the problem has been approached by molecular dynamics calculations [8.125–128]. As the number of molecules

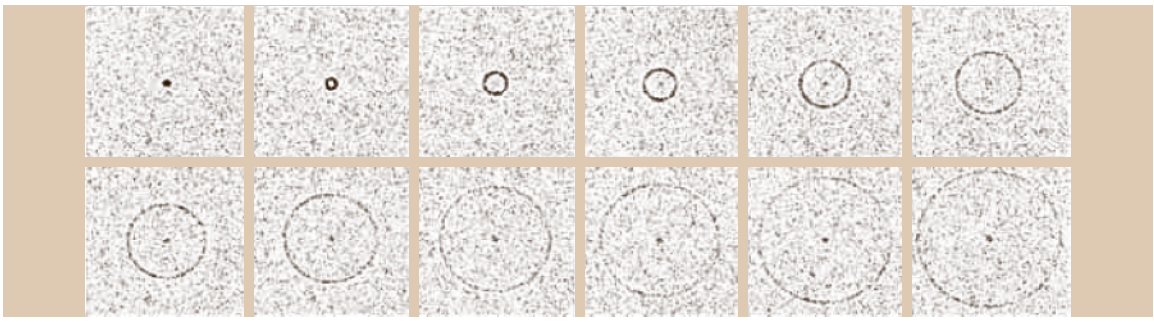


Fig. 8.18 Shock wave from a trapped, sonoluminescing bubble driven at 21.4 kHz and a pressure amplitude of 132 kPa. The interframe time is 30 ns. Picture size is 160 × 160 µm. (Courtesy of R. Geisler)

Amazon
EX1010 Page 303

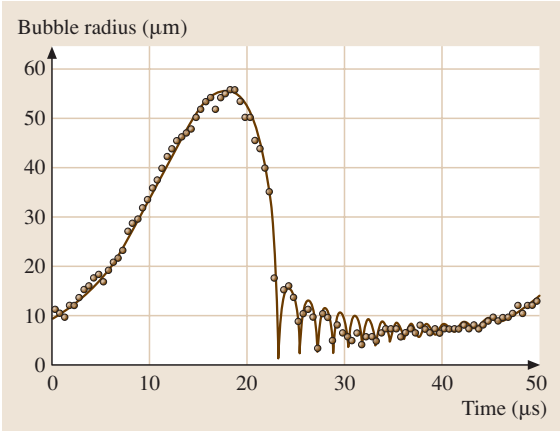


Fig. 8.19 Radius-time curve of a trapped bubble in a water-glycerine mixture derived from photographic observations. A numerically calculated curve (Gilmore model) is superimposed on the experimental data points (*open circles*). The calculation is based on the following parameters: driving frequency $f_0 = 21.4\,\text{kHz}$, ambient pressure $p_0 = 100\,\text{kPa}$, driving pressure $p_0 = 132\,\text{kPa}$, vapor pressure $p_v = 0$, equilibrium radius $R_n = 8.1\,\mu\text{m}$, density of the liquid $\rho = 1000\,\text{kg/m}^3$, viscosity $\mu = 0.0018\,\text{Ns/m}^2$ (measured) and surface tension $\sigma = 0.0725\,\text{N/m}$. The gas within the bubble is assumed to obey the adiabatic equation of state for an ideal gas with $\kappa = 1.2$. (Measured points courtesy of R. Geisler)

in a small bubble is relatively small, around 10^9 to 10^{10} molecules, this approach promises progress for the question of internal shock waves. At present molecular dynamics simulations are feasible with several million particles inside the bubble. Figure 8.20 gives a graphical view on the internal temperature distribution inside a collapsing sonoluminescence bubble with near-adiabatic conditions (reflection of the molecules at the inner boundary of the bubble) for six different times around maximum compression. The liquid

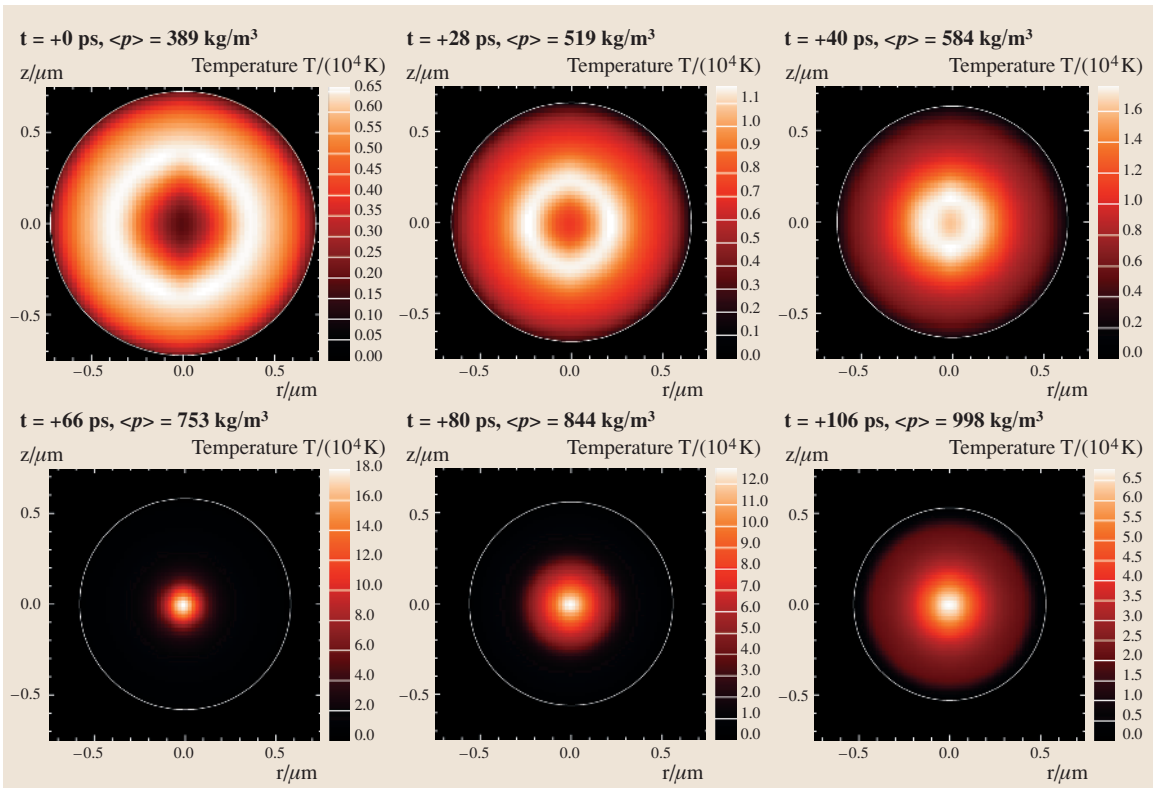


Fig. 8.20 Temperature distribution inside a collapsing sonoluminescence bubble filled with argon, one million particles, radius of the bubble at rest 4.5 μm, sound pressure amplitude 130 kPa, sound field frequency 26.5 kHz, total time covered 106 ps. (Courtesy of B. Metten [8.126])

Amazon
EX1010 Page 304

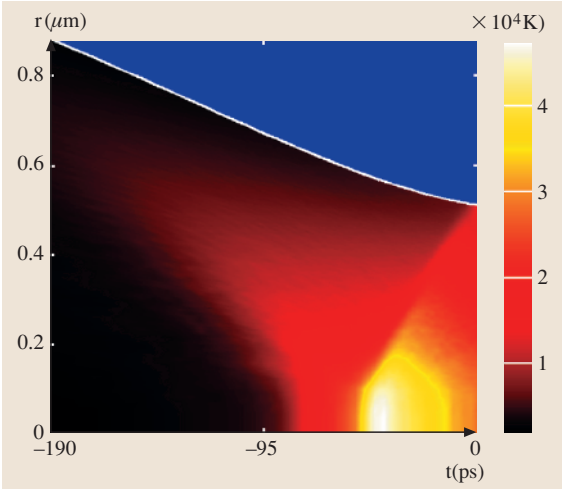


Fig. 8.21 Distribution of temperature inside an acoustically driven bubble in dependence on time. Molecular dynamics calculation with argon and water vapor including chemical reactions. (after [8.128])

motion and the inner molecular dynamics calculations are coupled via the gas pressure (at the interface), which is determined from the molecular dynamics of the 10^6 particles and inserted into the Rayleigh–Plesset equation giving the motion of the bubble wall. A strong focusing of energy inside the bubble is observed under these conditions. An inward-traveling compression wave focuses at the center and yields a core temperature of more than 10^5 K. This temperature is an overestimate as no energy-consuming effects are included.

The temperature variation inside the bubble with time can be visualized for spherical bubbles in a single picture in the following way (Fig. 8.21). The vertical axis represents the radial direction from the bubble center, the horizontal axis represents time and the color gives the temperature in Kelvin according to the color-coded scale (bar aside the figure). The upper solid line in the figure depicts the bubble wall; the blue part is water. In this case an argon bubble with water vapor is taken and chemical reactions are included. Then the temperature is lowered significantly by the endothermal processes of chemical species formation, for instance of OH^- radicals. The temperature drops to about 40 000 K in the center [8.128].

8.12 Acoustic Chaos

Nonlinearity in acoustics not only leads to shock waves and, as just demonstrated, to light emission, but to even deeper questions of nonlinear physics in general [8.4]. In his curiosity, man wants to know the future. Knowledge of the future may also be of help to master one's life by taking proper provisions. The question therefore arises: how far can we look into the future and where are the difficulties in doing so? This is the question of predictability or unpredictability. In the attempt to solve this question we find deterministic systems, stochastic systems and, nowadays, chaotic systems. The latter are special in that they combine deterministic laws that nevertheless give unpredictable output. They thus form a link between deterministic and stochastic systems.

8.12.1 Methods of Chaos Physics

A description of the methods developed to handle chaotic systems, in particular in acoustics, has been given in [8.32]. The main question in the context

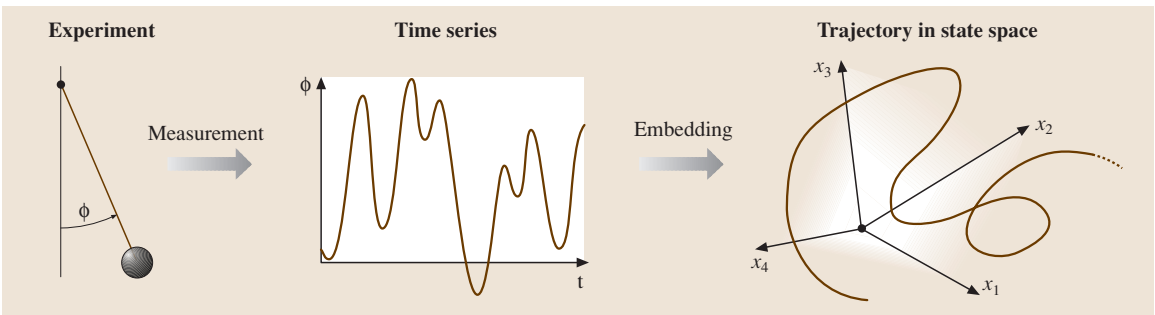


Fig. 8.22 Visualization of the embedding procedure

Amazon
EX1010 Page 305

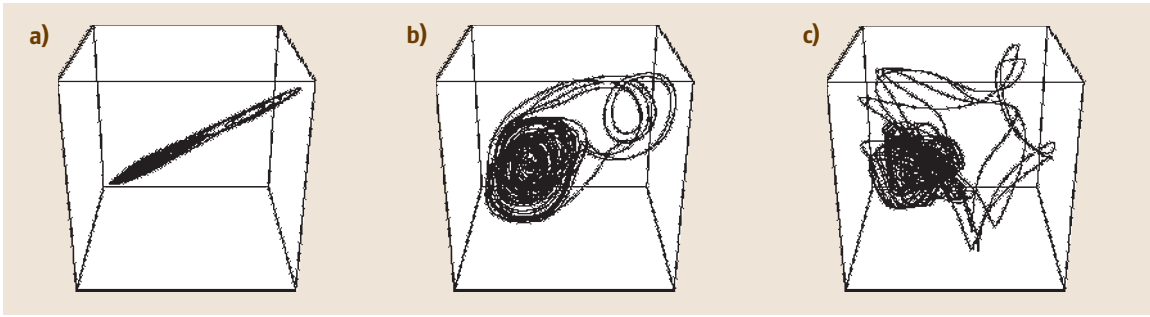


Fig. 8.23 Three embeddings with different delay times t_l for experimental data obtained from a chaotically oscillating, periodically driven pendulum. (Courtesy of U. Parlitz)

of experiments is how to connect the typically one-dimensional measurements (a time series) with the high-dimensional state space of theory (given by the number of variables describing the system). This is done by what is called *embedding* Fig. 8.22 [8.129, 130] and has led to a new field called *nonlinear time-series analysis* [8.131–133].

The embedding procedure runs as follows. Let $\{p(kt_s), k = 1, 2, \ldots, N\}$ be the measured time series, then an embedding into a n-dimensional state space is achieved by grouping n elements each of the time series to vectors $\boldsymbol{p}_k^{(n)} = [p(kt_s), p(kt_s + t_l), \ldots, p(kt_s + (n-1)t_l)]$, $k = 1, 2, \ldots, N-n$, in the n-dimensional state space. There t_s is the sampling interval at which samples of the variable p are taken. The delay time t_l is usually taken as a multiple of t_s, $t_l = lt_s$, $l = 1, 2, \ldots$, to avoid interpolation. The sampling time t_s, the delay time t_l and the embedding dimension n must all be chosen properly according to the problem under investigation. Figure 8.23 demonstrates the effect of different delay times with experimental data from a chaotically oscillating periodically driven pendulum. When the delay time t_l is too small then from one embedding vector to the next there is little difference and the embedded points all lie along the diagonal in the embedding space Fig. 8.23a. On the other hand, when the delay time t_l is too large, the reconstructed trajectory obtained by connecting successive vectors in the embedding space becomes folded and the reconstruction becomes fuzzy Fig. 8.23c. The embedding dimension n is usually not known beforehand when an unknown system is investigated for its properties. Therefore the embedding is done for increasing n until some criterion is fulfilled. The basic idea for a criterion is that a structure in the point set obtained by the embedding should appear. Then some law must be at work that generates it. The task after embedding is therefore to find and characterize the structure and to find the laws behind it. The characterization of the point set obtained can be done by determining its static structure (e.g., its dimension) and its dynamic structure (e.g., its expansion properties via the dynamics of nearby points).

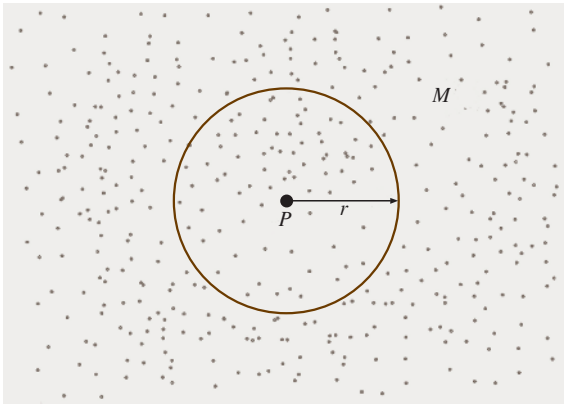


Fig. 8.24 Notations for the definition of the pointwise dimension

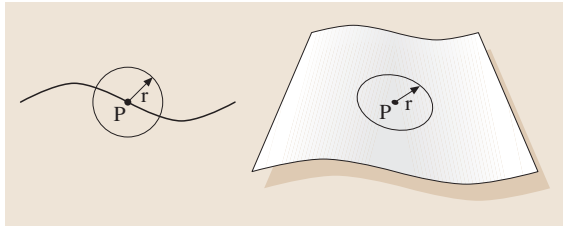


Fig. 8.25 Example of pointwise dimensions for one-dimensional (a curve) and two-dimensional (a surface) point sets

The dimension easiest to understand is the pointwise dimension. It is defined at a point P of a point set M by $N(r) \sim r^D$, $r \to 0$, where $N(r)$ is the number of

Amazon
EX1010 Page 306



Fig. 8.26 The point set of a strange attractor of an experimental, driven pendulum. (Courtesy of M. Kaufmann)

points of the set M inside the ball of radius r around P (Fig. 8.24). Examples for a line and a surface give the right integer dimensions of one and two (Fig. 8.25), because for a line we have $N(r) \sim r^1$ for $r \to 0$ and thus $D = 1$, and for a surface we have $N(r) \sim r^2$ for $r \to 0$ and thus $D = 2$.

Chaotic or strange attractors usually give a fractal (noninteger) dimension. The pointwise dimension may not be the same in this case for each point P. The distribution of dimensions then gives a measure of the inhomogeneity of the point set. Figure 8.26 gives an example of a fractal point set. It has been obtained by sampling the angle and the angular velocity of a pendulum at a given phase of the periodic driving for parameters in a chaotic regime.

To investigate the dynamic properties of a (strange or chaotic) set the succession of the points must be retained. As chaotic dynamics is brought about by a stretching and folding mechanism and shows sensitive dependence on initial conditions (see, e.g., [8.32]) the behavior of two nearby points is of interest: do they separate or approach under the dynamics? This

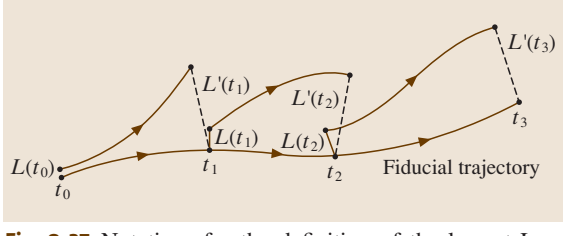


Fig. 8.27 Notations for the definition of the largest Lyapunov exponent

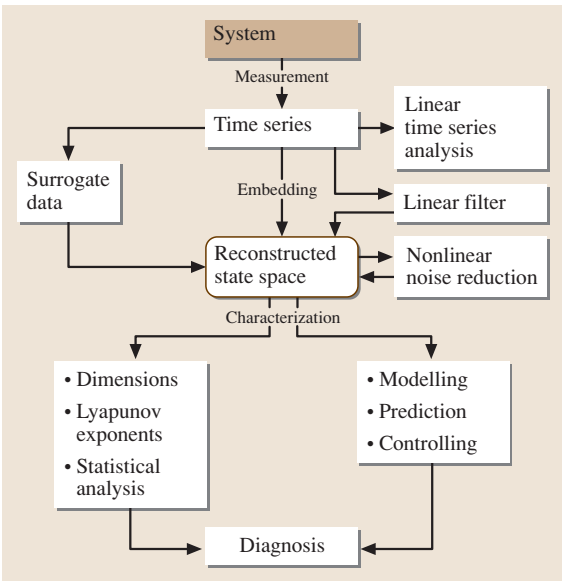


Fig. 8.28 Operations in nonlinear time-series analysis. (Courtesy of U. Parlitz)

behavior is quantified by the notion of the Lyapunov exponent. In Fig. 8.27 the calculation scheme [8.134] is depicted. It gives the maximum Lyapunov exponent via the formula

$$\lambda_{\max} = \frac{1}{t_m - t_0} \sum_{k=1}^{m} \log_2 \frac{L'(t_k)}{L(t_{k-1})} \quad \left[\frac{\text{bits}}{\text{s}}\right]. \qquad (8.224)$$

As space does not permit us to dig deeper into the operations possible with embedded data, only a graph depicting the possible operations in nonlinear time-series analysis is given in Fig. 8.28. Starting from the time series obtained by some measurement, the usual approach is to do a linear time-series analysis, for instance by calculating the Fourier transform or some correlation. The new way for chaotic systems proceeds via embedding to a reconstructed state space. There may be some filtering involved in between, but this is a dangerous operation as the results are often difficult to predict. For the surrogate data operation and nonlinear noise reduction the reader is referred to [8.131–133]. From the characterization operations we have mentioned here the dimension estimation and the largest Lyapunov exponent. Various statistical analyses can be done and the data can also be used for modeling, prediction and controlling the system. Overall, nonlinear time series analysis is a new diagnostic tool for describing (nonlinear) systems.

Amazon
EX1010 Page 307

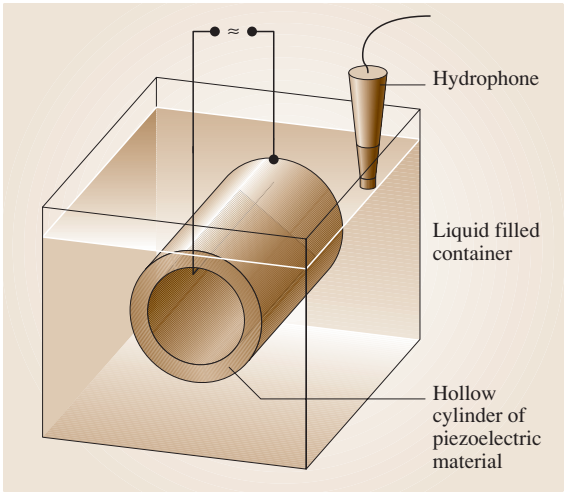


Fig. 8.29 Cylindrical transducer submerged in water for bubble oscillation, cavitation noise, and sonoluminescence studies

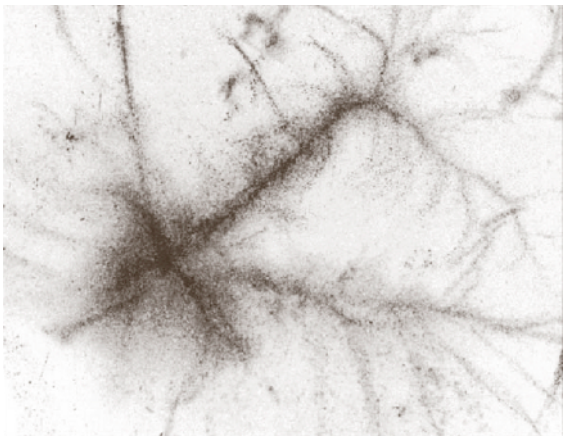
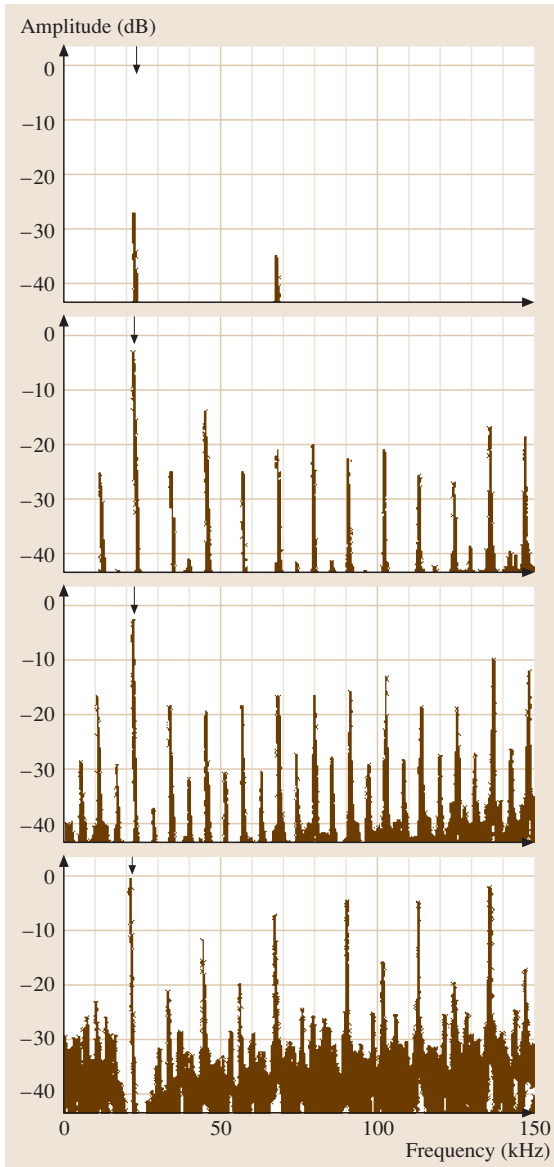


Fig. 8.30 Example of the filamentary bubble pattern (acoustic Lichtenberg figure) inside the cylinder in the projection along the axis of the transducer. (Courtesy of A. Billo)

Fig. 8.31 Power spectra of cavitation noise taken at a driving frequency of $f_0 = 23\,\text{kHz}$, marked in the figures by small triangle. The driving pressure was increased from one graph to the next, giving first a periodic, anharmonic signal (*top*), then subharmonic motion with lines at multiples of $f_0/2$ (period-2 motion, *top next*), then period-4 motion with lines at multiples of $f_0/4$ (*third plot*) and finally a broadband spectrum indicative of chaotic behavior (*bottom*)▶

8.12.2 Chaotic Sound Waves

One of the first examples of chaotic dynamics and where these methods were first applied was acoustic cavitation [8.4, 135, 136]. To investigate this phenomenon, the rupture of liquids by sound waves and the phenomena associated with it, an experimental arrangement as depicted in Fig. 8.29 was used. A cylindrical transducer of piezoelectric material is used to generate a strong sound field in water. A typical transducer was of 76 mm



Amazon
EX1010 Page 308

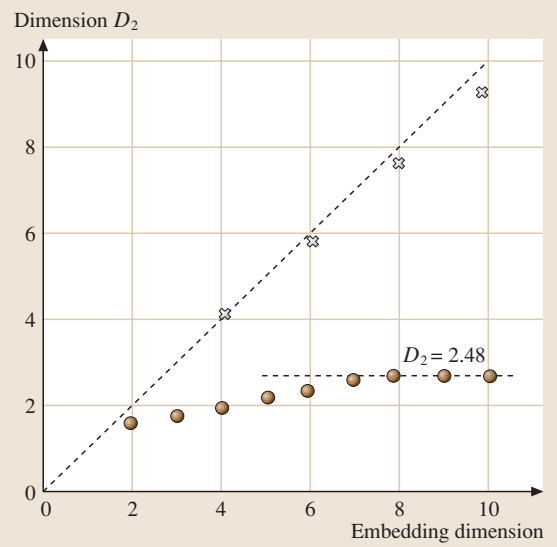


Fig. 8.32 Dimension estimation by embedding experimental acoustic cavitation sound pressure data into spaces of increasing dimension (*dots*). The *crosses* (×) are from an experiment, where noise from a noise generator has been embedded

length, 76 mm inner diameter, and 5 mm wall thickness submerged in a water-filled glass container. Cylinders of different size were available driven at different frequencies between 7 kHz and 23 kHz. A standing acoustic wave is set up inside the cylinder having its maximum pressure amplitude along the axis of the transducer. A hydrophone monitors the sound output of the liquid. Some electronics and a computer surround the experiment to drive the cylinder and to store the sampled pressure data from the hydrophone. When cavitation is fully developed, a dentritic filamentary bubble pattern is set up in the cylinder (Fig. 8.30).

When the sound field amplitude is raised the whole bubble field undergoes a period-doubling cascade to chaos [8.81, 137], a strong indication that chaotic dynamics really has been reached and that the broadband spectrum then encountered (Fig. 8.31) is not of stochastic origin. The cascade of period-doubled sound in the liquid has its origin in the cascade of period-doubled oscillations of the nonlinearly oscillating bubbles [8.81], and thus shows chaotic sound.

Embedding of the sound data into spaces of increasing dimension yields a structure with low fractal dimensions between two and three (Fig. 8.32). This is a quite surprising result in view of the thousands of oscillating bubbles of different sizes. Indeed, new results on the superposition of the sound output of a population of driven bubbles have indicated that the low dimensionality may be a result of the (weak) synchronization of their motion from the periodic driving and the scale of observation [8.138].

Chaotic sound waves also appear in other contexts [8.139]. In musical acoustics several instruments are susceptible to chaotic sound emission. Examples are the bowed string [8.140, 141], the clarinet [8.142] and gongs and cymbals [8.143].

The human speech production process is intrinsically nonlinear. To produce voice sounds the vocal cords are set into vibration through the air flow between them. The cords are a coupled system of nonlinear oscillators giving rise to bifurcations and chaos [8.144].

Sound can be generated by heat. When a gas-filled tube, closed at one end and open at the other is heated at the closed end and/or cooled at the open end, sound waves are emitted at a sufficiently high temperature difference (Sondhauss and Taconis oscillation). This phenomenon has been used to study its route to chaos [8.145]. It has been used to build a new type of refrigerator and heat pump [8.146].

References

8.1 M.F. Hamilton, D.T. Blackstock (Eds.): *Nonlinear Acoustics* (Academic, San Diego 1998)

8.2 K. Naugolnykh, L. Ostrovsky: *Nonlinear Wave Processes in Acoustics* (Cambridge Univ. Press, Cambridge 1998)

8.3 R.T. Beyer: *Nonlinear Acoustics* (Acoust. Soc. Am., Woodbury 1997)

8.4 W. Lauterborn, T. Kurz, U. Parlitz: Experimental nonlinear physics, Int. J. Bifurcation Chaos **7**, 2003–2033 (1997)

8.5 A.L. Thuras, R.T. Jenkins, H.T. O'Neil: Extraneous frequencies generated in air carrying intense sound waves, J. Acoust. Soc. Am. **6**, 173–180 (1935)

8.6 D.T. Blackstock, M.J. Crocker, D.G. Crighton, E.C. Everbach, M.A. Breazeale, A.B. Coppens, A.A. Atchley, M.F. Hamilton, W.E. Zorumski, W. Lauterborn, K.S. Suslick, L.A. Crum: Part II, Nonlinear Acoustics and Cavitation. In: *Encyclopedia of Acoustics*, Vol. 281, ed. by M.J. Crocker (Wiley, New York 1997) pp. 191–281

Amazon
EX1010 Page 309

8.7 N.S. Bakhvalov, Y.M. Zhileikin, E.A. Zabolotskaya: *Nonlinear Theory of Sound Beams* (American Institute of Physics, Melville 1987)
8.8 B.K. Novikov, O.V. Rudenko, V.I. Timoshenko: *Nonlinear Underwater Acoustics* (American Institute of Physics, New York 1987)
8.9 O.V. Rudenko, S.I. Soluyan: *Theoretical Foundations of Nonlinear Acoustics* (Consultants Bureau, London 1977)
8.10 G.B. Whitham: *Linear and Nonlinear Waves* (Wiley, London 1974)
8.11 L.D. Rozenberg (Ed.): *High-Intensity Ultrasonic Fields* (Plenum, New York 1971)
8.12 M.F. Hamilton, D.T. Blackstock (Eds.): *Frontiers of Nonlinear Acoustics* (Elsevier, London 1990)
8.13 H. Hobaek (Ed.): *Advances in Nonlinear Acoustics* (World Scientific, Singapore 1993)
8.14 R.J. Wei (Ed.): *Nonlinear Acoustics in Perspective* (Nanjing Univ. Press, Nanjing 1996)
8.15 W. Lauterborn, T. Kurz (Eds.): *Nonlinear Acoustics at the Turn of the Millennium* (American Institute of Physics, Melville 2000)
8.16 O.V. Rudenko, O.A. Sapozhnikov (Eds.): *Nonlinear Acoustics at the Beginning of the 21st Century* (Faculty of Physics, Moscow State University, Moscow 2002)
8.17 S. Makarov, M. Ochmann: Nonlinear and thermoviscous phenomena in acoustics, Part I, Acustica **82**, 579–606 (1996)
8.18 S. Makarov, M. Ochmann: Nonlinear and thermoviscous phenomena in acoustics, Part II, Acustica **83**, 197–222 (1997)
8.19 S. Makarov, M. Ochmann: Nonlinear and thermoviscous phenomena in acoustics, Part III, Acustica **83**, 827–864 (1997)
8.20 C.E. Brennen: *Cavitation and Bubble Dynamics* (Oxford Univ. Press, Oxford 1995)
8.21 T.G. Leighton: *The Acoustic Bubble* (Academic, London 1994)
8.22 J.R. Blake, J.M. Boulton-Stone, N.H. Thomas (Eds.): *Bubble Dynamics and Interface Phenomena* (Kluwer, Dordrecht 1994)
8.23 F.R. Young: *Cavitation* (McGraw-Hill, London 1989)
8.24 L. van Wijngaarden (Ed.): *Mechanics and Physics of Bubbles in Liquids* (Martinus Nijhoff, The Hague 1982)
8.25 W. Lauterborn (Ed.): *Cavitation and Inhomogeneities in Underwater Acoustics* (Springer, Berlin, Heidelberg 1980)
8.26 E.A. Neppiras: Acoustic cavitation, Phys. Rep. **61**, 159–251 (1980)
8.27 H.G. Flynn: Physics of acoustic cavitation. In: *Physical Acoustics*, ed. by W.P. Mason (Academic, New York 1964) pp. 57–172
8.28 F.R. Young: *Sonoluminescence* (CRC, Boca Raton 2005)
8.29 T.J. Mason, J.P. Lorimer: *Applied Sonochemistry* (Wiley-VCH, Weinheim 2002)
8.30 K.S. Suslick (Ed.): *Ultrasound: Its Chemical, Physical and Biological Effects* (VCH, New York 1988)
8.31 W. Lauterborn: Acoustic chaos. In: *Encyclopedia of Physical Science and Technology*, 3rd edn., ed. by R.A. Meyers (Academic, San Diego 2002) pp. 117–127
8.32 W. Lauterborn, U. Parlitz: Methods of chaos physics and their application to acoustics, J. Acoust. Soc. Am. **84**, 1975–1993 (1988)
8.33 F.E. Fox, W.A. Wallace: Absorption of finite amplitude sound waves, J. Acoust. Soc. Am. **26**, 994–1006 (1954)
8.34 R.T. Beyer: Parameter of nonlinearity in fluids, J. Acoust. Soc. Am. **32**, 719–721 (1960)
8.35 A.B. Coppens, R.T. Beyer, M.B. Seiden, J. Donohue, F. Guepin, R.H. Hodson, C. Townsend: Parameter of nonlinearity. II, J. Acoust. Soc. Am. **38**, 797–804 (1965)
8.36 R.T. Beyer: *Nonlinear Acoustics* (Naval Ship Systems Command, Washington 1974), Table 3-1
8.37 E.C. Everbach: *Tissue Composition Determination via Measurement of the Acoustic Nonlinearity Parameter B/A, Ph.D. Dissertation* (Yale Univ., New Haven 1989) p. 66
8.38 Z. Zhu, M.S. Roos, W.N. Cobb, K. Jensen: Determination of the acoustic nonlinearity parameter B/A from phase measurements, J. Acoust. Soc. Am. **74**, 1518–1521 (1983)
8.39 X. Gong, Z. Zhu, T. Shi, J. Huang: Determination of the acoustic nonlinearity parameter in biological media using FAIS and ITD methods, J. Acoust. Soc. Am. **86**, 1–5 (1989)
8.40 W.K. Law, L.A. Frizell, F. Dunn: Determination of the nonlinearity parameter B/A of biological media, Ultrasound Med. Biol. **11**, 307–318 (1985)
8.41 J. Zhang, F. Dunn: A small volume thermodynamic system for B/A measurement, J. Acoust. Soc. Am. **89**, 73–79 (1991)
8.42 F. Plantier, J.L. Daridon, B. Lagourette: Measurement of the B/A nonlinearity parameter under high pressure: Application to water, J. Acoust. Soc. Am. **111**, 707–715 (2002)
8.43 E.C. Everbach: Parameters of nonlinearity of acoustic media. In: *Encyclopedia of Acoustics*, ed. by M.J. Crocker (Wiley, New York 1997) pp. 219–226
8.44 I. Rudnick: On the attenuation of finite amplitude waves in a liquid, J. Acoust. Soc. Am. **30**, 564–567 (1958)
8.45 J. Banchet, J.D.N. Cheeke: Measurements of the acoustic nonlinearity parameter B/A in solvents: Dependence on chain length and sound velocity, J. Acoust. Soc. Am. **108**, 2754–2758 (2000)
8.46 A.B. Coppens, R.T. Beyer, M.B. Seiden, J. Donohue, F. Guepin, R.H. Hodson, C. Townsend: Parameter of nonlinearity in fluids II, J. Acoust. Soc. Am. **38**, 797–804 (1965)

Amazon
EX1010 Page 310

8.47 O. Nomoto: Nonlinear parameter of the 'Rao Liquid', J. Phys. Soc. Jpn. **21**, 569–571 (1966)
8.48 R.T. Beyer: Parameter of nonlinearity in fluids, J. Acoust. Soc. Am. **32**, 719–721 (1960)
8.49 K.L. Narayana, K.M. Swamy: Acoustic nonlinear parameter (B/A) in n-pentane, Acustica **49**, 336–339 (1981)
8.50 S.K. Kor, U.S. Tandon: Scattering of sound by sound from Beyers (B/A) parameters, Acustica **28**, 129–130 (1973)
8.51 K.M. Swamy, K.L. Narayana, P.S. Swamy: A study of (B/A) in liquified gases as a function of temperature and pressure from ultrasonic velocity measurements, Acustica **32**, 339–341 (1975)
8.52 H.A. Kashkooli, P.J. Dolan Jr., C.W. Smith: Measurement of the acoustic nonlinearity parameter in water, methanol, liquid nitrogen, and liquid helium-II by two different methods: A comparison, J. Acoust. Soc. Am. **82**, 2086–2089 (1987)
8.53 R.T. Beyer: The parameter B/A. In: *Nonlinear Acoustics*, ed. by M.F. Hamilton, D.T. Blackstock (Academic, San Diego 1998) pp. 25–39
8.54 L. Bjørnø: Acoustic nonlinearity of bubbly liquids, Appl. Sci. Res. **38**, 291–296 (1982)
8.55 J. Wu, Z. Zhu: Measurement of the effective nonlinearity parameter B/A of water containing trapped cylindrical bubbles, J. Acoust. Soc. Am. **89**, 2634–2639 (1991)
8.56 M.P. Hagelberg, G. Holton, S. Kao: Calculation of B/A for water from measurements of ultrasonic velocity versus temperature and pressure to 10 000 kg/cm^2, J. Acoust. Soc. Am. **41**, 564–567 (1967)
8.57 B. Riemann: Ueber die Fortpflanzung ebener Luftwellen von endlicher Schwingungsweite (On the propagation of plane waves of finite amplitude), Abhandl. Ges. Wiss. Göttingen **8**, 43–65 (1860), in German
8.58 S. Earnshaw: On the mathematical theory of sound, Philos. Trans. R. Soc. London **150**, 133–148 (1860)
8.59 D.T. Blackstock: Propagation of plane sound waves of finite amplitude in nondissipative fluids, J. Acoust. Soc. Am. **34**, 9–30 (1962)
8.60 M.F. Hamilton, D.T. Blackstock: On the coefficient of nonlinearity β in nonlinear acoustics, J. Acoust. Soc. Am. **83**, 74–77 (1988), Erratum, ibid, p. 1976
8.61 D.G. Crighton: Propagation of finite-amplitude waves in fluids. In: *Encyclopedia of Acoustics*, ed. by M.J. Crocker (Wiley, New York 1997) pp. 203–218
8.62 B.D. Cook: New procedure for computing finite-amplitude distortion, J. Acoust. Soc. Am. **34**, 941–946 (1962), see also the footnote on page 312 of 8.1
8.63 W. Keck, R.T. Beyer: Frequency spectrum of finite amplitude ultrasonic waves in liquids, Phys. Fluids **3**, 346–352 (1960)
8.64 L.E. Hargrove: Fourier series for the finite amplitude sound waveform in a dissipationless medium, J. Acoust. Soc. Am. **32**, 511–512 (1960)
8.65 E. Fubini Ghiron: Anomalie nella propagazione di onde acustiche di grande ampiezza (Anomalies in the propagation of acoustic waves of large amplitude), Alta Frequenza **4**, 530–581 (1935), in Italian
8.66 D.T. Blackstock: Nonlinear Acoustics (Theoretical). In: *American Institute of Physics Handbook*, 3rd edn., ed. by D.E. Gray (McGraw Hill, New York 1972) pp. 3/183–3/205
8.67 A. Hirschberg, J. Gilbert, R. Msallam, A.P.J. Wijnands: Shock waves in trombones, J. Acoust. Soc. Am. **99**, 1754–1758 (1996)
8.68 M.J. Lighthill: Viscosity effects in sound waves of finite amplitude. In: *Surveys in Mechanics*, ed. by G.K. Batchelor, R.M. Davies (Cambridge Univ. Press, Cambridge 1956) pp. 249–350
8.69 J. Lighthill: *Waves in Fluids* (Cambridge Univ. Press, Cambridge 1980)
8.70 J.S. Mendousse: Nonlinear dissipative distortion of progressive sound waves at moderate amplitudes, J. Acoust. Soc. Am. **25**, 51–54 (1953)
8.71 Z.A. Gol'dberg: Second approximation acoustic equations and the propagation of plane waves of finite amplitude, Sov. Phys.-Acoust. **2**, 346–350 (1956)
8.72 D.T. Blackstock: Thermoviscous attenuation of plane, periodic, finite amplitude sound waves, J. Acoust. Soc. Am. **36**, 534–542 (1964)
8.73 E. Hopf: The partial differential equation $u_t + uu_x = \mu u_{xx}$, Comm. Pure Appl. Math. **3**, 201–230 (1950)
8.74 J.D. Cole: On a quasi-linear parabolic equation occurring in aerodynamics, Quart. Appl. Math. **9**, 225–236 (1951)
8.75 M. Abramowitz, I.A. Stegun (Eds.): *Handbook of Mathematical Functions* (Dover, New York 1970)
8.76 L.S. Gradsteyn, I.M. Ryshik: *Table of Integrals, Series and Products* (Academic, Orlando 1980)
8.77 D.T. Blackstock: Connection between the Fay and Fubini solutions for plane sound waves of finite amplitude, J. Acoust. Soc. Am. **39**, 1019–1026 (1966)
8.78 R.D. Fay: Plane sound waves of finite amplitude, J. Acoust. Soc. Am. **3**, 222–241 (1931)
8.79 R.V. Khokhlov, S.I. Soluyan: Propagation of acoustic waves of moderate amplitude through dissipative and relaxing media, Acustica **14**, 241–246 (1964)
8.80 I.S. Akhatov, R.I. Nigmatulin, R.T. Lahey Jr.: The analysis of linear and nonlinear bubble cluster dynamics, Multiphase Sci. Technol. **17**, 225–256 (2005)
8.81 W. Lauterborn, T. Kurz, R. Mettin, C.D. Ohl: Experimental and theoretical bubble dynamics, Adv. Chem. Phys. **110**, 295–380 (1999)
8.82 C. Chaussy (Ed.): *Extracorporeal Shock Wave Lithotripsy* (Karger, New York 1986)
8.83 G.A. Askar'yan: Self-focusing of powerful sound during the production of bubbles, J. Exp. Theor. Phys. Lett. **13**, 283–284 (1971)
8.84 P. Ciuti, G. Jernetti, M.S. Sagoo: Optical visualization of non-linear acoustic propagation in cavitating liquids, Ultrasonics **18**, 111–114 (1980)

Amazon
EX1010 Page 311

8.85 Yu.A. Kobelev, L.A. Ostrovsky: Nonlinear acoustic phenomena due to bubble drift in a gas-liquid mixture, J. Acoust. Soc. Am. **85**, 621–627 (1989)

8.86 S.L. Lopatnikov: Acoustic phase echo in liquid with gas bubbles, Sov. Tech. Phys. Lett. **6**, 270–271 (1980)

8.87 I.Sh. Akhatov, V.A. Baikov: Propagation of sound perturbations in heterogeneous gas-liquid systems, J. Eng. Phys. **9**, 276–280 (1986)

8.88 I.Sh. Akhatov, V.A. Baikov, R.A. Baikov: Propagation of nonlinear waves in gas-liquid media with a gas content variable in space, Fluid Dyn. **7**, 161–164 (1986)

8.89 E. Zabolotskaya: Nonlinear waves in liquid with gas bubbles, Trudi IOFAN (Institute of General Physics of the Academy of Sciences, Moscow) **18**, 121–155 (1989), in Russian

8.90 I.Akhatov, U. Parlitz, W. Lauterborn: Pattern formation in acoustic cavitation, J. Acoust. Soc. Am. **96**, 3627–3635 (1994)

8.91 I.Akhatov, U. Parlitz, W. Lauterborn: Towards a theory of self-organization phenomena in bubble-liquid mixtures, Phys. Rev. E **54**, 4990–5003 (1996)

8.92 O.A. Druzhinin, L.A. Ostrovsky, A. Prosperetti: Low-frequency acoustic wave generation in a resonant bubble-layer, J. Acoust. Soc. Am. **100**, 3570–3580 (1996)

8.93 L.A. Ostrovsky, A.M. Sutin, I.A. Soustova, A.I. Matveyev, A.I. Potapov: Nonlinear, low-frequency sound generation in a bubble layer: Theory and laboratory experiment, J. Acoust. Soc. Am. **104**, 722–726 (1998)

8.94 R.I. Nigmatulin: *Dynamics of Multiphase Systems* (Hemisphere, New York 1991)

8.95 V.E. Nakoryakov, V.G. Pokusaev, I.R. Shreiber: *Propagation of Waves in Gas- and Vapour-liquid Media* (Institute of Thermophysics, Novosibirsk 1983)

8.96 L. van Wijngaarden: One-dimensional flow of liquids containing small gas bubbles, Ann. Rev. Fluid Mech. **4**, 369–396 (1972)

8.97 U. Parlitz, R. Mettin, S. Luther, I. Akhatov, M. Voss, W. Lauterborn: Spatiotemporal dynamics of acoustic cavitation bubble clouds, Philos. Trans. R. Soc. London Ser. A **357**, 313–334 (1999)

8.98 J.G. McDaniel, I. Akhatov, R.G. Holt: Inviscid dynamics of a wet foam drop with monodisperse bubble size distribution, Phys. Fluids **14**, 1886–1984 (2002)

8.99 A. Prosperetti, A. Lezzi: Bubble dynamics in a compressible liquid. Part 1. First order theory, J. Fluid Mech. **168**, 457–478 (1986)

8.100 R.I. Nigmatulin, I.S. Akhatov, N.K. Vakhitova, R.T. Lahey Jr.: On the forced oscillations of a small gas bubble in a spherical liquid-filled flask, J. Fluid Mech. **414**, 47–73 (2000)

8.101 A. Jeffrey, T. Kawahara: *Asymptotic Methods in Nonlinear Wave Theory* (Pitman, London 1982)

8.102 L. van Wijngaarden: On the equations of motion for mixtures of fluid and gas bubbles, J. Fluid Mech. **33**, 465–474 (1968)

8.103 N.A. Gumerov: Propagation of long waves of finite amplitude in a liquid with polydispersed gas bubbles, J. Appl. Mech. Tech. Phys. **1**, 79–85 (1992)

8.104 A. Hasegawa: *Plasma Instabilities and Nonlinear Effects* (Springer, Berlin, Heidelberg 1975)

8.105 N.A. Gumerov: The weak non-linear fluctuations in the radius of a condensed drop in an acoustic field, J. Appl. Math. Mech. (PMM U.S.S.R.) **53**, 203–211 (1989)

8.106 N.A. Gumerov: Weakly non-linear oscillations of the radius of a vapour bubble in an acoustic field, J. Appl. Math. Mech. **55**, 205–211 (1991)

8.107 N.A. Gumerov: On quasi-monochromatic weakly nonlinear waves in a low-dissipative bubbly liquid, J. Appl. Math. Mech. **56**, 50–59 (1992)

8.108 S. Gavrilyuk: Large amplitude oscillations and their "thermodynamics" for continua with "memory", Euro. J. Mech. B/Fluids **13**, 753–764 (1994)

8.109 S.L. Gavrilyuk, V.M. Teshukov: Generalized vorticity for bubbly liquid and dispersive shallow water equations, Continuum Mech. Thermodyn. **13**, 365–382 (2001)

8.110 L.F. McGoldrick: Resonant interactions among capillary-gravity waves, J. Fluid Mech. **21**, 305–331 (1965)

8.111 D.J. Benney: A general theory for interactions between long and short waves, Studies Appl. Math. **56**, 81–94 (1977)

8.112 I.Sh. Akhatov, D.B. Khismatulin: Effect of dissipation on the interaction between long and short waves in bubbly liquids, Fluid Dyn. **35**, 573–583 (2000)

8.113 I.Sh. Akhatov, D.B. Khismatulin: Two-dimensional mechanisms of interaction between ultrasound and sound in bubbly liquids: Interaction equations, Acoust. Phys. **47**, 10–15 (2001)

8.114 I.Sh. Akhatov, D.B. Khismatulin: Mechanisms of interaction between ultrasound and sound in liquids with bubbles: Singular focusing, Acoust. Phys. **47**, 140–144 (2001)

8.115 D.B. Khismatulin, I.Sh. Akhatov: Sound – ultrasound interaction in bubbly fluids: Theory and possible applications, Phys. Fluids **13**, 3582–3598 (2001)

8.116 V.E. Zakharov: Collapse of Langmuir waves, Sov. Phys. J. Exp. Theor. Phys. **72**, 908–914 (1972)

8.117 D.F. Gaitan, L.A. Crum, C.C. Church, R.A. Roy: An experimental investigation of acoustic cavitation and sonoluminescence from a single bubble, J. Acoust. Soc. Am. **91**, 3166–3183 (1992)

8.118 Y. Tian, J.A. Ketterling, R.E. Apfel: Direct observations of microbubble oscillations, J. Acoust. Soc. Am. **100**, 3976–3978 (1996)

8.119 J. Holzfuss, M. Rüggeberg, A. Billo: Shock wave emission of a sonoluminescing bubble, Phys. Rev. Lett. **81**, 5434–5437 (1998)

8.120 R. Pecha, B. Gompf: Microimplosions: Cavitation collapse and shock wave emission on a nanosecond time scale, Phys. Rev. Lett. **84**, 1328–1330 (2000)

Amazon
EX1010 Page 312

8.121 E. Heim: Über das Zustandekommen der Sonoluminеszenz (On the origin of sonoluminescence). In: *Proceedings of the Third International Congress on Acoustics, Stuttgart, 1959*, ed. by L. Cremer (Elsevier, Amsterdam 1961) pp. 343–346, in German

8.122 C.C. Wu, P.H. Roberts: A model of sonoluminescence, Proc. R. Soc. Lond. A **445**, 323–349 (1994)

8.123 W.C. Moss, D.B. Clarke, D.A. Young: Calculated pulse widths and spectra of a single sonoluminescing bubble, Science **276**, 1398–1401 (1997)

8.124 V.Q. Vuong, A.J. Szeri, D.A. Young: Shock formation within sonoluminescence bubbles, Phys. Fluids **11**, 10–17 (1999)

8.125 B. Metten, W. Lauterborn: Molecular dynamics approach to single-bubble sonoluminescence. In: *Nonlinear Acoustics at the Turn of the Millennium*, ed. by W. Lauterborn, T. Kurz (Am. Inst. Physics, Melville 2000) pp. 429–432

8.126 B. Metten: *Molekulardynamik-Simulationen zur Sonolumineszenz*, *Dissertation* (Georg-August Universität, Göttingen 2000)

8.127 S.J. Ruuth, S. Putterman, B. Merriman: Molecular dynamics simulation of the response of a gas to a spherical piston: Implication for sonoluminescence, Phys. Rev. E **66**, 1–14 (2002), 036310

8.128 W. Lauterborn, T. Kurz, B. Metten, R. Geisler, D. Schanz: Molecular dynamics approach to sonoluminescent bubbles. In: *Theoretical and Computational Acoustics 2003*, ed. by A. Tolstoy, Yu-Chiung Teng, E.C. Shang (World Scientific, New Jersey 2004) pp. 233–243

8.129 N.H. Packard, J.P. Crutchfield, J.D. Farmer, R.S. Shaw: Geometry from a time series, Phys. Rev. Lett. **45**, 712–716 (1980)

8.130 F. Takens: Detecting strange attractors in turbulence. In: *Dynamical Systems and Turbulence*, ed. by D.A. Rand, L.S. Young (Springer, Berlin, Heidelberg 1981) pp. 366–381

8.131 H.D.I. Abarbanel: *Analysis of Observed Chaotic Data* (Springer, Berlin, New York 1996)

8.132 H. Kantz, T. Schreiber: *Nonlinear Time Series Analysis* (Cambridge Univ. Press, Cambridge 1997)

8.133 U. Parlitz: Nonlinear time serie analysis. In: *Nonlinear Modeling – Advanced Black Box Techniques*, ed. by J.A.K. Suykens, J. Vandewalle (Kluwer Academic, Dordrecht 1998) pp. 209–239

8.134 A. Wolf, J.B. Swift, H.L. Swinney, J.A. Vastano: Determining Lyapunov exponents from time series, Physica D **16**, 285–317 (1985)

8.135 W. Lauterborn, E. Cramer: Subharmonic route to chaos observed in acoustics, Phys. Rev. Lett. **47**, 1445–1448 (1981)

8.136 W. Lauterborn, J. Holzfuss: Acoustic chaos, Int. J. Bifurcation Chaos **1**, 13–26 (1991)

8.137 W. Lauterborn, A. Koch: Holographic observation of period-doubled and chaotic bubble oscillations in acoustic cavitation, Phys. Rev. A **35**, 1774–1976 (1987)

8.138 S. Luther, M. Sushchik, U. Parlitz, I. Akhatov, W. Lauterborn: Is cavitation noise governed by a low-dimensional chaotic attractor?. In: *Nonlinear Acoustics at the Turn of the Millennium*, ed. by W. Lauterborn, T. Kurz (Am. Inst. Physics, Melville 2000) pp. 355–358

8.139 W. Lauterborn: Nonlinear dynamics in acoustics, Acustica acta acustica Suppl. 1 **82**, S46–S55 (1996)

8.140 M.E. McIntyre, R.T. Schumacher, J. Woodhouse: On the oscillation of musical instruments, J. Acoust. Soc. Am. **74**, 1325–1345 (1983)

8.141 N.B. Tuffilaro: Nonlinear and chaotic string vibrations, Am. J. Phys. **57**, 408–414 (1989)

8.142 C. Maganza, R. Caussé, Laloë: Bifurcations, period doublings and chaos in clarinet-like systems, Europhys. Lett. **1**, 295–302 (1986)

8.143 K.A. Legge, N.H. Fletcher: Nonlinearity, chaos, and the sound of shallow gongs, J. Acoust. Soc. Am. **86**, 2439–2443 (1989)

8.144 H. Herzel: Bifurcation and chaos in voice signals, Appl. Mech. Rev. **46**, 399–413 (1993)

8.145 T. Yazaki: Experimental observation of thermoacoustic turbulence and universal properties at the quasiperiodic transition to chaos, Phys. Rev. **E48**, 1806–1818 (1993)

8.146 G.W. Swift: Thermoacoustic engines, J. Acoust. Soc. Am. **84**, 1145–1180 (1988)

Amazon
EX1010 Page 313

Part C Architectural Acoustics

9 Acoustics in Halls for Speech and Music
Anders Christian Gade, Lyngby, Denmark

10 Concert Hall Acoustics Based on Subjective Preference Theory
Yoichi Ando, Makizono, Kirishima, Japan

11 Building Acoustics
James Cowan, White River Junction, USA

Amazon
EX1010 Page 314

9. Acoustics in Halls for Speech and Music

This chapter deals specifically with concepts, tools, and architectural variables of importance when designing auditoria for speech and music. The focus will be on cultivating the useful components of the sound in the room rather than on avoiding noise from outside or from installations, which is dealt with in Chap. 11. The chapter starts by presenting the subjective aspects of the room acoustic experience according to consensus at the time of writing. Then follows a description of their objective counterparts, the objective room acoustic parameters, among which the classical *reverberation time* measure is only one of many, but still of fundamental value. After explanations on how these parameters can be measured and predicted during the design phase, the remainder of the chapter deals with how the acoustic properties can be controlled by the architectural design of auditoria. This is done by presenting the influence of individual design elements as well as brief descriptions of halls designed for specific purposes, such as drama, opera, and symphonic concerts. Finally, some important aspects of loudspeaker installations in auditoria are briefly touched upon.

9.1 **Room Acoustic Concepts** 302

9.2 **Subjective Room Acoustics** 303
- 9.2.1 The Impulse Response 303
- 9.2.2 Subjective Room Acoustic Experiment Techniques 303
- 9.2.3 Subjective Effects of Audible Reflections 305

9.3 **Subjective and Objective Room Acoustic Parameters** 306
- 9.3.1 Reverberation Time 306
- 9.3.2 Clarity 308
- 9.3.3 Sound Strength 308
- 9.3.4 Measures of Spaciousness 309
- 9.3.5 Parameters Relating to Timbre or Tonal Color 310
- 9.3.6 Measures of Conditions for Performers 310
- 9.3.7 Speech Intelligibility 311
- 9.3.8 Isn't One Objective Parameter Enough? 312
- 9.3.9 Recommended Values of Objective Parameters 313

9.4 **Measurement of Objective Parameters** ... 314
- 9.4.1 The Schroeder Method for the Measurement of Decay Curves 314
- 9.4.2 Frequency Range of Measurements 314
- 9.4.3 Sound Sources 315
- 9.4.4 Microphones 315
- 9.4.5 Signal Storage and Processing 315

9.5 **Prediction of Room Acoustic Parameters** 316
- 9.5.1 Prediction of Reverberation Time by Means of Classical Reverberation Theory 316
- 9.5.2 Prediction of Reverberation in Coupled Rooms 318
- 9.5.3 Absorption Data for Seats and Audiences 319
- 9.5.4 Prediction by Computer Simulations 320
- 9.5.5 Scale Model Predictions 321
- 9.5.6 Prediction from Empirical Data ... 322

9.6 **Geometric Design Considerations** 323
- 9.6.1 General Room Shape and Seating Layout 323
- 9.6.2 Seating Arrangement in Section .. 326
- 9.6.3 Balcony Design 327
- 9.6.4 Volume and Ceiling Height 328
- 9.6.5 Main Dimensions and Risks of Echoes 329
- 9.6.6 Room Shape Details Causing Risks of Focusing and Flutter 329
- 9.6.7 Cultivating Early Reflections 330
- 9.6.8 Suspended Reflectors 331
- 9.6.9 Sound-Diffusing Surfaces 333

9.7 **Room Acoustic Design of Auditoria for Specific Purposes** 334
- 9.7.1 Speech Auditoria, Drama Theaters and Lecture Halls 334

Amazon
EX1010 Page 315

9.7.2 Opera Halls 335
9.7.3 Concert Halls for Classical Music .. 338
9.7.4 Multipurpose Halls 342
9.7.5 Halls for Rhythmic Music 344
9.7.6 Worship Spaces/Churches 346
9.8 **Sound Systems for Auditoria** 346
9.8.1 PA Systems 346
9.8.2 Reverberation-Enhancement Systems 348
References 349

Current knowledge about room acoustic design is based on several centuries of practical (trial-and-error) experience plus a single century of scientific research. Over the last couple of decades scientific knowledge has matured to a level where it can explain to a usable degree:

1. the subjective aspects related to how we perceive the acoustics of rooms
2. how these subjective aspects are governed by objective properties in the sound fields
3. how these objective properties of the sound field are governed by the physical variables in the architectural design

This chapter is organized in the same manner. The various subjective acoustic aspects will form the basis for our discussion and be a guide through most aspects of relevance in room acoustic design. However, some trends in current design practice based on the experience and intuition of individual acoustical designers will also be commented on. It is hoped that this approach will also have the advantage of stimulating the reader's ability to judge a room from her/his own listening experience, an ability which is important not only for designers of concert halls, but also for those responsible for creating and enjoying the sound in these halls: musicians, sound-system designers, recording engineers and concert enthusiasts.

9.1 Room Acoustic Concepts

In order to help the reader maintain a clear perspective all the way through this chapter, Fig. 9.1 illustrates the universe of architectural acoustics.

In the upper half of the figure, we have the phenomena experienced in the real world. Going from left to right, we have the auditoria, in which we can experience objective sound fields causing subjective impressions of the acoustic conditions. In all of these three domains, we find a huge number of degrees of freedom: halls can differ in a myriad of ways (from overall dimensions to detailed shaping of small details like door handles), the sound fields which we describe by the impulse response concept – as explained in a moment – contain a wealth of individual sound components (reflections), each being a function of time, level, direction and frequency. Also, every individual may have his/her own way of expressing what the room does to the sound heard.

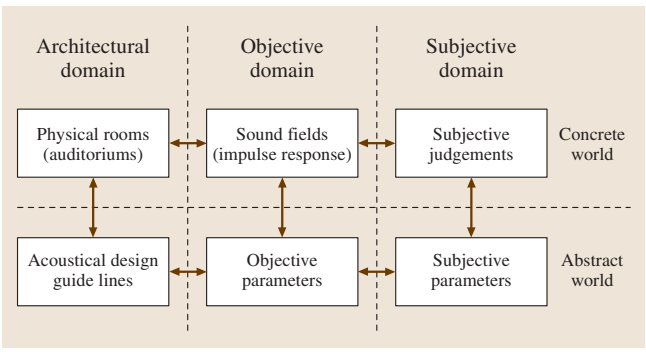


Fig. 9.1 Overview of concepts related to subjective room acoustics (after [9.1])

In other words, like in many other aspects of life, the real world is so complex that we need to simplify the problem – reduce the degrees of freedom – through definition of abstract, well-formulated and meaningful concepts and parameters in all three domains (the lower row of boxes). First, we must try to define a vocabulary to describe the subjective acoustic impression: we will isolate a set of subjective acoustic parameters that are valid to most people's listening experience (as indicated by the box in the lower-right corner), then we will try to deduce those properties from the sound fields that are responsible for our experience of each of the subjective aspects: we will define a set of objective, measurable parameters that correlate well with the subjective parameters, and finally – in order to be able to guide the architect – we must find out which aspects of the design govern the important objective and in turn the subjective

Amazon
EX1010 Page 316

parameters, so we can assist in building halls meeting the specific needs of their users.

A rough historical overview: systematic search for objective acoustic parameters peaked in the 1960s and 1970s, while the relationships between the objective parameters and design variables were the topic of many research efforts in the 1980s and 1990s. However, we cannot yet claim to have the answers to all questions regarding the acoustic design of auditoria. Hopefully, there will always be room for intuition and individual judgment, not only in room acoustic design; but also as a source of inspiration for continued research efforts. Still it should be clear that room acoustic design today is based on solid research; it is not a snake-oil business.

9.2 Subjective Room Acoustics

9.2.1 The Impulse Response

The basic source of information regarding the audible properties of the sound field in a room is the impulse response signal. Actually, this signal – when recorded with a multichannel technique preserving the information about direction of incidence – can be shown to contain all information about the acoustics of a room between two specific source and receiver positions.

Consider a short sound impulse being emitted by the source on the stage, as shown in Fig. 9.2. A spherical wave propagates away from the source in all directions and the sound first heard in the listener position originates from that part of the wave that has propagated directly from the source to the receiver, called *the direct sound*. This is shown on the left in the lower part of Fig. 9.2, which shows the received signal versus time at a given position in the room.

This component is soon followed by other parts of the wave that have been reflected one or more times by the room boundaries or by objects in the room before reaching the receiver, called *the early reflections*. Besides arriving later than the direct sound, normally these reflections are also weaker because the intensity is reduced as the area of the spherical wavefront increases with time (spherical distance attenuation) and because a fraction of the energy is being absorbed each time the wave hits a more or less sound-absorbing room boundary or object in the room.

The sound wave will continue to be reflected and to pass the receiver position until all the energy has been absorbed by the boundaries/objects or by the air. The density of these later reflections increases with time (proportional to t^2), but the attenuation due to absorption at the room boundaries ensures that eventually all sound dies out. This decay is often heard as reverberation in the room, as Sabine did, when he carried out his famous experiment in the Fogg Art Museum more than 100 years ago [9.2]. This event marked the start of subjective room acoustics as a science.

9.2.2 Subjective Room Acoustic Experiment Techniques

With each of the reflections specified in time, level, spectrum and direction of incidence, the impulse response contains a huge amount of information. Now, the question is how we can reduce this to what is necessary for an explanation of why we perceive the acoustics in different rooms as being different.

Experiments trying to answer this question have mainly been carried out in the second half of the 20th century when electro-acoustic means for recording, measurement and simulation of sound fields had become available. Such experiments take place in the four rightmost boxes in Fig. 9.1: a number of impulse responses – or rather, music or speech convolved (filtered) through these responses – are presented to a number of subjects. The subjective evaluations are collected either as simple preferences between the sound fields presented in pairs or as scalings along specific subjective parameters suggested by the experimenter. The experimenter will also choose a number of different objective parameters, and calculate their values for each of the impulse responses presented. The level of correlation between these objective values and the objective scalings will then indicate which of the parameters and therefore which properties of the impulse responses are responsible for the subjective evaluations.

As can be imagined, the results of such experiments will be strongly dependent on the range of variation and degree of realism of the impulse responses presented – as well as by the sound quality of the equipment used for the presentation. Besides, the results will always be limited by the imagination of the experimenter regarding his/her:

1. suggestions of proper semantic descriptors for the subjects' evaluation (except in cases where the subjects are only asked to give preferences) and

Amazon
EX1010 Page 317

2. suggestions of calculation of parameters from the impulse response.

In other words, before the experiments, the experimenter must have some good hypotheses regarding the contents of the lower-mid and lower-right boxes in Fig. 9.1.

Over the years, a variety of different techniques have been applied for presenting room sound fields to test subjects:

1. Collection of opinions about existing halls recalled from the memory of qualified listeners
2. Listening tests in different halls or in a hall with variable acoustics
3. Listening tests with presentation of recordings from existing halls or of *dry* speech/music convolved with impulse responses recorded in existing halls
4. Listening tests with sound fields synthesized in anechoic rooms (via multiple loudspeakers in an anechoic room) or impulse responses generated/modified by computer convolved with *dry* speech/music and presented over headphones.

It should be mentioned here that our acoustic memory is very short. Therefore, unless the subjects are highly experienced in evaluating concert hall acoustics, comparison of acoustic experiences separated by days,

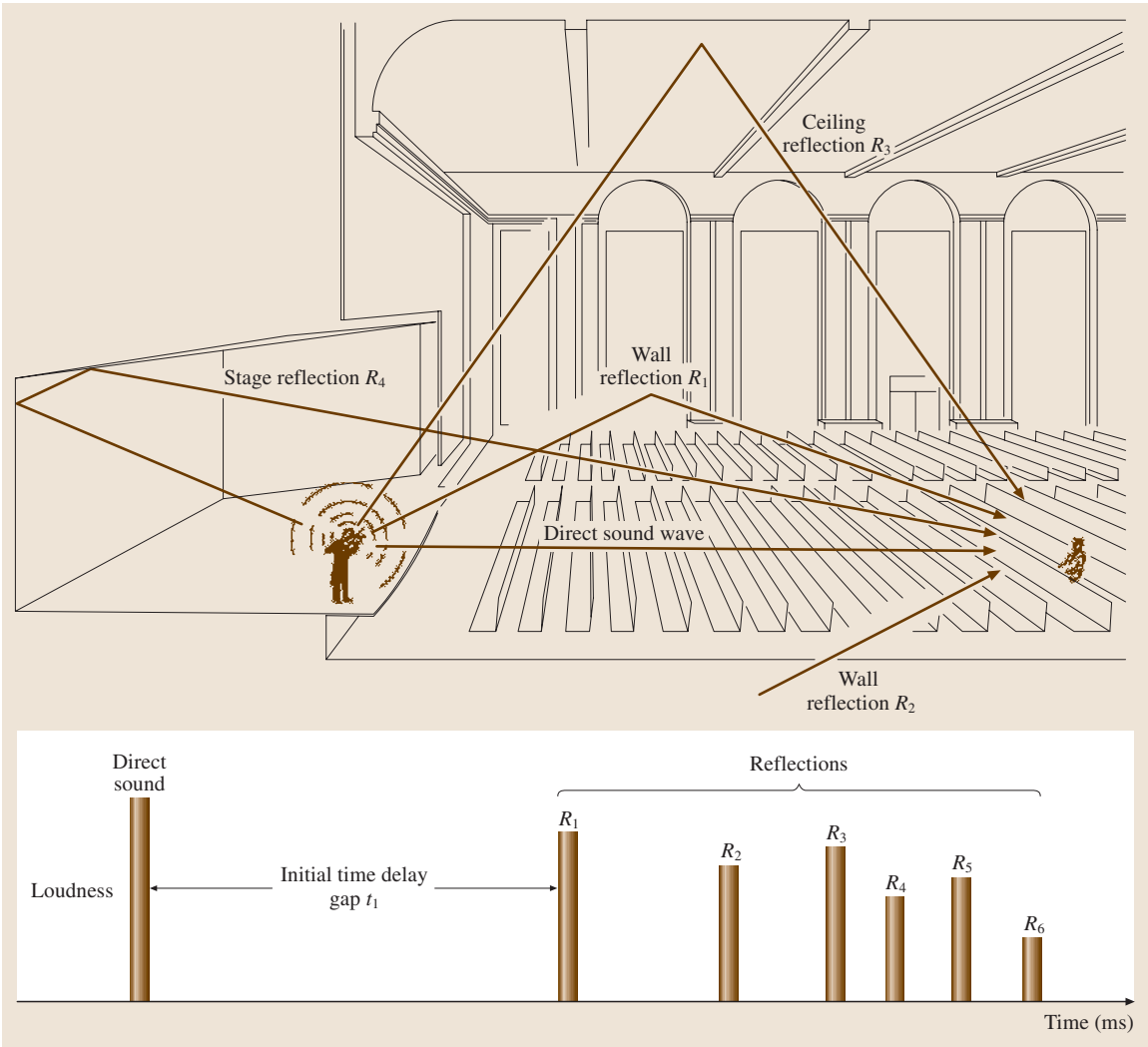


Fig. 9.2 Diagram illustrating the generation of an impulse response in a room (after [9.3])

Amazon
EX1010 Page 318

weeks or even years is less reliable than comparison in the lab, where different recordings can be presented immediately one after the other. On the other hand, it is often difficult to get really qualified people to come to the lab to participate in scientific tests. Therefore, results from interview surveys can still be highly relevant.

These different techniques for presenting the sound fields all have different limitations. Experiments in the lab involving electro-acoustic reproduction or the generation of sound fields may lack fidelity, while listening in a real hall to a real orchestra will normally lack flexibility and control of the independent variables. Another important difference between these two methods is the absence of realistic visual cues in the lab. Enjoyment of a performance is a holistic experience, a fact which is now given increased scientific attention. In all cases elaborate statistical analysis of the results are needed in order to separate the significant facts from the error variance present in any experiment involving subjective judgements. Since the 1960s, multidimensional statistical tool such as factor analysis and multidimensional scaling have been very useful in distinguishing between the different subjective parameters which are present – consciously or not – in our evaluation. In any case, published results are more likely to be close to the truth, if they have been verified by several experiments – and experimenters – using different experimental approaches.

9.2.3 Subjective Effects of Audible Reflections

As the impulse response consists of the direct sound followed by a series of reflections, the simplest case possible would be to have only the direct sound plus a single reflection (and perhaps some late, artificial reverberation). Many experiments in simulated sound fields have been conducted using such a simple setup, and in spite of the obvious lack of realism, we can still learn a lot about the subjective effects of reflections from these experiments.

First of all, due to the psycho-acoustic phenomenon called forward masking, the reflection will be inaudible if it arrives very soon after the direct sound and/or its level is very low relative to the direct sound. Thus, there exists a level threshold of audibility depending on delay and direction of incidence relative to the direct sound. Only if the level of the reflection is above this threshold will the reflection have an audible effect, which again depends on its level, delay and direction of incidence. The possible effects are (at least):

- Increased level (energy addition)
- Increased clarity, if it arrives within 50–80 ms after the direct sound
- Increased spaciousness, if the reflection direction in the horizontal plane is different from that of the direct as this causes the signals received at the two ears to be different (If the angle between the direct and reflected sounds differs in the vertical plane only, the effect is rather a change in *timbre* or coloration of the sound.)
- Echo, typically observed for delays beyond 50 ms and at high reflection levels. If the delay is very long, say 200 ms, then the echo may even be detected at a much lower level;
- Coloration. If the delay is short, say below 30 ms, and the level is high, phase addition of the direct sound and the reflection will create a *comb filter* effect, which severely deteriorates the original frequency spectrum
- Change in localization direction, in cases where the reflection is louder than the direct sound. This may happen either due to amplification of the reflection via a concave surface or due to excess attenuation of the direct sound, for instance by an orchestra pit rail.

Audibility thresholds, echo risk and other effects also depend on spectral and temporal properties of the signal itself. Thus, with speech and fast, staccato played music (not to speak of artificial, impulsive *click* sounds), echoes are much easier to detect than when the signal

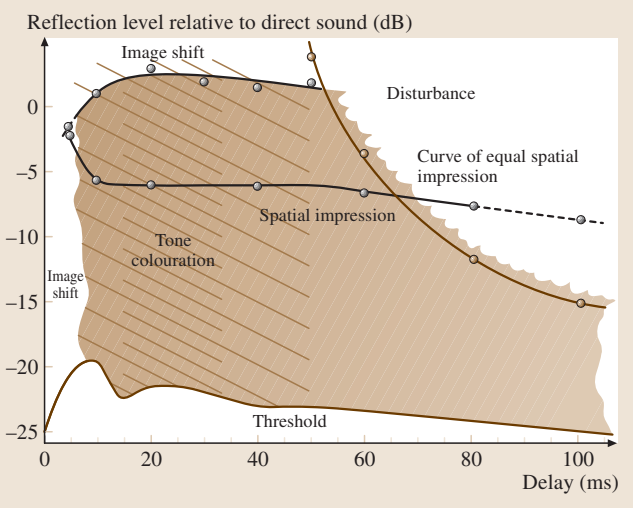


Fig. 9.3 Various audible effects of a single reflection arriving from the side. The signal used was music (after [9.4])

Amazon
EX1010 Page 319

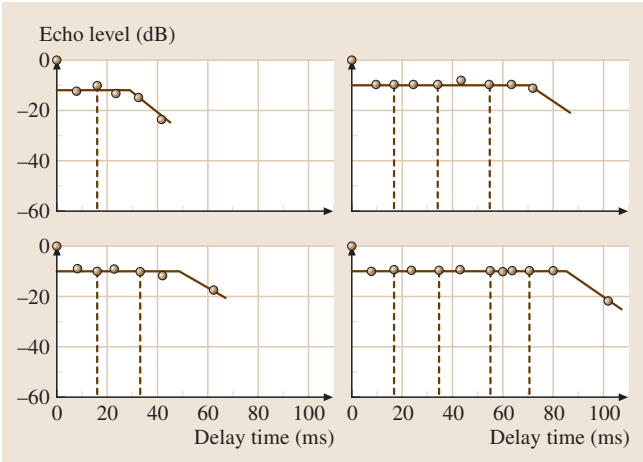


Fig. 9.4 Thresholds of perception of a new reflection (*circles* and *horizontal lines*) being added to impulse responses already containing one, two, three, or four other reflections with delay and relative levels, as indicated by the *vertical lines* (after [9.5])

is slow, legato music. On the other hand, these slower signals are more sensitive for the detection of coloration effects.

The temporal properties of sounds are sometimes described by the autocorrelation function. According to Ando (see Chap. 10 in this book) not only the thresholds of audibility but also the preferred delay of early reflections and the preferred reverberation time depend strongly on the autocorrelation of the signal. However, such a strong effect on concert hall preference – derived from listening experiments in rather simplified simulated sound fields in the lab – is not in accordance with everyday listening experiences in concert halls, in which we gladly accept listening to different music pieces of different tempo from different seats (different reflection delays) in the same hall (fixed reverberation time).

Figure 9.3 illustrates the various audible effects of a single reflection arriving from a 40° angle relative to a frontal direct sound. In this experiment music was used as the stimulus signal. Below the lower threshold (reflection level below about −20 dB and almost independent of the delay), the reflection is inaudible. In the upper-right region it causes a distinct echo, while in the shaded area we experience *spatial impression* or a broadening of the area from which the sound seem to originate. For delays lower than about 30 ms, this single reflection also causes an unpleasant change in *timbre* or *tonal color*, which is due to the combination of the direct and reflected signal forming a comb filter giving systematic changes in the spectrum. If the level of the reflection is increased to be louder than the direct sound (above 0 dB) while the delay is still below say 50 ms, we experience an *image shift* or a change in localization from the direction of the direct sound towards the direction from which the reflection is coming.

In practice, of course, the impulse response from a room contains many reflections, and we therefore need to know how the threshold of perceptibility of the incoming reflection changes in cases where the impulse response contains other reflections already. As seen from Fig. 9.4, the threshold level increases substantially in the delay range already occupied by other reflections. This phenomenon is primarily due to masking.

From this we can conclude that many of the details in a complex impulse response will be masked and only some of the dominant components or some of its overall characteristics seriously influence our perception of the acoustics. This is the reason why it is possible to create rather simple objective room acoustic parameters, as listed in the following section, which still describe the main features of the room acoustic experience. Thus, we seem to have some success describing the complex real world (the upper-middle and right boxes in Fig. 9.1) by simpler, abstract concepts. Also, it will be seen that the subjective effects caused by a single reflection remain important in the evaluation of more-realistic and complicated impulse responses.

9.3 Subjective and Objective Room Acoustic Parameters

From a consensus of numerous subjective experiments in real rooms and in simulated sound fields (representing all of the previously mentioned subjective research techniques), we now have a number of subjective parameters and corresponding objective measures available. Most of these are generally recognized as relevant descriptors of major aspects in our experience of the acoustics in rooms. This situation has promoted standardization of measurement methods and many of the objective parameters are now described in an appendix to the International Organization for Standardization (ISO) standard [9.6]. In order to maintain a clear distinction between the subjective and objective parameters in the following, the names for the subjective parameters will be printed in italics.

Amazon
EX1010 Page 320

9.3.1 Reverberation Time

Reverberance is probably the best known of all subjective room acoustic aspects. When a room creates too much *reverberance*, speech loses intelligibility because important details (consonants) are masked by louder, lingering speech sounds (the vowels). For many forms of music, however, *reverberance* can add an attractive fullness to the sound by bonding adjacent notes together and blending the sounds from the different instruments/voices in an ensemble.

The reverberation time T which is the traditional objective measure of this quality, was invented 100 years ago by W. C. Sabine. T is defined as the time it takes for the sound level in the room to decrease by 60 dB after a continuous sound source has been shut off. In practice, the evaluation is limited to a smaller interval of the decay curve, from −5 dB to −35 dB (or −5 dB to −25 dB) below the start value; but still relating to a 60 dB decay (Fig. 9.5), i. e.:

$$T = 60\,\mathrm{dB}\,\frac{(t_{-35}) - (t_{-5})}{(-5\,\mathrm{dB}) - (-35\,\mathrm{dB})}. \tag{9.1}$$

In this equation, t_{-x} denotes the time when the decay has decreased to XdB below its start value, or, if we let $R(t)$ represent the squared value of the decaying sound pressure and shut off the sound source at time $t = 0$:

$$10\log_{10}\left(\frac{R(t_{-X})}{R(0)}\right) = -X\,\mathrm{dB}\,. \tag{9.2}$$

With the fluctuations always present in decay curves, T should rather be determined from the decay rate, A dB/s, as found from a least-squares regression line (determined from the relevant interval of the decay curve). Hereby we get for T:

$$T = \frac{60\,\mathrm{dB}}{A\,\frac{\mathrm{dB}}{\mathrm{s}}} = \frac{60}{A}\mathrm{s}\,. \tag{9.3}$$

Ways to obtain the decay curve from the impulse response will be further explained in the section on measurement techniques.

Due to masking, the entire decay process is only perceivable during breaks in the speech or music. Besides, the rate of decay is often different in the beginning and further down the decay curve. During running music or speech, the later, weaker part of the reverberation will be masked by the next syllable or musical note. Therefore an alternative measure, early decay time (EDT) has turned out to be better correlated with the *reverberance* perceived during running speech and music. This parameter, like T, also measures the rate of the decay; but now evaluated from the initial part, the interval between 0 and −10 dB, only. Thus,

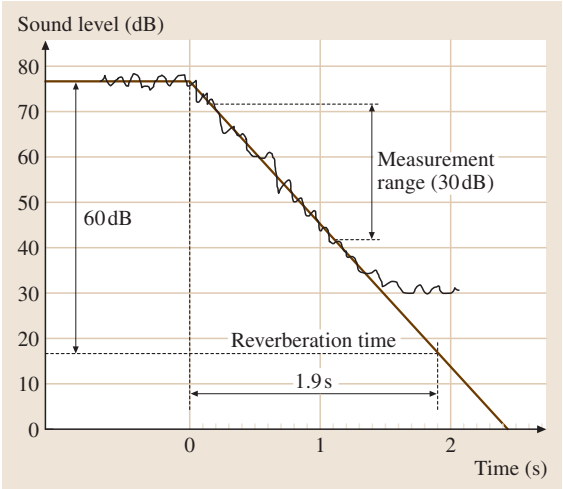


Fig. 9.5 The definition of reverberation time (after [9.4])

$$\mathrm{EDT} = 6(t_{-10}) \quad \text{or} \quad \mathrm{EDT} = \frac{60}{A_{(0\,\mathrm{dB}\to-10\,\mathrm{dB})}}\mathrm{s}\,. \tag{9.4}$$

The detailed behavior of the early part of the reverberation curve is influenced by the relative levels and distribution in time of the early reflections, which in turn vary depending on the positions of the source and receiver in the room. Likewise, the value of EDT is often found to vary throughout a hall, which is seldom the case with T.

In spite of the fact that EDT is a better descriptor of *reverberance* than T, T is still regarded the basic and most important objective parameter. This is mainly due to the general relationship between T and many of the other room acoustic parameters and because a lot of room acoustic theory relates to this concept, not least diffuse field theory, which is the basis for measurements of sound power, sound absorption, and sound insulation. T is also important by being referred to in legislation regarding room acoustic conditions in buildings.

Talking about diffuse field theory, it is often of relevance to compare the measured values of certain objective parameters with their expected values according to diffuse field theory and the measured or calculated reverberation time. As diffuse field theory predicts the decay to be purely exponential, the distribution in time of the impulse response squared should

Amazon
EX1010 Page 321

follow the function:

$$h^2(t) = A \exp\left(\frac{-13.8}{T} t\right) , \tag{9.5}$$

in which the constant −13.8 is determined by the requirement that for $t = T$:

$$10 \log_{10}\left(\exp\left(\frac{-13.8}{T} t\right)\right) = 60\,\text{dB} . \tag{9.6}$$

With an exponential decay, the decay curve in dB becomes a straight line. Consequently, the expected value of EDT, EDT_{exp}, equals T.

When evaluating measurement results, it is also relevant to compare differences with the smallest change that can be detected subjectively. For EDT, this so-called subjective difference limen is about 5% [9.7].

9.3.2 Clarity

Clarity describes the degree to which every detail of the performance can be perceived as opposed to everything being blurred together by later-arriving, reverberant sound components. Thus, *clarity* is to a large extent a property complementary to *reverberance*.

When reflections are delayed by no more than 50–80 ms relative to the direct sound, the ear will integrate these contributions and the direct sound together, which means that we mainly perceive the effect as if the clear, original sound has been amplified relative to the later, reverberant energy. Thus, an objective parameter that compares the ratio between energy in the impulse response before and after 80 ms has been found to be a reasonably good descriptor of *clarity*

$$C = 10 \log_{10}\left[\int_0^{80\,\text{ms}} h^2(t)\,\text{d}t \Big/ \int_{80\,\text{ms}}^{\infty} h^2(t)\,\text{d}t\right] . \tag{9.7}$$

The higher the value of C, the more the early sound dominates, and the higher the impression of *clarity*.

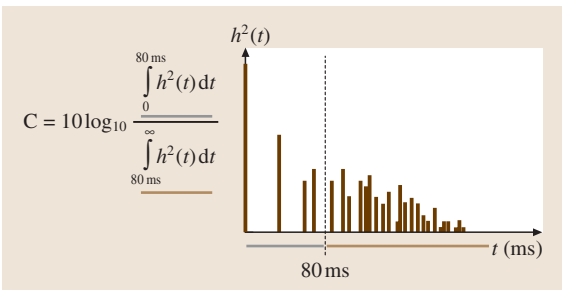


Fig. 9.6 The definition of C: the ratio between early and late energy in the impulse response

With exponential decay, the expected value of C becomes a function of T alone:

$$C_{\text{exp}} = 10 \log_{10}\left[\exp\left(\frac{1.104}{T}\right) - 1\right] \text{dB} . \tag{9.8}$$

The subjective difference limen for C (the equal best difference perceivable) is about 0.5 dB.

The definition of C is illustrated in Fig. 9.6.

Another parameter, which is also used to describe the balance between early and late sound or the balance between *clarity* and *reverberance*, is the center time t_s, which describes the center of gravity of the squared impulse response:

$$t_s = \int_0^{\infty} t h^2(t)\,\text{d}t \Big/ \int_0^{\infty} h^2(t)\,\text{d}t . \tag{9.9}$$

A low value of t_s corresponds to a clear sound, whereas higher values indicate dominance of the late, reverberant energy. The main advantage of t_s is that it does not contain a sharp time limit between early and late energy, since this sharp distinction is not justified by our knowledge about the functioning of our hearing system. The subjective difference limen for t_s is about 10 ms, and the expected diffuse field value is simply given by:

$$t_{s,\text{exp}} = \frac{T}{13.8} \tag{9.10}$$

9.3.3 Sound Strength

The influence of the room on the perceived *loudness* is another important aspect of room acoustics. A relevant measurement of this property is simply the difference in dB between the level of a continuous, calibrated sound source measured in the room and the level the same source generates at 10 m distance in anechoic surroundings. This objective measure called the (relative) strength G can also be obtained from impulse response recordings from the ratio between the total energy of the impulse response and the energy of the direct sound with the latter being recorded at a fixed distance (10 m) from the impulsive sound source:

$$G = 10 \log_{10} \frac{\int_0^{\infty} h^2(t)\,\text{d}t}{\int_0^{t_{\text{dir}}} h^2_{10\,\text{m}}(t)\,\text{d}t} . \tag{9.11}$$

Here the upper integration limit in the denominator t_{dir} should be limited to the duration of the direct sound pulse (which in practice will depend on the bandwidth

Amazon
EX1010 Page 322

selected). A distance different from 10 m can be used, if a correction for the distance attenuation is applied as well.

The expected value of G according to diffuse field theory becomes a function of T as well as of the room volume, V:

$$G_{\mathrm{exp}} = 10\log_{10}\left(\frac{T}{V}\right) + 45\,\mathrm{dB}\,. \qquad (9.12)$$

The subjective difference limen for G is about 1.0 dB. The definition of G is illustrated in Fig. 9.7.

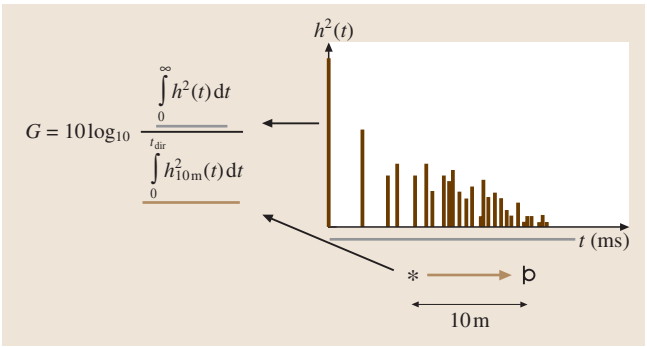


Fig. 9.7 The definition of strength G: the total energy in the impulse response measured relative to the direct sound level at 10 m distance from the source

9.3.4 Measures of Spaciousness

Spaciousness is the feeling that the sound is arriving from many different directions in contrast to a monophonic impression of all sound reaching the listener through a narrow opening. It is now clear that there are two aspects of *spaciousness*, both of which are attractive, particularly when listening to music:

- *apparent source width* (ASW): the impression that the sound image is wider than the visual, physical extent of the source(s) on stage. This should not be confused with localization errors, which of course should be avoided.

and

- *listener envelopment* (LEV): the impression of being inside and surrounded by the reverberant sound field in the room.

Both aspects have been found to be dependent on the direction of incidence of the impulse response reflections. When a larger portion of the early reflection energy (up to about 80 ms) arrives from lateral directions (from the sides) the ASW increases. When the level of the late, lateral reflections is high, strong LEV results.

The lateral components of the impulse response energy can be recorded using a figure-of-eight microphone with the sensitive axis held horizontal and perpendicular to the direction towards the sound source (so that the source lies in the deaf plane of the microphone). For measurement of the lateral energy fraction (LEF), the early part (up to 80 ms) of this lateral sound energy is compared with the energy of the direct sound plus all early reflections picked up by an ordinary omnidirectional microphone:

$$\mathrm{LEF} = \int_{t=5\,\mathrm{ms}}^{t=80\,\mathrm{ms}} h_1^2(t)\,dt \Big/ \int_{t=0\,\mathrm{ms}}^{t=80\,\mathrm{ms}} h^2(t)\,dt\,, \qquad (9.13)$$

where h_1 is the impulse response pressure recorded with a figure-of-eight microphone, whereas h is captured through the (usual) omnidirectional microphone.

It is mainly the energy at low and mid frequencies that contribute to the *spaciousness*. Consequently, LEF is normally averaged over the four octaves 125–1000 Hz. The higher the value of LEF, the wider the ASW. The literature contains many data on LEF values in different, existing concert halls.

LEF does not have an expected value related to T. In a completely diffuse field, LEF would be constant with a value of 0.33, which is higher than that normally found in real halls. The subjective difference limen for LEF is about 5%.

The definition of LEF is illustrated in Fig. 9.8.

The ASW aspect of *spaciousness* is not only dependent on the ratio between early lateral and total early

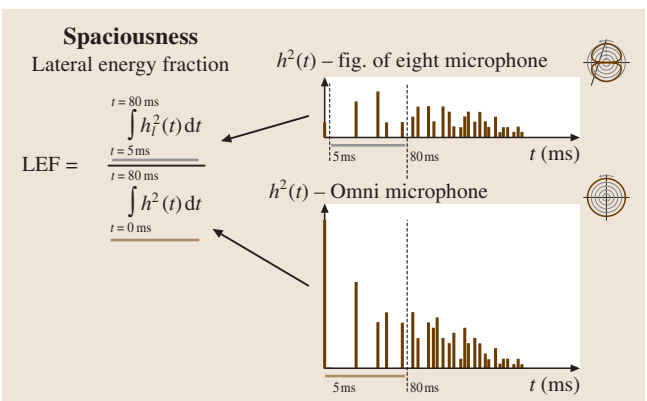


Fig. 9.8 The definition of lateral energy fraction LEF: the ratio between early reflection energy arriving from the sides and total early energy

Amazon
EX1010 Page 323

sound; but also on the total level of the sound. The higher the G value (and the louder the sound source), the broader the acoustic image of the source. However, at the time of writing, there is no solid way of incorporating the influence of level into the objective measure.

Listener envelopment seems to be determined mainly by the spatial distribution and the level of the late reflections (arriving after 80 ms). A parameter called *late lateral strength* (LG) relating the late lateral energy to the direct sound at 10 m distance from the source has been proposed to measure this quality [9.8]:

$$\mathrm{LG} = \int_{t=80\,\mathrm{ms}}^{t=\infty} h_1^2(t)\,\mathrm{d}t \Big/ \int_{t=0\,\mathrm{ms}}^{t=t_{\mathrm{dir}}} h_{10\,\mathrm{m}}^2(t)\,\mathrm{d}t\,. \qquad (9.14)$$

LG is likely to be included in the ISO 3382 standard (from 2007); but so far LG has only been found correlating with subjective responses in laboratory experiments using synthetic sound fields. Therefore, it may be wise not to put too much emphasis on this parameter until its value has also been confirmed by experiments in real halls.

In contrast to reflections arriving in the median plane, lateral reflections will cause the instantaneous pressure at the two ears of the listener to be different. Such a dissimilarity of the signals at the two ears can also be measured by means of the interaural cross-correlation coefficient IACC:

$$\mathrm{IACC}_{t_1,t_2} = \max \left| \frac{\int_{t_1}^{t_2} h_{\mathrm{L}}(t) h_{\mathrm{R}}(t+\tau)\,\mathrm{d}t}{\sqrt{\int_{t_1}^{t_2} h_{\mathrm{L}}^2(t)\,\mathrm{d}t \int_{t_1}^{t_2} h_{\mathrm{R}}^2(t)\,\mathrm{d}t}} \right| \qquad (9.15)$$

in which t_1 and t_2 define the time interval of the impulse response within which the correlation is calculated, h_{L} and h_{R} represent the impulse response measured at the entrance of the left and right ear, respectively, and τ is the interval within which we search for the maximum of the correlation. Normally, the range of τ is chosen between -1 and $+1$ ms, covering roughly the time it takes for sound to travel the distance from one ear to the other. As the correlation is normalized by the product of the energy of h_{L} and h_{R}, the IACC will take a value between 0 and 1. Results are often reported as $1-\mathrm{IACC}$ in order to obtain a value increasing with increasing dissimilarity, corresponding to an increasing impression of *spaciousness*. If the time interval for the calculation (t_1, t_2) is (0 ms, 100 ms), then the IACC will measure the ASW, while a later interval $(t_1, t_2) = (100\,\mathrm{ms}, 1000\,\mathrm{ms})$ may be used to describe the LEV. The literature on measured values in halls mainly contain data on IACC related to the 0–100 ms time interval.

Although the LEF and IACC parameters relate to the same subjective quality, they are not highly correlated in practice. Another puzzling fact is that LEF and IACC emphasize different frequency regions being of importance. LEF is primarily measured in the four lowest octaves, 125 Hz, 250 Hz, 500 Hz and 1000 Hz while IACC should rather be measured in the octave bands above 500 Hz. IACC values would always be high in the lower octaves, because the distance between the ears (< 30 cm) is small compared to 1/4 of the wave length (≈ 70 cm at 125 Hz).

9.3.5 Parameters Relating to Timbre or Tonal Color

Timbre describes the degree to which the room influences the frequency balance between high, middle and low frequencies, i. e. whether the sound is *harsh*, *bright*, *hollow*, *warm*, or whatever other adjective one would use to describe *tonal color*. Traditionally, a graph of the frequency variation of T (per 1/1 or 1/3 octave) has been used to indicate this quality; but a convenient single-number parameter intended to measure the warmth of the hall has been suggested [9.9]: the bass ratio (BR) given by:

$$\mathrm{BR} = \frac{T_{125\,\mathrm{Hz}} + T_{250\,\mathrm{Hz}}}{T_{500\,\mathrm{Hz}} + T_{1000\,\mathrm{Hz}}}\,. \qquad (9.16)$$

Likewise, a *treble ratio* (TR) can be formed as:

$$\mathrm{TR} = \frac{T_{2000\,\mathrm{Hz}} + T_{4000\,\mathrm{Hz}}}{T_{500\,\mathrm{Hz}} + T_{1000\,\mathrm{Hz}}}\,. \qquad (9.17)$$

However, in some halls, a lack of bass sound is experienced in spite of high T values at low frequencies. Therefore EDT or perhaps G versus frequency would be a better – and intuitively more logical – parameter for measurement of *timbre*. Likewise, BR or TR could be based on G rather than T values.

Besides the subjective parameters mentioned above, a quality called *intimacy* is also regarded as being important when listening in auditoria. *Beranek* [9.9] originally suggested this quality to be related to the initial time delay gap ITDG; but this has not been experimentally verified (At the time of writing, Beranek no longer advocates this idea but mentions the observation that, if the ITDG exceeds 45 ms, the hall has no intimacy [9.10]). It is likely that *intimacy* is related to a combination of some of the other parameters already mentioned, such as a high sound level combined with a clear and envelop-

Amazon
EX1010 Page 324

ing sound, as will naturally be experienced fairly close to the source or in small rooms.

9.3.6 Measures of Conditions for Performers

In rooms for performance of music it is also relevant to consider the acoustic conditions for the musicians, partly because it is important to ensure that the musicians are given the best working conditions possible and partly because the product as heard by the audience will also be better if the conditions are optimal for the performers.

Musicians will be concerned about *reverberance* and *timbre* as mentioned above; but also about at least two aspects which are unique for their situation: *ease of ensemble* and *support* [9.11] and [9.12].

Ease of ensemble relate to how well musicians can hear – and play together with – their colleagues. If ensemble is difficult to achieve, the result – as perceived by musicians and listeners alike – might be less precision in rhythm and intonation and a lack of balance between the various instruments. *Ease of ensemble* has been found to be related to the amount of early reflection energy being distributed on the stage. So far, the only widely recognized objective parameter suggested for objective measurement of this quality is *early support* $\mathrm{ST}_{\mathrm{early}}$.

$\mathrm{ST}_{\mathrm{early}}$ is calculated from the ratio between the early reflection energy and the direct sound in an impulse response recorded on the stage with a distance of only one meter between the source and receiver:

$$\mathrm{ST}_{\mathrm{early}} = 10\log_{10}\frac{\int_{20\,\mathrm{ms}}^{100\,\mathrm{ms}} h^2_{1\,\mathrm{m}}(t)\,\mathrm{d}t}{\int_{0\,\mathrm{ms}}^{t_{\mathrm{dir}}} h^2_{1\,\mathrm{m}}(t)\,\mathrm{d}t}\,. \tag{9.18}$$

Support relates to the degree to which the room supports the musicians' efforts to create the tone on their own instruments, whether they find it easy to play or whether they have to force their instruments to fill the room. Having to force the instrument leads to playing fatigue and inferior quality of the sound.

Support is also related to the amount of reflected energy on the stage measured using only a one meter source/microphone distance. For measurement of *support*, however, one needs to consider also the later reflections. This is because for many types of instruments, (especially strings), the early reflections will be masked by the strong direct sound from the instrument itself. Consequently, it seems relevant to define a measure

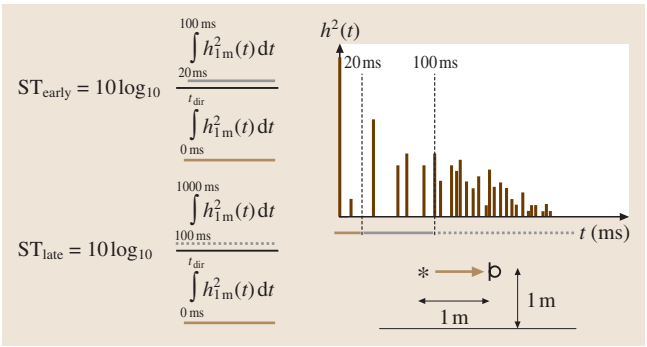


Fig. 9.9 The definition of early support $\mathrm{ST}_{\mathrm{early}}$ and late support $\mathrm{ST}_{\mathrm{late}}$, the ratio between early and late reflection energy respectively and the direct sound in the impulse response. Both are measured at 1 m distance from the source

such as *late support*, $\mathrm{ST}_{\mathrm{late}}$:

$$\mathrm{ST}_{\mathrm{late}} = 10\log_{10}\frac{\int_{100\,\mathrm{ms}}^{1000\,\mathrm{ms}} h^2_{1\,\mathrm{m}}(t)\,\mathrm{d}t}{\int_{0\,\mathrm{ms}}^{t_{\mathrm{dir}}} h^2_{1\,\mathrm{m}}(t)\,\mathrm{d}t} \tag{9.19}$$

which relates to late response (after 100 ms) from the room to the sound emitted.

$\mathrm{ST}_{\mathrm{early}}$ and $\mathrm{ST}_{\mathrm{late}}$ are typically measured in the four octaves 150 Hz, 500 Hz, 1000 Hz, 2000 Hz. The lowest octave is omitted primarily because it is not possible to isolate the direct sound from the early reflections in a narrow band measurement. The definitions of early and late support are illustrated in Fig. 9.9.

Also the support parameters are planned to be included in the ISO 3382 standard (from 2007); but like LG the experiences and amount of data available from existing halls are still rather limited.

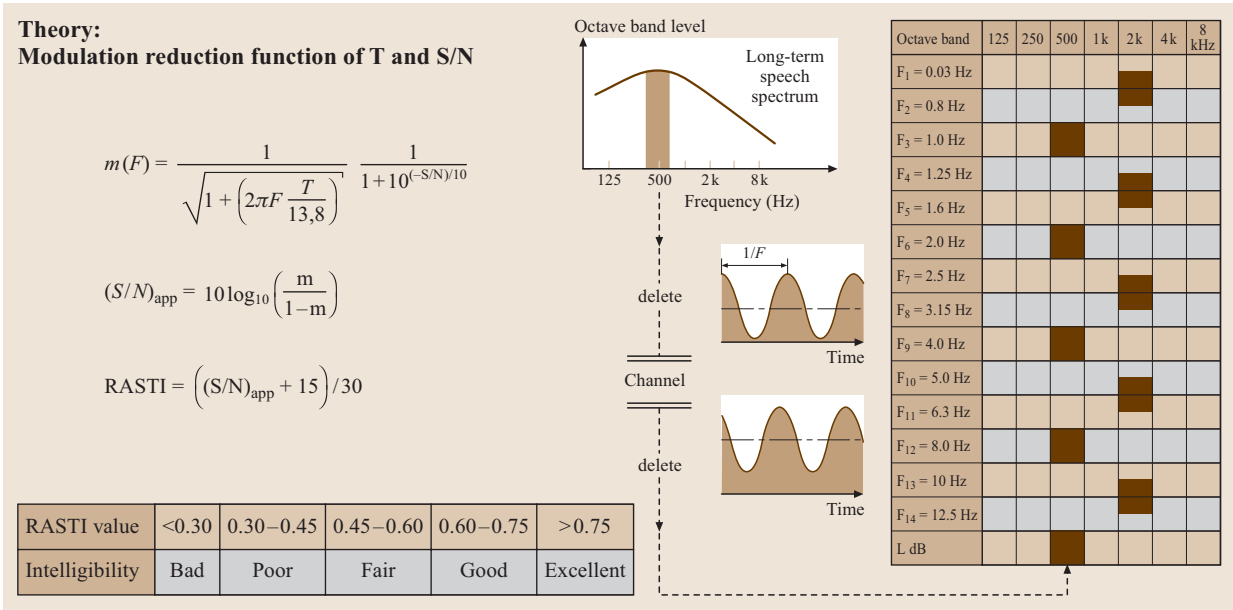
The amount of *reverberance* on the stage may be measured by means of EDT, (with a source–receiver distance of, say, 5 m or more).

9.3.7 Speech Intelligibility

All the objective parameters mentioned above (except the basic T parameter), are mainly relevant in larger auditoria intended for performance of music. In auditoria used for speech, such as lecture halls or theaters, the influence of the acoustics on intelligibility is a major issue.

Currently, the most common way to assess objectively *speech intelligibility* in rooms is by measurement of the speech transmission index STI.

Amazon
EX1010 Page 325



RASTI value	<0.30	0.30–0.45	0.45–0.60	0.60–0.75	>0.75
Intelligibility	Bad	Poor	Fair	Good	Excellent

Fig. 9.10 Illustration of the theory and principle in the measurement of STI or RASTI. The scale for the evaluation of RASTI values is shown at the bottom (after [9.13])

As illustrated in Fig. 9.10, this measure is based on the idea that speech can be regarded as an amplitude-modulated signal in which the degree of modulation carries the speech information. If the transmission path adds noise or reverberation to the signal, the degree of modulation in the signal will be reduced, resulting in reduced intelligibility.

The modulation transfer is tested by emitting noise in seven octave bands, each modulated with 14 different modulation frequencies as listed in the table in Fig. 9.10 and then calculating the ratio between the original and the received degree of modulation, the modulation reduction factor, in each of these 98 combinations. A weighted average of the modulation reduction factor then results in a number between 0 and 1, corresponding to very poor and excellent conditions respectively.

A faster measurement method using only two carrier bands of noises and four plus five modulation frequencies (indicated by the dark squares in Fig. 9.10) is called rapid STI (RASTI). The STI/RASTI method is described in an International Electrotechnical Commission (IEC) standard: IEC 286-16.

Although the original method of STI or RASTI measurement employs modulated noise signals, it is also possible to calculate the modulation reduction factor from the impulse response. Thus, the modulation reduction factor versus modulation frequency F, which is called the modulation transfer function (MTF), can be found as the Fourier transform of the squared impulse response normalized by the total impulse response energy.

According to *Bradley* [9.14], a simpler parameter, called the *useful-to-detrimental sound ratio* U_{80} is equally suitable for measurement of speech intelligibility. U_{80} is simply a modified version of the clarity parameter defined in Sect. 9.3.2, in which a correction is made according to the ratio between the levels of speech and background noise.

9.3.8 Isn't One Objective Parameter Enough?

It is important to notice that all the parameters mentioned above – apart from T – may show large differences between different seats within the same hall. Actually, differences within a single hall are sometimes as large (both objectively and subjectively) as the differences between two different halls.

It should also be mentioned that the objective parameters related to the three subjectively different aspects: *reverberance/clarity*, *loudness* and *spaciousness* show low mutual correlation when measured in different seats or in different halls. In other words, they behave as orthogonal factors and do not monitor the same properties

Amazon
EX1010 Page 326

of the sound fields. Consequently, it is obviously necessary to apply one objective parameter for each of these subjective aspects.

It is also clear that different listeners will judge the importance of the various subjective parameters differently. While some may base their judgment primarily on *loudness* or *reverberance* others may be more concerned about *spaciousness* or *timbre*.

For these reasons, one should be very sceptical when people attempt to rank concert halls along a single, universal, one-dimensional quality scale or speak about the best hall in the world. Fortunately, the diversity of room acoustic design and the complexity of our perception does not justify such simplifications.

9.3.9 Recommended Values of Objective Parameters

In view of the remarks above, it may be regarded risky to recommend values for the various objective acoustic parameters. On the other hand, there is a long tradition of suggesting optimal values for reverberation time T as a function of hall volume and type of performance. Besides, most of the other parameters will seldom deviate drastically from the expected value determined by T. As we shall see later, this deviation is primarily influenced by how we shape the room to control early reflections. Designing for strong early reflections can increase *clarity*, *sound strength* and *spaciousness*. Current taste regarding concert hall acoustics for classical music seems to be in favor of high values for these factors in addition to strong *reverberance*. This could lead to suggested ranges for the various parameters in small and large halls, as shown in Table 9.1. These values relate to empty halls with well-upholstered seating, assuming that, when fully occupied with musicians and audience, the T values will drop by no more than say 0.2 s. The reason for relating the values to the unoccupied condition is that it is seldom possible to make acoustic measurements in the occupied state and almost all reference data existing regarding parameters other than T are from unoccupied halls. On the other hand, suggesting well-upholstered seats is a sound recommendation in most cases, which will ensure only small changes depending on the degree of occupancy. This will also justify extrapolation of the unoccupied values of the other parameters to the occupied condition, as mentioned later in this section.

The values listed in the table were arrived at by first choosing values for T ensuring high *reverberance*, while the correlative values for EDT, G and C stem from the diffuse field expected values; but these have been slightly changed to promote high *clarity* and high *levels*. As this is particularly important in larger halls, it has been suggested to use an EDT value 0.1 s lower than T ($=\mathrm{EDT}_{\mathrm{exp}}$) and C values 1 dB higher than C_{exp} in a 2500 m^3 hall, but 0.2 s less than T and 2 dB higher than C_{exp}, respectively, in the 25 000 m^2 hall. Likewise, it is suggested to use G values 2 dB less than G_{exp} in the small halls; but only 1 dB less than or even equal to G_{exp} in large halls. For halls of size between the 2500 and 25 000 m^3 listed in the table, one may of course interpolate to taste. Please note that, in general, G is found to be 2–3 dB lower that G_{exp} (Sect. 9.5.6) so the G values suggested here are actually 1–2 dB higher than those found in "normal" halls.

In the occupied condition, one may expect EDT, C and G to be reduced by amounts equal to the difference between the expected values calculated using T for the empty and occupied conditions respectively. In any case,

Table 9.1 Suggested position-averaged values of objective room acoustic parameters in unoccupied concert halls for classical music. It is assumed that the seats are highly absorptive, so that T will be reduced by no more than 0.2 s when the hall is fully occupied. 2.4 s should be regarded as an upper limit mainly suitable for terraced arena or DRS halls with large volumes per seat (Sect. 9.7.3), whereas 2.0 s will be more suitable for shoe-box-shaped halls, which are often found to be equally reverberant with lower T values and lower volumes per seat

Parameter	Symbol	Chamber music	Symphony
Hall size	V/N	2500 m^3/300 seats	25 000 m^3/2000 seats
Reverberation time	T	1.5 s	2.0–2.4 s
Early decay time	EDT	1.4 s	2.2 s
Strength	G	10 dB	3 dB
Clarity	C	3 dB	−1 dB
Lateral energy fraction	LEF	0.15–0.20	0.20–0.25
Interaural cross correlation	1 − IACC	0.6	0.7
Early support	$\mathrm{ST}_{\mathrm{early}}$	−10 dB	−14 dB

Amazon
EX1010 Page 327

if the empty–occupied difference in T is limited to 0.2 s, as suggested here, then the difference in these parameters will be fairly limited, with changes in both C and G being less than one dB - given that the audience does not introduce additional grazing incidence attenuation of direct sound and early reflections (Sect. 9.6.2).

For opera, one may aim towards the same relationships between the diffuse field expected and the desired values of EDT, C and G, as mentioned above for symphonic halls; but the goal for the reverberation time will normally be set somewhat lower, 1.4–1.8 s in order to obtain a certain intelligibility of the libretto and perhaps to make breaks in the music sound more dramatic (Sect. 9.7.2).

For rhythmic music, T values of 0.8–1.5 s, depending on room size, are appropriate, and certainly the value should not increase towards low frequencies in this case. In very large rock venues such as sports arenas, it may actually be very difficult to get T below 3–5 s; but even then the conditions can be satisfactory with a properly designed sound system. The reason is that in such large room volumes the level of the reverberant sound can often be controlled, if highly directive loudspeakers are being used. In these spaces, the biggest challenge is often to avoid highly delayed echoes, which are very annoying. For amplified music, only recommendations for T are relevant, because the acoustic aspects related to the other parameters will be determined primarily by the sound system (Sect. 9.7.5).

In order to ensure adequate speech intelligibility in lecture halls and theaters, values for STI/RASTI should be at least 0.6. In reverberant houses of worship values higher than 0.55 are hard to achieve even with a well-designed loudspeaker system.

9.4 Measurement of Objective Parameters

Whenever the acoustic specifications of a building are of importance we need to be able to predict the acoustic conditions during the design process as well as document the conditions after completion. Therefore, in this and the following sections, techniques for measurement and prediction of room acoustic conditions will be presented.

In Sect. 9.2.1 it was claimed that the impulse response contains all relevant information about the acoustic conditions in a room. If this is correct, it must also be true that all relevant acoustic parameters can be derived from impulse response measurements. Fortunately, this has also turned out to be the truth.

9.4.1 The Schroeder Method for the Measurement of Decay Curves

Originally, reverberation decays were recorded from the decay of the sound level following the termination of a stationary sound source. However, *Schroeder* [9.15] has shown that the reverberation curve can be measured with increased precision by *backwards* integration of the impulse response, $h(t)$, as follows:

$$R(t) = \int_t^\infty h^2(t)\,\mathrm{d}t = \int_0^\infty h^2(t)\,\mathrm{d}t - \int_0^t h^2(t)\,\mathrm{d}t \quad (9.20)$$

in which $R(t)$ is equivalent to the decay of the squared pressure decay. The method is called backwards integration because the fixed upper integration limit, *infinite time*, is not known when we start the recording. Therefore, in the days of magnetic tape recorders, the integration was done by playing the tape backwards. In this context *infinite time* means the duration of the recording, which should be comparable with the reverberation time. Traditional noise decays contain substantial, random fluctuations because of interference by the different eigenmodes present within the frequency range of the measurement (normally 1/3 or 1/1 octaves). These fluctuations will be different each time the measurement is carried out because the modes will be excited with random phase by the random noise (and the random time of the noise interruption). When, instead, the room is exited by a repeatable impulse, the response will be repeatable as well without such random fluctuations. In fact, Schroeder showed that the ensemble average of interrupted noise decays (recorded in the same source and receiver positions) will converge towards $R(t)$ as the number of averages goes towards infinity.

In (9.20), the right-hand side indicates that the impulse response decay can be derived by subtracting the running integration (from time zero to t) from the total energy. Contrary to the registration of noise decays, this means that the entire impulse response must be stored before the decay function is calculated. However, with modern digital measurement equipment, this is not a problem. From the $R(t)$ data, T is calculated by linear regression as explained in Sect. 9.3.1. As the EDT is evaluated from a smaller interval of the decay curve than T, the EDT is more sensitive to random decay fluctuations than is T. Therefore, EDT should never

Amazon
EX1010 Page 328

be derived from interrupted noise decays – only from integrated impulse responses.

9.4.2 Frequency Range of Measurements

T may be measured per 1/3 octave; but regarding the other objective parameters mentioned in this chapter, it makes no sense to use a frequency resolution higher than 1/1 octave. The reason is that the combination of narrow frequency intervals and narrow time windows in the other parameters will lead to extreme fluctuations with position of the measured values due to the acoustic relation of uncertainty. Such fluctuations have no parallel in our subjective experience. *Bradley* [9.16] has shown that, with 1/1 octave resolution, a change in microphone position of only 30 cm can already cause fluctuations in the clarity C and strength G of about 0.5–1 dB, which is equal to the subjective difference limen. Higher fluctuations would not make sense, as normally we do not experience an audible change when moving our head 30 cm in a concert hall.

The frequency range in which room acoustic measurements are made is normally the six octaves from 125 to 4000 Hz, but it may be extended to 63–8000 Hz when possible. Particularly for reverberation measurements in halls for amplified music, the 63 Hz octave is important.

9.4.3 Sound Sources

With the possibility of deriving all of the objective parameters described above from impulse response measurements, techniques for creating impulses are described briefly in the following.

Basically, the measurements require an omnidirectional sound source emitting short sound pulses (or other signals that can be processed to become impulses) covering the frequency interval of interest, an omnidirectional microphone and a medium for the storage of the electrical signal generated by the microphone.

Impulsive sources such as pistols firing blank cartridges, bursting balloons, or paper bags and electrical spark sources may be used; but these sources are primarily used for noncritical measurements, as their directivity and acoustic power are not easy to control.

For measurements requiring higher precision and repeatability, omnidirectional loudspeakers are preferable, as the power and directivity characteristics of loudspeakers are more stable and well defined. Omnidirectional loudspeakers are often built as six units placed into the sides of a cube, 12 units placed into a dodecahedron or 20 units in an icosahedron, see Fig. 9.11. The requirements regarding omnidirectivity of the source are described in the ISO 3382 standard.

Loudspeakers, however, cannot always emit sufficient acoustic power if an impulsive signal is applied directly. Therefore, special signals of longer duration such as maximum-length sequences or tone sweeps have been developed, which have the interesting property that their autocorrelation functions are band-limited delta pulses. This means that the loudspeaker can emit a large amount of energy without challenging its limited peak-power capability while impulse responses with high time resolution can still be obtained afterwards through post-processing (a correlation/convolution process) of the recorded noise or sweep responses.

In certain cases, other source directivity patterns than omnidirectional can be of interest. For example, a directivity like that of a human talker may be relevant if the measurement is related to the intelligibility of speech or to measurements on the stage in an opera house. A suitable talker/singer directivity can be obtained by using a small loudspeaker unit (membrane diameter about three to four inches) mounted in a closed box of size comparable to that of the human head. Using only one of the loudspeakers in a cube or dodecahedron speaker of limited size is another possibility.

9.4.4 Microphones

For most of the parameters mentioned, the microphone should be omnidirectional, while omni plus figure-of-eight directivity and dummy heads are used when the impulse responses are to be used for the calculation of LEF and IACC.

Three-dimensional intensity probes, sound field microphones or microphone arrays have also been suggested in attempts to obtain more-complete information about the amplitude and direction of incidence of individual reflections [9.17] or for wave field analysis [9.18]. However, such measurements are mainly for research or diagnostic purposes. As such, they do not fulfill the goal set up in Sect. 9.1 of reducing the information to what is known to be subjectively relevant. A selection of relevant microphones are shown in Fig. 9.12.

9.4.5 Signal Storage and Processing

For the storage of the impulse responses the following choices appear.

- The hard disk on a personal computer (PC) equipped with a sound card or special analog-to-digital (A/D) converter card

Amazon
EX1010 Page 329

- Real-time (1/3 and 1/1 octave) analyzers or sound level meters with sufficient memory for storage of a series of short time-averaged root-mean-square (RMS) values
- Fast Fourier transform (FFT) analysers capable of recording adequately long records
- Tape recorders, preferably a digital audio tape (DAT) recorder, or even MP3 recorders given that the data reduction does not deteriorate the signal.

Of these, real-time analyzers and sound level meters will process the signal through an RMS detector before storage, which means that not the full signal, but only energy with a limited time resolution will be recorded.

Today, calculation of the objective parameters will always be carried out by a PC or by a computer built into a dedicated instrument. A large number of PC-based systems and software packages particularly suited for room acoustic measurements are available. Some systems come with a specific analog-to-digital (A/D), digital-to-analog (D/A) and signal-processing card, which must be installed in or connected to the PC, while others can use the sound card already available in most PCs as well as external sound cards for hobby music use.

9.5 Prediction of Room Acoustic Parameters

Beyond theoretical calculation of the reverberation time, the prediction techniques presented in this section range from computer simulations and scale model measurements to simple linear models based on empirical data collected from existing halls.

In all cases, the main objective is the prediction of the acoustic conditions described in terms of the acoustic parameters presented in Sect. 9.3. Just as we can record the sound in a hall, both scale models and numerical computer simulations can also provide *auralizations*, which are synthesized audible signals that allow the client and architect to listen to and participate in the acoustic evaluation of proposed design alternatives. Such audible simulations will often have much greater impact and be more convincing than the acoustician's verbal interpretation of the numerical results. Therefore, the acoustician must be very careful to judge the fidelity and the degree of realism before presenting auralizations.

9.5.1 Prediction of Reverberation Time by Means of Classical Reverberation Theory

Reverberation time as defined in Sect. 9.3.1 is still the most important objective parameter for the characterization of the acoustics of a room. Consequently, the prediction of T is a basic tool in room acoustic design. Calculation of reverberation time according to the Sabine equation was the first attempt in this direction and today is still the most commonly used. However, during the 100 years since its invention, several other reverberation time formulae have been suggested (by Eyring, Fitzroy, Millerton and Sette, Metha and Mulholland Kuttruff and others), all with the purpose of correcting some obvious shortcomings of the Sabine method.

The Sabine equation has been described in Sect. 11.1.4. In larger rooms, the absorption in the air plays a major role at high frequencies. If we include this factor, the Sabine equation reads:

$$T = \frac{0.161V}{S\alpha^* + 4mV}\,, \tag{9.21}$$

where V is the room volume, S is the total area of the room surfaces, α^* is the area-weighted average absorption coefficient of the room surfaces

$$\alpha^* = \overline{\alpha} = \frac{1}{S}\sum_i S_i\alpha_i \tag{9.22}$$

and m accounts for the air absorption, which is a function of the relative humidity and increases rapidly with fre-



Fig. 9.11 Two types of omnidirectional sound sources for room acoustic measurements: blank pistol (in the *raised hand of the seated person*) and an omnidirectional loudspeaker (icosahedron with 20 units)

Amazon
EX1010 Page 330

Table 9.2 Air absorption coefficient m for different frequencies and relative humidity; valid for an air temperature of 20 °C (after [9.19])

Relative humidity (%)	0.5 kHz	1 kHz	2 kHz	4 kHz	8 kHz	Air absorption
40	0.4	1.1	2.6	7.2	23.7	$10^{-3}\,\mathrm{m}^{-1}$
50	0.4	1.0	2.4	6.1	19.2	$10^{-3}\,\mathrm{m}^{-1}$
60	0.4	0.9	2.3	5.6	16.2	$10^{-3}\,\mathrm{m}^{-1}$
70	0.4	0.9	2.1	5.3	14.3	$10^{-3}\,\mathrm{m}^{-1}$
80	0.3	0.8	2.0	5.1	13.3	$10^{-3}\,\mathrm{m}^{-1}$

quency [9.19]. Values of m versus frequency and relative humidity are listed in Table 9.2.

The Sabine equation assumes the absorption to be evenly distributed on all surfaces, and that the sound field is *diffuse*, which means that in each point of the room:

1. the energy density is the same, and
2. there is equal probability of the sound propagating in all directions.

Among the alternative reverberation formulae, only the Eyring method will be described here, as it may give more-accurate predictions in cases where the room is highly absorptive.

In contrast to Sabine, the Eyring theory assumes that the sound field is composed of plane sound waves that lose a fraction of their energy equal to the absorption coefficient of the surface whenever the wave hits a surface in the room. Thus, after n reflections, the energy in all wavefronts and the average energy density in the room has been reduced to $(1-\overline{\alpha})^n$ times the original value. The average distance of propagation during this process is $l_\mathrm{m} n = ct$, in which l_m is the *mean free path*, equal to the average distance traveled by the wave between two reflections, and t is the time elapsed since the wave propagation started. *Kosten* [9.20] has shown, that regardless of the room shape, l_m equals $4V/S$, if all directions of propagation are equally probable. These assumptions lead to the Eyring formula, which can be expressed by substituting α^* in (9.21) by

$$\alpha^* = \alpha_\mathrm{e} = \ln\left(\frac{1}{1-\overline{\alpha}}\right) \tag{9.23}$$

For low values of $\overline{\alpha}$, $\overline{\alpha}$ and α_e are almost identical, causing the Sabine and the Eyring formulae to give nearly identical results; but the difference becomes noticeable when $\overline{\alpha}$ exceeds about 0.3. In general, α_e will always be larger than $\overline{\alpha}$, leading to $T_\mathrm{Sabine} > T_\mathrm{Eyring}$. In the extreme case of the mean absorption approaching 1, α_e converges towards ∞, whereby $T_\mathrm{Eyring} \to 0$ as one would expect for a totally absorbing room. However, T_Sabine converges towards the finite positive value 0.16 V/S, which of course is unrealistic.

Both the Sabine and the Eyring theories suffer from at least two shortcomings. Neither of them consider the actual distribution of the free paths (see the comments on the *mean free path* above), which is highly dependent on the room shape, nor the often very uneven distribution of the absorption in the room, which causes different directions of sound propagation not to be equally probable. Typical situations where these factors become important are rooms with highly absorbing acoustic ceilings and hard walls and floors – or the reverse situation of an auditorium, where almost all absorption is found in the seating. In these situations the energy is certainly not evenly distributed, there is a considerable distribution of the path lengths, and there is a much higher probability for sound energy to travel towards the absorbing surface than away from it.

A common example in which the Sabine and Eyring theories fall short is the simple case of a rectangular room with plane walls, absorbing ceiling and low height compared to length and width. In such a room the main part of the late reverberant energy will be stored in

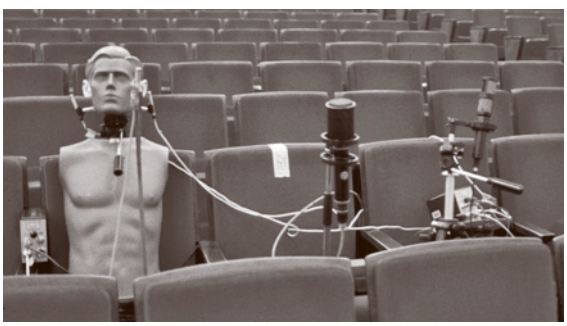


Fig. 9.12 A selection of microphones types used for recording impulse responses in rooms. *From left*: artificial head (with both internal and external microphones), *sound field microphone* (with four capsules for 3-D recordings of reflections) and a two-channel (stereo) microphone with omnidirectional and figure-of-eight capsules

Amazon
EX1010 Page 331

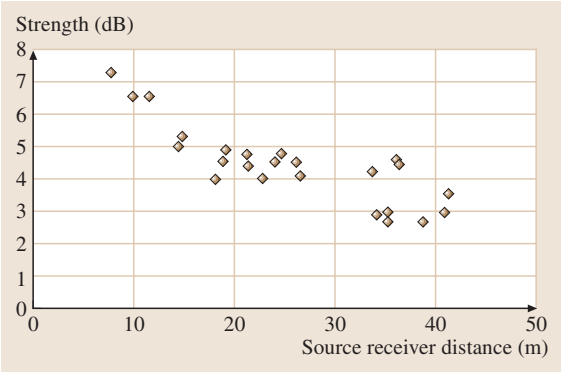


Fig. 9.13 Strength versus distance measured in the Boston Symphony Hall; values averaged over the four octaves 250–2000 Hz. The reverberation distance in this hall is about 5 m

one- and two-dimensional horizontal room modes with long free paths, whereas the three-dimensional modes with shorter free paths will soon have lost their energy by interacting with the absorbing ceiling. Hereby, different modes end up having very different decay rates, leading to bent or double-sloped decay curves and to measured T values often longer than calculated. In fact, only the unnatural situation with an even absorption distribution and all free paths of equal length will result in a straight-line decay and a well-defined T value.

From practical measurements of the distribution of G values, it is also clear that the assumption of an even distribution of the energy density is not met in large auditoria. Contrary to the Sabine theory, which predicts a constant level beyond the reverberation distance (Fig. 11.6), we observe that the level continues to decrease with distance from the source – even far beyond the reverberation distance, where the contribution of the direct sound is negligible. An example of this is seen in Fig. 9.13. (Based on empirical data, simple equations predicting this attenuation of G with distance as a function of room geometry have been derived as described in Sect. 9.5.6.)

Still, rather than relying on another of the reverberation formulas to provide a more correct result, today it may be wiser just to apply the Sabine and perhaps the Eyring equations, keeping in mind their limitations. Thus, *Beranek* [9.21] has suggested that, for Sabine calculations in concert halls, one should apply different sets of seat absorption values depending on the room shape. These values should be measured in nearly the same type of room as the hall in question.

When higher prediction accuracy is required, it is recommended to carry out simulations in a computer model as described in Sect. 9.5.4. However, also with this calculation approach, the question about which absorption values to use is relevant.

9.5.2 Prediction of Reverberation in Coupled Rooms

Auditoria with coupled spaces form another situation in which the decay curve may end up being nonlinear and the energy density will be different in different areas of the room. Typical of such cases are open-plan office floors coupled to an atrium covering several storeys, seating areas in auditoria subdivided by (deep) balconies, theaters with proscenium openings between the auditorium and the stage house, churches subdivided into main and side naves and concert halls with reverberation chambers. Diffuse field theory can be used to illuminate important properties of the reverberation conditions in coupled rooms.

We consider a sound source placed in a room, room 1, with volume V_1 and physical absorption area A_{10}. This room is coupled by an opening with area S to another room, room 2, with volume V_2 and absorption area A_{20}. From diffuse field theory (the energy balance equations) we find that the apparent absorption area of room 1, A_1, depends on the ratio between the absorption area of the attached room A_{20} and the area of the opening S:

$$A_1 = A_{10} + \frac{A_{20}S}{A_{20}+S} \,. \tag{9.24}$$

It is seen that for small openings, $S \ll A_{20}$, $A_1 \approx A_{10} + S$, and for large openings, $S \gg A_{20}$, $A_1 \approx A_{10} + A_{20}$, as we would expect.

As for the reverberation curve, a double slope may be observed, particularly if both source and receiver are placed in the less reverberant of the two rooms. The two reverberation times T_I and T_II defining the double slope can be described in terms of the reverberation times for each of the two rooms separately if we consider the opening to be totally absorbing:

$$T_1 = \frac{0.161V_1}{A_{10}+S} \quad \text{and} \quad T_2 = \frac{0.161V_2}{A_{20}+S} \,. \tag{9.25}$$

However, for our purpose the math gets simpler if we apply damping coefficients: $\delta_1 = 6.9/T_1$ and $\delta_2 = 6.9/T_2$ instead of the reverberation times. Then, with coupling, the two damping coefficients, δ_I and δ_II, corresponding to the slope in the first and second part of the decay,

Amazon
EX1010 Page 332

respectively, can be calculated from:

$$\delta_{\mathrm{I,II}} = \frac{\delta_1 + \delta_2}{2} \pm \sqrt{\frac{(\delta_1 - \delta_2)^2}{4} + \frac{S^2 \delta_1 \delta_2}{(A_{10} + S)\,(A_{20} + S)}} \tag{9.26}$$

upon which

$$T_{\mathrm{I}} = 6.9/\delta_{\mathrm{I}} \quad \text{and} \quad T_{\mathrm{II}} = 6.9/\delta_{\mathrm{II}}\,. \tag{9.27}$$

Another important feature of the double-slope decay is how far down the knee point appears. If the opening area is large and/or the source or receiver is placed close to the opening, then a substantial exchange of energy can occur and the knee point may appear so early that even the EDT can be influenced by the decay from the coupled room with longer T. If the opening area is small, then the knee point appears late and far down on the curve, in which case the influence of the coupled room can only be perceived after final cords. This is the case with some of the existing concert halls equipped with coupled reverberation chambers. Further descriptions of coupled spaces can be found in [9.5].

9.5.3 Absorption Data for Seats and Audiences

Regardless of which reverberation formula is used, the availability of reliable absorption values is fundamental for the accurate prediction of T as well as of most other room acoustic parameters. Beyond the absorption values of various building materials (as listed in Table 11.1), realistic figures for the absorption of the chairs and seated audience are of special concern, because these elements normally account for most of the absorption in auditoria. The absorption of chairs – both with and without seated people – depends strongly on the degree of upholstery. Average values of absorption for three different degrees of chair upholstery have been published by *Beranek* [9.22] and quoted in Table 9.3. As mentioned earlier, chair absorption values for use specifically in Sabine calculations and for different types of hall geometries can be found in [9.21].

Sometimes audience absorption data are quoted as absorption area per chair or per person. However, as demonstrated by *Beranek* [9.3], the use of absorption coefficients multiplied by the area covered by the seats plus an exposed perimeter correction is more representative than absorption area per person, because audience absorption tends to vary proportionally with the area covered, while the absorption coefficient does not change much if the density of chairs is changed within that area.

Minimizing the total sound absorption area is often attempted in auditoria for classical music in order to obtain a strong, reverberant sound field. One way to achieve this is not to make the row-to-row distance and the width of the chairs larger than absolutely necessary. Another factor is the seat design itself. Here one should aim at a compromise between minimum absorption and still a minimum difference between the absorption of the occupied and empty seat. This is facilitated by back rests not being higher than the shoulders of the seated person and only the surfaces covered by the person being upholstered. The rear side of the back rest should be made from a hard material like varnished wood. On the other hand, a minimum difference between the occupied and empty chair implies that the upholstery on the seat and back rest should be fairly thick (e.g., 80 mm on the

Table 9.3 Absorption coefficients of seating areas in concert halls for three different degrees of upholstery; both empty and occupied (after [9.22])

Octave centre frequency (Hz)	125	250	500	1000	2000	4000
Heavily upholstered chairs Unoccupied	0.70	0.76	0.81	0.84	0.84	0.81
Heavily upholstered chairs Occupied	0.72	0.80	0.86	0.89	0.90	0.90
Medium upholstered chairs Unoccupied	0.54	0.62	0.68	0.70	0.68	0.66
Medium upholstered chairs Occupied	0.62	0.72	0.80	0.83	0.84	0.85
Lightly upholstered chairs Unoccupied	0.36	0.47	0.57	0.62	0.62	0.60
Lightly upholstered chairs Occupied	0.51	0.64	0.75	0.80	0.82	0.83

Amazon
EX1010 Page 333

seat and 50 mm on the back rest), the bottom of the tip-up seats should be perforated or otherwise absorptive, and when the seat is in its vertical position, there should be a wide opening between the seat and the back rest so that the sound can still access the upholstered areas.

9.5.4 Prediction by Computer Simulations

Computer simulations take into account the geometry and actual distribution of the absorption materials in a room as well as the actual source and receiver positions. The results provided are values for all relevant acoustic parameters as well as the generation of audio samples for subjective judgments. Computer simulation is useful not only for the design of concert halls and theaters, but also for large spaces such as factories, open-plan offices, atria, traffic terminals, in which both reverberation, intelligibility and noise-mapping predictions are of interest. Besides, they can be used in *archaeological acoustics* for virtual reconstruction of the acoustics of ancient buildings such as Roman theaters (http://server.oersted.dtu.dk/www/oldat/erato/).

The first computer models appeared in the 1960s, and today a number of commercially available software packages are in regular use by acoustic consultants as well as by researchers all over the world.

In computer simulations the room geometry is represented by a three-dimensional (3-D) computer-aided design (CAD) model. Thus, the geometry information can often be imported from a 3-D model file already cre-

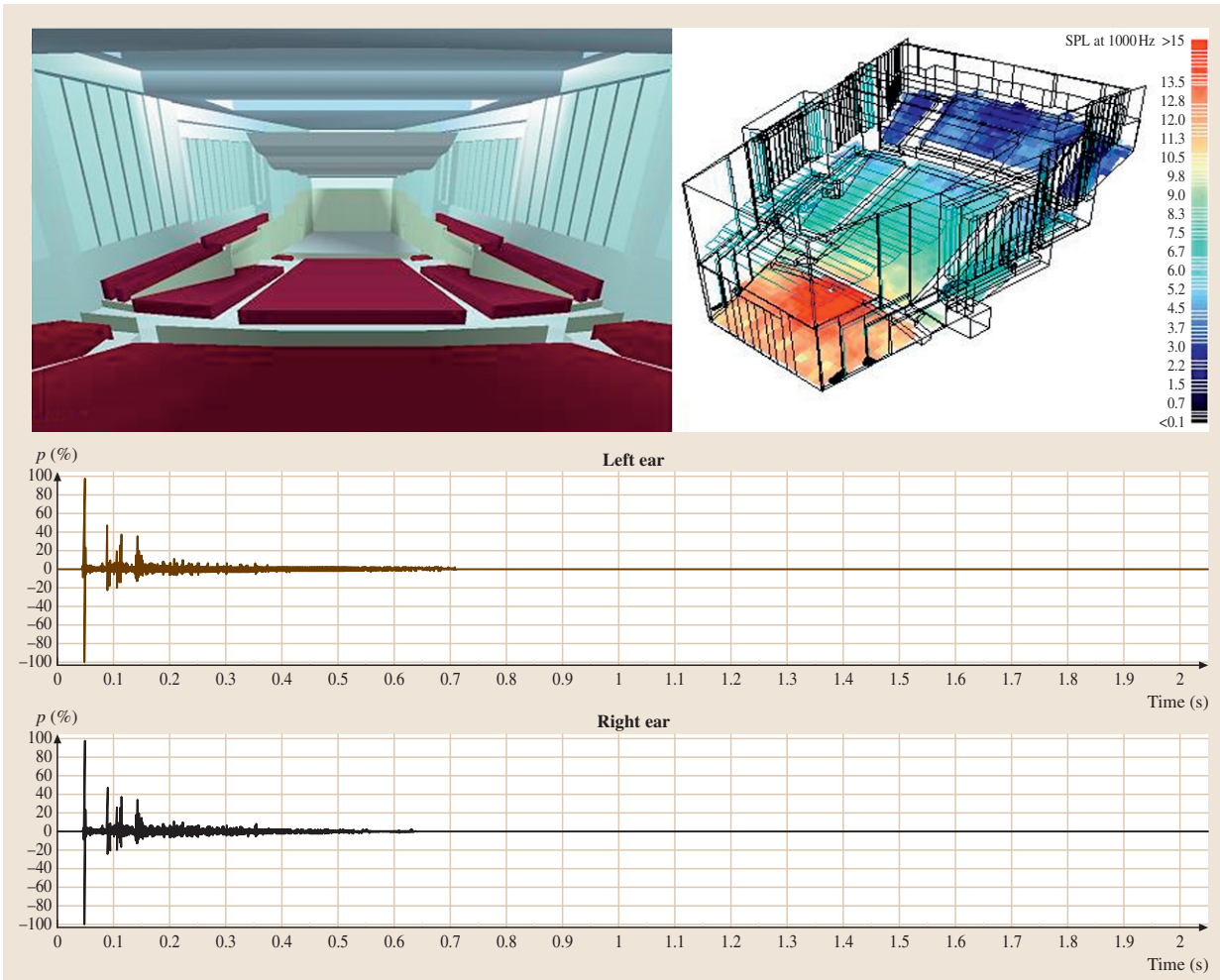


Fig. 9.14 Examples of output from a room acoustic simulation software package (ODEON); see text for explanation

Amazon
EX1010 Page 334

ated by the architects. However, one needs to break up eventual curved surfaces into plane elements and often it is also advisable to simplify details in the geometry provided by the architect. Alternatively, the acoustician can build the room model by writing a file of coordinate points or mathematical expressions for all surface corners. Of course this will be more time consuming in cases of complex room geometry, but some programs offer intelligent programming routines for the modeling of geometric elements.

When the geometry has been completed, the absorption values for each octave band, the scatter, and the eventual degree of acoustic transparency have to be assigned to each surface. In addition, the source and receiver characteristics (power and directivity versus frequency, position and orientation) must also be entered.

In the calculation of sound propagation, most models disregard phase properties and use an energy approximation. The sound propagation is studied by means of rays (up to millions depending on the room complexity) being traced from the source position through reflections until their energy has been reduced below the dynamic range of interest (often determined by T or the signal-to-noise ratio in auralizations). Reflection directions are chosen so that angle of reflection equals angle of incidence or with more or less random angles depending on the scatter value attributed to the surface. For the calculation of early reflections, some models also apply image source theory, which actually makes phase considerations possible if the complex impedances of the various surface materials and not just their energy absorption coefficients are known. However, the late reverberation part is normally calculated by some kind of ray method, as image source calculations become impractical after a few orders of reflection. Recently, however, attempts to carry out complete calculations inspired by finite-element (FEM) or boundary-element (BEM) methods have been reported even for rather complex rooms [9.23], whereby phase and diffraction phenomena can be handled.

As a result of tracing the history of all rays emitted in the room model, source and receiver specific impulse responses are produced with detailed information about the direction of incidence, delay and level versus frequency of each reflection component. From these, all the parameters mentioned in Sect. 9.3 can be calculated. Most programs can generate a grid of receiver point over selected audience areas and code the numeric results using a color scale to facilitate a fast overview of the detailed position results for any of the parameters. Also, automatic plots of relevant statistics regarding the distribution with frequency and position are provided.

Impulse responses suitable for use in *auralization* can be generated by applying available head-related transfer functions, which have been recorded as a function of direction of sound incidence on an artificial head. Such transfer functions not only represent the directivity of the human receiver, but are also important for correct perception of direction of incidence of sound field components when listening through headphones. Alternatively, the directional information of the individual reflections making up the impulse response can be coded into a surround-sound format for listening via a multiple-loudspeaker setup.

Figure 9.14 shows a view of a room model as well as two binaural impulse responses and a color mapping of a calculated parameter (generated by the ODEON software).

9.5.5 Scale Model Predictions

Acoustic scale models have been used since the 1930s [9.24] to study the behavior of sound in rooms. With proper care in detailing the geometry and the choice of materials for building the model, this technique can provide quite accurate predictions of impulse responses and acoustic parameters. Actually, scale modeling is still regarded as more reliable than computer models in cases where the room contains a lot of irregular surfaces or objects that diffuse or diffract sound waves. However, the use of physical scale models is limited to larger, acoustically demanding projects, as building and testing the model is far more time consuming and costly than computer modeling.

The diffusion and diffraction caused by an object or surface in a room depends on the ratio between the linear dimensions and the wavelength of the sound: l/λ. Therefore, in a $1:M$ scale model, the diffraction/diffusion conditions will be modeled correctly if the wavelengths of the measurement signals in the model are chosen such that:

$$\frac{l}{\lambda} = \frac{l_{\mathrm{M}}}{\lambda_{\mathrm{M}}} = \frac{l/M}{\lambda/M} \quad \Rightarrow \quad f_{\mathrm{M}} = fM\,. \tag{9.28}$$

This means that we should increase the frequency used in the model measurements by the factor M. Fortunately, sound sources and microphones exist that are capable of handling frequencies up to around 100 kHz, whereby the frequency range up to 10 kHz can be handled in a 1 : 10 scale model or 2 kHz in a 1 : 50 scale model. The sources may be small loudspeaker units (piezoelectric or

Amazon
EX1010 Page 335

electro magnetic) and the microphones 1/4" or even 1/8" condenser types.

Ideally, the absorption coefficient α_M of the materials chosen for building each surface in the hall model should fulfil the equation:

$$\alpha_M(fM) = \alpha(f) \,. \tag{9.29}$$

In practice, however, we need only to distinguish between mainly reflecting and mainly absorptive materials. The reflecting surfaces are quite easy, as these can be made of any hard material (plywood, plaster) with a couple of layers of varnish if necessary. It is far more important to build the seats/audience so that both head diffraction and absorption is correct for the scale chosen. In the end it is often necessary to fine-tune the reverberation time in the model by applying absorption to some secondary surfaces (surfaces that do not generate primary early reflections).

Another important issue is to compensate for the excessive air absorption at high frequencies in the model. This can be achieved either by drying the air in the model, by exchanging the air for nitrogen, or simply as a calculated compensation since the attenuation is a simple linear function of time once the, frequency, humidity and temperature have been specified. However, in the case of compensation the signal-to-noise ratio at high frequencies will be severely limited, which reduces the decay range for the estimation of T and the sound quality if auralization is attempted. Figures 9.15 and 9.16 show an example of a 1:10 scale model and its audience respectively.

9.5.6 Prediction from Empirical Data

In the 1980s, when most of the current objective acoustic parameters had been defined, several researchers started making systematic measurement surveys of concert, opera and multipurpose halls. Many of these measured data were published in [9.3]. Combining acoustic data with data on the geometry of the halls has made it possible to derive some simple rules of thumb regarding how, and how much, acoustic parameters are affected by the choice of gross room shape and dimensions.

Through statistical multiple linear-regression analysis of data from more than 50 halls, a number of relationships between acoustical and geometrical properties have been found [9.25]. A number of the linear regression models derived are shown in Table 9.4. In these models, the variations in the acoustic parameters are described as functions of the expected value according to diffuse field theory (G_{exp} and C_{exp}, Sect. 9.3) plus various geometrical variables such as: average room height H, average width W, room volume V, number of seats N, number of rear balcony levels 'no. rear balc.' etc. When the models were derived, the measured reverberation time (T) was used to calculate the expected values of strength G_{exp} and clarity C_{exp}. When using these models for prediction of the values in a hall not yet built, the expected values could be based on a Sabine calculation of T instead. It should be mentioned that, apart from $\Delta G(10\,\text{m})$, the attenuation in strength per 10 m increase in source–receiver distance, the predicted values should be considered as representing the position average of values to be found in the hall.

The three rightmost columns in Table 9.4 contain information about how well each prediction formula matched the measured data. When comparing the amounts of variance explained by the different models, it is seen that the diffuse field prediction is responsible for the largest portion of the variance. This may be interpreted as hall volume and total absorption area being the most important factors governing the behavior

Table 9.4 Regression models for the relationships between room acoustic parameters and room design variables as derived from a database containing data from more than 50 halls (after [9.25])

Room acoustic parameter	Regression models: $f(\text{PAR}_{expected}, \text{geometry})$	Correlation coefficient	% of variance	STD residuals
C (dB)	$-0.1+1.0C_{exp}$	0.76	58	1.0 dB
	$-1.4+0.95C_{exp}+0.47W/H+0.031$ floor slope	0.83	68	0.9 dB
	$-1.2+1.03C_{exp}+0.43W/H+0.013$ wall angle	0.84	70	0.9 dB
	$-1.77+1.10C_{exp}+0.055W+0.027$ stage ceil. angle	0.86	74	0.8 dB
G (dB)	$-2.0+0.94G_{exp}$	0.91	83	0.9 dB
	$-5.61+1.06G_{exp}+0.17V/N+0.04$ distance	0.94	89	0.9 dB
$\Delta G(10\,\text{m})$ (dB)	$-1.85+0.42$ no. rear balc.	0.50	25	0.7 dB
	$-1.41+0.35$ no. rear balc. -3.93 distance$/(HW)$	0.55	31	0.6 dB
LEF (–)	$0.39-0.0061$ width	0.70	49	0.05
	$0.37-0.0051$ width -0.00069 wall angle	0.72	53	0.05

Amazon
EX1010 Page 336

of C and G. However, as all the independent variables listed gave a significant improvement of the model accuracy, this also demonstrated that consideration of the geometrical factors can improve the prediction accuracy. Equally importantly, the acoustic effects of changes in certain design variables can be quantified quickly.

Prediction of Clarity

The first C-model illustrates that absorption and volume, as reflected in T, are responsible for the main part of the variation in C. The other three models all illustrate the positive, but sometimes unwanted, effect of average hall width on clarity. Moreover, it is seen that introducing a moderate 15° slope of the main audience floor (without changing the other variables: average width-to-height ratio, volume and absorption area) causes C to increase by about 0.5 dB on average. Similarly, changing the basic design from rectangular to a 70° fan shape makes C increase by about 1 dB. The last C-model illustrates the effect of tilting the angle of the stage ceiling towards the audience. Changing the slope from horizontal to 20° results in about 0.5 dB higher C values.

Predictions of Strength

The G model only considering G_{exp} is rather accurate. The constants in both G-models illustrate the fact that G is always a few dB lower than G_{exp}, as also predicted by *Barron's revised theory* [9.26].

The second G-model contains an independent variable: the ratio between the volume and the number of seats. The positive influence of this ratio is not immediately evident because V/N, which is strongly correlated with T, is expected to be incorporated into the variable G_{exp} already (although this result has also been confirmed by other researchers [9.27]).

As mentioned earlier, G shows a steady and significant decrease with distance in most halls, as was also found by *Barron* [9.26]. This phenomenon is described quantitatively by the two models for estimation of the rate of decrease in G per 10 m source–receiver distance $\Delta G(10\,\text{m})$.

Both listed $\Delta G(10\,\text{m})$ models indicate a reduced distance attenuation when the number of rear balconies is increased. This may be related to the fact that the level is increased in the more-distant seats when these are placed on a balcony, whereby they are closer to the stage and to the reflecting ceiling.

In the second $\Delta G(10\,\text{m})$ model, distance/HW appears as an independent variable. This variable equals the distance from the stage to the rearmost seat divided by the product of the average room height H and average hall width W. As the coefficient to this variable is negative, the natural result appears to be that attenuation with distance will increase if the hall is long, narrow or has a low ceiling.

Predictions of Lateral Energy Fraction

At the bottom of Table 9.4 are listed two models for LEF as a function of hall geometry only, as diffuse field theory has no effect on LEF variation. The effects of the width and angle between the side walls are understandable.

Simple prediction formulae as listed in Table 9.4 are particularly useful in the very early phases of the design process, in which it is natural for the architect to produce and test many different sketches in short succession, leaving no time to carry out computer simulation of each proposal. The importance of the knowledge embedded in these rule-of-thumb equations is highlighted by the fact that many aspects of the acoustics of a new hall are settled when one of these sketches is selected for the further development of the project.

9.6 Geometric Design Considerations

With the connections between room acoustic parameters and hall geometry described in the previous section, we have made the first approach to the third question set up in the introduction to this chapter, which is of real interest to the acoustic designer: how do we control the acoustic parameters by the architectural design variables? Referring again to Fig. 9.1, we are beginning to fill the lower-left box with architectural parameters and establish the relationship between these and the objective parameters. The major geometric factors of importance in auditorium design will be dealt with in the present section: seating layout in plan (determining the gross plan shape of the room) and in section (determining sight lines), use of balconies, choice of wall structure, room height, ceiling shape and use of free-hanging reflectors.

9.6.1 General Room Shape and Seating Layout

When people stop to watch or listen to a spontaneous performance, for instance in an open square in the city, the way they arrange themselves depends on the type

Amazon
EX1010 Page 337



Fig. 9.15 A 1:10 scale model of the Danish Broadcasting concert hall in Ørestad, Copenhagen. The model is fitted with audience and orchestra (acoustic design by Nagata Acoustics, Japan)

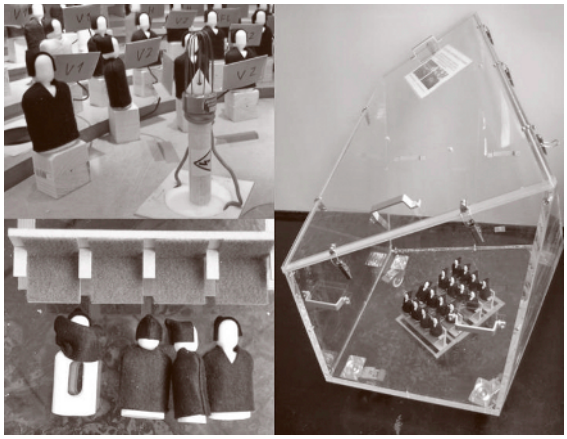


Fig. 9.16 Model audience used in a 1:10 scale model of the Danish Broadcasting concert hall shown in Fig. 9.15. *Upper-left corner*: Close view of model orchestra musicians and spark sound source. *Lower left*: close-up view of model chairs and polystyrene audience with hollow chest. Dress and hair is made from wool felt. *Right*: model audience and chairs placed in model reverberation chamber for absorption testing (reverberation room designed by Nagata Acoustics)

of performance. It will be governed by the fact that any newcomer will look for the best position available relative to his/her need to see or hear properly. The choice will be a compromise between choosing a position close to the performer(s) and next to other members of the audience or farther away but close to an eventual main center line for vision and sound radiation. In Fig. 9.17,

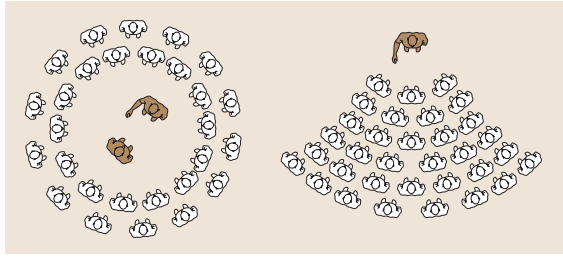


Fig. 9.17 *Organic* formations of audience depending on the type of performance

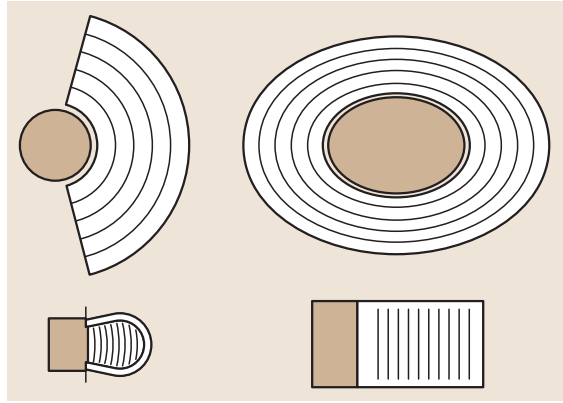


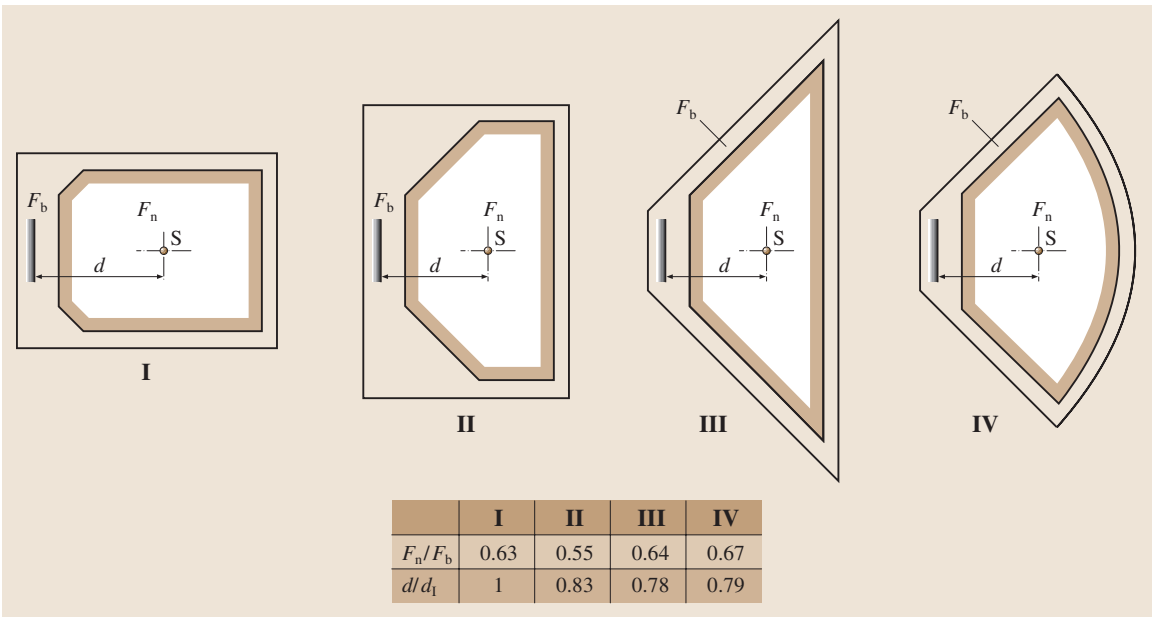
Fig. 9.18 Basic room shapes (after [9.4])

such organic audience arrangements are shown for two different types of performances:

1. action or dialogue theater such as dancing, fighting, debating, circus performance, for which the visual and acoustic emission are more or less omnidirectional and
2. monologue or proscenium stage theater performance and concerts with acoustic instruments – all of which have a more-limited visual and/or acoustic directivity.

When we set up walls around the gathered people, we arrive at two classical plan shapes of auditoria developed early during our cultural history. These are shown at the top of Fig. 9.18: the fan-shaped Greek/Roman theater (left), and the amphitheater, circus or arena (right). Both were originally open theaters; but the shapes were maintained in roofed buildings. In the bottom of Fig. 9.18, later, basic forms are shown: the horseshoe, the Italian opera plan and the rectangular concert hall. The latter form was originally a result of traditional building forms and limitations in roof span with wooden beams.

Amazon
EX1010 Page 338



	I	II	III	IV
F_n/F_b	0.63	0.55	0.64	0.67
d/d_I	1	0.83	0.78	0.79

Fig. 9.19 Mean stage–listener distance and net efficiency of floor area for four different room shapes. F_n is the net area occupied by the audience, F_b is the total floor area, d is the average source–listener distance; $d_I = d$ for case I (after [9.28])

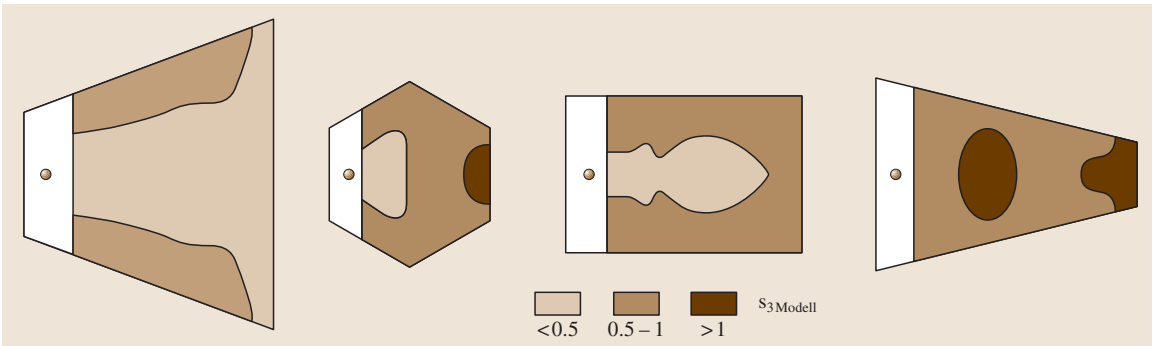


Fig. 9.20 Calculated distributions of early lateral reflection levels in rooms of different plan shape: fan, hexagon, rectangular and reverse fan. *Darker areas* represent higher LEF levels (after [9.5])

When building an auditorium, efficient use of the available floor space and the average proximity of the audience to the performers are very important parameters. Depending on the plan shape of the room different values appear as shown in Fig. 9.19.

Low average distance is the main reason for the frequent use of the fan shape (III and IV in Fig. 9.19), although the directivity of sound sources (like the human voice) as well as the quality of lines of sight sets limits on the opening angle of the fan.

Another limitation of the fan shape is that it does not generate the strong lateral reflections so important in halls for classical music. This was already seen in the empirical equations in Sect. 9.5.6 and confirmed in Fig. 9.20, showing the calculated distributions of early lateral reflection levels in rooms of different plan shapes.

The reason is that sound waves from the source hitting the side walls will produce reflections that will run almost parallel to the direct sound and so hit the listener from an almost frontal direction, therefore not contribut-

Amazon
EX1010 Page 339

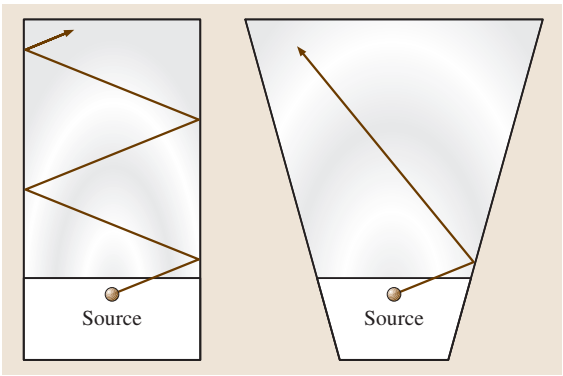


Fig. 9.21 Directions of side-wall reflections depending on room shape (after [9.4])

ing to the LEF or causing dissimilarity between the two ear signals. This is also illustrated in Fig. 9.21. In addition, many of the side-wall reflections will not reach the center of the hall at all.

9.6.2 Seating Arrangement in Section

When several rows of seated audience are placed on a flat floor, the direct sound from a source on the stage and the reflection off the audience surface will hit a receiver in this audience area after having traveled almost identical distances, and the reflection will hit the audience surface at a very small angle relative to the surface plane. At this grazing angle of incidence, all the energy will be reflected regardless of the diffuse absorption value of the surface, but the phase of the pressure in the reflected wave will also be shifted 180°. Hereby the direct sound and the grazing incidence reflection will almost cancel each other over a wide frequency range. Typical attenuation values found at seats beyond the tenth row can amount to 10–20 dB in the range 100–800 Hz relative to an unobstructed direct sound. Moreover, the higher frequencies above 1000 Hz will also be attenuated by 10 dB or more due to scattering of the sound by the heads of people sitting in the rows in front.

The same values of attenuation mentioned above for the direct sound are likely also to be valid for first-order reflections off vertical side walls. The result will be weaker direct sound and early reflections in the horizontal stalls area and subjective impressions of reduced *clarity*, *intimacy* and *warmth* in the stalls seats.

To avoid this grazing incidence attenuation, the seating needs to be sloped relative to the direction towards the source. The vertical angle of the audience floor can be designed to be constant or to vary gradually with

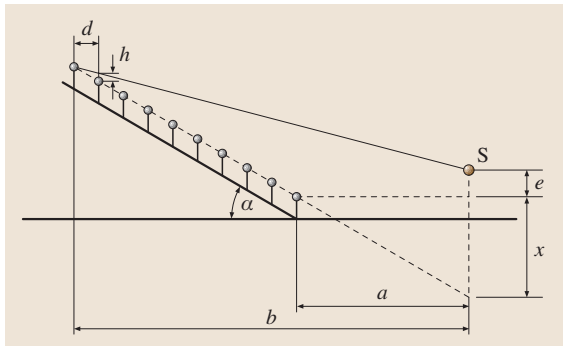


Fig. 9.22 Relevant parameters for the calculation of the necessary angle α for a constantly sloping floor section. a: distance from the source to the first seating row, b: distance from the source to the last seating row, d: distance between the seat rows, e: source height above the head of listeners in the first row (determined by the height of the stage floor over the stalls floor), h: line-of-sight clearance at the last row. Rows closer to the source will have clearance values larger than h (after [9.28])

distance. If a constant slope is planned, the angle α necessary to obtain a certain clearance h at the last row (equal to the vertical distance between sight lines from this and the preceding row) can be calculated from the variables indicated in Fig. 9.22:

$$\tan\alpha = \frac{hb}{da} - \frac{e}{a} \,. \tag{9.30}$$

In particular, it is of interest to use this formula to see how far away from the source it is possible to maintain a certain slope (one obvious example being $\alpha = 0$, corresponding to a horizontal floor):

$$b = \frac{d}{h}\,(e + a\tan\alpha) \,. \tag{9.31}$$

Normally, a clearance value of minimum 8 cm will be sufficient to avoid grazing-incidence attenuation; but sight lines will still be unsatisfactory unless staggered seating is applied so that each listener is looking towards the stage between two other heads and not over a person sitting directly in front. However, if the clearance is increased to about 12 cm, then both the acoustic and visual conditions will be satisfactory, but this implies a steeper floor slope.

In rows closer to the sound source a linear slope will cause the clearance to be higher than the design goal – and so higher than necessary. Often this is not desirable as it may cause the last row to be elevated high above the source and the steeply sloped floor will reduce

Amazon
EX1010 Page 340

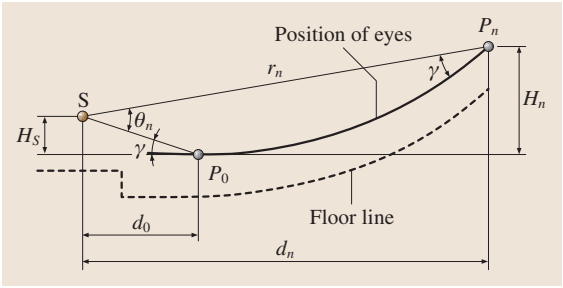


Fig. 9.23 Relevant parameters for the calculation of a floor slope with constant clearance. The variables are explained in the text (after [9.29])

the effective volume of the room. Therefore, it can be relevant to consider instead a curved floor slope with constant clearance, as illustrated in Fig. 9.23.

In Fig. 9.23, the height of a person's head in the n-th row H_n relative to the height of the head in the first row is calculated according to the formula (derived from a logarithmic spiral)

$$H_n = d_0\gamma + d\,(\theta - \gamma) = \gamma\left[d_n \log_e\left(\frac{d_n}{d_0}\right) - (d_n - d_0)\right] . \qquad (9.32)$$

In this expression d_0 is the distance from the source to the first row, d_n the distance to the n-th row and γ the desired angle between the tangent to the seating plane and the line of sight to the source. For a one meter row-to-row distance, an angle γ of 8° will correspond to a clearance of about 12 cm.

A curved slope can also be obtained by simply applying the linear-slope formula to each of smaller sections of seat rows successively (e.g. for every five rows). In this case the variables a and e in (9.30) should refer to the first row in the relevant section.

As mentioned earlier, a steep slope will reduce the volume and so the reverberation time T. Besides, geometric factors may reduce T beyond what a Sabine calculation may predict. The reason is that the elevated seating – and its mirror image in the ceiling – will cover a larger solid angle as seen from the source. Hereby a larger part of the emitted sound energy will quickly reach the absorbing seating and leave less for fueling a reverberant sound field in the room. The result is higher *clarity* and less *reverberance* in halls with steeply raked seating. This is in line with the empirical equation for clarity as a function of T (C_{exp}) and floor slope listed in Table 9.4, Sect. 9.5.6. Consequently, it is a good idea to limit the clearance/angle in halls for classical music to about 8 cm or 6°, whereas for speech auditoriums and drama theaters, in which both intelligibility and good visual sight lines have priority, values closer to 12–15 cm or 8°–10° may be preferable.

9.6.3 Balcony Design

The introduction of balconies allows a hall with a larger seat count to be built where a limited footprint area is available; but often balconies are introduced simply in order to avoid longer distances between stage and listeners. The average stage–listener distance can be reduced significantly by elevating the rearmost seat rows and moving them forward on rear or side balconies above parts of the audience in the stalls. In this way not only is the direct sound increased by shortening the direct sound path, but the elevated seats also become closer to a possibly reflecting ceiling. The result is higher strength as well as higher clarity in the balcony seats compared to the alternative placement of seats at the back of an even deeper hall.

Since the line-of-sight and clearance criteria still have to be fulfilled for balcony seats, the slope often becomes quite steep on balconies, as illustrated in Fig. 9.24 showing a long section in a hall with constant clearance on main floor and balcony seats. For safety reasons the slope must be limited to no more than about 35°.

When balconies are introduced, the acoustics in the seats below the balconies need special attention. It is important to ensure sufficient opening height below balcony fronts relative to the depth of the seating under the balcony (Fig. 9.25). Otherwise, particularly the level of the reverberant energy in the overhung seats will be reduced, causing the overall sound level to be weak and lacking in fullness. Rules of thumb in design are $H \geq 2D$ for theaters (in which reverberant sound is less important) and $H \geq D$ for concert halls (in which fullness is

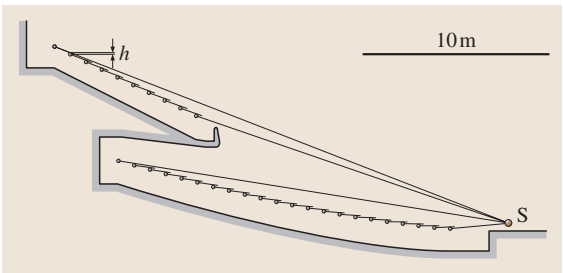


Fig. 9.24 Section of a hall with a rear balcony and constant clearance. The result is an increased slope for the elevated balcony (after [9.30])

Amazon
EX1010 Page 341

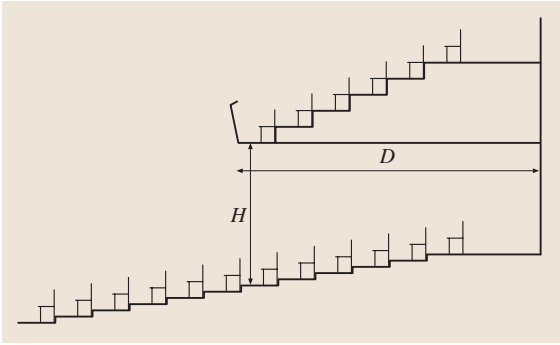


Fig. 9.25 Important parameters for maintaining proper sound in seats overhung by balconies (after [9.9])

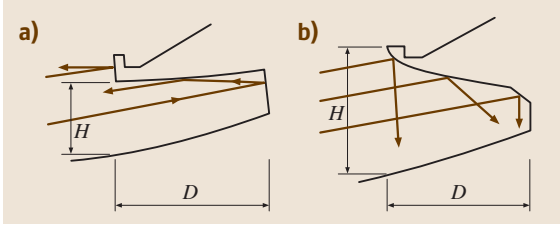


Fig. 9.26a,b Poor (**a**) and good (**b**) design of balcony profile (after [9.29])

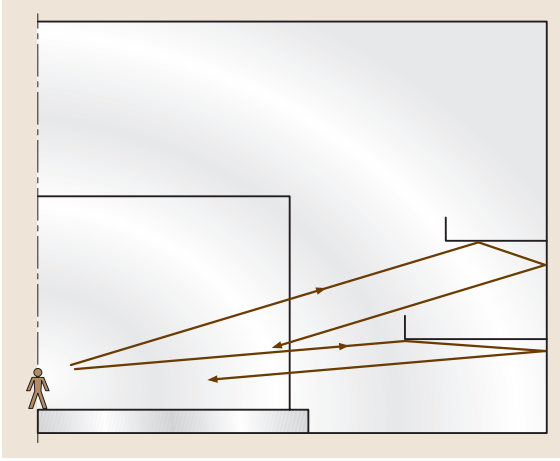


Fig. 9.27 A half cross section of a hall with side balconies that, in combination with the side wall, return early reflection energy towards the stalls area from a lateral angle (after [9.4])

more important) [9.9]. The criteria may also be stated in terms of the vertical viewing angle from the seat to the main hall volume. Recently, *Beranek* [9.3] has suggested this be a minimum of 45°.

Sometimes, the requirement for limited depth of balcony overhangs is also specified as a percentage of the ceiling area needed to be visible from the last row of seating or as a vertical opening angle β between the balcony soffit and the head of listener below the balcony front as seen from the last row. In the latter case, Barron has suggested 25° as suitable for drama halls and 35° for concert halls.

As illustrated in Fig. 9.26, it is often advantageous to let the soffit be sloped, so that it will help distribute reflected sound to the overhung seats. If a diffusing profile is added to the balcony soffit, the reflection off this surface may even gain a lateral component, so that *spaciousness* will not be reduced. The drawing also illustrates how the otherwise vertical balcony front and the right angle between the rear wall and balcony soffit have been modified to avoid sound being reflected back to the stage where it could generate an echo. However, in a rectangular hall with balconies along the side walls, vertical soffits in combination with the side-wall surface can increase the early and lateral reflection energy in the stalls area as shown in the half cross section in Fig. 9.27.

In general, as large-scale modulations in the hall geometry, balconies also provide low-frequency diffusion, which is considered an advantage.

9.6.4 Volume and Ceiling Height

As the people present are often the main source of sound absorption in an auditorium, the ratio between the volume and area covered by the audience and performers is an important factor for the reverberation time achievable. The general relationship valid for concert halls is shown in Fig. 9.28.

Because the variation in area per person does not vary significantly between halls, the volume per seat is also used as a rule of thumb for the calculation of the required volume. For speech theaters, a volume per seat of 5–7 m^3 will result in a reverberation time around 1 s, whereas at least 10 m^3 per seat is needed to obtain a T value of 2 s.

Since the audience normally occupies most of the floor area, the volume criterion can also be translated to a ceiling height criterion. In such cases, the abscissa in Fig. 9.28 can be interpreted as roughly equal to the required room height. A ceiling height of about 15 m is required if a T value of 2 s is the target, whereas a height of just 5–6 m will result in an auditorium with a reverberation time of about 1 s. It should be emphasized that, in the discussion above, we have assumed the other room surfaces to be reflective.

Amazon
EX1010 Page 342

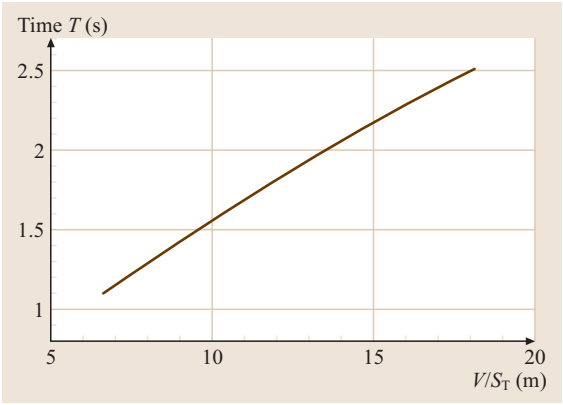


Fig. 9.28 Reverberation time T in occupied concert halls versus the ratio between the volume V and area occupied by the audience and orchestra S_T (including aisle space up to 1 m width). Derived from empirical data (after [9.9])

These guidelines on volume should be regarded as rough rules of thumb only, as room shape, floor slope, the presence of balconies and the distribution of absorption on other surfaces can cause significant variations in the objective values obtained for T and other parameters. In smaller halls (say below 1500 seats) for symphonic concerts, it is better to start with a volume slightly larger than required rather than the opposite, as one can always add a little absorption – but not more volume – to a hall near completion. On the other hand, in larger halls, where maintaining a suitably high G value is also of concern, a better strategy is to limit the volume and minimize the absorption instead. One way of minimizing absorption is to place some of the seats under balcony overhangs, where they are less exposed to the reverberant sound field. However, the other side of the coin is the poor conditions in these seats, as explained in Sect. 9.6.3.

9.6.5 Main Dimensions and Risks of Echoes

In order for early reflections to contribute to the *intelligibility* of speech or to the *clarity* of music, they must not be delayed more than about 30 ms and 80 ms, respectively, relative to the direct sound. If the first reflection arrives later than 50 ms, it is likely to be perceived as a disturbing echo when impulsive sounds are emitted (Sect. 9.2).

In large rooms it is a challenge to shape the surfaces so that reflections from the main reflecting areas arrive within 50 ms at all seats. It is possible to identify which surfaces are able to generate echoes at the receiver point

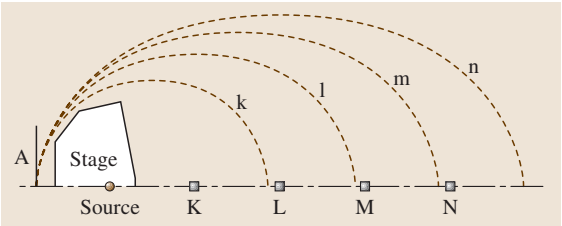


Fig. 9.29 Echo ellipses drawn over the plan of an auditorium (after [9.4])

in question by means of simple geometrical studies of plan and sectional drawings as seen in Fig. 9.29. Ellipses are drawn so that the source and relevant receiver positions are placed at the focal points and so that the sum of distances from the focal points to any point on the ellipse equals the distance between the focal points plus 17 m (times the scale of the drawing). Then, if a surface outside the ellipse marked "m" in the figure directs sound towards seats near point M, this surface must be made absorbing, diffusing or be reoriented so that the reflection is directed towards areas farther away from the source than M.

In particular, it is important to check the risk of echoes being generated by the rear wall behind the audience and from a high ceiling.

9.6.6 Room Shape Details Causing Risks of Focusing and Flutter

Concave surfaces can cause problems as they may focus the sound in certain areas while leaving others with too little sound. Thus, vaulted ceilings as seen in Fig. 9.30 are only acceptable if the radius of curvature is less than half the height of the room (or rather half the distance from peoples' heads to the ceiling) so that the focus center is placed high above the listeners. Situations with

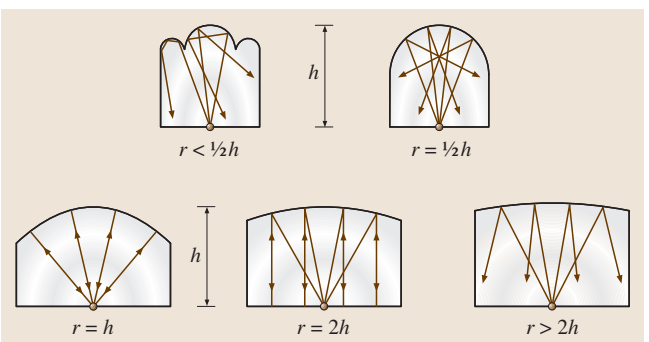


Fig. 9.30 Focusing by concave ceilings (after [9.31])

Amazon
EX1010 Page 343

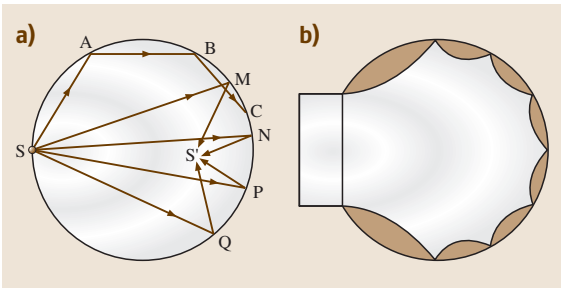


Fig. 9.31a,b Circular room with focused and creeping waves **(a)**, and with the surface shape modified **(b)** so that these phenomena are avoided

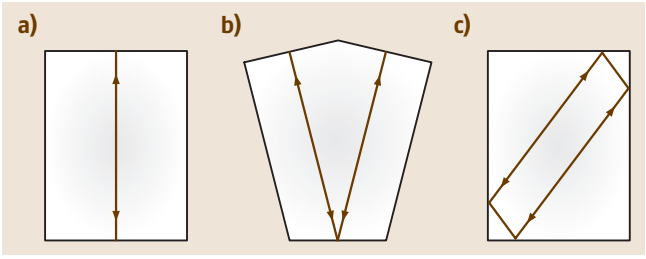


Fig. 9.32 Room shapes causing risk of flutter echoes

a slight curvature, $r \geq 2h$, may also be acceptable if the floor is covered with absorptive seating so that multiple reflections between floor and ceiling will not arise.

Circular rooms are also unfavorable both due to the risk of focusing and the risk of a whispering-gallery effect (boundary waves creeping along the wall). Modifications of the concave wall within the overall circular shape as shown in Fig. 9.31 can solve the problem, at least at mid and high frequencies.

Another frequent problem is regular, repeated reflections, so-called flutter echoes, which arise between parallel, smooth reflecting walls or along other simple reflection paths that can repeat themselves as shown in Fig. 9.32. Particularly in small rooms such reflections may cause strong coloration of the sound (through comb filtering as explained in Sect. 9.2.3) while in larger rooms they may be perceived as a long series of distinct echoes evenly spaced in time.

In any case, the flutter can be avoided by simple absorptive or diffusive treatment of at least one of the opposite reflecting surfaces, as shown in Fig. 9.33. Besides, if it is possible to change the angle between the opposite walls just by a few degrees (3–5°), the problem will also disappear.

9.6.7 Cultivating Early Reflections

In most rooms accommodating more than say 25 listeners, it is of relevance to consider how early reflections can help distribute the sound evenly from the source(s) to the audience. This will increase the early reflection energy and so improve *clarity/intelligibility* and perhaps even reduce the reverberation time by directing more sound energy towards the absorbing audience.

In rooms for speech, the ceiling height should be moderate (Sect. 9.6.4) so that this surface becomes the main surface for the distribution of early reflection energy to the audience. Figure 9.34 shows examples of how this can be accomplished in rooms with both low and high ceilings.

In this figure the two situations at the top need improvement. In the low-ceiling room to the left the echo from the rear wall/ceiling combination can be removed by introducing a slanted reflector covering the corner. In this way the sound is redirected to benefit the last rows, which may need this to compensate for the weak direct sound at this large distance. Alternatively, the energy from this rear corner may simply be attenuated by one or both surfaces near the corner being supplied with absorption.

If the ceiling is so high that echoes can be generated in the front part of the room, as shown to the right, the front part may likewise be treated with slanted reflectors that redirect the sound to the remote seat rows, or this ceiling area may simply be made sound absorbing. The lower-right section in the figure also illustrates how the

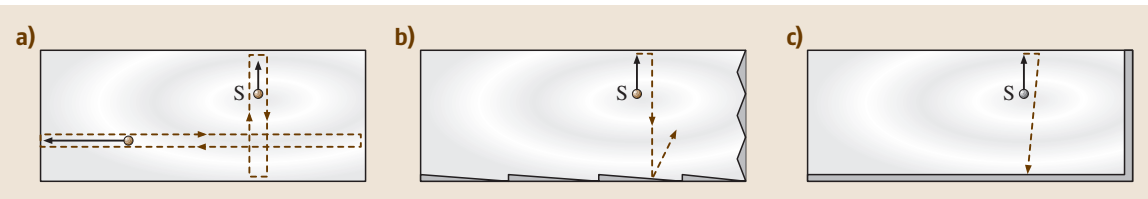


Fig. 9.33a–c Room with flutter echoes **(a)**, and measures against this by means of diffusion **(b)** or absorption **(c)** (after [9.28])

Amazon
EX1010 Page 344

floor can be tilted to reduce volume and allow the rear seats benefit from being closer to the reflecting ceiling.

If for architectural reasons the ceiling is higher than necessary in a room for speech or rhythmic music, substantial areas of the room surfaces must be treated with sound-absorbing material to control the reverberation time. However, more sound absorption will reduce the overall sound level in the room so this is only recommended if the sound can be amplified.

If the ceiling is to be partly absorbing, the ceiling area that should be kept reflecting in order to distribute useful first-order reflections to all listeners can be generated geometrically by drawing the image of the source in the ceiling surface and connecting lines from this image point to the boundaries of the seating area. Where these lines cross the actual ceiling we find the boundaries for the useful reflecting area, as shown in Fig. 9.35.

In larger auditoria, a more-detailed shaping of the ceiling profile may be needed to ensure even distribution of the reflected sound to the listeners. Notice in Fig. 9.36 that the concave overall shape of the ceiling can be maintained if just the size of the ceiling panel segments is large enough to redirect the reflections at suitably low frequencies.

Local reshaping of surfaces while maintaining the overall form is also illustrated in Fig. 9.37, in which the weak lateral reflections in a fan-shaped hall are improved by giving the walls a zigzag shape with almost parallel sets of smaller areas along the splayed side walls. In the example shown in the photo, the panels are even separated from the wall surface and tilted downward.

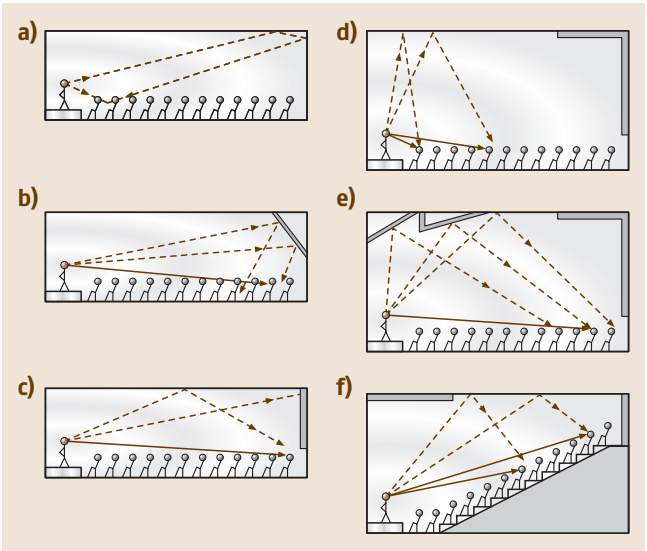


Fig. 9.34 Means of controlling early reflections in auditoria (after [9.28])

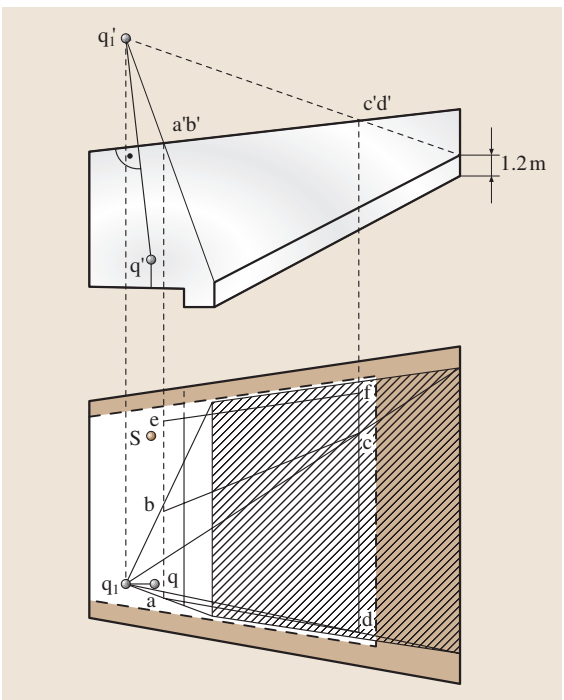


Fig. 9.35 Sketch identifying the area responsible for covering the audience area with a first-order ceiling reflection (after [9.32])

9.6.8 Suspended Reflectors

In many cases it is advantageous to reduce the delay and increase the level of a reflection without changing the room volume. In this case it is obvious to suggest individual reflecting surfaces suspended within the room boundaries, as shown to the right in Fig. 9.38. If the reflector is placed over an orchestra pit, it can improve mutual hearing among the musicians in the pit as well as increase the early energy from the singing on the stage to the seating primarily in the stalls area.

Suspended reflectors are also suitable for acoustic renovation of existing, listed buildings, because the main building structure is not seriously affected (as in the case of the Royal Albert Hall in London [9.3]).

For a given source position, a small reflector will cover only a limited area of receiver positions. There-

Amazon
EX1010 Page 345

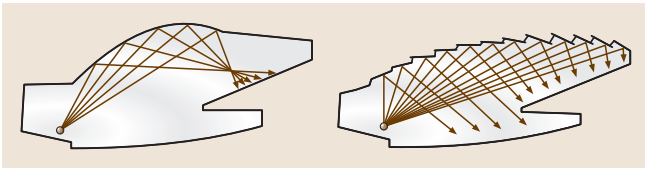


Fig. 9.36 Reshaping of ceiling profile to avoid focusing and provide more-even sound distribution

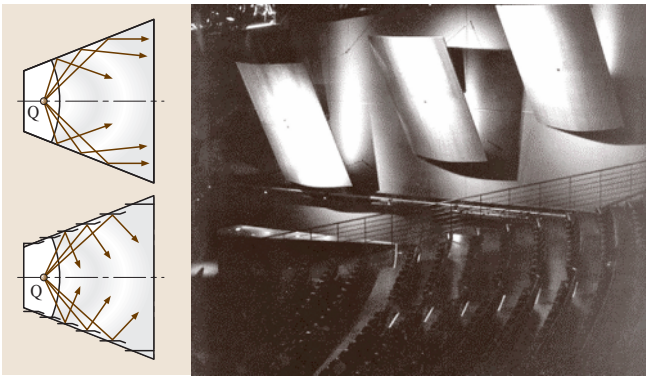


Fig. 9.37 Improvement of side-wall reflections in a fan-shaped hall by local reshaping or adding of panels parallel to the long axis of the room (drawing after [9.32])

fore, how the reflector(s) influence the balance heard between different sources such as the different sections in a symphony orchestra must be thoroughly considered. With small reflectors, the balance between sections may be perceived as very different in different parts of the audience. Often it will be advantageous to give the reflector(s) a slightly convex shape to extend the area covered by the reflection and to soften its level.

The nature of the reflection off a panel of limited size is strongly frequency dependent and may be influenced by several factors: distance to source and receiver, absorption by the panel material, diffraction governed by the ratio between panel size and the wavelength, and focusing/diffusion due to panel curvature.

The attenuation with distance is as for a spherical wave in free field: 6 dB per doubling of the total distance from the source to the reflector a_1 plus the distance from the reflector to the receiver a_2. Normally, the attenuation due to absorption is negligible, as reflectors should obviously be made from a reflective material. The only exception could be when a thin, lightweight material is used, such as plastic foil or coated canvas. In this case the attenuation ΔL_{abs} can be calculated from the mass law

$$\Delta L_{\text{abs}} = -10 \log_{10} \left[1 + \left(\frac{\rho c}{\pi f m \cos\theta} \right)^2 \right] \qquad (9.33)$$

where ρc equals the specific impedance of air ($\approx 414\,\text{kg}\,\text{m}^{-2}\,\text{s}^{-1}$), f is the frequency in Hz, m is the mass per square meter of the material and θ is the angle of incidence relative to the normal direction.

As a simple design guide, diffraction can be said to cause the specular reflection to be attenuated by 6 dB per octave below a limiting frequency f_{g} given by:

$$f_{\text{g}} = \frac{ca^*}{2S\cos\theta} \qquad (9.34)$$

where a^* is the weighted *characteristic distance* of the reflector from the source and receiver:

$$a^* = \frac{2a_1 a_2}{a_1 + a_2}\,, \qquad (9.35)$$

S is the area of the reflector, and θ is the angle of incidence as before. Above the frequency specified in (9.34), the influence of diffraction can be neglected.

If the reflector is curved, the attenuation ΔL_{curv} can be calculated as:

$$\Delta L_{\text{curv}} = -10 \log_{10} \left| 1 + \frac{a^*}{R\cos\theta} \right|\,. \qquad (9.36)$$

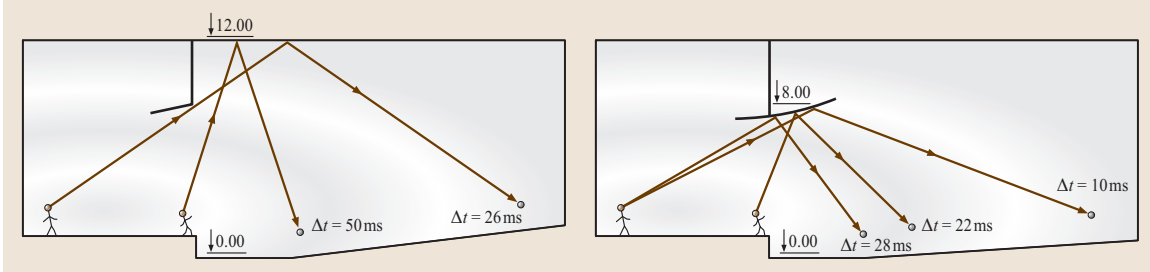


Fig. 9.38 The influence on reflection paths of a reflecting panel suspended in front of a stage (after [9.33])

Amazon
EX1010 Page 346

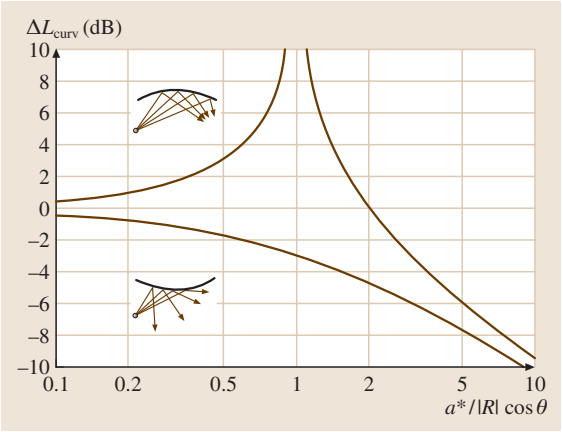


Fig. 9.39 Attenuation of a reflection caused by concave and convex reflectors (after [9.34])

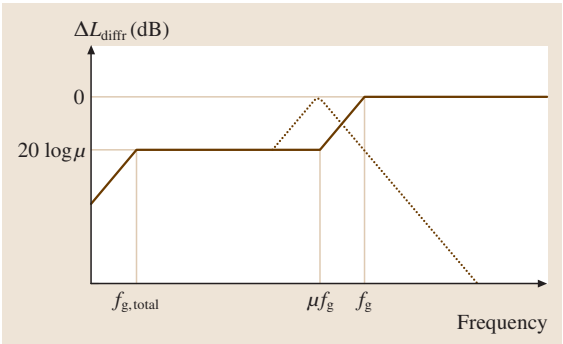


Fig. 9.40 Approximate attenuation due to diffraction from a reflector array. All non-horizontal lines have a slope of 6 dB per octave. See text for further explanation (after [9.34])

Here, the only new variable R is the radius of curvature. R should be entered positive for convex surfaces and negative for concave surfaces. When the reflector is concave, strong focussing occurs when $R = -a^*/\cos\theta$. In Fig. 9.39, graphs of ΔL_{curv} are shown for both the concave and convex cases. It is noted that the values can be both positive and negative. In the case where the surface is curved in both the x- and y-directions of the reflecting plane, the ΔL_{curv} correction should be applied twice using the appropriate radii of curvature in the two directions.

In certain cases an array of (identical) reflectors are suspended as an alternative to having one large reflector. Such an array can be characterized by the area of each element, S, the total area covered by the array S_{total} and the degree of coverage, μ, equal to the ratio between the total area of the n reflector elements nS and S_{total}. In this case, the attenuation due to diffraction depends on frequency as shown in Fig. 9.40.

Here, f_g is the limit frequency of the individual elements calculated according to (9.34), while $f_{g,\text{total}}$ is the lower-limit frequency related to the entire array area S_{total}

$$f_{g,\text{total}} = \frac{ca^*}{2S_{\text{total}}\cos\theta} \,. \tag{9.37}$$

First we look at the situation above the frequency f_g in Fig. 9.40. As in the case of the single reflector, the attenuation is zero as long as the specular reflection point falls on one of the reflector elements. If the specular point falls between two elements, the attenuation can be approximated by the dotted line, according to which we have an attenuation of 6 dB per octave as frequency increases. In the frequency range between $f_{g,\text{total}}$ and μf_g, the attenuation is roughly frequency independent and governed by the array density μ, and below $f_{g,\text{total}}$ the level again rolls off by 6 dB per octave. It is seen that, in order to obtain a wide range of frequency-independent reflection, one should aim to use many small reflectors rather than fewer, larger elements. Fortunately, the strong position-dependent variation in reflection level at high frequencies can be reduced by making the individual elements slightly convex.

It should be remembered that whenever surfaces are shaped with the purpose of efficiently directing sound energy from the source towards the absorbing audience, this energy is no longer available for the creation of the reverberant sound field. In other words, the more we try to improve the *clarity* and *intelligibility*, the more we reduce reverberation in terms of T and EDT (regardless of the physical absorption area), and the more the sound field will deviate from the diffuse field predicted by any simple reverberation formula. If substantial reverberation is needed as well, the solution may be to increase the volume per seat beyond the $10\,\text{m}^3$ as already suggested for large halls in Table 9.1. As seen in Sect. 9.7.3 this is in line with the current trend in concert hall design.

9.6.9 Sound-Diffusing Surfaces

It is often stated that diffusion of sound from irregular surfaces adds a pleasant, smooth character to the sound in a concert hall. It is a fact that reflections from large smooth surfaces can produce an unpleasant harsh sound. It is also a fact that most of the surfaces in famous old and highly cherished halls such as the Musikvereinsaal

Amazon
EX1010 Page 347

break up and scatter the reflected sound in many directions due to rich ornamentation, many window and door niches and the coffered ceiling (Fig. 9.45). Even the large chandeliers in this hall break up the sound waves.

Many present-day architects are influenced by modernism and are less enthusiastic about filling their designs with rich ornamentation. Therefore, close cooperation is often needed between architect and acoustician in order to reach a surface structure that will scatter the sound sufficiently, although this is difficult to define exactly as good guidelines do not exist for what percentage of the wall/ceiling area one should make diffusive.

Schroeder [9.35] has done pioneering work on creating algorithms for the design of surface profiles that will ensure uniform distribution of scattered sound within a well-defined frequency range. These algorithms are based on number theory using the maximum length, quadratic residue or primitive root number sequences. However, in most cases of practical auditorium design, perfectly uniform scattering is not needed, and good results can be obtained even after a relaxed architectural adaptation of the ideas, as shown in Fig. 9.41.

The primary requirement to achieve diffusion is that the profile depth of the relief is comparable with a quarter of the wavelength and the linear extension of the diffusing element (before it is eventually repeated) is comparable with the wavelength at the lowest frequency of interest to be diffused. Given this, many different solutions can be imagined such as soft, curved forms cast in plaster, broken stone surfaces, wooden sticks, irregular brick walls etc.

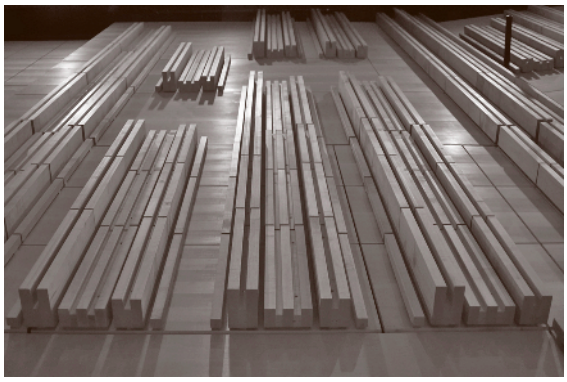


Fig. 9.41 Diffusion treatment by means of wooden sticks screwed on an otherwise plane, wooden wall surface

Finally, it should be mentioned that strict periodic structures with sharp edges equally spaced along the surface can cause problems of harsh sound at frequencies above the design frequency range. Actually, it is safer to apply more-organic, chaotic structures, or to ask the workers not to be too careful with the ruler.

9.7 Room Acoustic Design of Auditoria for Specific Purposes

This section will present some examples showing how the principles outlined in Sect. 9.5 are implemented in the current design of different types of auditoria. The main focus will be on concert halls for classical music as well as drama and opera theaters. It will also be shown that design choices are not only compromises between acoustic and other concerns, but sometimes even between different room acoustic aspects. This is often the case with multipurpose auditoria. In any case, the compromises are more serious the larger the seating capacity.

9.7.1 Speech Auditoria, Drama Theaters and Lecture Halls

In the Western world, rooms for spoken drama as well as for opera have their roots in the Greek and Roman theaters in which the audience is arranged in sloping concentric rows, the *cavea*. In Roman times, this audience area covered a 180° angle around the orchestra or apron stage. The advantage of such an arrangement is of course the possibility to accommodate a large audience within a limited maximum distance from the stage. Many modern theaters and speech auditoria have adopted this layout – perhaps extended with one or more sets of balconies.

An example of such a modern speech auditorium (the lecture hall at Herlev Hospital, Denmark) is seen in Fig. 9.42 along with a Roman theater for comparison.

In a drama theater, a moderate reverberation time around 1 s will provide a good compromise between high intelligibility and a high strength value, as both are needed for unamplified speech. The T value may be reduced to about 0.5 s in small rooms for 50–100 people and also increased slightly for audiences above 1000. To obtain a high strength value in a large theater, it is important to choose a modest volume per seat (about 5 m^3) rather than to control the reverberation in an unneces-

Amazon
EX1010 Page 348

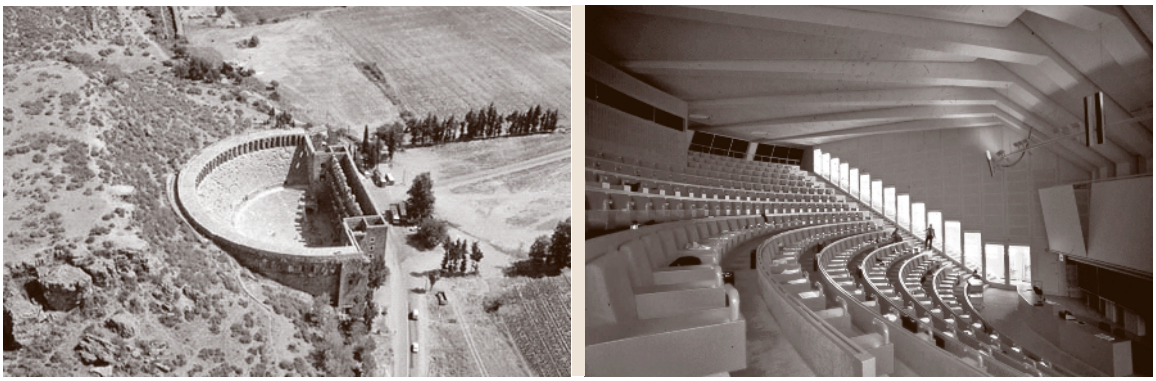


Fig. 9.42 Photos of Roman theater (in Aspendos, Turkey) and of a modern speech auditorium (Herlev Hospital, Denmark)

sarily large volume by applying additional absorption beyond that provided by the audience chairs. Thus, the height of the ceiling should be chosen fairly low – which is also advantageous for its ability to distribute early reflections to the audience. According to diffuse field theory, the steady-state energy density equivalent to G_{exp} is inversely proportional to the total absorption area A in the room.

High *clarity* and sound *level* are also promoted by careful shaping of the reflecting ceiling and a substantial sloping of the audience floor. Due to the directivity of the human voice, a reflecting rear wall (or stage scenery in a theatre) is of less importance, unless an actor should turn his back to the audience. Also the wall surfaces close to the stage opening are important, because they will send sound across the room so that sound also reaches people behind the speaker when he turns the head towards one side. The rear wall/balcony soffits behind/over the rear part of the audience should diffuse or redirect the sound to benefit nearby listeners.

As *spaciousness* is not a quality of particular importance in a speech auditorium, reflections from the side walls farther from the stage are often given lower priority than a low average stage-to-audience distance, which is promoted by a fan-shaped floor plan. However, as indicated by the problems encountered in the Olivier Theater in London [9.4], there should be limits to the opening angle of large fan-shaped theaters.

In a modern theater, the floor slope will often be more modest than seen in Fig. 9.42. In contrast to the lecture hall, a modern drama theater also needs to be highly flexible regarding the layout of stage and audience areas.

The classical proscenium frame inherited from the Italian Baroque theater is often considered to limit intimacy as well as the creativity of the stage-set designers and directors. If the classical proscenium stage is not needed, intimacy and audience involvement can be maximized by an arena arrangement, with audience all around the stage. In other cases, the stage can be extended into the audience chamber, for instance by removing the first rows of seats and raising the floor below to stage level. If such a flexible forestage is considered, the line-of-sight design should be adjusted accordingly, particularly if the hall features balconies.

An example of a flexible modern theater (without balcony) is seen in Fig. 9.43. In this room, the circular side/rear wall was made highly sound absorbing, leaving most of the distribution of early reflection energy to the ceiling.

Dedicated drama theaters are seldom built with a seat count higher than 500–1000, because visual as well as acoustic intimacy, including close view of facial expressions and freedom from artificial amplification, are given high priority. Thus, the maximum distance from the stage front to any seat should not exceed about 20 m for drama performances.

From this discussion it can be concluded that a reflecting ceiling of modest height is the main source of early reflection energy in theaters. However, lighting staff will often want to penetrate this surface with slots for stage lights and rigging or place light bridges across the room, which will act as possible barriers for the sound paths going via the ceiling. This challenge must always be considered in the acoustic design of drama theaters.

9.7.2 Opera Halls

There is a 350 year tradition of performing opera in halls of the Italian Baroque theater style. These are halls with a horse-shoe plan shape with several balcony levels running continuously from one side of the proscenium arch

Amazon
EX1010 Page 349

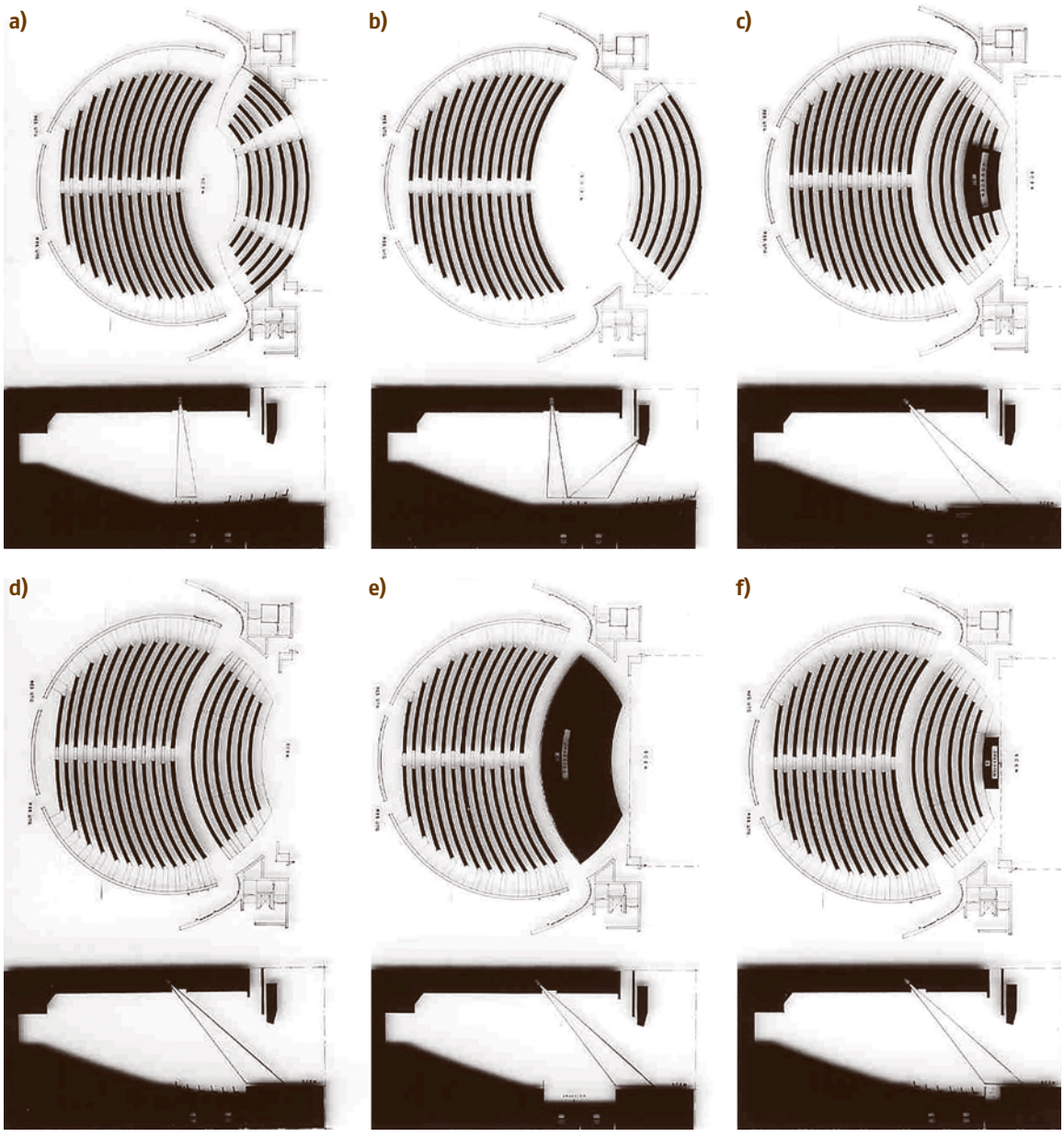


Fig. 9.43a–f Plans showing a flexible theater in Hëlsingborg, Sweden, with different layouts of the stage, orchestra pit and audience seating. **(a)** and **(b)**: arena with small and large stage respectively, **(c)**, **(e)**, and **(f)**: proscenium theater with three different sizes of orchestra pits. **(d)**: proscenium theater without pit

to the other along the curved side and rear walls. The balconies are either divided into boxes separated by thin walls or are open with long seat rows. The orchestra is placed in front of the proscenium opening that connects the auditorium with the stage house.

This tradition has undergone few changes during the past 350 years. Since the 19th century, the orchestra has been placed in a lowered pit separated from the stalls by a closed barrier. In this arrangement, seats in the stalls and lower rear bal-

Amazon
EX1010 Page 350

cony experience an attenuation of the direct sound from the orchestra, because the pit rail blocks the free line of sight to the orchestra. The result may be an improved singer-to-orchestra balance in these seating areas. The pit rail will also reflect sound back and forth between the stage and pit, giving improved contact between the singers and the lowered orchestra.

Another development is that the separate boxes have been exchanged for open balconies, which improves the possibility for the now exposed side walls to help distribute the sound to seating farther backwards in the auditorium. This development is the result of advances in building technology as well as of changes in social attitudes.

The multiple levels of horseshoe-shaped balconies facilitates a short average distance between the audience and the singers, promoting both the visual and the acoustic intimacy, which is important for both parties. However, balcony seats close to the proscenium and on the upper balcony levels often have a very restricted view of the stage.

The short audience–singer distance obtained by the horseshoe form gives high levels of both strength and clarity. On the other hand, the horseshoe form and the proscenium arch also cause some acoustic problems:

- with all wall surfaces covered by balconies, only small free wall areas are left to generate the early reflections that assist an even distribution of the sound, clarity and the generation of reverberation in the room;
- often focusing effects occur from the curved wall surfaces and a cupola-shaped ceiling which, along with the placement of the orchestra out of sight in the pit, give a high risk of false localization of certain instruments;
- only part of the energy generated by the singer will reach the auditorium, because the singers are placed in a large stage house coupled to the auditorium via a proscenium opening of limited size, and this energy even depends on the acoustic properties of the ever-changing stage sets.

Recent developments in the acoustic design of opera halls have mainly aimed at avoiding these problems. Only a few attempts have been tried to radically change the overall shape (e.g. the Deutsche Oper in Berlin, and the Opéra Bastille in Paris) but without much success. Therefore, we are left with tradition and acoustic properties of horseshoe halls to shape the current acoustic ideals for opera, which are

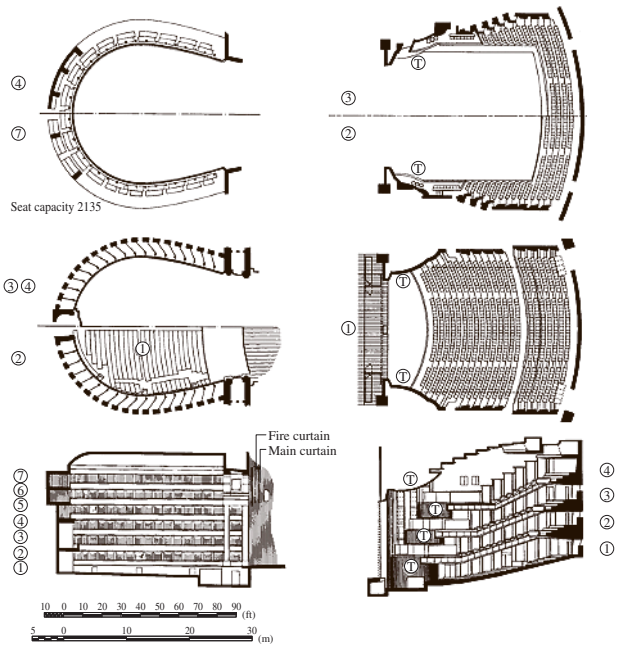


Fig. 9.44 Plan and section drawings of the Teatro alla Scala, Milan, Italy, from 1778 (*left*) and the New National Theatre Opera, Tokyo, Japan, from 1997 (*right*) (after [9.3])

- sufficient level of the singers' voices relative to the orchestra,
- some emphasis on *clarity* and *intelligibility* (although not as much as in speech auditoria),
- a certain *fullness of tone* and *reverberance*; but less than in a classical concert hall.

In recent years the trend has moved towards higher T values than found in the old halls, like Opéra Garnier, Paris (2131 seats, 1.1 s), Teatro Alla Scala, Milano (2289 seats, 1.2 s). This might well be due to the tendency to perform operas in the original language and display the translated text on a text board above the proscenium. Thus, for many recent opera halls we find T values of 1.4–1.8 s. Examples are: Göteborg (1390 seats, $T = 1.7$ s), Glyndebourne (1200 seats, $T = 1.4$ s), Tokyo (1810 seats, $T = 1.5$ s), and Semper Oper, Dresden (reconstruction, 1290 seats, $T = 1.6$ s).

As the width of the traditional horseshoe shape is about equal to its length, the lateral sound is not very pronounced and so *spaciousness* is seldom regarded a factor of particular importance in opera hall acoustics.

In order to ensure a sufficient level and *clarity* of the singers' sound, efficient sound reflections off the proscenium frame, ceiling, balcony fronts and from the

Amazon
EX1010 Page 351

corners between balcony soffits and rear/side walls are important. Of course the scenery may also be designed to help in this respect, but generally this is out of the hands of the acoustician.

If a seat count larger than, say, 1500 is demanded it is better to extend the top balcony backwards, as seen in Covent Garden in London and the Metropolitan in New York rather than increase the overall dimensions of the horseshoe, which would give poorer acoustics for all seats. As this extended balcony is close to the ceiling surface, the acoustics here can often be very intimate, clear and loud, in spite of the physical and visual distance to the stage being very large. In the Metropolitan Opera in New York the farthest seat is about 60 m from the stage.

The culmination of the old Baroque theater tradition is represented by the Teatro alla Scala in Milan, Italy, which dates from 1778. Drawings of this theater are shown in Fig. 9.44 along with a modern opera with almost the same number of seats, the New National Opera in Tokyo from 1997.

The horseshoe-shaped Milan opera contains six levels of balconies subdivided into boxes with the openings covered with curtains so that the audience could decide whether to concentrate on the play or on socializing with their guests or family in the box. The audience in the boxes receive a rather weak sound unless they are very close to the opening.

This aspect has been improved in the modern opera with open balconies. Steeper slopes on the stalls floor and even on the side balconies have also improved the direct sound propagation to all seats. Fewer balcony levels have created higher openings at the balcony fronts, allowing the reverberant sound to reach the seats in the last rows below the balconies, providing more early reflection energy from the walls to all seats.

In the Tokyo opera, much emphasis has been put on retracting the balconies away from the proscenium so that extensive side-wall areas close to the proscenium are available for projecting the sound from the stage into the auditorium. Along with the ceiling above the pit, these wall areas almost form a trumpet flare. In the section, it is also seen that the side balconies are tilted downwards towards the stage in order to improve lines of sight. Finally, the side-wall areas and the side-balcony fronts have been made straight to avoid focusing and improve lateral reflection energy.

9.7.3 Concert Halls for Classical Music

Public concerts with large orchestras started in Europe about 250 years ago in halls that resembled those in which the composers normally found audience for their nonreligious music such as the salons and ballrooms of the nobility and courts. It is likely that this tradition as well as the limited span of wooden beam ceilings are the main reasons why many of the old concert rooms were built in what we now call the classical shoe-box shape: a narrow rectangle with a flat floor and ceiling and with the orchestra placed on a platform at one end.

The most famous of the shoe-box-shaped halls is the Musikvereinsaal in Vienna, Austria, shown in Fig. 9.45. This hall, dating from 1870, has a volume of 15 000 m^3 and seats 1670 people. Today, we understand many of the factors responsible for its highly praised acoustics:

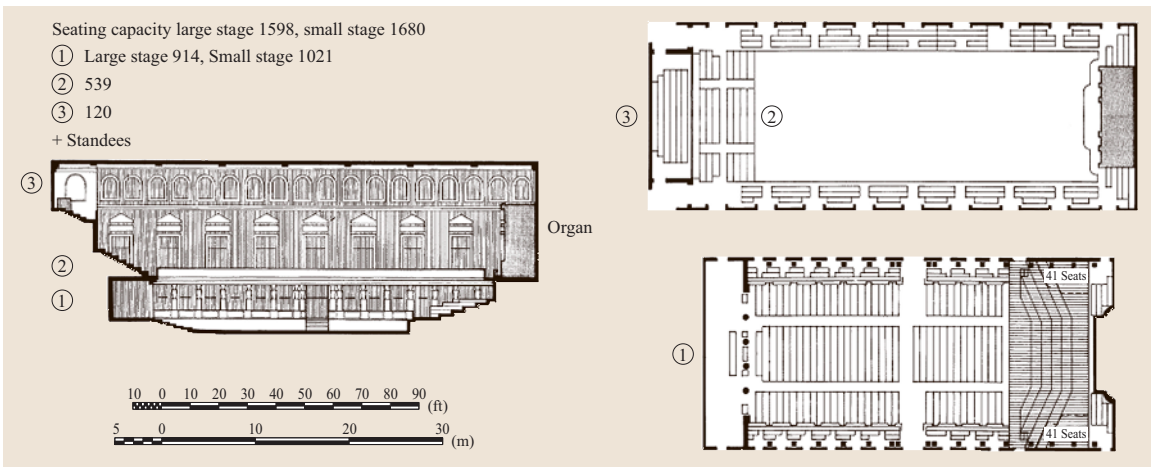


Fig. 9.45 The Musikvereinsaal, Vienna. Balcony and floor plans and long section (after [9.3])

Amazon
EX1010 Page 352

- The volume per seat is only 9 m^3; but T is still 2.0 s in the fully occupied hall because the seating area is relatively small (the seats are narrow and the row-to-row distance is small) and because of the flat main floor. Thus, the sound becomes both loud and reverberant.
- The reverberation also benefits from the fact that the absorbing audience (apart from a few on the top rear balcony) is placed in the lower half of the volume, whereby a *reservoir* of reverberant energy can exist in the upper part of the room.
- The close side walls create strong lateral reflections giving high *clarity* and *envelopment*, and all surfaces are modulated with rich ornamentation, which prevents echoes and causes the room reflections to sound soft and pleasant.

There are however elements of the acoustics, and lack of comfort, that we would not accept in a modern concert hall. The sound is somewhat unclear and remote in the rear part of the flat main floor due to grazing-incidence attenuation. Also, in the side balconies only people sitting close to the balcony front can see well. Other old and famous shoe-box halls (such as the Boston Symphony Hall) have too-shallow balcony overhangs, which results in weak reverberant energy below the balconies.

Because of the general and proven success of the shoe-box design, many new halls are built with this shape. However, in most of the modern shoe-box halls, the drawbacks mentioned above are avoided by a slightly sloping stalls floor and a different layout of the side balconies.

One of the modern shoe-box halls in which the above modifications have been introduced is the Kyoto Concert Hall, Japan, shown in Fig. 9.46. Comparing Fig. 9.45 and Fig. 9.46, the increased floor slope and the subdivided side balconies turned towards the stage are clearly seen.

Recalling the influence of floor slope on T (and other parameters, Sect. 9.5.6) the increased slope will result in a reduced T and higher C. In modern designs T will also tend to be reduced by more-spacious seating and less-shallow balcony overhangs, which result in a larger absorptive audience area being exposed to the sound field. All these factors call for a larger volume per seat in modern shoe-box halls than found in the classical ones, if a high T value is to be maintained. On the other hand, this might well be the reason why the newer halls seldom provide the same intensity and warmth as experienced when listening from one of the sparsely upholstered wooden chairs in Vienna.

Early in the 20th century the development of concrete building technology allowed architects to shape the halls more freely. At the same time it became popular to treat sound as light, by designing the surfaces by means of geometric acoustics and by trying to transmit the sound as efficiently as possible from the source on stage to the (absorbing) audience. Another desire was to put the audience as close as possible to the stage.

The result was the fan-shaped concert hall, which dominated modernist architecture between about 1920 and 1980. An example is seen in Fig. 9.47: Kleinhans Music Hall in Buffalo, USA. Comparison with Fig. 9.45 reveals a very wide hall with a relatively low ceiling and the stage surrounded by concave, almost parabolic, walls and with the ceiling projecting the sound into the absorbing audience area after just a single reflection. This phenomenon, as well as the low volume per seat (about 6.4 m^3), are the reasons for the resulting low reverberation time and the weak sense of *reverberance*. The audience receives most of the sound from frontal directions or from the ceiling, so the sound is clear but lacks envelopment. Other examples of modernist fan-shaped halls are, the Salle Pleyel in Paris (1927) and the old Danish Broadcasting Concert Hall (Copenhagen, 1946). In conclusion, few concert halls from the modernist era have been acoustically successful.

Fortunately, mainly as a result of advances in room acoustic research, two alternative and more-promising designs appeared in the 1960s and 1970s: the *vineyard*

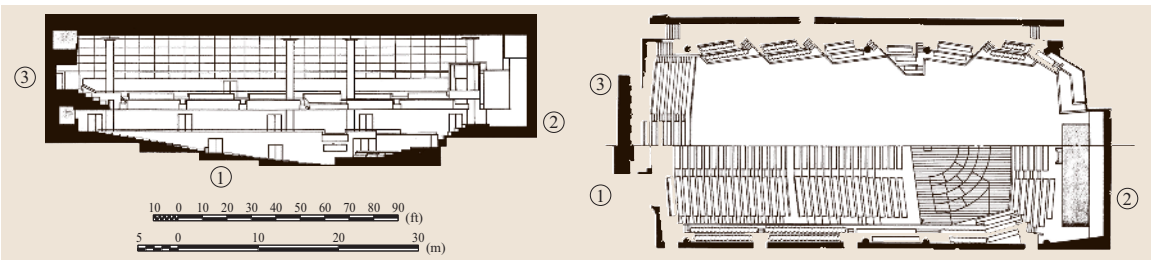


Fig. 9.46 Kyoto Concert Hall, Japan. Built 1995, volume 20 000 m^3, 1840 seats, RT = 2.0 s (after [9.3])

Amazon
EX1010 Page 353

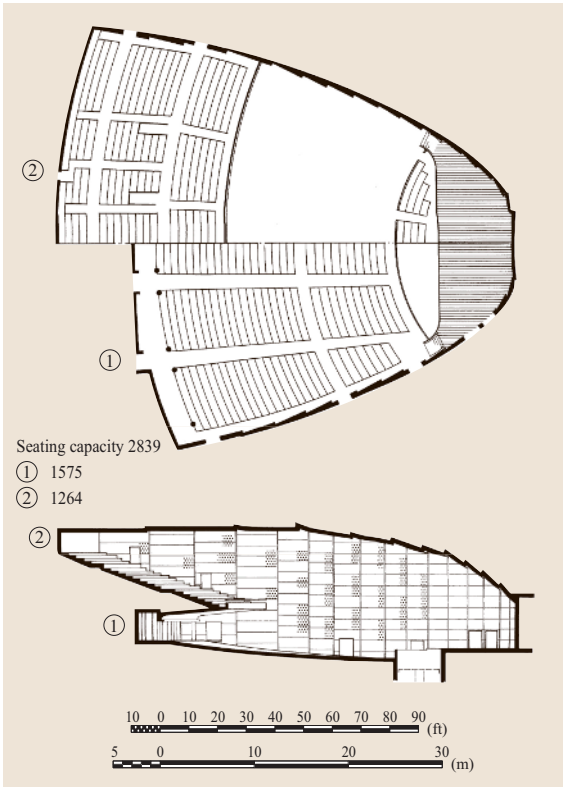


Fig. 9.47 Kleinhans Music Hall, Buffalo, USA. Built 1940, volume 18 240 m^3, 2839 seats, RT = 1.5 s. Plans and long section (after [9.3])

and the *directed reflection sequence* (DRS). Both are arena-shaped with the possibility of the audience being placed all around the orchestra platform. Even more than the fan shape, this causes the audience to come closer to the orchestra for the sake of intimacy. However, both designs are primarily relevant for larger halls, say more than 1500 seats. For halls seating more than about 2000, these designs may even be more successful than the classical rectangular shape, which, with so many seats, possess a risk of some listeners being placed too far from the stage.

The first vineyard concert hall was the Philharmonie Berlin, shown in Fig. 9.48, which opened in 1963. This hall has no balconies. Instead, the seating area is subdivided into terraces elevated relative to each other, whereby the terrace fronts and sides can act as *local* reflectors for specific seating areas. By careful design of these terraces, it is possible to provide plenty of early, and even lateral, reflections to most of the seats in an arena-shaped hall. With no seats being overhung by balconies, a large absorptive area is exposed to the sound, whereby a generous volume per seat is recommended. Thus, in the Sapporo Concert Hall in Japan (1997) as well as in the new Danish Radio Concert Hall in Copenhagen, the volume per seat is about 14 m^3. This is a quite high value for concert halls, as a 2 s T value should normally be obtained with just 10 m^3 per seat.

In *directed reflection sequence* halls such as the Christchurch Town Hall shown in Fig. 9.49, most of the early reflections are provided by huge, suspended and tilted reflectors. These are distinctly separate from

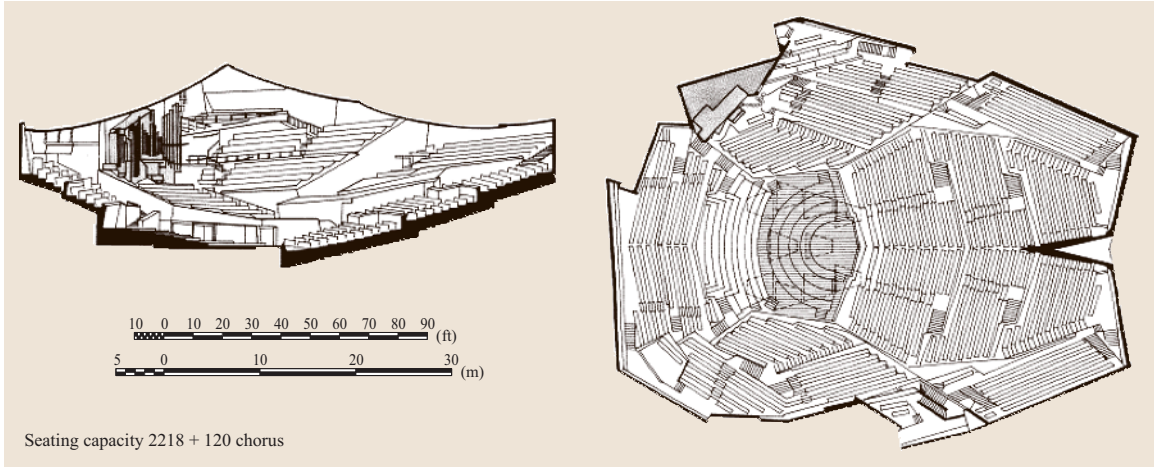


Fig. 9.48 Plan and section of Philharmonie Berlin, Germany. (Built 1963, 2335 seats, $V = 21\,000\,m^3$, $T = 2.1$ s) Acoustician: Lothar Cremer (after [9.3])

Amazon
EX1010 Page 354

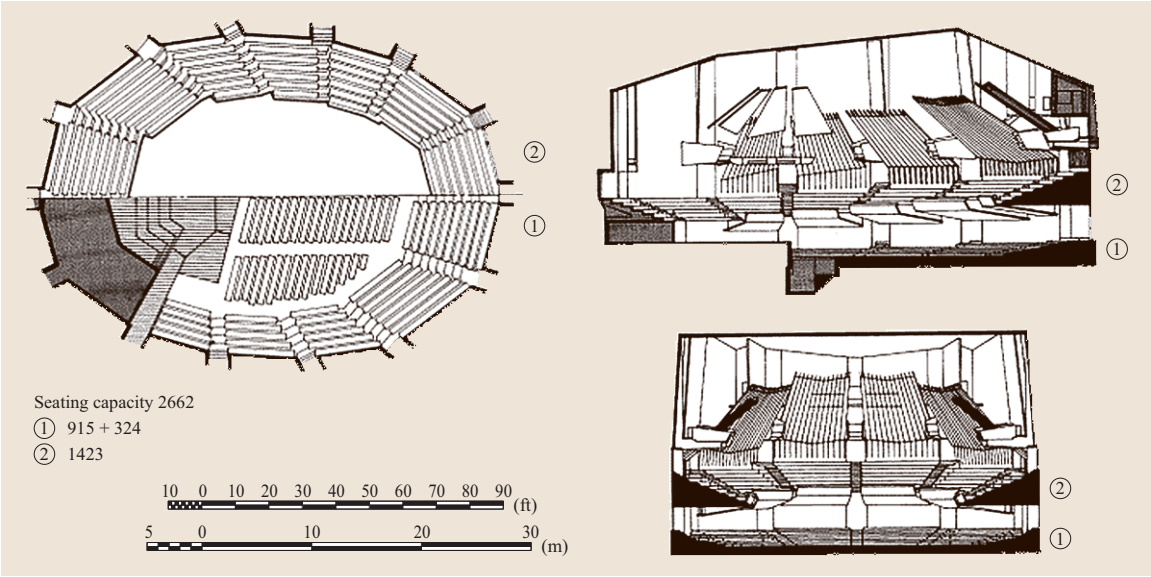


Fig. 9.49 Christchurch Town Town Hall, New Zealand. (Built 1972, 2662 seats, $V = 20\,500\,\mathrm{m}^3$, $T = 2.4\,\mathrm{s}$) Acoustician: Harold Marshall (after [9.3])

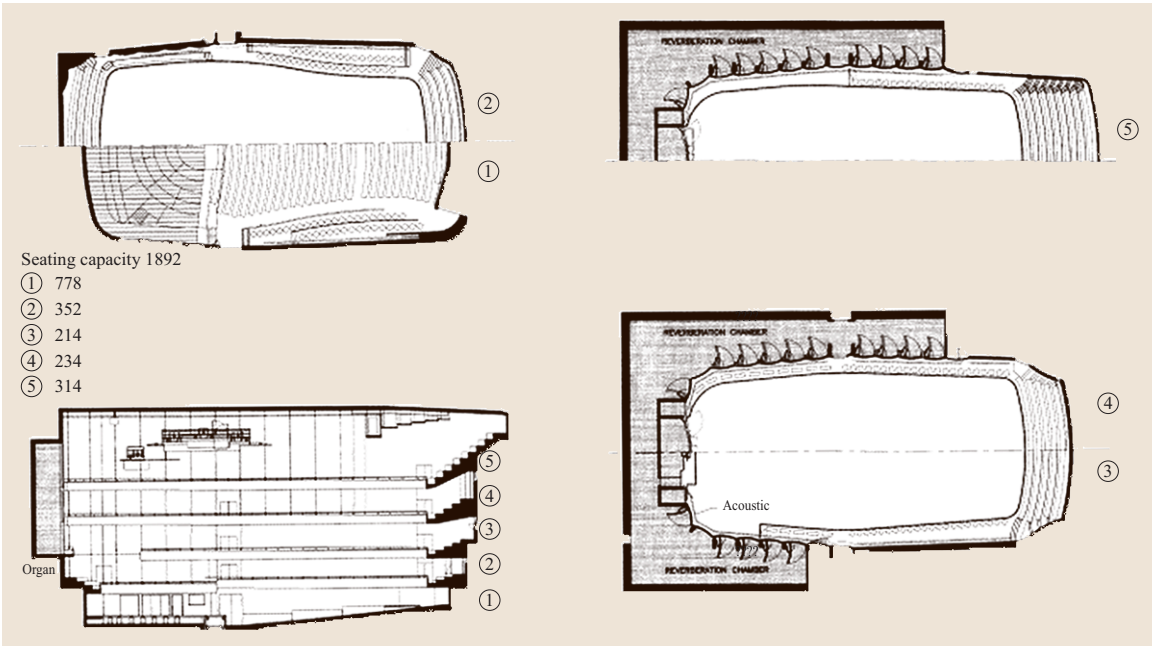


Fig. 9.50 The KKL Concert hall in Luzern, Switzerland. (Built 1999, 1892 seats, $V = 17800 + 6200\,\mathrm{m}^3$, $T = 1.8–2.2\,\mathrm{s}$) Acoustician: Russell Johnson (after [9.3])

the boundaries, which define the reverberant volume. The fronts and soffits of the sectioned balconies surrounding the main floor and stage in the elliptical plan provide additional early reflections. Because of the arena layout combined with the extensive use of balconies (containing more than half of the seats) the hall is very

Amazon
EX1010 Page 355

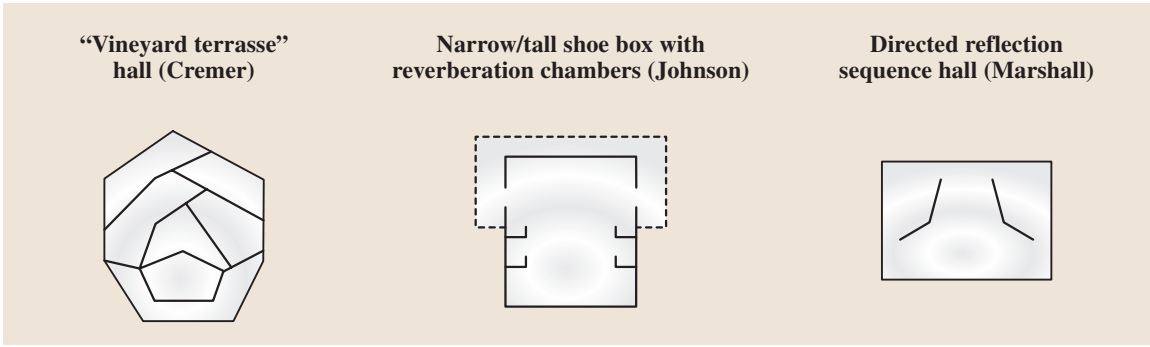


Fig. 9.51 Three concert hall concepts with the potential of combining high clarity with long reverberation. *From left to right*: vineyard (plan), shoe box with coupled reverberation chambers (cross section), and directed reflection sequence (cross section)

intimate, and the large reflecting surfaces provide a stunningly clear, dynamic and almost too loud sound. Still, the reverberation is long and rich because of the significant volume without absorption above/behind the reflectors.

This aim towards a combination of high *clarity* and high *reverberance*, probably developed through our extensive listening to recorded music, requires close reflecting surfaces as well as a large volume. The natural consequence of this demand is to separate the early reflecting surfaces from the room boundaries. Both the terrace fronts in the vineyard halls and the suspended reflectors in the DRS halls offer this possibility. A third way to achieve high *clarity* as well as high *reverberance* is a narrow shoe box with added surrounding volume, as found in a number of halls since about 1990. In these halls the volume of the narrow tall shoe-box hall providing the early reflections is quite moderate; but an extra volume is coupled to the main hall through openings that can be closed by heavy doors, so that the total volume can be varied. However, in such halls one should be careful to make the coupling area large enough for the added volume to have any significant effect (unless one sits close to one of the open doors), otherwise it is hard to justify the enormous costs of the extra volume and door system. With weak coupling, a double-sloped decay curve with a knee point perhaps 20 dB down is created, whereby the added, longer reverberation becomes barely audible except during breaks in the music.

A recent design of such a rectangular hall with a coupled volume is shown in Fig. 9.50.

The sketches in Fig. 9.51 summarize the basic design of the three types of halls mentioned. It is seen that they all possess the possibility of separating the surfaces that generate the early reflections from the volume boundaries that generate the reverberation.

9.7.4 Multipurpose Halls

Many modern halls built for cultural purposes often have to accommodate a variety of different types of events, from classical to pop/rock concerts, drama and musicals, opera, conferences, banquets, exhibitions, cinema and perhaps even sports events. From an acoustical point of view, the first concern in these cases is whether a variable reverberation time will be necessary. The answer is yes in most cases where some functions primarily require intelligibility of speech while others require a substantial reverberation, such as for classical music.

A hall in which these demands have been met by means of variable absorption is Dronningesalen, at the Royal Library in Copenhagen (Fig. 9.52). For this hall both chamber-music concerts and conferences with amplified speech were given high priority. The variable absorption is provided by means of moveable panels on the side walls as well as by folded curtains and roller blinds on the end walls. Combining these measures in different ways, T values in the range from 1.1 to above 1.8 s can be obtained (in the empty hall) as seen in Fig. 9.52.

In many cases, stage performances with extensive scenery are also required. The most common way to accomplish this is to design a stage house, mount an orchestra shell on the stage and raise the pit to stage level for concerts. If a hall is also to be used for banquets and exhibitions requiring a flat floor, it is common to place the stalls seats on a telescopic riser system on a flat floor instead of having a fixed, sloped seating. When not in use, this riser system is stored along the rear wall or un-

Amazon
EX1010 Page 356

der a balcony. If the reverberation time suits classical music concerts with the sloped seating in place, a substantial area of variable absorption is needed to reduce the T value when the chairs are absent. Another problem may be that the telescopic systems offer only a rather steep and linear slope, which is not optimal for classical concerts. If the chairs are fixed on the riser steps, the minimum step height is about 25 cm, corresponding to a rake of about 25%.

If a change in T is accomplished by means of variable absorption, G will be reduced along with lowering T. However, if instead T is lowered by reducing the volume, for instance by moving a wall or lowering the ceiling, G will remain approximately constant or perhaps even increase. This can be advantageous when the low-T setting is to be used, for instance for unamplified drama or for chamber music in a larger symphony concert hall.

An example of a hall with variable volume is found in Umeå, Sweden (Fig. 9.53). In this hall the auditorium volume can be adjusted by moving the proscenium wall between three positions. When the proscenium is stored against the rear wall in the *concert* format, the entire volume is available for concerts with large symphonic orchestras on an open stage. In this situation, the stage tower can be closed off by horizontal panels at ceiling level. But when the proscenium is moved forward to the *opera* setting, the auditorium becomes smaller and a proscenium stage area is created, while the ceiling panels are removed for access to the fly tower above. In the third position, *drama*, the auditorium volume is further reduced to create an intimate theater. The variable elements also include a hinged side-wall section to improve the shape of the room for theater as well as moveable reflectors and variable absorption curtains above the grid ceiling level.

It should be mentioned that many of the problems related to the successful design of speech and music auditoria become more severe with increased size of the room. In other words, it is much easier to design a hall for less than 1000 people, like the two examples presented above, than for 2000 plus. The problems become even more complicated if multipurpose function is requested.

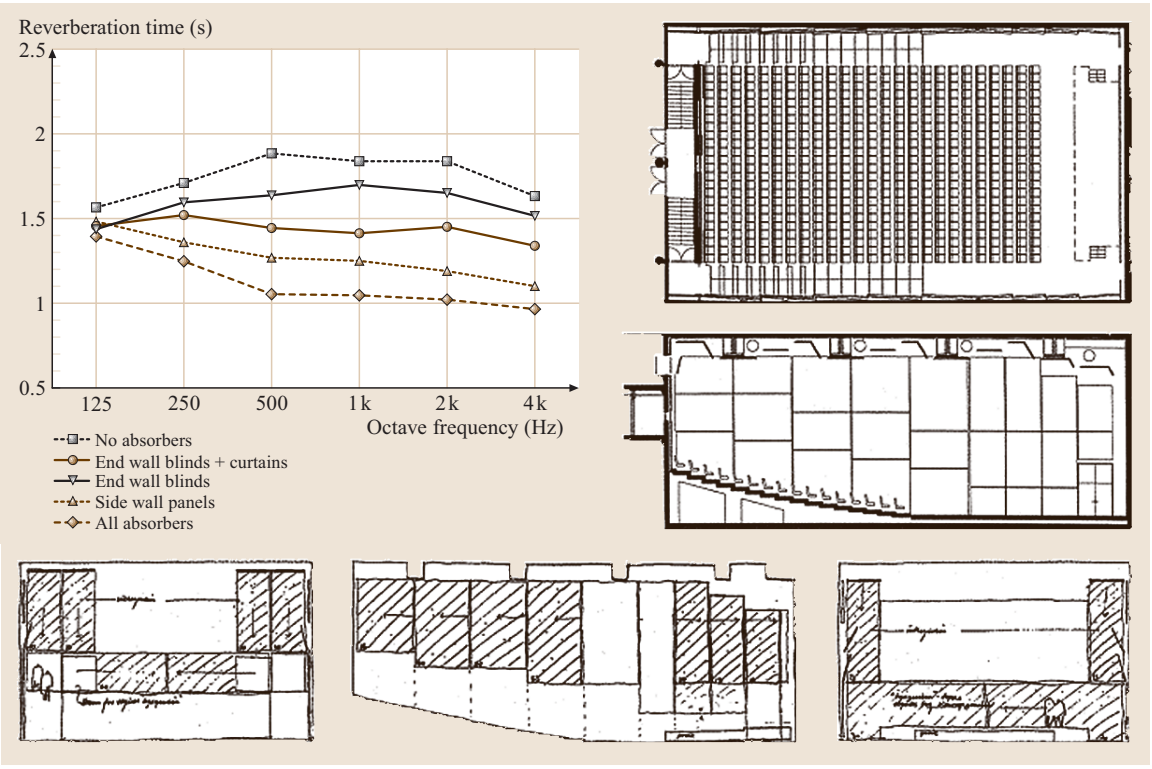


Fig. 9.52 Dronningesalen in the Royal Library in Copenhagen, Denmark; 1999, 400–600 seats. Reverberation time curves, plan, section and wall elevations with *hatched areas* indicating variable absorption

Amazon
EX1010 Page 357

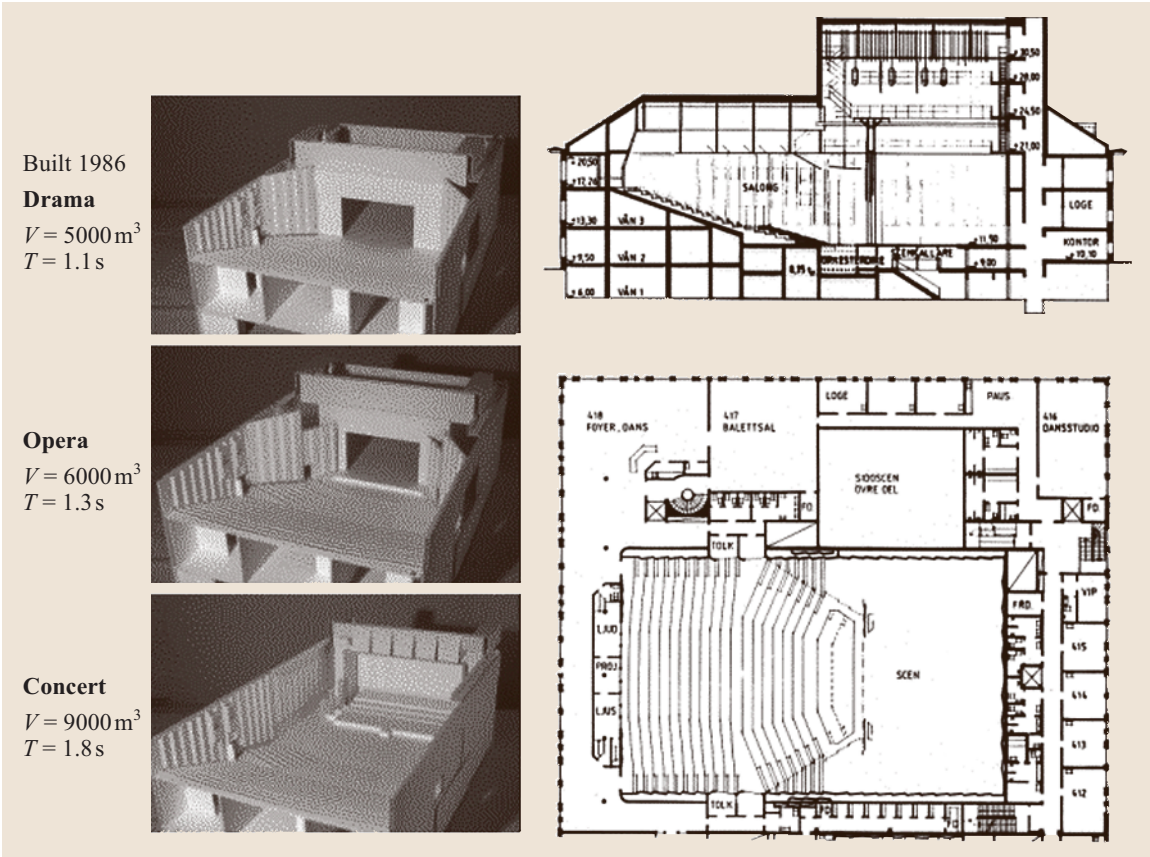


Fig. 9.53 The Idun multipurpose hall in Umeå, Sweden, with variable volume and stage configurations. The hall seats up to 860 people. Brief data (*left*), photos from cardboard model, long section and plan (*right*)

Still, a few examples of such successful designs exist. The most innovative is probably the Segerstrom Hall in Orange County, California, USA, which is shown in Fig. 9.54. This hall features a special layout of the almost 3000 audience seats, which are distributed on four levels. Each of these forms an almost rectangular, or even reverse fan, shape. However, the orientation of each level is shifted so that the overall plan becomes a wide fan. In this way the virtues of the fan shape for audience proximity to the stage are combined with the advantages of the rectangular shape for strong, early reflections from lateral directions. Thus, although the total width is about 50 m, the lateral energy level in this hall resembles that found in rectangular, 25 m-wide concert halls with typical seating capacity up to, say, 2000 people [9.36].

9.7.5 Halls for Rhythmic Music

Halls intended for rhythmic, amplified music concerts range in size from less than 100 to perhaps more than 50 000 listeners (in roofed sports arenas). The reason for this broad range of audience capacity is that the size and number of the sound amplification loudspeakers as well as of event video screens can be chosen at will to ensure good vision and adequate (often too high) sound levels for any size of audience. In any case, the reverberation time should be close to the optimal for speech, i. e., not more than 1 s if possible.

In huge arenas, of course, the reverberation time will be higher; but if efficient absorption is applied to the critical surfaces, a higher reverberation time need not compromise clarity. This is because the reverber-

Amazon
EX1010 Page 358

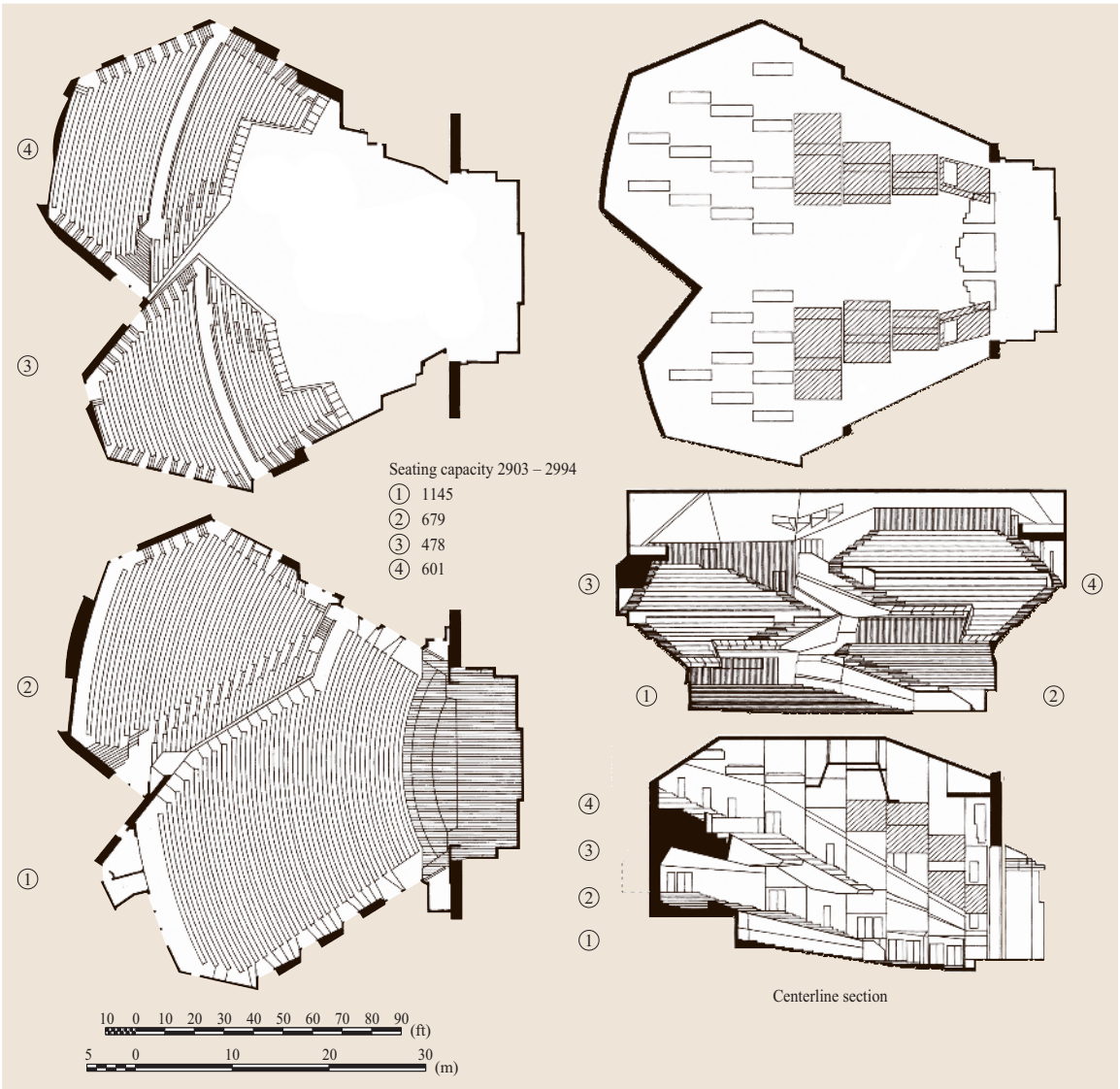


Fig. 9.54 Segerstrom Hall, Orange County, California, seating 2900 people. Acoustic design: Marshall, Hyde, Paoletti (after [9.3])

ation level will be low compared to the direct sound from the loudspeakers. In large spaces, designed to have a moderate T value, one must be careful to avoid echoes from distant, hard surfaces facing the often highly directional loudspeakers. Even small surfaces such as doors can cause echo problems if most other surfaces in the room are efficiently absorbing.

It is also very important to maintain modest low-frequency T values. A bass ratio larger than unity can create serious problems with control of the low-frequency levels. This is largely because most loudspeakers are almost omnidirectional at low frequencies, at which they willingly excite the room *reverberance*. In contrast, with high loudspeaker directivity in mid- and high-frequency range, it is easy to control the level in the audience area at these frequencies without spilling additional sound energy into the room.

Amazon
EX1010 Page 359

Unfortunately, low-frequency reverberation control can be difficult to achieve, because low-frequency absorbers are normally less efficient (have lower α values) than mid-/high-frequency absorbers, and in a room in which these already occupy most of the available surfaces, it can be difficult to also find spaces for dedicated low-frequency absorbers. In particular, this poses a problem in buildings made from heavy concrete or masonry (which on the other hand is favorable for insulation of low-frequency sound towards the neighbors). When the low-frequency reverberation is too high the string bass and pedal drum will sound muddy. The audience area layout should be shaped to allow an even coverage by a sensible loudspeaker set up, and in large halls, a sloping floor is not suitable if a standing audience is expected. Fortunately, a sloping floor is not always mandatory, since in larger venues, the loudspeakers can be elevated to avoid grazing-incidence attenuation and elevated video projection screens improve the visual experience. It is advantageous to design the hall as well as the loudspeaker system so that zones with lower levels are also created, whereby people can have a chance to rest their ears, for instance while picking up refreshments in the bar. This may be accomplished by placing the bar in a smaller, partly decoupled, space with a shallower room height and an efficiently absorbing ceiling.

9.7.6 Worship Spaces/Churches

The liturgies in old Christian and Muslim worship were developed in highly reverberant cathedrals and mosques, both of which have their roots in Byzantine architecture. When new churches are built for the traditional Catholic or Protestant Christian denominations, it is customary to aim at a rich reverberation, which suit the pipe organ literature and congregational singing, while the intelligibility of the words by the priests is taken care of by a distributed public address (PA) sound system.

The same is true for new large mosques, in which the speech is amplified while the long reverberation supports traditional singing by the imams. Apart form these songs music is not performed in mosques.

In contrast to this, several Christian denominations, particularly in the US, have built new churches or temples (often accommodating several thousand people) and brought in newer art forms making use of large rock-music sound systems. In these spaces, therefore, the solution is often for the acoustician to create fairly dry, natural acoustics and to install both a heavy PA sound system as well as an artificial, electronic reverberation-enhancement system. Both types of sound systems are briefly described in Sect. 9.8.

9.8 Sound Systems for Auditoria

It is important to realize that sound systems will always be installed in both new and existing halls. As these systems are often used to amplify natural sound sources appearing on the stage in the hall, they may be regarded as a means for creating variable acoustics of the space. In this regard, the following will focus on how these systems interact with the natural acoustics, rather than talking about specific details or trends in the design of the loudspeakers themselves.

In principle, one may consider two different types of loudspeaker to be installed in an auditorium: traditional PA systems intended for the modification of the early part of the impulse response of the hall, and reverberation-enhancement systems intended for modification of the later part. Below, important aspects of both types will be briefly explored.

9.8.1 PA Systems

Normally, PA sound systems are installed with the purpose of increasing the sound level and/or the intelligibility of the performance. Use of the sound system for the reproduction of prerecorded sounds is of less interest in this context, as in this case it just acts like any other sound source working under the acoustic conditions provided by the natural acoustics of the room. In Sect. 9.2 we learned that, in order to improve *clarity/intelligibility* as well as the *level*, we need to increase the clarity C by adding sound components to the early part of the impulse response. (The alternative, to increase C by reducing the late part, can so far only be accomplished by adding physical absorption; but some day in the future, active systems with multiple microphones and loudspeakers integrated into *acoustic wallpaper* could be imagined as well.) Doing this requires that the main part of the sound energy leaving the loudspeakers hits the absorbing audience area. Alternatively, if substantial parts of the energy hit other, reflecting room surfaces, it may be reflected randomly and feed the reverberant field, which will reduce the clarity. For this reason, it is very important to apply loudspeakers with well-controlled directivity for this purpose, espe-

Amazon
EX1010 Page 360

cially in auditoria with T values larger than optimal for speech.

For the acoustician, the most important technical specification for PA loudspeakers relates to their directivity, either in terms of vertical and horizontal radiation angles or in terms of the Q factor. Sometimes, the term *directivity index* $\mathrm{DI} = 10\log(Q)$ is used instead. Q is defined as the ratio between

1. the intensity emitted in the axis direction of the directive loudspeaker, and
2. the averaged intensity emitted by the same loudspeaker integrated over all directions.

The higher the Q value, the more the sound emitted will be concentrated in the forward direction (or rather, within the radiation angles specified).

When the loudspeaker is placed in a room, the sound field close to the loudspeaker will be dominated by the direct sound, whereas at longer distances, this component is negligible compared to the (diffuse) reverberant sound, as illustrated in Fig. 11.6. The (squared) sound pressure as a function of distance from the source in a room can be written as follows:

$$p^2(r) = \rho c\, P_{\mathrm{SP}} \left(\frac{Q_{\mathrm{SP}}}{4\pi r^2} + \frac{4}{A} \right) . \qquad (9.38)$$

In (9.38) the first term in the parenthesis is the direct sound component and the second one, $4/A$, the diffuse, reverberant component, P_{SP} is the emitted sound power, Q_{SP} is the Q factor of the loudspeaker, and A is the total sound absorption area of the room. Notice that in (9.38), for simplification, we assume a diffuse field intensity that is constant throughout the room, although in Sect. 9.5.1 and Fig. 9.13 we demonstrated that this is seldom the case.

Equation (9.38) shows that the direct component will dominate as long as the direct term is larger than the diffuse term. This will be the case for distances below the *critical distance* or the *reverberation distance*, $r_{\mathrm{cr,SP}}$. At this distance, the two components have equal magnitude, whereby

$$r_{\mathrm{cr,SP}} = \sqrt{\frac{Q_{\mathrm{SP}} A}{16\pi}} = \sqrt{\frac{Q_{\mathrm{SP}} V}{100\pi T}} . \qquad (9.39)$$

As seen from (9.39), we maximize the range within which we are able to provide the listeners with a clear sound from the speakers by increasing Q (as well as A).

One should be careful not to apply a larger number of loudspeakers than needed for coverage of the audience area, as each new loudspeaker will contribute to the generation of the reverberant diffuse field, while only one at a time will send direct sound towards a given audience position. Likewise, the number of open microphones should be minimized (which is often done automatically by an intelligent microphone mixer), as all open microphones will pick up and amplify the unclear reverberant field in the room.

The number of active loudspeakers and microphones should also be minimized in order to reduce the risk of feedback, which is a consequence of the microphone(s) picking up the sound from the loudspeaker(s) and the amplifier gain being set to high. If the amplification through the entire closed loop (microphone–amplifier–loudspeaker–room and back to the microphone) exceeds unity, the system will start to oscillate at a random frequency, which is emitted at maximum power level into the room, a most annoying experience.

The risk of feedback can be reduced by minimizing the loudspeaker–listener distance and the source–microphone distance, whereby a suitable listening level can be obtained with a moderate amplifier gain setting. Use of head-borne microphones represents the ultimate reduction of the source–microphone distance. Consequently, with such microphones the risk of feedback is substantially reduced. Also, the microphone–loudspeaker distance should be maximized and directional microphones and loudspeakers should be used and positioned so that the transmission from the loudspeaker back into the microphone is minimized. Thus, the loudspeakers and the microphones should be placed pointing away from each other with the microphone pointing towards the stage and the loudspeaker pointing toward the audience.

Considering the factors mentioned above, we still need to choose a configuration of the loudspeakers for a given room. Often the choice is between

1. a central system, consisting of a single or a limited number of highly directional units arranged close together in a cluster over the stage, or
2. a distributed system of several smaller units placed closer to the listeners.

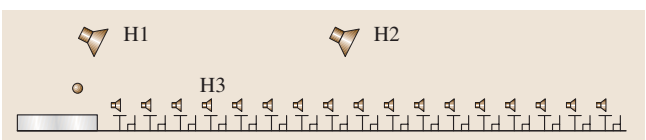


Fig. 9.55 Alternative solutions for loudspeaker coverage in an auditorium: a central (cluster) system H1, the same with a delayed secondary unit H2, or a highly distributed (pew back) system with small loudspeakers placed in each row of seats

Amazon
EX1010 Page 361

These options are illustrated schematically in Fig. 9.55 as H1 and H3, respectively. H2 illustrates a compromise with a secondary unit or cluster assisting the main cluster, H1.

In meeting rooms or churches, highly distributed systems with small loudspeakers built into fixed meeting tables or pews can be very successful. With each loudspeaker being within a distance of say 1 m from the listener, each unit can be set to a very moderate level. Therefore, it is often possible to serve the listeners with a clear direct sound from such speakers without the total number of speakers exciting too much of the room reverberation. If the system is subdivided into independent sections, it is even possible to install automatic switches that only activate loudspeakers in zones where people are sitting. In this way, the reverberant field can be even further reduced in cases of fewer people attending the meeting or service. This is actually very fortunate as, especially in churches, fewer people also means less absorption and louder reverberation. The performance regarding intelligibility of pew-back systems with perhaps one hundred, moderately directive speakers is often equal to or better than when a highly directive central-cluster system is used. This is simply due to the moderate sound level needed from each of the closely placed loudspeakers compared to the much higher level needed for the cluster to reach the distant listeners. As can be imagined, the sound level distribution produced by the pew-back system will also be more uniform.

Of course, the highly distributed systems are not suitable for amplification of stage performances, where a high sound level of music is needed. For this purpose, a main cluster over the stage or a stereo system with loudspeakers on each side of the stage is preferable. For such systems, it is also more important to maintain a correct localization of the sound as coming from the performers on the stage.

In cases where some additional, distributed loudspeakers are needed to assist coverage in certain parts of the room, for instance on and under deep balconies, these are equipped with an electronic delay. If this delay is set so that the sound from the distributed assisting loudspeakers arrives 5–25 ms after the sound from the main loudspeakers, the listener will still perceive the sound as coming from the direction of the source. This is even true when the assisting loudspeakers are up to 5 dB louder than the main cluster at the listener's position. This very convenient phenomenon, called the precedence effect or Hass effect, is generally used as a guideline for the choice of level and delay settings in distributed loudspeaker systems.

9.8.2 Reverberation-Enhancement Systems

For auditoria where a long reverberation time is only needed occasionally or when the available room volume is simply inadequate, one may consider creating more reverberation by means of an electronic reverberation-enhancement system. Like the systems described in the previous section, these also consist of a number of loudspeakers and microphones connected by amplifiers; but there are many important differences.

The basic difference is that enhancement systems primarily attempt to add energy to the late part of the impulse response. Therefore, delays must be built into the signal processing between microphones and loudspeakers. In the first systems of this kind, *assisted*

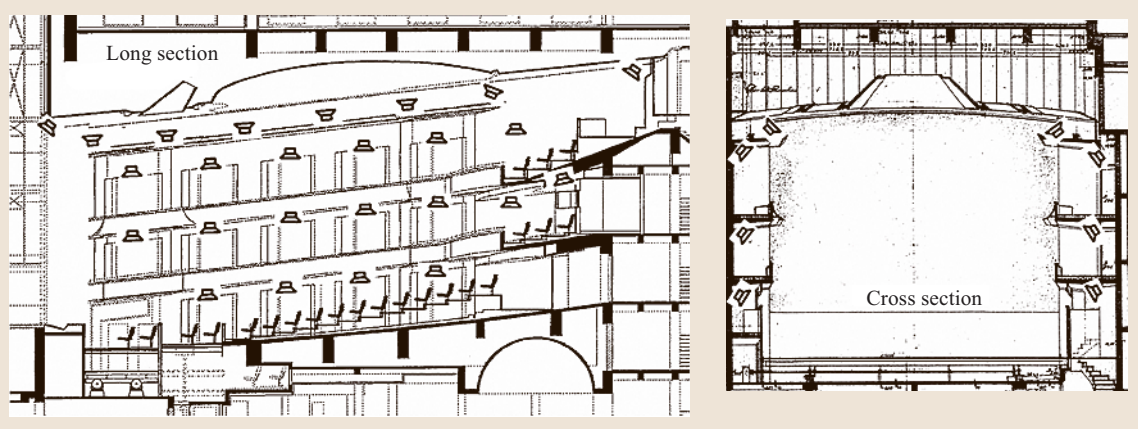


Fig. 9.56 Example of distribution of loudspeakers for reverberation enhancement in a theatre

Amazon
EX1010 Page 362

resonance (AR) and *multichannel reverberation* (MCR), which appeared in the 1960s, this delay was provided by letting the loop gain of a large number of microphone–loudspeaker channels be tuned to just below the feedback limit. By spacing the microphones and loudspeakers far apart in the room (normally close to the ceiling), the sound would spend sufficient time traveling several times between loudspeakers and microphones for an audible prolongation of the reverberation to be perceived. In more-modern systems, electronic delays and reverberators are normally used.

In order to create the illusion of diffuse reverberation coming from the room itself, a large number of loudspeakers with low directivity must be distributed over the main surfaces in the room, as illustrated in Fig. 9.56. Since many speakers are needed, each can be fairly small and with limited acoustic power capability. The density and placement of these speakers as well as the balancing of their levels is essential to prevent localization of individual loudspeakers from any seat.

Regarding the microphones, these may be highly directive, but they must be placed quite far from the sound sources (and preferably out of sight) in order to cover the stage without the reverberant level being strongly dependent on the position of the sound source.

In view of what was explained in Sect. 9.8.1 about the measures needed to reduce the risk of feedback in loudspeaker systems, it is no wonder that most reverberation-enhancement manufacturers have to implement a solid strategy against uncontrolled feedback. One very efficient approach is to introduce time-varying delays in the sound-processing equipment, as this seems to destroy sharp room resonances when they start to build up to form a hauling frequency. Still, most enhancement systems work with a loop gain close to the feedback limit (which is actually participating actively in increasing the reverberation time), which is acceptable as long as it is under control and does not cause audible coloration of the sound.

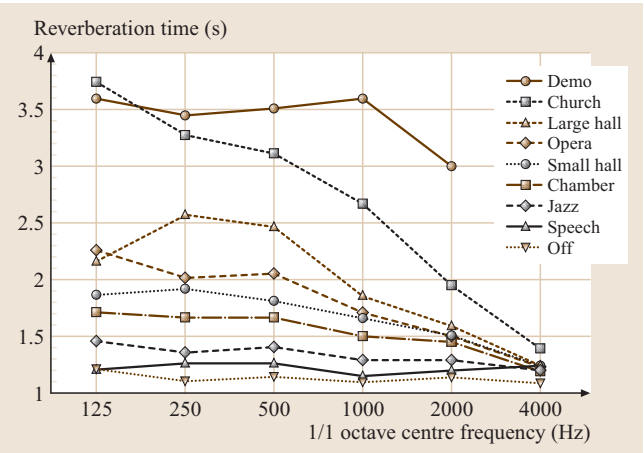


Fig. 9.57 Reverberation time values measured in a hall for different settings of the reverberation enhancement system (LARES)

It is essential for the acceptance of enhancement systems that neither audience nor performers experience the sound as coming from a loudspeaker system. Likewise, artefacts such as coloration due to feedback or the poor frequency characteristics of speakers are unacceptable.

The maximum increase in reverberation time possible with feedback-based systems like AR and MCR was typically about 50%. With modern digital reverberators, a much larger range can be achieved, as shown in Fig. 9.57. Increasing the reverberation time by a factor of three or more is not impossible. However, the illusion, when you still see the physical, much-dryer room around you, tends to break down when the value increases much above the 50%, which ironically is what the old systems could produce.

From a purist standpoint, reverberation enhancement can be regarded as an acoustic prosthesis, but in many cases a pragmatic approach to the use of these systems can increase the range of programs that a cultural venue can host.

References

9.1 A.C. Gade: *Subjective Room Acoustic Experiments with Musicians. PhD thesis, Rep. No. 32* (Technical University of Denmark, Copenhagen 1982)

9.2 W.C. Sabine: *Collected Papers on Acoustics* (Peninsula, Los Altos 1994), Reissued

9.3 L.L. Beranek: *Concert Halls and Opera Houses, Music Acoustics and Architecture*, 2nd edn. (Springer, Berlin, New York 2004)

9.4 M.F.E. Barron: *Auditorium Acoustics and Architectural Design* (Spun, London 1993)

9.5 H. Kuttruff: *Room Acoustics* (Applied Science, London 1976)

9.6 ISO: *ISO 3382*, Acoustics – Measurement of the Reverberation Time of Rooms with Reference to Other Acoustical Parameters (ISO, Geneva 1997)

Amazon
EX1010 Page 363

9.7 M. Vorländer: *International Round Robin on Room Acoustical Computer Simulations, Proc. 15th ICA* (Trondheim, Norway 1995) pp. 689–692

9.8 J.S. Bradley, G.A. Soloudre: The influence of late arriving energy on spetial impression, J. Acoust. Soc. Am. **97**(4), 2263–2271 (1995)

9.9 L.L. Beranek: *Music, Acoustics and Architecture* (Wiley, New York 1962)

9.10 Personal communication (summer 2006)

9.11 A.C. Gade: Investigations of musicians' room acoustic conditions in concert halls I, methods and laboratory experiments, Acustica **69**, 193–203 (1989)

9.12 A.C. Gade: Investigations of musicians' room acoustic conditions in concert halls II, Field experiments and synthesis of results, Acustica **69**, 249–262 (1989)

9.13 T. Houtgast, H.J.M. Steeneken: A tool for evaluating auditoria, Brüel Kjær Tech. Rev. **3**, 3–12 (1985)

9.14 J.S. Bradley: Predictors of speech intelligibility in rooms, J. Acoust. Soc. Am. **80**, 837–845 (1986)

9.15 M.R. Schroeder: New method of measuring reverberation time, J. Acoust. Soc. Am. **37**, 409 (1965)

9.16 J.S. Bradley: Accuracy and reproducibility of auditorium acoustics measures, Proc. IOA **10**, 399–406 (1988), Part 2

9.17 K. Sekigouchi, S. Kimura, T. Hanyuu: Analysisi of sound field on spatial information using a four-channel microphone system based on regular tetrahedron peak point method, Appl. Acoust. **37**, 305–323 (1992)

9.18 D. de Vries, A.J. Berkhout, J.J. Sonke: *Array Technology for Measurement and Analysis of Sound Fields in Enclosures, AES 100th Convention 1996 Copenhagen, Preprint 4266 (R-4)* (AES, San Francisco 1996)

9.19 C.M. Harris: Absorption of air versus humidity and temperature, J. Acoust. Soc. Am. **40**, 148–159 (1966)

9.20 C.W. Kosten: The mean free path in room acoustics, Acustica **10**, 245 (1960)

9.21 L.L. Beranek: Analysis of Sabine and Eyring equations and their applications to concert hall audience and chair absorption, J. Acoust. Soc. Am. **120** (2006)

9.22 L.L. Beranek, T. Hidaka: Sound absorption in concert halls by seats, occupied and unoccupied, and by the hall's interior surfaces, J. Acoust. Soc. Am. **104**, 3169–3177 (1998)

9.23 S. Sakamoto, T. Yokota, H. Tachibana: Numerical sound field analysis in halls using the finite difference time domain method. In: *Proc. Int. Symp. Room Acoustics: Design and Science (RADS)*, Awaji Island (ICA, Kyoto 2004)

9.24 F. Spandöck: Raumakustische Modellversuche, Ann. Phys. **20**, 345 (1934)

9.25 A.C. Gade: Room acoustic properties of concert halls: quantifying the influence of size, shape and absorption area, J. Acoust. Soc. Am. **100**, 2802 (1996)

9.26 M. Barron, L.-J. Lee: Energy relations in Concert Auditoria, J. Acoust. Soc. Am. **84**, 618–628 (1988)

9.27 W.-H. Chiang: *Effects of Various Architectural Parameters on Six Room Acoustical Measures in Auditoria, PhD thesis* (University of Florida, Gainesville 1994)

9.28 W. Fasold, H. Winkler: *Bauphysikalische Entwurfslehre, Band 5; Raumakustik* (Verlag Bauwesen, Berlin 1976)

9.29 Z. Maekawa, P. Lord: *Environmental and Architectural Acoustics* (Spon, London 1994)

9.30 W. Furrer, A. Lauber: *Raum- und Bauakustik Lärmabwehr* (Birkhaüser, Basel 1976)

9.31 J.H. Rindel: *Anvendt Rumakustik, Note 4201, Oersted DTU* (Technical University of Denmark, Copenhagen 1984), (In Danish)

9.32 L.I. Makrinenko: *Acoustics of Auditoriums in Public Buildings* (ASA, Melville 1994)

9.33 J. Sadowski: *Akustyka architektoniczna* (PWN, Warszawa 1976)

9.34 J.H. Rindel: *Acoustic design of reflectors in Auditoria, Note 4212 Oersted DTU* (Technical University of Denmark, Copenhagen 1999)

9.35 M.R. Schroeder: Binaural dissimilarity and optimum ceilings for concert halls: More lateral sound diffusion, J. Acoust. Soc. Am. **65**, 958–963 (1979)

9.36 J.R. Hyde: *Segerstrom Hall in Orange County – Design, Measurements and Results after years of operation*, Proc. IOA, Vol. 10 (IOA, St. Albans 1988), Part 2

Amazon
EX1010 Page 364

10. Concert Hall Acoustics Based on Subjective Preference Theory

This chapter describes the theory of subjective preference for the sound field applied to designing concert halls. Special attention is paid to the process of obtaining scientific results, rather than only describing a final design method. Attention has also been given to enhancing satisfaction in the selection of the most preferred seat for each individual in a given hall. We begin with a brief historical review of concert hall acoustics and related fields since 1900.

A neurally grounded theory of subjective preference for the sound field in a concert hall, based on a model of the human auditory–brain system, is described [10.1]. Most generally, subjective preference itself is regarded as a primitive response of a living creature and entails judgments that steer an organism in the direction of maintaining its life. Brain activities relating to the scale value of subjective preference, obtained by paired-comparison tests, have been determined. The model represents *relativity*, relating the autocorrelation function (ACF) mechanism and the interaural cross-correlation function (IACF) mechanism for signals arriving at the two ear entrances. The representations of ACF have a firm neural basis in the temporal patterning signal at each of the two ears, while the IACF describes the correlations between the signals arriving at the two ear entrances. Since Helmholtz, it has been well appreciated that the cochlea carries out a rough spectral analysis of sound signals. However, by the use the of the spectrum of an acoustic signal, it was hard to obtain factors or cues to describe subjective responses directly. The auditory representations from the cochlea to the cortex that have been found to be related to subjective preference in a deep way involve these temporal response patterns, which have a very different character from those related to power spectrum analyses. The scale value of subjective preference of the sound field is well described by four orthogonal factors. Two are temporal factors (the initial delay time between the direct sound and the first reflection, Δt_1, and the reverberation time, T_{sub}) associated with the left cerebral hemisphere, and two are spatial factors [the binaural listening level (LL) and the magnitude of the IACF, the IACC] associated with the right hemisphere. The theory of subjective preference enables us to calculate the acoustical quality at any seat in a proposed concert hall, which leads to a seat selection system.

The temporal treatment enables musicians to choose the music program and/or performing style most suited to a performance in a particular concert hall. Also, for designing the stage enclosure for music performers, a temporal factor is proposed. Acoustical quality at each seating position examined in a real hall is confirmed by both temporal and spatial factors.

10.1 **Theory of Subjective Preference for the Sound Field** 353
10.1.1 Sound Fields with a Single Reflection 353
10.1.2 Optimal Conditions Maximizing Subjective Preference 356
10.1.3 Theory of Subjective Preference for the Sound Field 357
10.1.4 Auditory Temporal Window for ACF and IACF Processing 360
10.1.5 Specialization of Cerebral Hemispheres for Temporal and Spatial Factors of the Sound Field 360
10.2 **Design Studies** 361
10.2.1 Study of a Space-Form Design by Genetic Algorithms (GA) 361
10.2.2 Actual Design Studies 365
10.3 **Individual Preferences of a Listener and a Performer** 370
10.3.1 Individual Subjective Preference of Each Listener 370
10.3.2 Individual Subjective Preference of Each Cellist 374
10.4 **Acoustical Measurements of the Sound Fields in Rooms** 377
10.4.1 Acoustic Test Techniques 377
10.4.2 Subjective Preference Test in an Existing Hall 380
10.4.3 Conclusions 383
References 384

Amazon
EX1010 Page 365

In the first half of the 20th century, studies were mostly concentrated on temporal aspects of the sound field. In 1900 *Sabine* [10.2] initiated the science of architectural acoustics, developing a formula to quantify reverberation time. In 1949, *Haas* [10.3] investigated the echo disturbance effect from adjustment of the delay time of the early reflection by moving head positions on a magnetic tape recorder. He showed the disturbance of speech echo to be a function of the delay time, with amplitude as a parameter.

After investigations with a number of existing concert halls throughout the world, *Beranek* in 1962 [10.4] proposed a rating scale with eight factors applied to sound fields from data obtained by questionnaires on existing halls given to experienced listeners. Too much attention, however, has been given to monaural temporal factors of the sound field since Sabine's formulation of reverberation theory. For example, the Philharmonic Hall of Lincoln Center in New York, opened in 1962, was not satisfactory to listeners even after many improvements.

On the spatial aspect of the sound field, *Damaske* in 1967 [10.5] investigated subjective diffuseness by arranging a number of loudspeakers around the listener. In 1968, *Keet* [10.6] reported the variation of apparent source width (ASW) in relation to the short-term cross-correlation coefficient between two signals fed into the stereo loudspeakers as well as the sound pressure level. *Marshall* in 1968 [10.7] stressed the importance of early lateral reflections of just 90 degrees, and *Barron* in 1971 [10.8] reported *spatial impressions* or *envelopment* of sound fields in relation to the short-term interaural cross-correlation coefficient.

As a typical spatial factor of the sound field, *Damaske* and *Ando* in 1972 [10.9] defined the IACC as the maximum absolute value of the interaural cross-correlation function (IACF) within the possible maximum interaural delay range for the human head, such that

$$\mathrm{IACC} = |\phi_{\mathrm{lr}}(\tau)|_{\max} \ , \text{for } |\tau| < 1\,\mathrm{ms} \qquad (10.1)$$

and proposed a method of calculating the IACF for a sound field. In 1974, *Schroeder* et al. in [10.10] reported results of paired-comparison tests asking listeners which of two music sound fields was preferred. In an anechoic chamber, sound fields in existing concert halls were reproduced at the ears of listeners through dummy head recordings and two loudspeaker systems, with filters reproducing spatial information. They found that two significant factors, the reverberation time and the IACC, had a strong influence on subjective preference.

In 1977, *Ando* discussed subjective preference in relation to the temporal and spatial factors of the sound field simulated with a single reflection [10.11]. In 1983, he described a theory of subjective preference in relation to four orthogonal factors consisting of the temporal and spatial factors for the sound field, which enable us to calculate the scale value of the subjective preference at each seat [10.12, 13]. *Cocchi* et al. reconfirmed this theory in an existing hall in 1990 [10.14]. In 1997, *Sato* et al. [10.15] reconfirmed this clearly by use of the paired-comparison judgment in an existing hall, switching identical loudspeakers located at different positions on the stage, instead of changing the seats of each subject. This method may avoid effects of other physical factors than the acoustic factors. In addition to the orthogonal factors, they found the interaural delay in the IACF, τ_{IACC}, as a measure of image shift of the sound source that is to be kept at zero realizes good balance in the sound field. Using this method, the dissimilarity distance has also been described by the temporal and spatial factors of the sound field in 2002 [10.16].

Thus far, the theory has been based on the global subjective attributes for a number of subjects. The theory may be applied for enhancing each individual's satisfaction by adjusting the weighting coefficient of each orthogonal factor [10.1], even though a certain amount of individual differences exist [10.17]. The seat selection system [10.18] was introduced in 1994 after construction of the Kirishima International Concert Hall.

For the purpose of identifying the model of the auditory–brain system, experiments point toward the possibility of developing the correlation between brain activities, measurable with electroencephalography (EEG) [10.19, 20]. Correspondences between subjective preference and brain activity have been found from EEG and magnetoencephalography (MEG) studies in human subjects [10.21, 22], but details of these results are not included in this chapter due to limited space. Results show that orthogonal factors comprise two temporal factors: the initial time delay gap between the direct sound and the first reflection (Δt_1) and the subsequent reverberation time (T_{sub}) are associated with the left hemisphere, and two spatial factors: the listening level (LL) and the magnitude of the IACF (IACC) are associated with the right hemisphere. The information corresponding to subjective preference of the sound field can be found in the effective duration of the autocorrelation function (ACF) of the alpha (α) waves of both EEG and MEG. A repetitive feature in the α-wave, as measured in its ACF at the preferred condition, has

Amazon
EX1010 Page 366

been found. The evidence ensures that the basic theory of subjective preference may also be applied to each individual preference [10.21].

Since individual differences of subjective preference in relation to the IACC in the spatial factor are small enough, at the first stage of acoustic design we can determine the architectural space form of the room. The temporal factors are closely related to the dimensions of a specific concert hall, which can be altered to exhibit specific types of music, such as organ music, chamber music or choral works.

On the neural mechanism in the auditory pathway, a possible mechanism for the interaural time difference and correlation processors in the time domain was proposed by *Jeffress* in 1948 [10.23], and by *Licklider* in 1951 [10.24]. By recording left and right auditory brainstem responses (ABR), Ando et al. in 1991 [10.25] revealed that the maximum neural activity (wave V at the inferior colliculus) corresponds well to the magnitude of the interaural cross-correlation function. Also, the left and right waves $IV_{l,r}$ are close to the sound energies at the right- and left-ear entrances. In fact, the time-domain analysis of the firing rate of the auditory nerve of a cat reveals a pattern of ACF rather than the frequency-domain analysis as reported by *Secker-Walker* and *Searle* in 1990 [10.26]. Cariani and Delgutte in 1996 showed that pooled inter-spike interval distributions resemble the short-time or the running autocorrelation function (ACF) for the low-frequency component. In addition, pooled interval distributions for sound stimuli consisting of the high-frequency component resemble the envelope for running ACF [10.27, 28].

Remarkably, primary sensations such as the pitch of the missing fundamental [10.29], loudness [10.30], and duration sensation [10.31] can be well described by the temporal factors extracted from the ACF [10.32, 33]. *Timbre* investigated by the dissimilarity judgment [10.16] of the sound field has been described by both the temporal and spatial factors. The typical spatial attributes of the sound field, such as subjective diffuseness [10.34] and apparent source width (ASW), as well as subjective preference, are well described by the spatial factor [10.32–36].

Besides the design of concert halls, other acoustical applications such as speech identification [10.36], environmental noise measurement [10.37], and sound localization in the median plane [10.38] should benefit from guidelines derived from this model.

10.1 Theory of Subjective Preference for the Sound Field

Subjective preference judgment is the most primitive response in any subjective attribute and entails judgments that steer an organism in the direction of maintaining and/or animating *life*. Subjective preference, therefore, may relate to an aesthetic issue. It is known that judgment in an absolute manner presents a problem in reliability; rather, data is judged in a relative manner such as by paired-comparison tests. This is the simplest method, in that any person may participate, and the resulting scale value may be utilized in the wide range of applications. From the results of subjective preference studies in relation to the temporal factor and the spatial factor of the sound field, the theory of subjective preference is derived. Examples of calculating subjective preference at each listener's position are demonstrated in Sect. 10.2 for the global listener and Sect. 10.3 for the individual listener. The relationship between the resulting scale value of subjective preference in an existing hall and the physical factors obtained by calculation using architectural plan drawings, has been examined by factor analysis in Sect. 10.4.

10.1.1 Sound Fields with a Single Reflection

Preferred Delay Time of a Single Reflection

First of all, the simplest sound field, which consists of the direct sound with the horizontal angle to a listener: $\xi_0 = 0°$ (the elevation angle $\eta_0 = 0°$), and a single reflection from a fixed direction $\xi_1 = 36°$ ($\eta_1 = 9°$), was investigated. These angles were selected since they are typical in a concert hall. The delay time Δt_1 of the reflection was adjusted in the range of 6–256 ms. The paired-comparison test was performed for all pairs in an anechoic chamber using normal hearing subjects with two different music motifs A and B (Table 10.1). The effective duration of the ACF of the sound source defined by τ_e may be obtained by the delay at which the envelope of the normalized autocorrelation function (ACF) becomes 0.1 (10-percentile delay) as shown in Fig. 10.1. The value of $(\tau_e)_{min}$ indicated in Table 10.1 is obtained from the minimum value of the running ACF, $2T$=2 s, with an interval of 100 ms. The recommended $2T$ is given by (10.14). As far as these source signals are concerned, values of (τ_e) extracted from the long-term ACF

Amazon
EX1010 Page 367

Table 10.1 Music and speech source signals and their minimum effective duration of the running ACF, $(\tau_e)_{min}$

Sound source	Title	Composer or writer	$(\tau_e)_{min}$ (ms)
Music motif A	Royal Pavane	Orlando Gibbons	125
Music motif B	Sinfonietta, opus 48; IV movement	Malcolm Arnold	40
Speech S	Poem read by a female	Doppo Kunikida	10

[1] The value of $(\tau_e)_{min}$ is the minimum value extracted from the running ACF, $2T = 2$ s, with a running interval of 100 ms. The recommended value of $2T$ is given by (10.14)

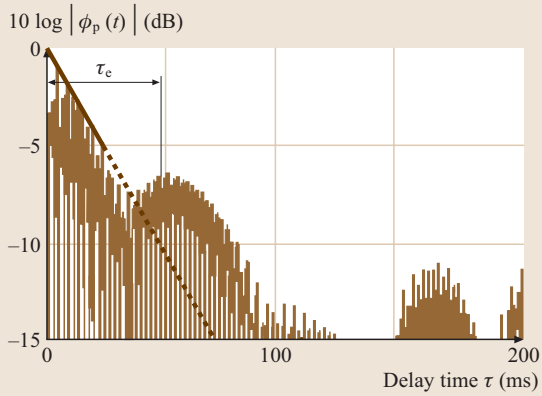


Fig. 10.1 Determination of the effective duration of the running ACF, τ_e. The value of τ_e may be obtained by the delay for which the envelope of the normalized ACF becomes 0.1 or −10 dB (10-percentile delay)

were similar to the minimum values from the running ACF, $(\tau_e)_{min}$.

For simplicity, the score was simply obtained, in this section, by accumulating a score giving +1 and −1 corresponding to positive and negative judgments, respectively, and the total score is divided by $S(F-1)$ to get the normalized score, where S is the number of subjects and F is the number of sound fields tested. The normalized scores for two motifs and the percentage of preference for speech signal as a function of the delay time are shown in Fig. 10.2.

Obviously, the most preferred delay time with the maximum score differs greatly between the two motifs. When the amplitude of reflection $A_1 = 1$, the most preferred delays are around 130 ms for music motif A, 35 ms for music motif B (Fig. 10.2a), and 16 ms for

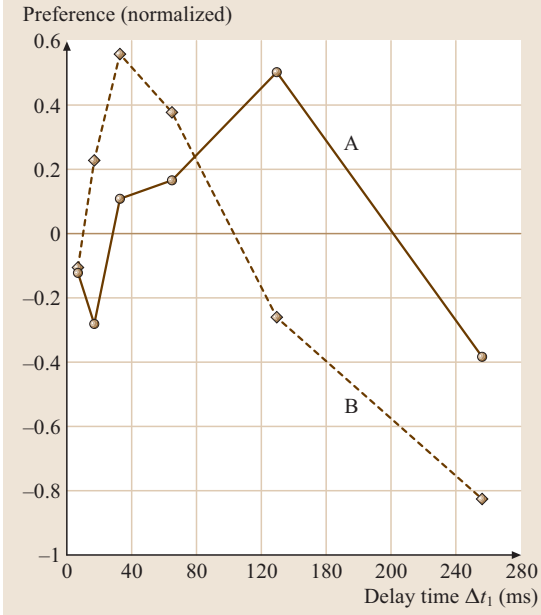


Fig. 10.2 Preference scores of the sound fields as a function of the delay time $A_1 = 1.0$ (six sound fields and 13 subjects [10.11]). Preference scores are directly obtained for each pair of sound fields by assigning the values +1 and −1, corresponding to positive and negative judgments, respectively. The normalized score is obtained by accumulating the scores for all sound fields (F) tested and all subjects (S), and then dividing by the factor $S(F-1)$ for 13 subjects. A: music motif A, Royal Pavane by Gibbons, $(\tau_e)_{min} = 125$ ms; B: music motif B, Sinfonietta, opus 48, III movement by Malcolm Arnold, $(\tau_e)_{min} = 40$ ms

speech [10.36]. Later, it was found that this corresponds well to the minimum values of the effective durations of the running ACF [10.39] of the source signals, so that the most preferred delay time were 125 ms (motif A), 40 ms (motif B) and 10 ms (speech). After inspection, the preferred delay is found roughly at certain durations of the ACF, defined by τ_p, such that the envelope of the ACF becomes $0.1A_1$. Thus, $[\Delta t_1]_p \approx \tau_e$ only when $A_1 = 1$. As shown in Fig. 10.3, changing the amplitude A_1, collected data of $[\Delta t_1]_p$ are expressed approximately by

$$[\Delta t_1]_p = \tau_p \approx (1 - \log_{10} A_1)(\tau_e)_{min} \,. \qquad (10.2)$$

Note that the amplitude of reflection relative to that of the direct sound should be measured by the most accurate method (ex. the square-root value of the ACF at the origin of the delay time).

Amazon
EX1010 Page 368

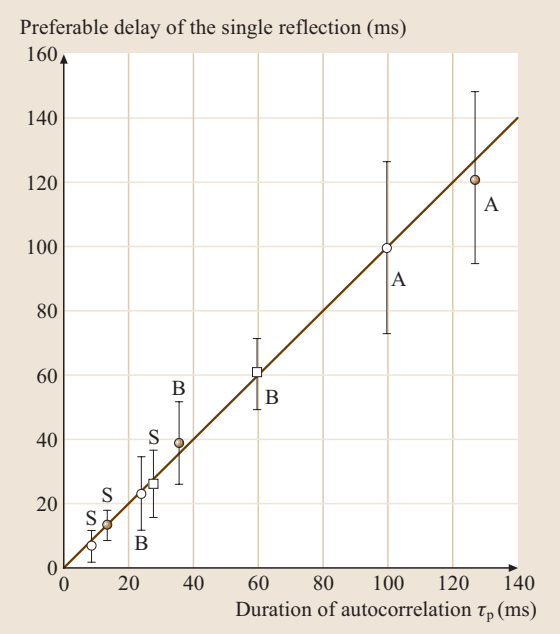


Fig. 10.3 The relationship between the preferred delay time of the single reflection and the duration of the ACF such that its envelope becomes 0.1 A_1 (for $k = 0.1$ and $c = 1.0$). The ranges of the preferred delays are graphically obtained at 0.1 below the maximum score. A, B and S refer to motif A, motif B, and speech, respectively. Different symbols indicate the center values obtained at the reflection amplitudes of +6 dB (○), 0 dB (●), and −6 dB (□), respectively (13–19 subjects). (After [10.11])

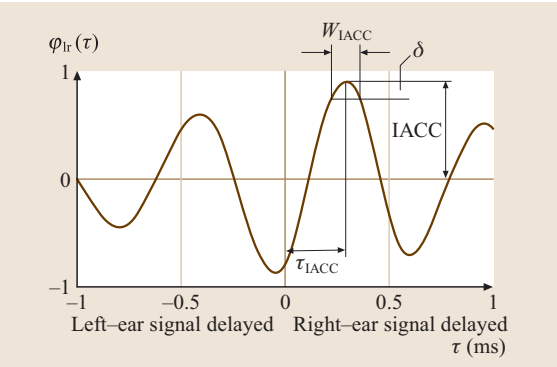


Fig. 10.4 Definition of the three spatial factors IACC, τ_{IACC} and W_{IACC}, extracted from the interaural cross-correlation function (IACF)

Two reasons can be given for why the preference decreases for the short delay range of reflection, $0 < \Delta t_1 < [\Delta t_1]_p$:

1. Tone coloration effects occur because of the interference phenomenon in the coherent time region; and
2. The IACC increases when Δt_1 is near 0. The definition of the IACC, which may be extracted from the IACF, as given by [10.1], is shown in Fig. 10.4.

On the other hand, echo disturbance effects can be observed when Δt_1 is greater than $[\Delta t_1]_p$.

Preferred Horizontal Direction of a Single Reflection to a Listener

The direction was specified by loudspeakers located at $\xi_1 = 0°$ ($\eta_1 = 27°$), and $\xi_1 = 18°, 36°, \ldots, 90°$ ($\eta_1 = 9°$), where the delay time of the reflection was fixed at 32 ms [10.11]. Results of the preference tests for the two motifs are shown in Fig. 10.5. No fundamental differences are observed between the curves of the sound source in spite of the large differences in the value of $(\tau_e)_{min}$. The preferred score increases roughly with decreasing IACC, the typical spatial factor. The correla-

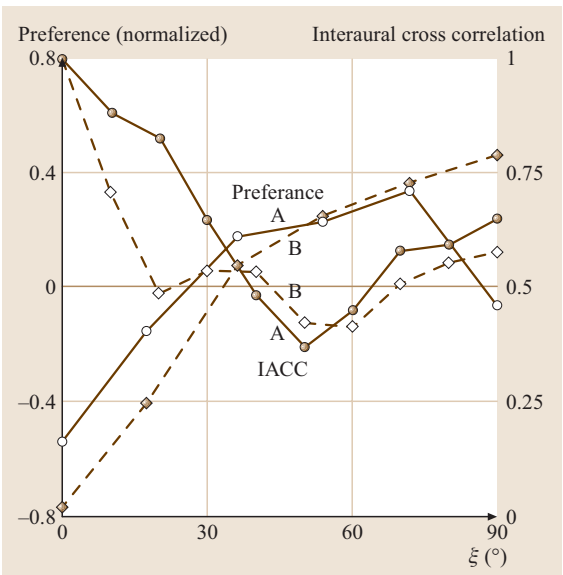


Fig. 10.5 Preference scores and the IACC of the sound fields with extreme music motifs A and B, as a function of the horizontal angle of a single reflection, A_1 = 0 dB (six sound fields and 13 subjects)

Amazon
EX1010 Page 369

tion coefficient between the score and the IACC is -0.8 ($p < 0.01$). The score with motif A at $\xi_1 = 90°$ drops to a negative value, indicating that the lateral reflections coming only from around $\xi_1 = 90°$, thus, are not always preferred. The figure shows that there is a preference for angles less than $\xi_1 = 90°$, and on average there may be an optimum range centered on about $\xi_1 = 55°$. Similar results can be seen in the data from speech signals [10.40]. These results are due to the spatial factor independent of the temporal factor, which consists of the source signal.

10.1.2 Optimal Conditions Maximizing Subjective Preference

According to a systematic investigation of simulating the sound field with multiple reflections and reverberation by the aid of a computer and the listening test, the optimum design objectives and the linear scale value of subjective preference may be derived. The optimum design objectives can be described in terms of the subjectively preferred sound qualities, which are related to the four orthogonal factors describing the sound signals arriving at the two ears. They clearly lead to comprehensive criteria for achieving the optimal design of concert halls as summarized below [10.11–13].

Listening Level (LL)

The listening level is, of course, the primary criterion for listening to sound in a concert hall. The preferred listening level depends upon the music and the particular passage being performed. The preferred levels obtained with 16 subjects were similar for two extreme music motifs: 77–79 dBA in peak ranges for music motif A (Royal Pavane by Gibbons) with a slow tempo, and 79–80 dBA for music motif B (Sinfonietta by Arnold) with a fast tempo Fig. 10.7a.

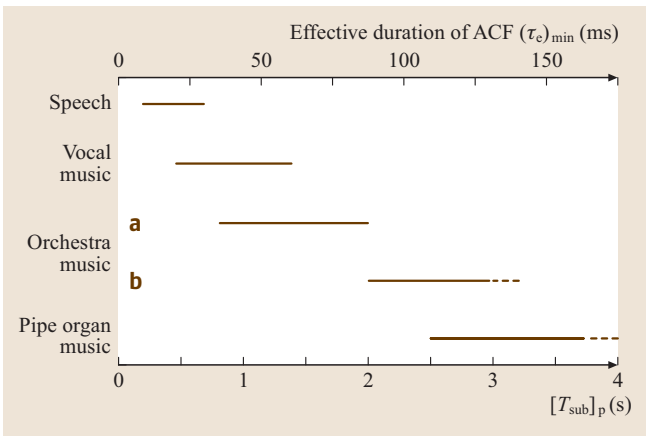


Fig. 10.6 Recommended reverberation time for several sound programs

Early Reflection after the Direct Sound (Δt_1)

An approximate relationship for the most preferred delay time has been discovered in terms of the ACF envelope of source signals and the total amplitude of reflections A. Generally, it is expressed by $[\Delta t_1]_p = \tau_p$

$$\left|\phi_p(\tau)\right|_{envelope} \approx kA^c, \text{ at } \tau = \tau_p\,, \tag{10.3}$$

where k and c are constants that depend on the subjective attributes [10.13, Fig. 42]. If the envelope of ACF is exponential, then

$$[\Delta t_1]_p = \tau_p \approx \left[\log_{10}(1/k) - c\log_{10} A\right](\tau_e)_{min}\,, \tag{10.4}$$

where the total pressure amplitude of reflection is given by

$$A = \left(A_1^2 + A_2^2 + A_3^2 + \ldots\right)^{1/2}\,. \tag{10.5}$$

The relationship given by (10.2) for a single reflection may be obtained by putting $A = A_1$, $k = 0.1$ and $c = 1$.

The value of $(\tau_e)_{min}$ is observed at the most active part of a piece of music containing artistic information such as a vibrato, a quick passage in the music flow, and/or a very sharp sound signal. Echo disturbance, therefore, may be perceived at $(\tau_e)_{min}$. Even for a long musical composition, the minimum part of $(\tau_e)_{min}$ of the running ACF in the whole music, which determines the preferred temporal condition, may be taken into consideration for the choice of music program to be performed in a given concert hall. A method of controlling the minimum value $(\tau_e)_{min}$ in performance, which determines the preferred temporal condition for vocal music has been discussed for blending the sound source and a given concert hall [10.41, 42]. If vibrato is introduced during singing, for example, it decreases $(\tau_e)_{min}$, blending the sound field with a short reverberation time.

Reverberation Time after the Early Reflection (T_{sub})

It has been observed that the most preferred frequency response to the reverberation time is a flat curve [10.39]. The preferred reverberation time, which is equivalent to that defined by *Sabine* [10.2], is expressed approxi-

Amazon
EX1010 Page 370

mately by

$$[T_{sub}]_p \approx 23(\tau_e)_{min} \,. \qquad (10.6)$$

The total amplitudes of reflections A tested were 1.1 and 4.1, which cover the usual conditions of sound fields in a room. Recommended reverberation times for several sound sources are shown in Fig. 10.6. A lecture and conference room must be designed for speech, and an opera house mainly for vocal music but also for orchestra music. For orchestral music, there may be two or three types of concert hall designs according to the effective duration of the ACF. For example, symphony no. 41 by Mozart, *Le Sacre du Printemps* by Stravinsky, and Arnold's Sinfonietta have short ACFs and fit orchestra music of type (A). On the other hand, symphony no. 4 by Brahms and symphony no. 7 by Bruckner are typical of orchestra music (B). Much longer ACFs are typical for pipe-organ music, for example, by Bach.

The most preferred reverberation times for each sound source given by (10.6) might play important roles for the selection of music motifs to be performed. Of interest is that the most preferred reverberation time expressed by (10.6) implies about four times the *reverberation time* containing the source signal itself.

Magnitude of the Interaural Cross-Correlation Function (IACC)

All individual data indicated a negative correlation between the magnitude of the IACC and subjective preference, i. e., dissimilarity of signals arriving at the two ears is preferred. This holds only under the condition that the maximum value of the IACF is maintained at the origin of the time delay, keeping a balance of the sound field at the two ears. If not, then an image shift of the source may occur (Sect. 10.4.2). To obtain a small magnitude of the IACC in the most effective manner, the directions from which the early reflections arrive at the listener should be kept within a certain range of angles from the median plane centered on ±55°. It is obvious that the sound arriving from the median plane ±0° makes the IACC greater. Sound arriving from ±90° in the horizontal plane is not always advantageous, because the similar detour paths around the head to both ears cannot decrease the IACC effectively, particularly for frequency ranges higher than 500 Hz. For example, the most effective angles for the frequency ranges of 1 kHz and 2 kHz are centered on ±55° and ±36°, respectively. To realize this condition simultaneously, a geometrical uneven surface has been proposed [10.43].

10.1.3 Theory of Subjective Preference for the Sound Field

Theory

Since the number of orthogonal acoustic factors of the sound field, which are included in the sound signals

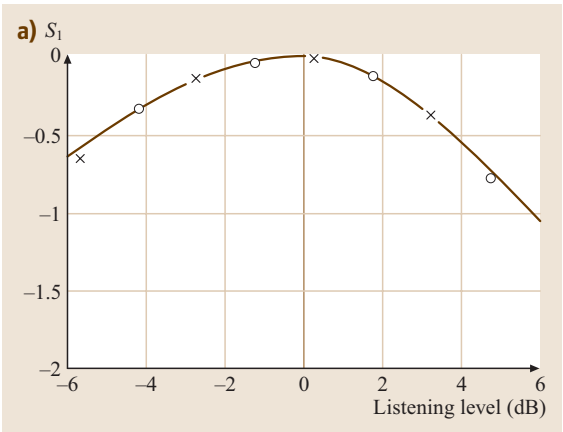


Fig. 10.7a–d Scale values of subjective preference obtained by the paired-comparison test for simulated sound fields in an anechoic chamber. Different symbols indicate scale values obtained from different source signals [10.12]. Even if different signals are used, a consistency of scale values as a function of each factor is observed, fitting a single curve. **(a)** As a function of the listening level, LL. The most preferred listening level, $[LL]_p = 0$ dB;

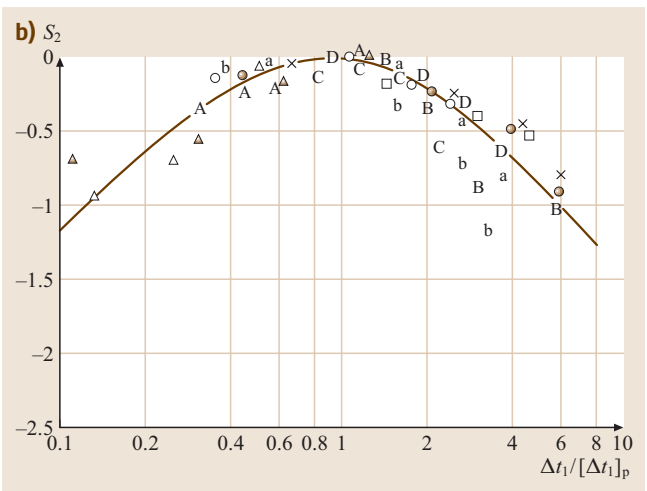


Fig. 10.7 (b) As a function of the normalized initial delay time of the first reflection by the most preferred delay time calculated by (10.4), $\Delta t_1/[\Delta t_1]_p$;

Amazon
EX1010 Page 371

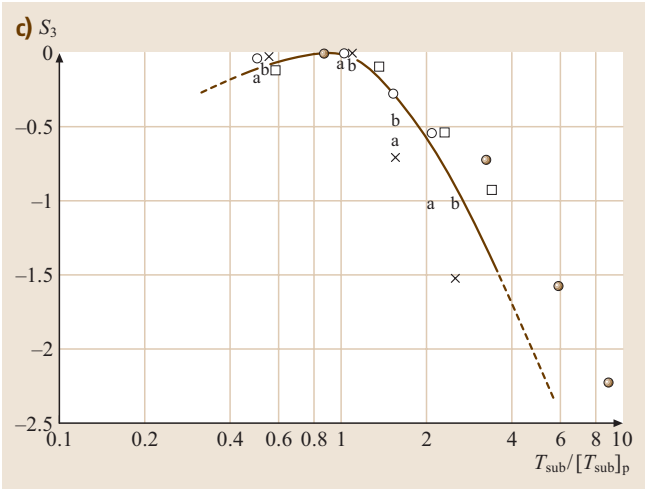


Fig. 10.7 (c) As a function of the normalized reverberation time for the most preferred calculated by (10.6), $T_{sub}/[T_{sub}]_p$;

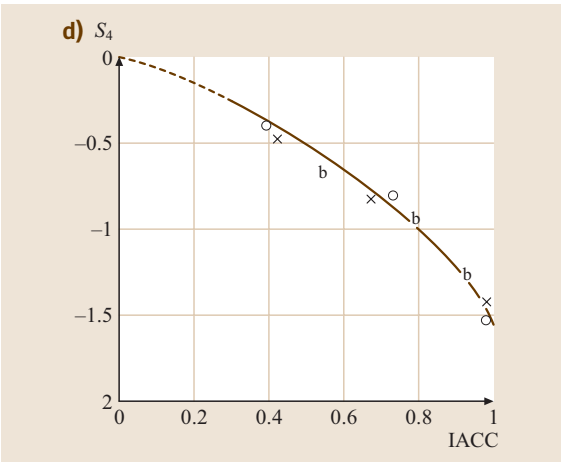


Fig. 10.7 (d) As a function of the IACC (After [10.12])

at both ears, is limited [10.12]; the scale value of any one-dimensional subjective response may be expressed by:

$$S = g(x_1, x_2, \ldots x_i) \,. \tag{10.7}$$

It has been verified by a series of experiments that four objective factors act independently on the scale value when changing two of the four factors simultaneously [10.13]. Results indicate that the units of the scale value of subjective preference derived by a series of experiments with different sound sources and different subjects have appeared to be constant [10.12], so that we may add scale values to obtain the total scale value such as

$$\begin{aligned} S &= g(x_1) + g(x_2) + g(x_3) + g(x_4) \\ &= S_1 + S_2 + S_3 + S_4 \,, \end{aligned} \tag{10.8}$$

where S_i $(i = 1, 2, 3, 4)$ is the scale value obtained relative to each objective parameter. Equation (10.8) indicates a four-dimensional continuity.

A Common Formula for the Four Normalized Orthogonal Factors

The dependence of the scale value on each objective parameter is shown graphically in Fig. 10.7. From the nature of the scale value, it is convenient to put a zero value at the most preferred conditions, as shown in this figure. These results of the scale value of subjective preference obtained from the different test series, using different music programs, yield the following common formula

$$S_i \approx -\alpha_i \, |x_i|^{3/2} \,, \quad i = 1, 2, 3, 4 \tag{10.9}$$

where values of α_i are weighting coefficients as listed in Table 10.2, which were obtained with a number of subjects. These coefficients depend on the individual. If α_i is close to zero, then a lesser contribution of the factor x_i on subjective preference is signified.

The factor x_1 is given by the sound pressure level (SPL) difference, measured by the A-weighted network, so that

$$x_1 = 20 \log P - 20 \log [P]_p \,, \tag{10.10}$$

P and $[P]_p$ being, respectively, the sound pressure at a specific seat and the most preferred sound pressure that may be assumed at a particular seat position in the

Table 10.2 Four orthogonal factors of the sound field and their weighting coefficients α_i obtained by a paired-comparison test of subjective preference with a number of subjects in conditions without any image shift of the source sound ($\tau_{IACC} = 0$)

i	x_i	α_i	
		$x_i > 0$	$x_i < 0$
1	$20 \log P - 20 \log [P]_p$ (dB)	0.07	0.04
2	$\log(\Delta t_1/[\Delta t_1]_p)$	1.42	1.11
3	$\log(T_{sub}/[T_{sub}]_p)$	$0.45 + 0.75A$	$2.36–0.42\,A$
4	IACC	1.45	–

Amazon
EX1010 Page 372

room under investigation:

$$x_2 = \log\left(\Delta t_1/[\Delta t_1]_p\right), \quad (10.11)$$

$$x_3 = \log\left(T_{sub}/[T_{sub}]_p\right), \quad (10.12)$$

$$x_4 = \text{IACC}. \quad (10.13)$$

Scale values of preference have been formulated approximately in terms of the 3/2 powers of the normalized objective parameters, expressed in the logarithm for the parameters, x_1, x_2 and x_3. Thus, scale values are not greatly changed in the neighborhood of the most preferred conditions, but decrease rapidly outside of this range. The remarkable fact is that the spatial binaural parameter x_4 is expressed in terms of the 3/2 powers of its real values, indicating a greater contribution than those of the temporal parameters.

Limitation of Theory

Since experiments were conducted to find the optimal conditions, this theory holds in the range of preferred conditions obtained by the test. In order to demonstrate the independence of the four orthogonal factors, under the conditions of fixed Δt_1 and T_{sub} around the preferred conditions, scale values of subjective preference calculated by (10.8) for the LL with (10.10) and the IACC with (10.13) with constants listed in Table 10.2 are shown in Fig. 10.8. Agreement between the calculated and observed values are satisfactory [10.13]. Even though both LL and the IACC are spatial factors, which are associated with the right cerebral hemisphere (Table 10.3), these are quite independent of each other. The same is true for the temporal factors of Δt_1 and T_{sub} associated with the left hemisphere. Of course, the spatial factor and the temporal factor are highly independent.

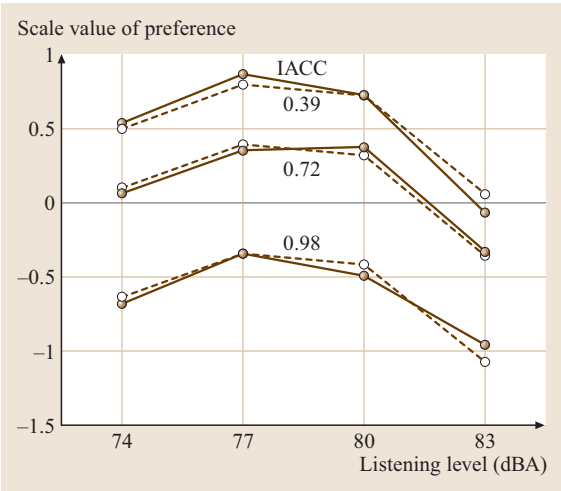


Fig. 10.8 Scale values of subjective preference for the sound field with music motif A as a function of the listening level and as a parameter of the IACC [10.13]. *Solid line*: calculated values based on (10.8) together with (10.9) taking the two factors (10.10) and (10.13) into consideration; *Dashed line*: measured values

Table 10.3 Hemispheric specializations determined by analyses of AEP (SVR), EEG and MEG[1]

Factors changed	AEP (SVR) $A(P_1 - N_1)$	EEG, ratio of ACF τ_e values of α-waves	MEG, ACF τ_e value of α-wave
Temporal			
Δt_1	L>R (speech)[2]	L>R (music)	L>R (speech)
T_{sub}	–	L>R (music)	–
Spatial			
LL	R>L (speech)	–	–
IACC	R>L (vowel /a/) R>L (band noise)	R>L (music)[3]	–

[1] See also [10.44] for a review of these investigations
[2] The sound source used in experiments is indicated in the bracket
[3] Flow of α-wave (EEG) from the right hemisphere to the left hemisphere for music stimuli when changing the IACC was observed by $|\phi(\tau)|_{max}$ between α-waves recorded at different electrodes [10.45]

Example of Calculating the Sound Quality at Each Seat

As a typical example, we shall discuss the quality of the sound field at each seating position in a concert hall with a shape similar to that of Symphony Hall in Boston. Suppose that a single source is located at the center, 1.2 m above the stage floor. Receiving points at a height of 1.1 m above the floor level correspond to the ear positions. Reflections with their amplitudes, delay times, and directions of arrival at the listeners are taken into account using the image method. Contour lines of the total scale value of preference calculated for music motif B are shown in Fig. 10.9. Results shown in Fig. 10.9b demonstrate the effects of the reflection from the sidewalls adjusted to the stage, which produce decreasing values of the IACC for the audience area. Thus the preference value at each seat is increased compared with that

Amazon
EX1010 Page 373

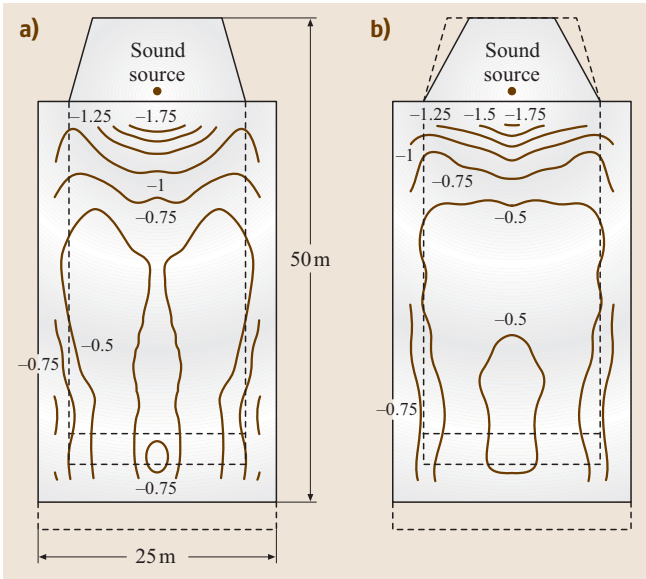


Fig. 10.9a,b An example of calculating the scale value with the four orthogonal factors using (10.8) through (10.13) with weighting coefficients (Table 10.2). **(a)** Contour lines of the total scale value for the Boston Symphony Hall, with original side reflectors on the stage. **(b)** Contour lines of the total scale values for the side reflectors optimized on the stage

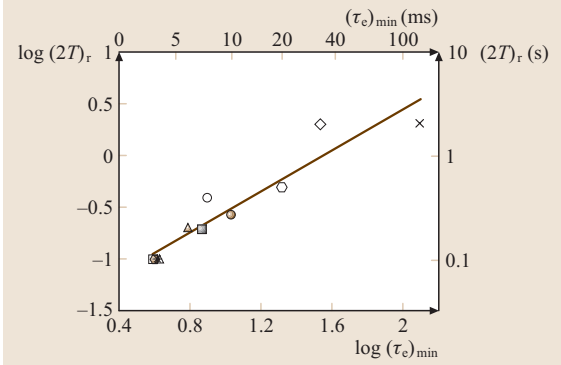


Fig. 10.10 Recommended temporal window $(2T)_r$ for the ACF proceeding as a function of the minimum value of effective duration of the ACF $(\tau_e)_{min}$. Different symbols represent experimental results using different sound sources

in Fig. 10.9a. In this calculation, the reverberation time is assumed to be 1.8 s throughout the hall and the most preferred listening level, $[LL]_p = 20\log[P]_p$ in (10.10), is set for a point on the center line 20 m from the source position.

10.1.4 Auditory Temporal Window for ACF and IACF Processing

Auditory Temporal Window for ACF Processing

In analyzing the running ACF, the so-called *auditory–temporal window* $2T$ must be carefully determined. The initial part of the ACF within the effective duration of the ACF contains important information about the source signal. In order to determine the auditory–temporal window, successive loudness judgments in pursuit of the running SPL have been conducted. Results shown in Fig. 10.10 indicate that the recommended signal duration $(2T)_r$ to be analyzed is approximately expressed by [10.46]

$$(2T)_r \approx 30(\tau_e)_{min}\,, \tag{10.14}$$

where $(\tau_e)_{min}$ is the minimum effective duration, extracted from the running ACF [10.47]. This signifies an adaptive temporal window depending on the temporal characteristics of the sound signal in the auditory system. For example, the temporal window may differ according to music pieces $[(2T)_r = 0.5–5\,s]$ and to the vowels $[(2T)_r = 50–100\,ms]$ and consonants $[(2T)_r = 5–10\,ms]$ in continuous speech signals. It is worth noticing that the time constant represented by "fast" or "slow" of the sound level meter should be replaced by the temporal window, which depends on the effective duration of the ACF of the source signal. The running step (R_s), which signifies a degree of overlap of signal to be analyzed, is not critical. It may be selected as $K_2(2T)_r$; K_2 is chosen, say, in the range 0.25–0.5.

Auditory Temporal Window for IACF Processing

For the sound source fixed on the stage in a concert hall as usual, the value of $2T$ can be selected longer than 1.0 s for the measurement of the spatial factor at a fixed audience seat. But, when a sound signal is moving in the horizontal direction on the stage, we must know a suitable temporal window for $2T$ in analyzing the running IACF, which describes the moving image of sound localization. For a sound source moving sinusoidally in the horizontal plane with less than 0.2 Hz, $2T$ may be selected in a wide range from 30 to 1000 ms. If a sound source is moving below and/or at 4.0 Hz, $2T = 30–100$ ms is acceptable. In order to obtain a reliable result, it is recommended that such a temporal window for the IACF covering a wide range of movement velocity in the horizontal localization be fixed at about 30 ms.

Amazon
EX1010 Page 374

10.1.5 Specialization of Cerebral Hemispheres for Temporal and Spatial Factors of the Sound Field

The independent influence of the aforementioned temporal and spatial factors on subjective preference judgments has been achieved by the specialization of the human cerebral hemispheres [10.44]. Recording over the left and right hemispheres of the slow vertex response (SVR) with latency of less than 500 ms, electroencephalograms (EEG) and magnetoencephalograms (MEG) have revealed various pieces of evidence (Table 10.3), with the most significant results being:

1. The left and right amplitudes of the evoked SVR, $A(P_1 - N_1)$ indicate that the left and right hemispheric dominance are due to temporal factors (Δt_1) and spatial factors (LL and IACC), respectively [10.48, 49].
2. Both left and right latencies of N_2 of SVR correspond well to the IACC [10.49].
3. Results of EEGs for the cerebral hemispheric specialization of the temporal factors, i. e., Δt_1 and T_{sub} indicated left-hemisphere dominance [10.50, 51], while the IACC indicated right-hemisphere dominance [10.45]. Thus, a high degree of independence between temporal and spatial factors was indicated.
4. The scale value of subjective preference is well described in relation to the value of τ_e extracted from the ACF of α-wave signals over the left hemisphere and the right hemisphere according to changes in temporal and spatial factors of the sound field, respectively [10.45, 50, 51].
5. Amplitudes of MEGs recorded when Δt_1 was changed reconfirm the left-hemisphere specialization [10.52].
6. The scale values of individual subjective preference relate directly to the value of τ_e extracted from the ACF of the α-wave of the MEG [10.52]. It is worth noting that the amplitudes of the α-wave in both the EEG and the MEG do not correspond well to the scale value of subjective preference.

In addition to the aforementioned activities in the time domain, in both the left and right hemispheres, spatial activity waves were analyzed by the cross-correlation function of alpha waves from the EEGs and MEGs. The results showed that a larger area of the brain is activated when the preferred sound field is presented [10.53] than when a less preferred one. This implies that the brain repeats a similar temporal rhythm in the α-wave range over a wider area of the scalp under the preferred conditions.

It has been reported that the left hemisphere is mainly associated with speech and time-sequential identifications, and the right is concerned with nonverbal and spatial identification [10.54, 55]. However, when the IACC was changed using speech and music signals, right-hemisphere dominance was observed, as indicated in Table 10.3. Therefore, hemispheric dominance is a relative response depending on which factor is changed in the comparison pair, and no absolute behavior could be observed.

To date, it has been discovered that the LL and the IACC are dominantly associated with the right cerebral hemisphere, and the temporal factors, Δt_1 and T_{sub} are associated with the left. This implies that such specialization of the human cerebral hemisphere may relate to the highly independent influence of spatial and temporal criteria on any subjective attribute. It is remarkable, for example, that *cocktail party effects* might well be explained by such specialization of the human brain, because speech is processed in the left hemisphere, and spatial information is processed in the right hemisphere independently.

10.2 Design Studies

Using the scale values in the four orthogonal factors of the sound field obtained by a number of listeners, the *principle of superposition* expressed by (10.8) together with (10.9) through (10.13) can be applied to calculate the scale value of preference for each seat. Comparison of the total preference values for different configurations of concert halls allows a designer to choose the best scheme. Temporal factors relating to its dimensions and the absorbing material on its walls are carefully determined according to the purpose of the hall in terms of a range of specific music programs (Fig. 10.6). In this section, we discuss mainly the spatial form of the hall, the magnitude of the interaural correlation function and the binaural listening level.

Amazon
EX1010 Page 375

10.2.1 Study of a Space-Form Design by Genetic Algorithms (GA)

A large number of concert halls have been built since the time of the ancient Greeks, but only the halls with good sound quality are well liked. In order to increase the measure of success, a genetic algorithm (GA) system [10.56], a form of evolutionary computing, can be applied to the acoustic design of concert halls [10.57,58]. The GA system is applied here to generate the alternative scheme on the left-hand side of Fig. 10.11 for listeners.

Procedure

In this calculation, linear scale values of subjective preference S_1 and S_4 given by (10.9) are employed as fitting functions due to the LL and IACC, because the geometrical shape of a hall is directly affected by these spatial factors. The spatial factor for a source on the stage was calculated at a number of seating positions. For the sake of convenience, the single omnidirectional source was assumed to be at the center of the stage, 1.5 m above the stage floor. The receiving points that correspond to the ear positions were 1.1 m above the floor of the hall. The image method was used to determine the amplitudes, delay times, and directions of arrival of reflections at these receiving points. Reflections were calculated up to the second order. In fact, there was no change in the relative relationship among the factors obtained from calculations performed up to the second, third, and fourth order of reflection. The averaged values of the IACC for five music motifs (motifs A through E [10.13]) were used for the calculation.

Those hall shapes that produced greater scale values are selected as parent chromosomes. An example of the encoding of the chromosome is given in Fig. 10.12. The first bit indicated the direction of motion for the vertex.

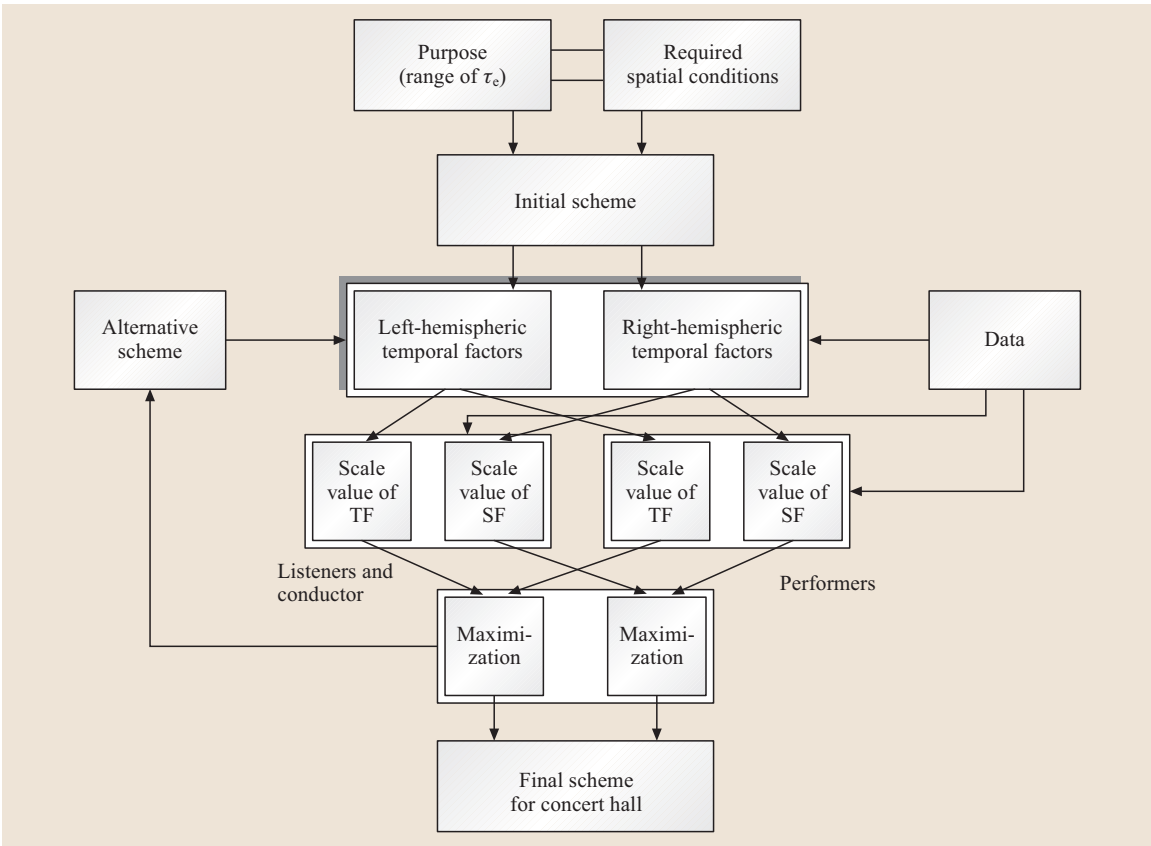


Fig. 10.11 The procedure for designing the sound field in a concert hall maximizing the scale values of subjective preference for a number of listeners (including a conductor) and performers. Data for global values of subjective preference may be utilized when designing a public hall

Amazon
EX1010 Page 376

The other $(n-1)$ bits indicated the range over which the vertex moved. To create a new generation, the room shapes are modified and the corresponding movement of the vertices of the walls is encoded in chromosomes, i. e., binary strings. After GA operations that include crossover and mutation, new offspring are created. The fitness of the offspring is then evaluated in terms of the scale value of subjective preference. This process is repeated until the end condition of about 2000 generations is satisfied.

Shoe-Box Optimized

First of all, the proportions of the shoe-box hall were optimized (model 1). The initial geometry is shown in Fig. 10.13. In this form, the hall was 20 m wide, the stage was 12 m deep, the room was 30 m long, and the ceiling was 15 m above the floor. The point source was located at the center of the stage and 4.0 m from the front of the stage; 72 listening positions were selected. The range of motion for each sidewall and the ceiling was ±5 m from the respective initial positions, and the distance through which each was moved was coded on the chromosome of the GA. Scale values at the listening positions other than those within 1 m of the sidewalls were included in the averages ($\overline{S_1}$ and $\overline{S_4}$). These values were employed as the measure of fitness. In this calculation, the most preferred listening level $[LL]_p$ was chosen at the frontal seat near the stage. Results of optimization of the hall for $\overline{S_1}$ and $\overline{S_4}$ are shown in Fig. 10.14a and Fig. 10.14b, respectively. The width and length were almost the same in the two results, but the indicated heights were quite different. The height of the ceiling that maximizes $\overline{S_1}$ was as low as possible within the allowed range of motion to obtain a constant LL (Fig. 10.14a). The height that maximizes $\overline{S_4}$, on the other hand, was at the upper limit of the allowed range of motion to obtain small values of the IACC (Fig. 10.14b). Table 10.4 shows the comparison of the proportions obtained here and those of the Grosser Musikvereinssaal, which is a typical example of an excellent concert hall. The length/width ratios are almost the same. The height/width ratio of

Table 10.4 Comparison of proportions for the optimized spatial form of *shoe-box* type and the *Grosser Musikvereinssaal*

	Length/width	Height/width
Optimized for $\overline{S_1}$ for the listening level	2.50	0.71
Optimized for $\overline{S_4}$ for the IACC	2.57	1.43
Grosser Musikvereinssaal	2.55	0.93

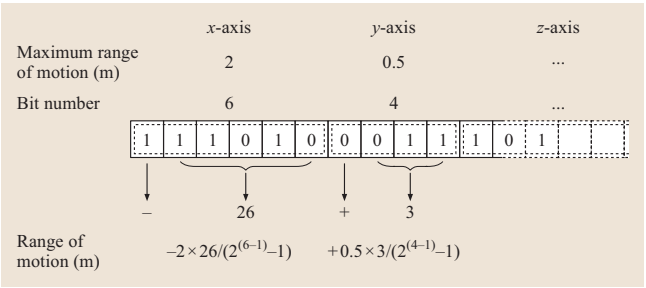


Fig. 10.12 An example of the binary strings used in encoding of the chromosome to represent modifications to the room shape

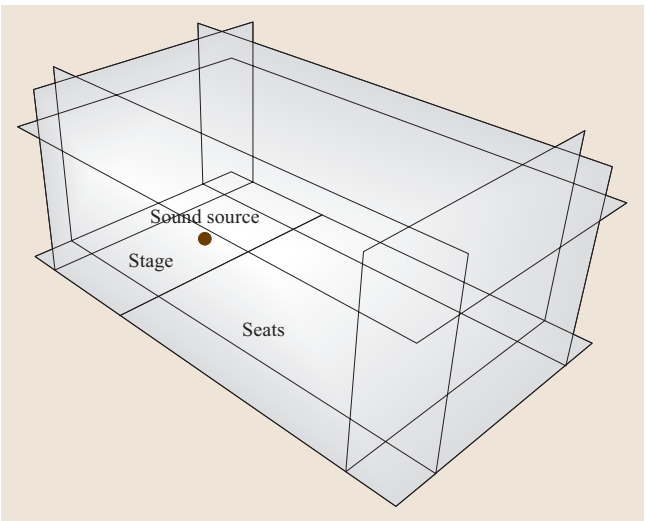


Fig. 10.13 The initial scheme of a concert hall (model 1). The range of sidewall and ceiling variation was ±5 m from the initial scheme

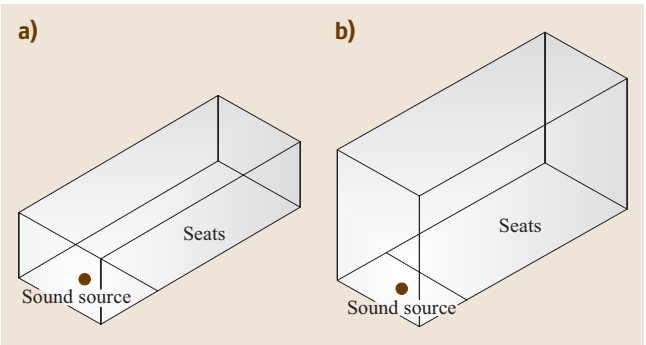


Fig. 10.14a,b Results for the model 1. **(a)** Geometry optimized for $\overline{S_1}$. **(b)** Geometry optimized for $\overline{S_4}$. (After [10.57])

Amazon
EX1010 Page 377

the Grosser Musikvereinsaal is intermediate between our results for the two factors. For the ceiling of the hall, the height that maximized $\overline{S_1}$ was the lowest within the allowed range of motion (Fig. 10.14a). This is due to the fact that more energy can be provided from the ceiling to the listening position throughout the seats. To maximize $\overline{S_4}$, on the other hand, the ceiling took on the maximum height in the possible range of motion (Fig. 10.14b). Reflections from the flat ceiling did not decrease the IACC, but those from the sidewalls did.

Modification from the *Shoe-Box*

Next, to obtain even better sound fields, a little more complicated form (model 2), as shown in Fig. 10.15, was examined. The floor plan optimized according to the above results was applied as a starting point. The hall in its initial form was 14 m wide, the stage was 9 m deep, the room was 27 m long, and the ceiling was 15 m above the stage floor. The sound source was again 4.0 m from the front of the stage, but was 0.5 m to one side of the centerline and 1.5 m above the stage floor. The front and rear walls were vertically bisected to obtain two faces, and each stretch of wall along the side of the seating area was divided into four faces. The walls were kept vertical (i. e., tilting was not allowed) to examine only the plan of the hall in terms of maximizing $\overline{S_1}$ and $\overline{S_4}$. Each wall was moved independently of the other walls. The openings between the walls, in the acoustical simulation using the image method, were assumed not to reflect the sound. Forty-nine listening positions distributing throughout the seating area on a 2 m×4 m grid were selected. In the GA operation, the sidewalls were moved, so that none of these 49 listening positions were excluded. The moving range of each vertex was ±2 m in the direction of the line normal to the surface. The coordinates of the two bottom vertices of each surface were encoded on the chromosomes for the GA. In this calculation, the most preferred listening level was set for a point on the hall's long axis (central line), 10 m from the source position.

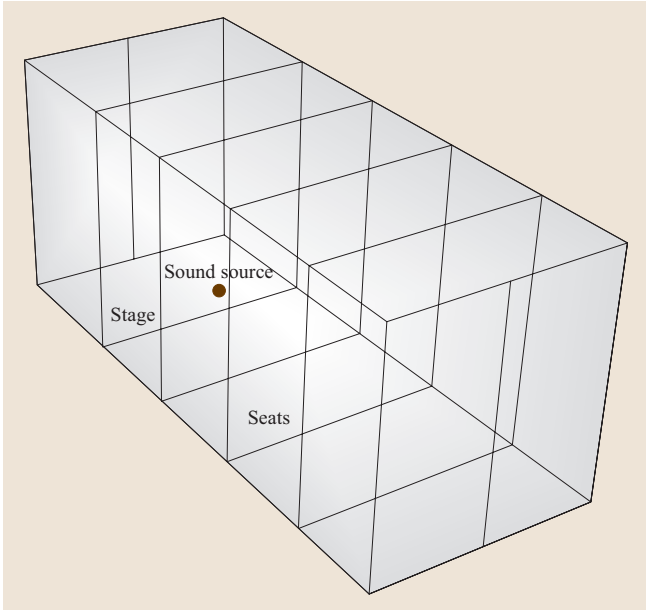


Fig. 10.15 Initial scheme of the concert hall (model 2). The rear wall of the stage and the rear wall of the audience area were divided into two. Sidewalls were divided into four

Leaf-Shape Concert Hall

The result of optimizing the hall for $\overline{S_1}$ is shown in Fig. 10.16 and the contour lines of equal $\overline{S_1}$ values are shown in Fig. 10.17. To maximize $\overline{S_1}$, the rear wall of the stage and the rear wall of the audience area took on concave shapes. The result of optimizing for $\overline{S_4}$ is shown in Fig. 10.18 and contour lines of equal $\overline{S_4}$ values are shown in Fig. 10.19. To maximize $\overline{S_4}$, on the other hand, the rear wall of the stage and the rear wall of the audience area took on convex shapes. With regard to the sidewalls, both $\overline{S_1}$ and $\overline{S_4}$ were maximized by the *leaf-shaped* plan, which is discussed in the following section.

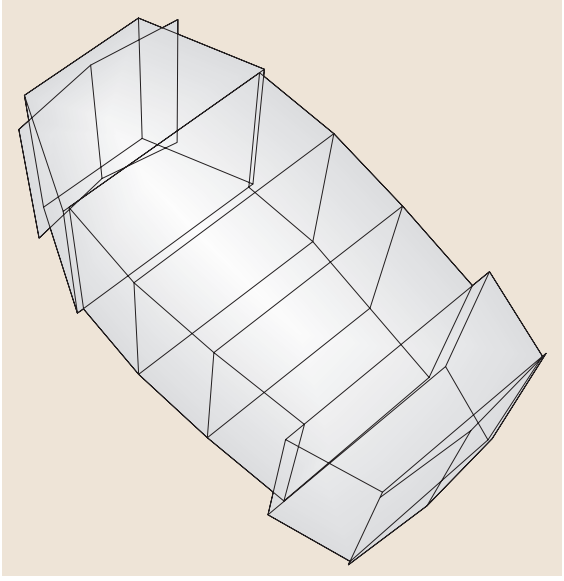


Fig. 10.16 A result for the model 2 optimized for $\overline{S_1}$

Amazon
EX1010 Page 378

As for the conflicting requirements for S_1 and S_4, the maximization of S_4 may take priority over that of S_1, because the preference increases with decreasing IACC without exception [10.1], while there is a large individual difference in the preferred LL [10.59]. It is worth noting that listeners themselves can usually choose the best seat with respect to the preferred LL in a real concert hall.

A conductor and/or music director must be aware of the sound field characteristics of a concert hall. One is then able to select a program of music so that the sound is best in that hall in terms of the temporal factors (Fig. 10.6).

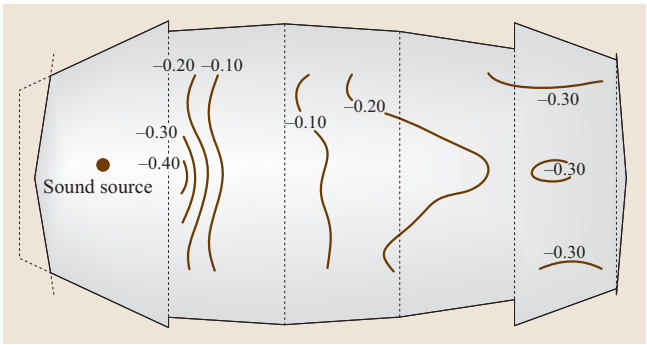


Fig. 10.17 Contour lines of equal $\overline{S_1}$ values calculated for the geometry shown in Fig. 10.16

10.2.2 Actual Design Studies

After testing more than 200 listeners, a small value of the IACC, which corresponds to different sound signals arriving at two ears, was demonstrated to be the preferred condition for individuals without exception. A practical application of this design theory was done in the Kirishima International Concert Hall (Miyama Conceru), which was characterized by a *leaf shape* (Fig. 10.20).

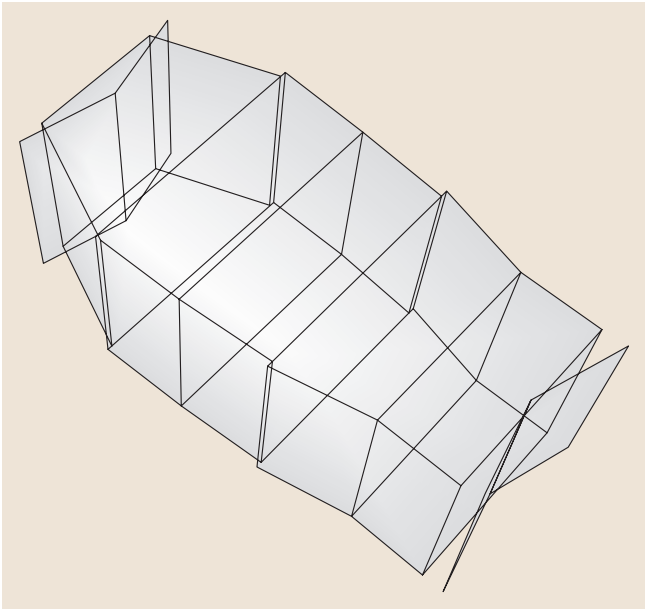


Fig. 10.18 A result for model 2 optimized for $\overline{S_4}$

Temporal Factors of the Sound Field for Listeners

When the space is designed for pipe-organ performance, the range of $(\tau_e)_{min}$, which may be selected to be centered on 200 ms, determines the typical temporal factor of the hall: $[T_{sub}]_p \approx 4.6$ s (10.6). When designed for the performance of chamber music, the range is selected to be near the value of 65 ms ($[T_{sub}]_p \approx 1.5$ s). The conductor and/or the sound coordinator select suitable musical motifs with a satisfactory range of effective duration of the ACF to achieve a music performance that blends the music and the sound field in a hall (Fig. 10.6). To adjust the preferred condition of Δt_1, on the other hand, since the value of $(\tau_e)_{min}$ for violins is usually shorter than that of contrabasses in the low-frequency range, the position of the violins is shifted closer to the left wall on the stage, and the position of the contrabasses is shifted closer to the center, as viewed from the audience.

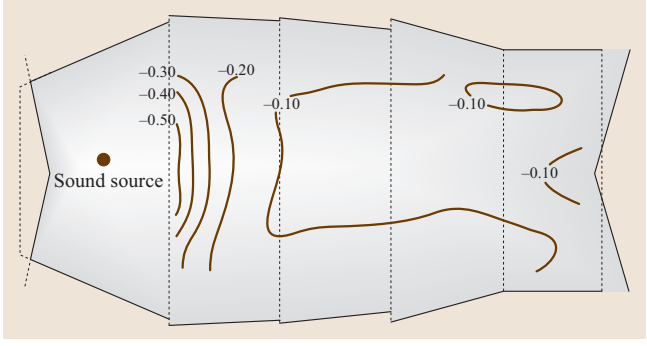


Fig. 10.19 Contour lines of equal $\overline{S_4}$ values calculated for the geometry shown in Fig. 10.18

Spatial Factors of the Sound Field for Listeners

The IACC should be kept as small as possible, maintaining $\tau_{IACC} = 0$. This is realized by suppressing the strong reflection from the ceiling, and by appropriate reflections from the sidewall at certain angles. When the source signal mainly contains frequency compo-

Amazon
EX1010 Page 379

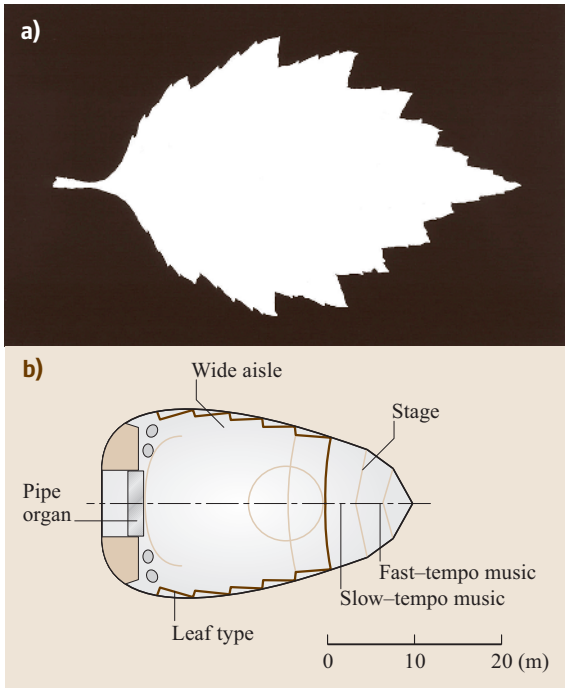


Fig. 10.20a,b A leaf shape for the plan proposed for the Kirishima International Concert Hall. **(a)** Original leaf shape. **(b)** Proposed shape for the plan. As usual, the sound field in *circled seating area* close to the stage must be carefully designed to obtain reflections from the walls on the stage and tilted sidewalls

nents around 1 kHz, the reflection from the side walls is adjusted to be centered roughly 55° to each listener, measured from the median plane. Under actual hearing conditions, the perceived IACC depends on whether or not the amplitudes of reflection exceed the hearing threshold level. This may be one of the reasons why a more diffuse sound field can be perceived with increasing power of the sound source. When the source is weak enough, that only the direct sound is heard, the actual IACC being processed in the auditory–brain system approaches unity, resulting in no diffuse sound impression. Thus, the IACC should be small enough with only strong early reflections.

Sound Field for Musicians

For music performers, the temporal factor is considered to be much more critical than the spatial factor (Sect. 10.3.2). Since musicians perform over a sequence of time, reflections with a suitable delay in terms of the value of $(\tau_e)_{min}$ of the source signals are of particular importance. Without any spatial subjective diffuseness, the preferred directions of reflections are in the median plane of music performers, resulting in IACC $\approx$ 1.0 [10.62, 63]. In order to satisfy these acoustic conditions, some design iterations are required, maximizing scale values for both musicians and listeners and leading to the final scheme of the concert hall as shown in Fig. 10.11.

Sound Field for the Conductor

It is recommended that the sound field for the conductor on the stage should be designed as that of a listener with appropriate reflections from the sidewalls on the stage [10.64].

Acoustic Design with Architects

From the historical viewpoint, architects have been more concerned with spatial criteria from the visual standpoint, and less so from the point of view of temporal criteria for blending human experience and the environment with design. On the other hand, acousticians

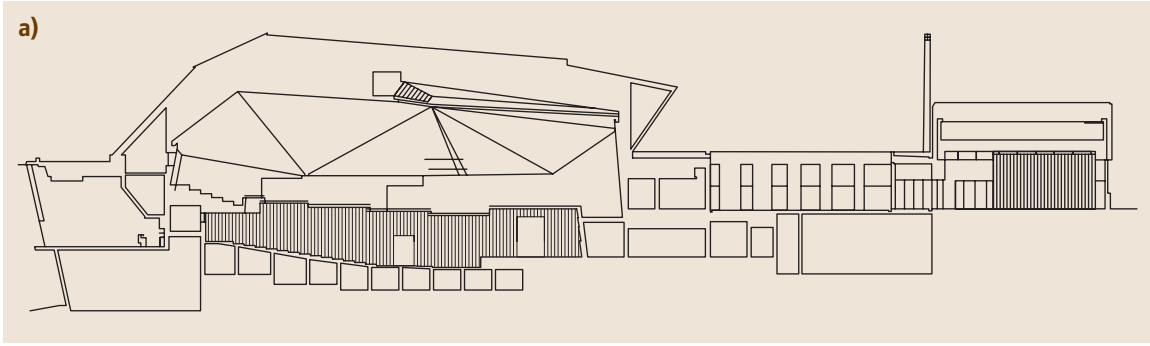


Fig. 10.21a–f Scheme of the Kirishima International Concert Hall, Kagoshima, Japan designed by the architect Maki and associates (1997) [10.60, 61].**(a)** Longitudinal section;

Amazon
EX1010 Page 380

have mainly been concerned with temporal criteria, represented primarily by the reverberation time, from the time of *Sabine* [10.2] onward. No comprehensive theory of design including the spatial criterion as represented by the IACC existed before 1977, so that discussions between acousticians and architects were rarely on the same subject. As a matter of fact, both temporal and spatial factors are deeply interrelated with both acoustic design and architectural design [10.65, 66].

As an initial design sketch of the Kirishima International Concert Hall, a plan shape like a leaf (Fig. 10.20a) was presented at the first meeting for discussion with the architect Fumihiko Maki and associates with the explanation of the temporal and spatial factors of sound field.

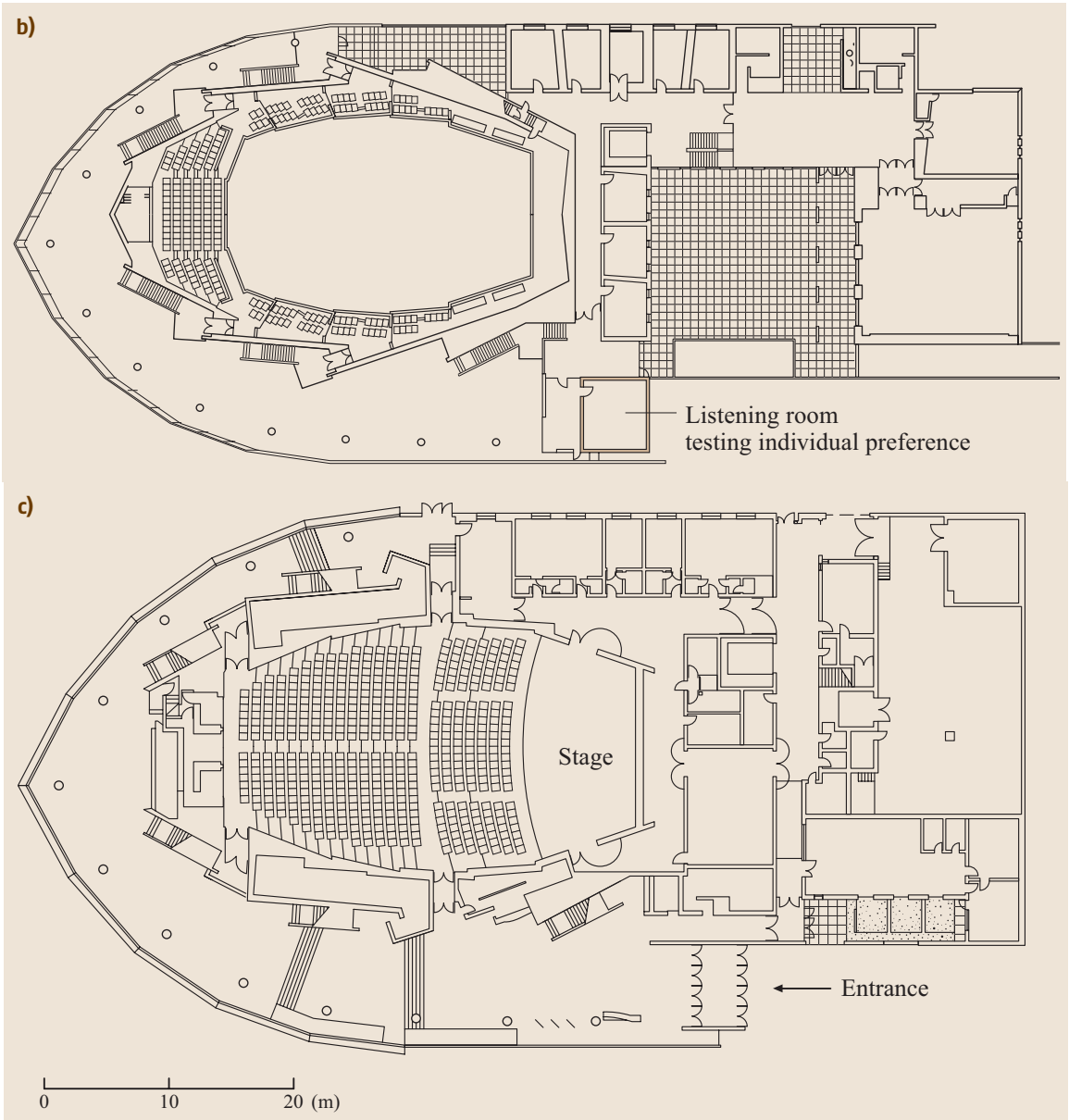


Fig. 10.21 (b) Plan of balcony level; (c) Plan of audience level

Amazon
EX1010 Page 381

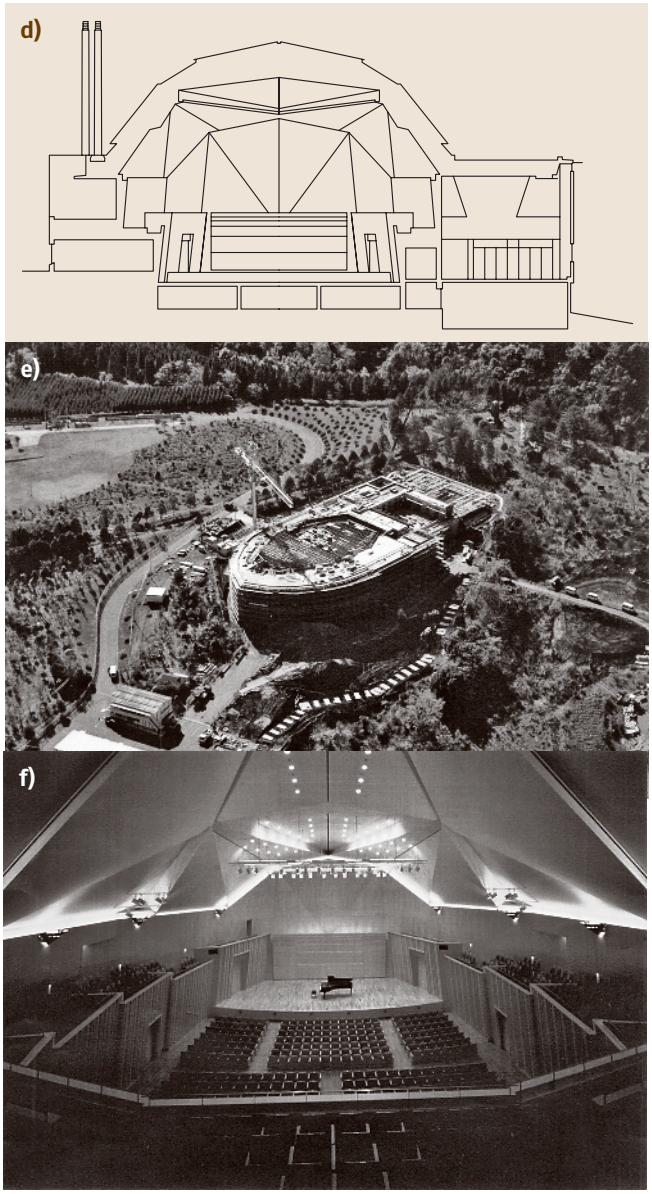


Fig. 10.21 (**d**) Cross section; (**e**) The Kirishima International Concert Hall, Kagoshima under construction. The leaf shape can be seen; (**f**) Tilt sidewalls and triangular ceilings after construction of the hall

After some weeks, Maki and Ikeda indicated a scheme of the concert hall as shown in Fig. 10.21 [10.60,61]. Without any change of plan and cross sections, the calculated results indicated the excellent sound field as shown in Fig. 10.22 [10.67,68].

The final architectural schemes, together with the special listening room for testing individual preference of sound field and selecting the appropriate seats for maximizing individual preference of the sound field, are shown in Fig. 10.21b. In these figures, the concert courtyard, the small concert hall, several rehearsal rooms and dressing rooms are also shown. The concert hall under construction is shown in Fig. 10.21e, in which the leaf shape may be seen; it was opened in 1994 (Fig. 10.21f).

Details of Acoustic Design

For listeners on the main floor. In order to obtain a small value of the IACC for most of the listeners, ceilings were designed using a number of triangular plates with adjusted angles, and the side walls were given a 10% tilt with respect to the main audience floor, as are shown in Fig. 10.21d and Fig. 10.23. In addition, diffusing elements were designed on the sidewalls to avoid the image shift of sound sources on the stage caused by the strong reflection in the high-frequency range above 2 kHz. These diffusers on the sidewalls were designed as a modification of the Schroeder diffuser [10.69] without the wells, as shown by the detail of Fig. 10.24.

For music performers on stage. In order to provide reflections from places near the median plane of each of the performers on the stage, the back wall on the stage is carefully designed as shown in the lower left in Fig. 10.23. The tilted back wall consists of six sub-walls with angles adjusted to provide appropriate reflections within the median plane of the performer. It is worth noting that the tilted sidewalls on the stage provide good reflections to the audience sitting close to the stage, at the same time resulting in a decrease of the IACC. Also, the sidewall on the stage of the left-hand side looking from the audience may provide useful reflections arriving from the back for a piano soloist.

Stage floor structure. For the purpose of suppressing the vibration [10.70] of the stage floor and anomalous sound radiation from the stage floor during a performance, the joists form triangles without any neighboring parallel structure, as shown in Fig. 10.25. The thickness of the floor is designed to be relatively thin (27 mm) in order to radiate sound effectively from the vibration of instruments such as the cello and contrabass. During rehearsal, music performers may control the radiation power somewhat by adjusting their position or by the use of a rubber pad between the floor and the instrument.

Amazon
EX1010 Page 382

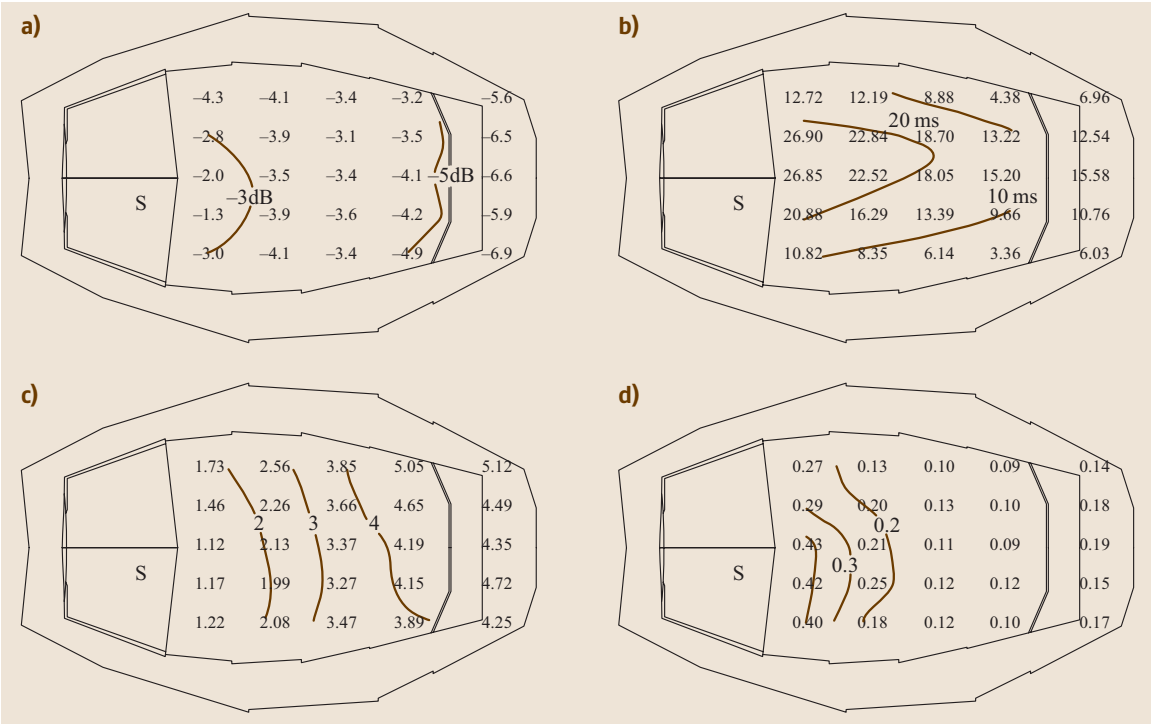


Fig. 10.22a–d Calculated orthogonal factors at each seat with a performing position *S* for an initial design of the hall. In the final design of the hall, the width was enlarged by about 1 m to increase the number of seats. The designed reverberation time was about 1.7 s for the 500 Hz band. **(a)** Relative listening level; **(b)** initial time delay gap between the direct sound and the first reflection Δt_1 [ms]; **(c)** *A*-value, the total amplitude of reflections; **(d)** IACC for white noise

Amazon
EX1010 Page 383

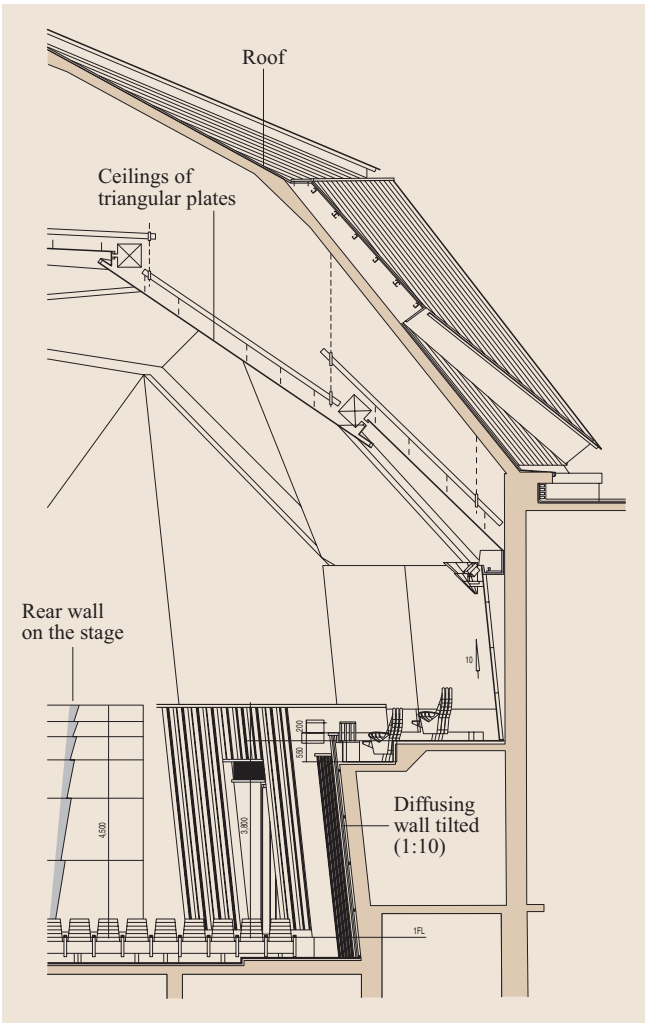


Fig. 10.23 Details of the cross section, including a sectional detail of the rear wall on the stage at the lower left of the figure

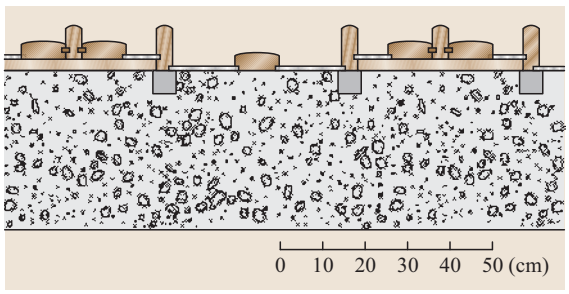


Fig. 10.24 Detail of the diffusing sidewalls effective for the higher-frequency range above 1.5 kHz, avoiding image shift of the sound source on the stage. The surface is deformed from the Schroeder diffuser by removal of the well partitions. (After [10.69])

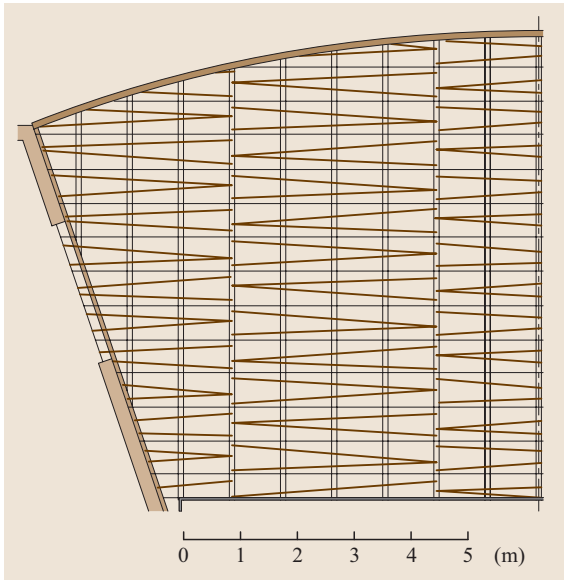


Fig. 10.25 Detail of the triangular joist arrangement for the stage floor, avoiding anomalous radiation due to the normal modes of vibration from certain music instruments that touch the floor

10.3 Individual Preferences of a Listener and a Performer

The minimum unit of society to be satisfied by the environment is one individual, which leads to a unique personal existence. Here, we demonstrate that the individual subjective preferences of each listener and each cellist may be described by the theory in Sect. 10.1, which resulted from observing a number of subjects.

10.3.1 Individual Subjective Preference of Each Listener

In order to enhance individual satisfaction for each listener, a special facility for seat selection, testing each listener's own subjective preference [10.59,71], was first

Amazon
EX1010 Page 384

introduced at the Kirishima International Concert Hall in 1994. The sound simulation system employed multiple loudspeakers. It used arrows for testing the subjective preference of four listeners at the same time. Since the four orthogonal factors of the sound field influence the preference judgment almost independently [10.1], each single factor is varied, while the other three are fixed at the preferred condition for the average listener. Results of testing acousticians who participated in the International Symposium on Music and Concert Hall Acoustics (MCHA95), which was held in Kirishima in May 1995, are presented here [10.1].

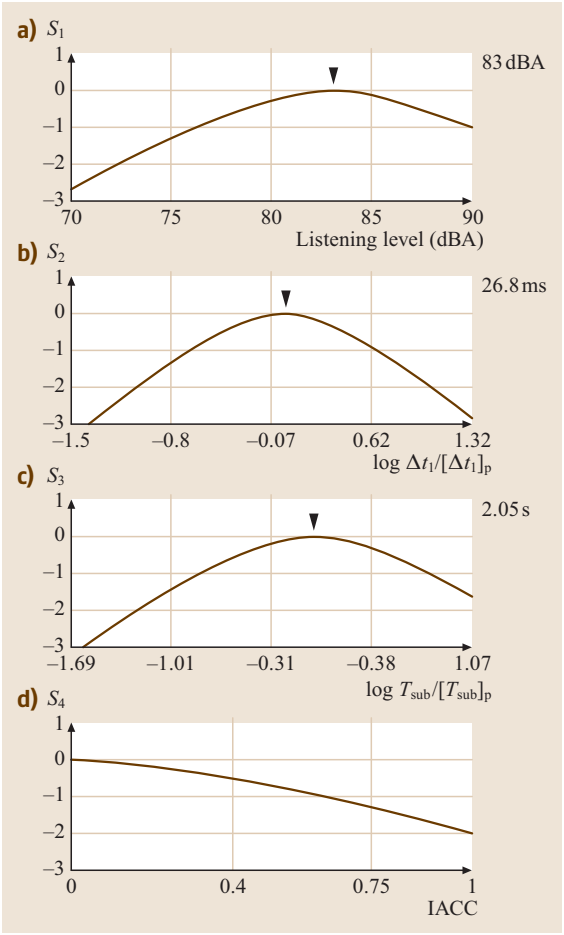


Fig. 10.26a–d Scale values of preference obtained by paired-comparison tests for the four orthogonal factors, subject BL. **(a)** The most preferred listening level was 83 dBA, the individual weighting coefficient in (10.9): $\alpha_1 = 0.06$; **(b)** the preferred initial time delay gap between the direct sound and first reflection was 26.8 ms, the individual weighting coefficient in (10.9): $\alpha_2 = 1.86$, where $[\Delta t_1]_p$ calculated by (10.4) with $(\tau_e)_{min}$ =62 ms for the music used ($A = 4$) is 24.8 ms; **(c)** the preferred subsequent reverberation time is 2.05 s, the individual weighting coefficient in (10.9): $\alpha_3 = 1.46$, where $[T_{sub}]_p$ calculated by (10.6) with $(\tau_e)_{min}$ =62 ms for the music used, is 1.43 s; **(d)** individual weighting coefficient in (10.9) for IACC: $\alpha_4 = 1.96$.

Individual Preference and Seat Selection

The music source was orchestral, the *Water Music* by Händel; the effective duration of the ACF was 62 ms [10.11]. The total number of listeners participating was 106. Typical examples of the test results for listener BL as a function of each factor are shown in Fig. 10.26. Scale values of this listener were rather close to the averages for subjects previously collected: the most preferred $[LL]_p$ was 83 dBA, the value

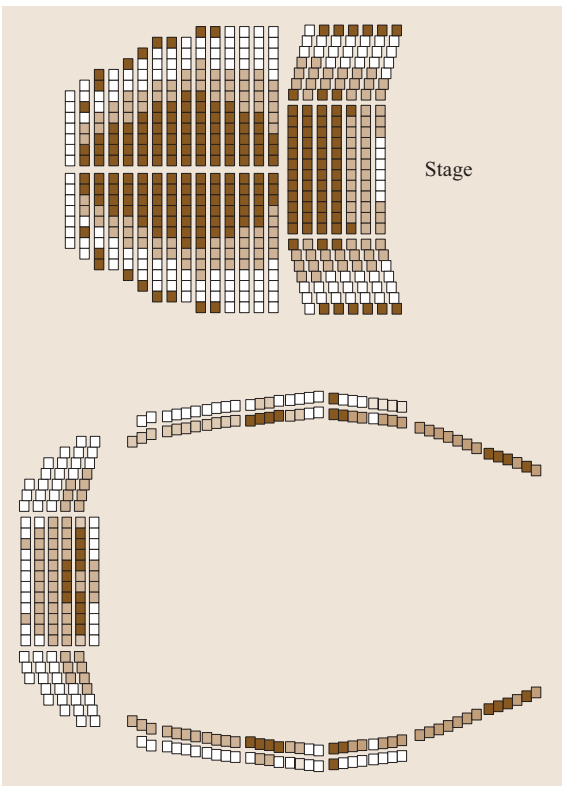


Fig. 10.27 Preferred seating area calculated for subject BL. The seats are classified in three parts according to the scale value of subjective preference calculated by the summation of S_1–S_4 (10.8) together with (10.9). Black indicates preferred seating areas, about one third of all seats in this concert hall, for subject BL

Amazon
EX1010 Page 385

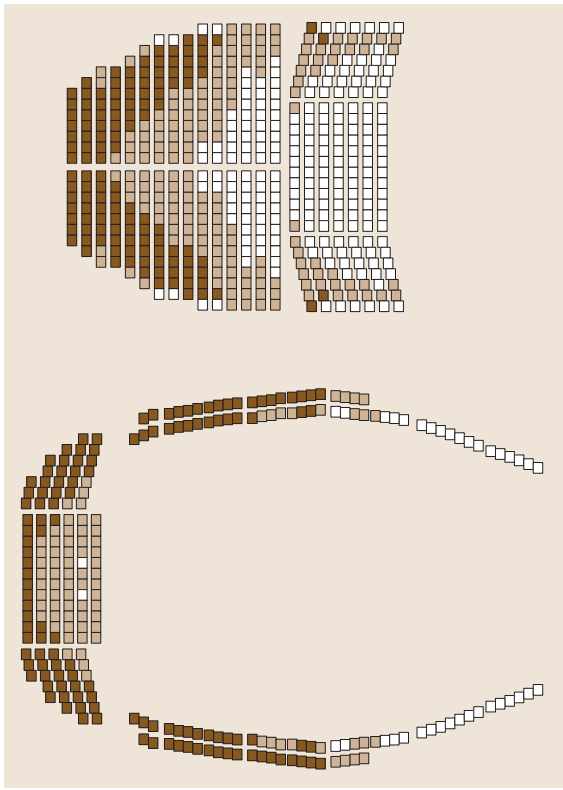


Fig. 10.28 Preferred seating area calculated for subject KH

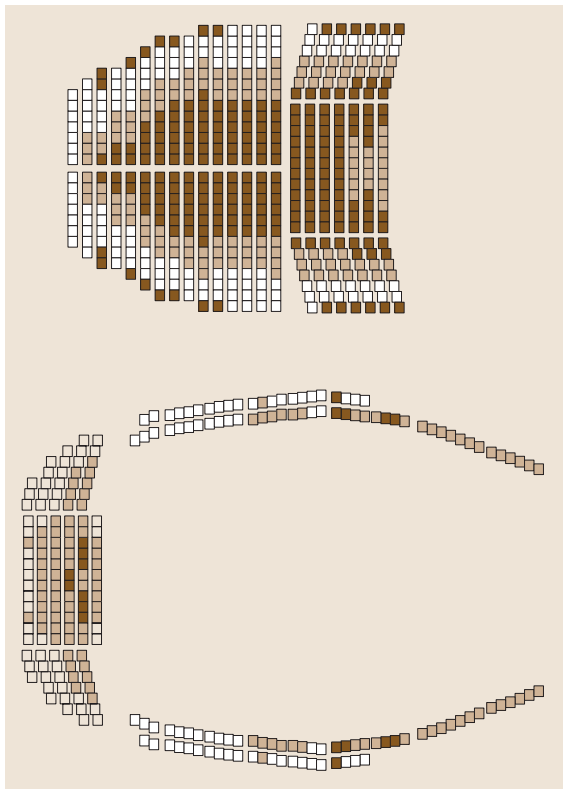


Fig. 10.29 Preferred seating area calculated for subject KK

$[\Delta t_1]_p \approx [(1 - \log_{10} A)(\tau_e)_{min}]$ was 26.8 ms (the global preferred value calculated by (10.4) with the total sound pressure as was simulated $A = 4.0$ is 24.8 ms. And the most preferred reverberation time is 2.05 s [the global preferred value calculated by (10.6) is 1.43 s]. Thus, as was designed, the center area of seats was preferred for listener BL (Fig. 10.27). With regard to the IACC, the result for all listeners was that the scale value of prefer-

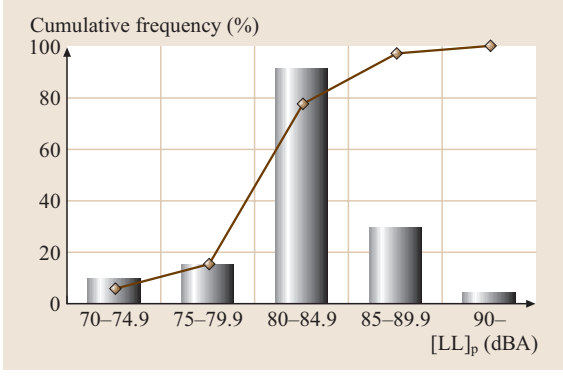


Fig. 10.30 Cumulative frequency of preferred listening level $[LL]_p$ (106 subjects). About 60% of subjects preferred the range of 80–84.9 dBA

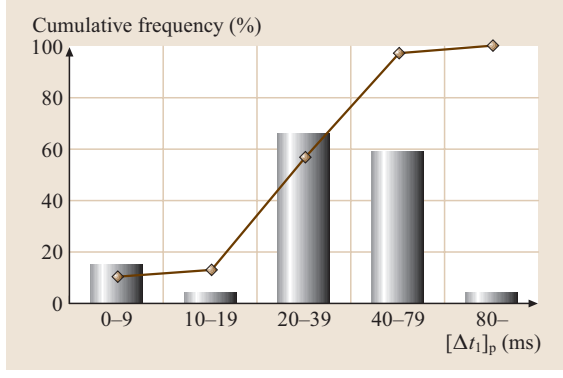


Fig. 10.31 Cumulative frequency of the preferred initial time delay gap between the direct sound and the first reflection $[\Delta t_1]_p$ (106 subjects). About 45% of subjects preferred the range of 20–39 ms. The value of $[\Delta t_1]_p$ calculated using (10.4) is 24.8 ms

Amazon
EX1010 Page 386

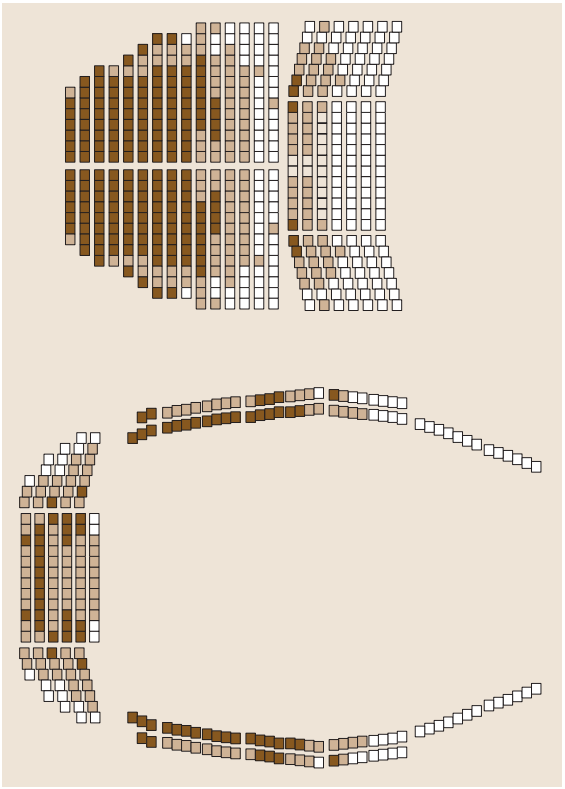


Fig. 10.32 Preferred seating area calculated for subject DP

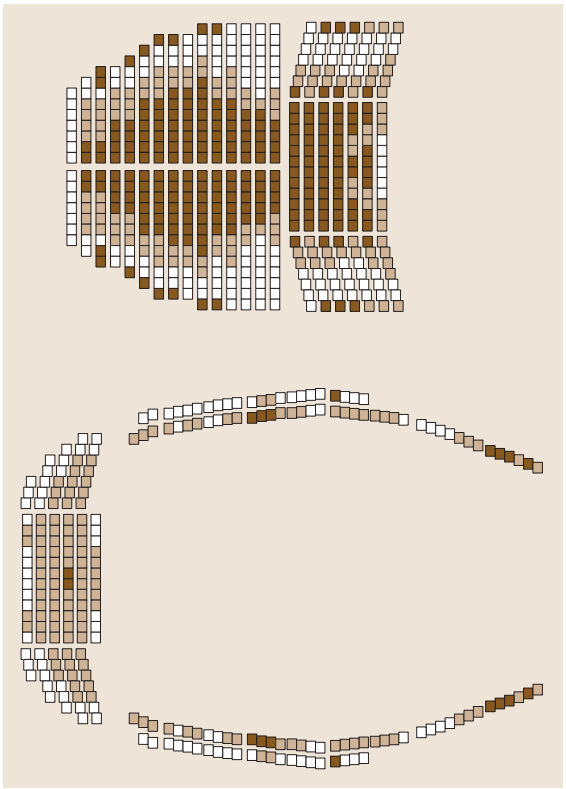


Fig. 10.33 Preferred seating area calculated for subject CA

ence increased with decreasing the IACC value. Since listener KH preferred a very short delay time of Δt_1, his preferred seats were located close to the boundary wall, as shown in Fig. 10.28. Listener KK indicated a preferred listening level exceeding 90 dBA. For this listener, the front seating area close to the stage was preferable, as shown in Fig. 10.29. For listener DP, whose preferred listening level was rather weak (76.0 dBA) and the preferred initial delay time was short (15.0 ms), the preferred seat was in the rear part of hall, as shown in Fig. 10.32. The preferred initial time delay gap for listener CA exceeds 100.0 ms, but was not critical. Thus, any initial delay times were acceptable, but the IACC was critical. Therefore, the preferred areas of seats were located as shown in Fig. 10.33.

Cumulative Frequency of Preferred Values

Cumulative frequencies of the preferred values with 106 listeners are shown in Fig. 10.30 through Fig. 10.34 for three factors. As indicated in Fig. 10.30, about 60% of listeners preferred the range 80–84.9 dBA when listening to music, but some listeners indicated that the most preferred LL was above 90 dBA, and the total range of the preferred LL was scattered, exceeding a 20 dB range. As shown in Fig. 10.31, about 45% of listeners preferred initial delay times of 20–39 ms, which were

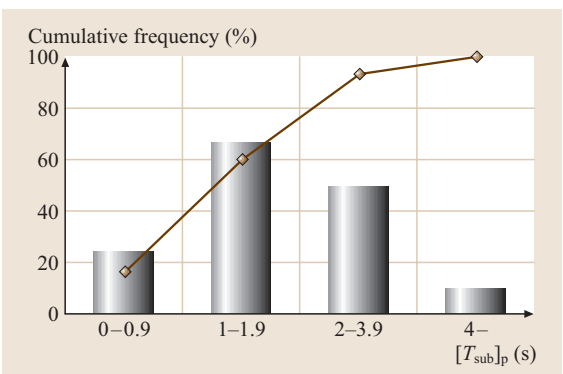


Fig. 10.34 Cumulative frequency of the preferred subsequent reverberation time $[T_{sub}]_p$ (106 subjects). About 45% of subjects preferred the range 1.0–1.9 s. The value of $[T_{sub}]_p$ calculated using (10.6) is 1.43 s

Amazon
EX1010 Page 387

around the calculated preference of 24.8 ms (10.4) with $k = 0.1$, $c = 1$ and $A = 4.0$; however, some listeners indicated 0–9 ms and others more than 80 ms. With regard to the reverberation time, as shown in Fig. 10.34, about 45% of listeners preferred 1.0–1.9 s, which is centered on the preferred value of 1.43 s calculated by (10.6), but some listeners indicated preferences lower than 0.9 s or more than 4.0 s.

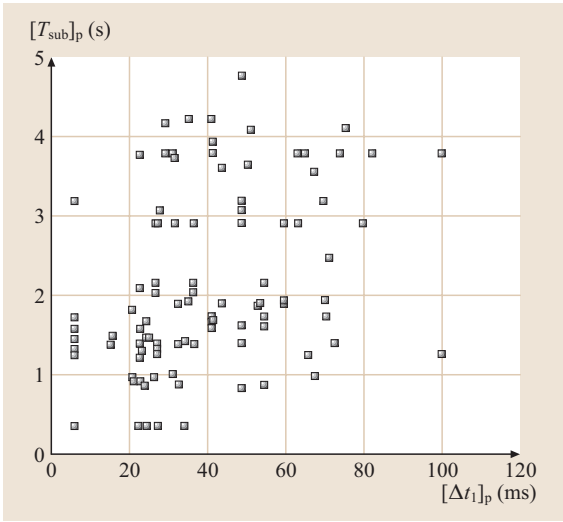


Fig. 10.35 The relationship between the preferred values of $[\Delta t_1]_p$ and $[T_{sub}]_p$ for each subject. No significant correlation between values was achieved

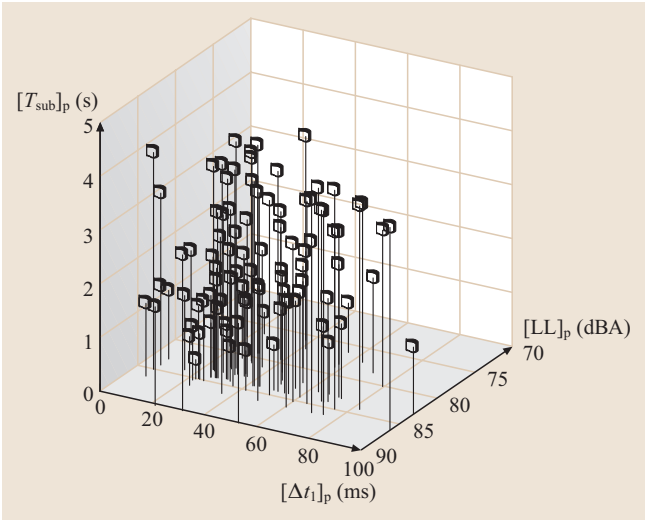


Fig. 10.36 Three-dimensional illustration of the three preferred orthogonal factors for the sound field for each individual subject (*squares*). All 106 listeners tested indicated that a smaller value of the IACC was preferred, and these data are not included in this figure. Preferred conditions are distributed in a certain range of each factor, so that subjects could not be classified into any specific groups

Independence of the Preferred Conditions

It was thought that both the initial delay time and the subsequent reverberation time appear to be mutually related, due to a kind of *liveness* of the sound field. Also, it was assumed that there is a strong interdependence between these factors for each individual. However, as shown in Fig. 10.35, there was little correlation between preference values of $[\Delta t_1]_p$ and $[T_{sub}]_p$ (the correlation is 0.06). The same is true for the correlation between values of $[T_{sub}]_p$ and $[LL]_p$ and for that between values of $[LL]_p$ and $[\Delta t_1]_p$, a correlation of less than 0.11. Figure 10.36 shows the three-dimensional plots of the preferred values of $[LL]_p$, $[\Delta t_1]_p$ and $[T_{sub}]_p$ for the 106 listeners. Looking at a continuous distribution in preferred values, no specific groupings of individuals can be classified from the data.

Another important fact is that there was no correlation between the weighting coefficients α_i and α_j, $i \neq j$ (i, $j = 1, 2, 3, 4$) in (10.9) for each individual listener [10.1]. A listener indicating a relatively small value of one factor will not always indicate a relatively small value for another factor. Thus, a listener can be critical about a preferred condition as a function of a certain factor, while insensitive to other factors, resulting in characteristic differences from other listeners.

10.3.2 Individual Subjective Preference of Each Cellist

To realize an excellent concert, we need to know the optimal conditions not only in the stage enclosure design for performers, but also in the style of the performance. The primary issue is that the stage enclosure is designed to provide a sound field in which performers can play easily. *Marshall* et al. [10.72] investigated the effects of stage size on the playing of an ensemble. The parameters related to stage size in their study were the delay time and the amplitude of reflections. *Gade* [10.73] performed a laboratory experiment to investigate the preferred conditions for the total amplitude of the reflections of performers. *Nakayama* [10.62] showed a relationship between the preferred delay time and the effective duration of the long-time ACF of the source signal for alto-recorder soloists (data was rearranged [10.1]). When we listen to a wide range of music signals containing a large fluctuation, it is more accurately expressed

Amazon
EX1010 Page 388

by the minimum value of the effective duration $(\tau_e)_{min}$ of the running ACF of the source signals [10.39]. For individual singers, *Noson* et al. [10.74, 75] reported that the most preferred condition of the single reflection for an individual singer may be described by $(\tau_e)_{min}$ and a modified amplitude of reflection according to the overestimate and bone conduction effects (for control of $(\tau_e)_{min}$ see [10.41, 42]).

Preferred Delay Time of the Single Reflection for Cellists

As a good example, the preferred delay time of the single reflection for individual cello soloist is described by the minimum value of the effective duration of the running ACF of the music motifs played by that cellist [10.76]. The same music motifs (motifs I and II) used in the experiment by Nakayama were applied here [10.62]. The tempo of motif I was faster than that of motif II, as shown in Fig. 10.37. A microphone in front of the cellist picked up the music signals performed three times by each of five cellists.

Figure 10.38 shows an example of the regression curve for the scale value of preference fitted by (10.9). The peak of this curve denotes the most preferred delay time $[\Delta t_1]_p$. The values for individual cellists are listed in Table 10.5. Global and individual results (except for that of subject E) for music motif II were longer than those for music motif I.

The most preferred delay time of a single reflection is approximately expressed by the duration τ'_p of the ACF as similar to that of listeners (10.4), so that

$$[\Delta t_1]_p = \tau'_p \approx \left[\log_{10}(1/k') - c' \log_{10} A'\right](\tau_e)_{min} , \quad (10.15)$$

where the values k' and c' are constants that depend on the individual performer and musical instrument used. A substantial difference from (10.4) of listeners is that the amplitude of the reflection A' is defined by $A' = 1$ relative to -10 dB of the direct sound as measured at the ear's entrance. This is due to the phenomenon of *missing reflection* (i. e., a performer overestimating the reflection) [10.1].

Individual Subjective Preference

Using the quasi-Newton method, the resulting constants on average were $k' \approx 1/2$ and $c' \approx 1$ for the five cellists. (It is worth noting that the coefficients k' and c' for alto-recorder soloists were 2/3 and 1/4, respectively [10.1].) After setting $k' = 1/2$, the coefficient c' for each individual was figured out as listed in Table 10.6. The average value of the coefficient c' for the five cellists

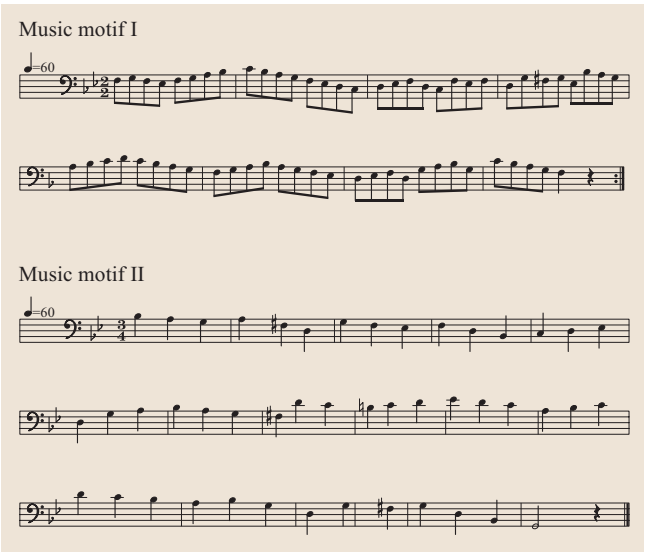


Fig. 10.37 Music motifs II and I composed by Tsuneko Okamoto for the investigation [10.62]

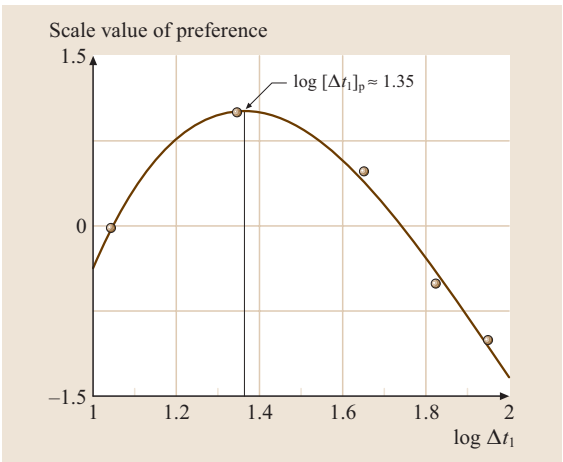


Fig. 10.38 An example of the regression curve for the preferred delay time (subject D, music motif I, −15 dB), $\log_{10}[\Delta t_1]_p \approx 1.35$, thus $[\Delta t_1]_p \approx 22.6$ ms

obtained was 1.03. The relationship between the most preferred delay time $[\Delta t_1]_p$ obtained by the judgment and the duration τ'_p $(= [\Delta t_1]_p)$ of the ACF calculated by (10.15) is shown in Fig. 10.40. Different symbols indicate values obtained in different test series with two music motifs. The correlation coefficient between calculated values of $[\Delta t_1]_p$ and measured values is 0.91 $(p < 0.01)$. The scale values of preference for each of the five cellists as a function of the delay time of the sin-

Amazon
EX1013 Page 389

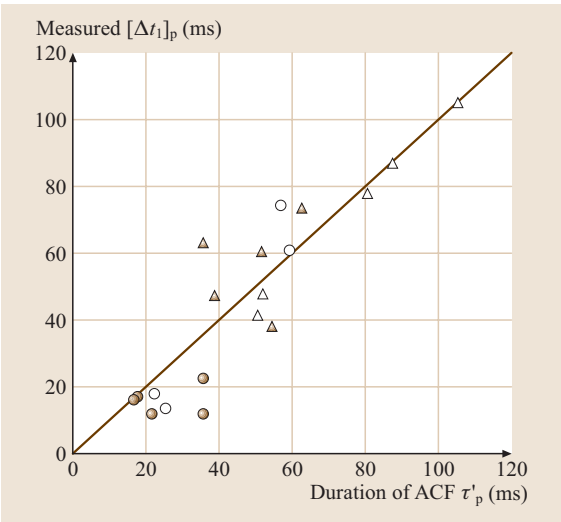


Fig. 10.39 The relationship between the most preferred delay time $[\Delta t_1]_p$ measured and the duration $[\Delta t_1]_p = \tau'_p$ calculated using (10.15). Correlation coefficient, $r = 0.91$ ($p < 0.01$). ●: music motif I, −15 dB; ○: music motif I, −21 dB; ▲: music motif II, −15 dB; △: music motif II, −21 dB

gle reflection normalized by the calculated $[\Delta t_1]_p$ are shown in Fig. 10.40.

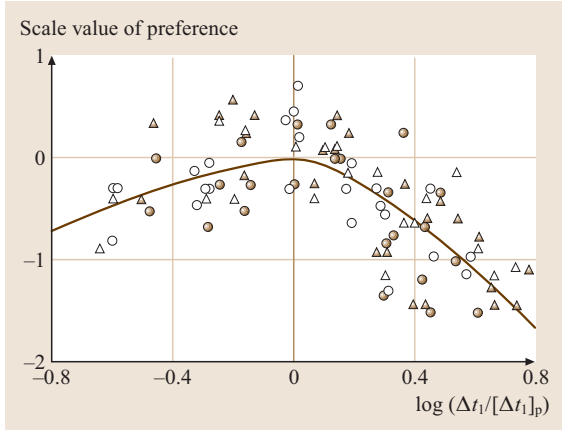


Fig. 10.40 Scale values of preference for each of five cellists as a function of the delay time of the single reflection normalized by its most preferred delay time calculated by (10.15). ●: music motif I, −15 dB; ○: music motif I, −21 dB; ▲: music motif II, −15 dB; △: music motif II, −21 dB. The regression curve is expressed by (10.9), $i = 2$

Table 10.5 Judged and calculated preferred delay times of a single reflection for each cello soloist. Calculated values of $[\Delta t_1]_p$ are obtained by (10.15) using the amplitude of the reflection A'_1 and $(\tau_e)_{min}$ for music signals performed by each cellist

A(dB)	A'(dB) (= $A+10$)	A'	Cellist	Judged $[\Delta t_1]_p$(ms)		Calculated $[\Delta t_1]_p$(ms)	
				Motif I	Motif II	Motif I	Motif II
−15	−5	0.56	A	16.2	47.9	16.3	38.5
			B	<12.0	73.8	35.2	62.7
			C	<12.0	60.8	211.3	51.3
			D	22.6	38.2	35.1	53.9
			E	17.6	63.6	17.3	35.2
			Global	18.0	48.3	24.3	47.5
−21	−11	0.28	A	18.1	48.4	21.8	51.5
			B	61.2	105.0	59.3	105.6
			C	–	77.9	–	80.6
			D	74.6	86.8	56.9	87.4
			E	<14.0	42.2	24.8	50.2
			Global	30.4	71.8	37.6	73.4

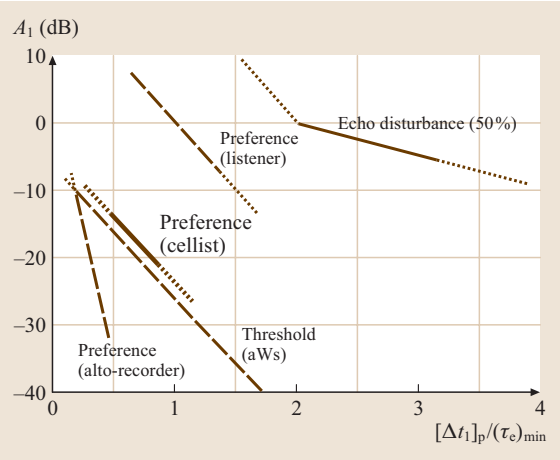
Table 10.6 The coefficient c' for each cellist in (10.15), calculating the preferred delay time of reflection for individual results and the global result, with $k' = 1/2$ (fixed)

	Cellist					Averaged
	A	B	C	D	E	(global)
Coefficient c'	0.47	1.61	1.10	1.30	0.67	≈ 1.03

Amazon
EX1010 Page 390

Subjective Responses as a Function of $[\Delta t_1]_p/(\tau_e)_{min}$

Figure 10.41 shows the relative amplitude of the single reflection to that of the direct sound for the preference of cello soloists as a function of the delay time of the single reflection normalized by the minimum value of the effective duration $(\tau_e)_{min}$ of the running ACF of the source signal. Several other subjective responses in terms of the amplitude are shown together as a function of the delay time of the single reflection normalized by the value of the effective duration τ_e of the long-time ACF. All these values can generally be expressed by (10.4) in relation to the effective duration of the ACF with the constants k and c, which depend on different subjective responses. An alto-recorder soloist's preference is also plotted in this figure [10.1]. The values for performers are below or close to the threshold of perception of listeners [10.77]. These reconfirm the phenomenon of *missing reflection* for performers.



In order to blend the source music under performance and the sound field in a given concert hall, a performer, to some extent, can control the value of $(\tau_e)_{min}$ by introducing vibrato. Such an introduction of vibrato may decease the value of $(\tau_e)_{min}$ to obtain a more preferred condition for listeners as well, even though there is a short reverberation time in a given concert hall [10.41, 42].

Fig. 10.41 Relative amplitude of the single reflection for the subjective preference of cello soloists as a function of the delay time of a single reflection normalized by the value of $(\tau_e)_{min}$. Also, the amplitudes of several subjective responses as a function of the delay time of the single reflection normalized by the value of τ_e of the source signal. Note that threshold has been rearranged using the typical ACF of the speech signal [10.1]

10.4 Acoustical Measurements of the Sound Fields in Rooms

Acoustical measurements were made in an existing hall for the purpose of testing acoustic factors that were calculated using the architectural scheme at the design stage. Also, subjective preference judgments for different source locations on the stage were performed by the paired-comparison test at each set of seats. The relationship between the resulting scale values of subjective preference and the physical factors obtained by simulation using architectural plan drawings was examined by factor analysis. The accumulation and understanding of the field data, in turn, may improve details of future methods for calculating acoustic factors.

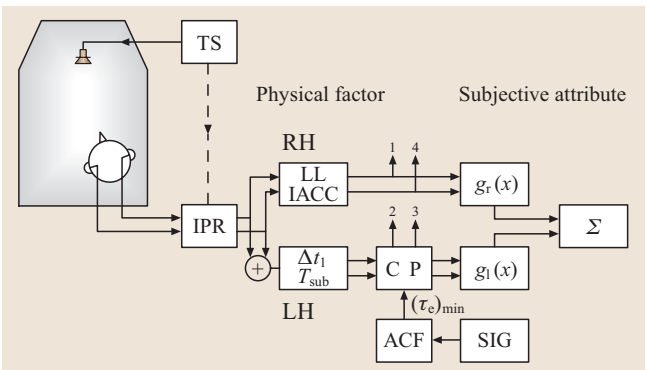


Fig. 10.42 A system for measuring the four orthogonal factors of sound fields and evaluating subjective qualities at each seat in a room. TS: test signal (maximum-length sequence signal); IPR: impulse response analyzer; RH: right-hemispheric factors (listening level and the IACC); LH: left-hemispheric factors (Δt_1, T_{sub}, and the A value); CP: comparators with the most preferred condition based on the effective duration of ACF, $(\tau_e)_{min}$; ACF: autocorrelation function; SIG: source signals; $g_r(x)$: scale values from the right-hemispheric factors; $g_l(x)$: scale values from the left-hemispheric factors; Σ: total scale value of subjective preference

Amazon
EX1010 Page 391

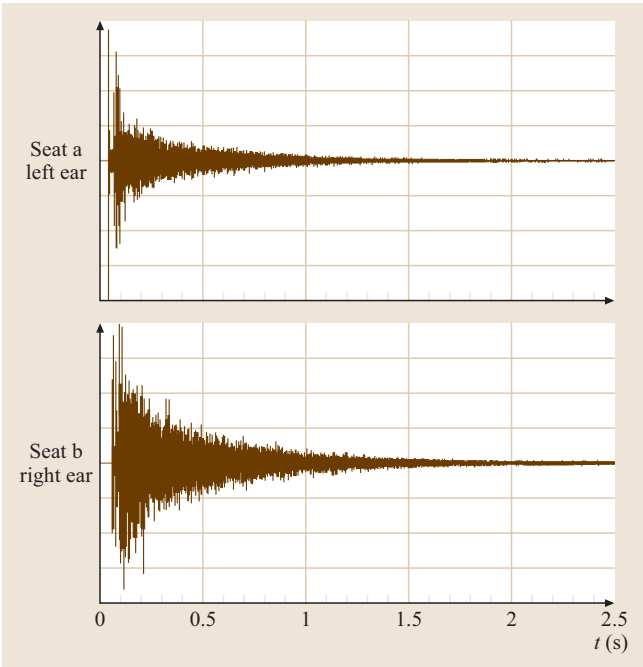
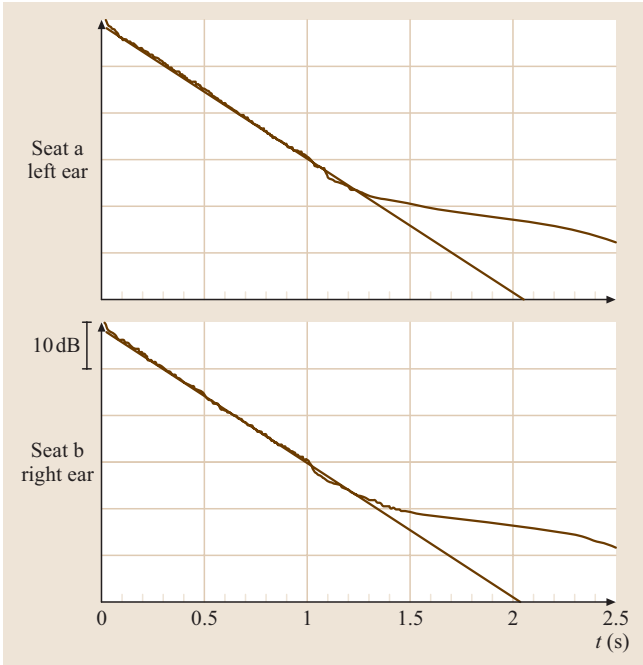


Fig. 10.43a,b Examples of the impulse response measured at seats: **(a)** (near to the stage) and **(b)** (far from the stage) in the Kirishima International Concert Hall. The amplitude of the impulse response measured at seat **(a)** is attenuated because of a strong direct sound.



10.4.1 Acoustic Test Techniques

Binaural Impulse Response

A diagnostic system for measuring the impulse response at the two ear entrances determining the four orthogonal factors, and for further evaluation of the subjective attributes of sound field at each seat in a hall is shown in Fig. 10.42. A test signal is radiated from the loudspeaker to measure impulse responses using two small microphones placed at the ear entrances of a real head (1.1 m above the floor). Then spatial factors associated with the right-hemisphere specialization (LL and IACC) and the temporal factors of left-hemisphere specialization (Δt_1 and T_{sub}) are analyzed. When the effective duration of the ACF of the source signal (τ_e) is calculated, the total scale value may be obtained by adding the scale values of the orthogonal factors referred to the most preferred conditions. The value of $(\tau_e)_{min}$ is used to determine the most preferred temporal values for $[\Delta t_1]_p$ and $[T_{sub}]_p$ (Sect. 10.1.2). If the source signal is fed into the ACF processor, then outputs (numbered 1–4) may be used to control the sound field simultaneously with an electroacoustic system, without any manual adjustment, preserving the preferred conditions of the four factors.

Examples of measuring binaural impulse responses at a seat close to the stage (seat a, left ear) and at a rear seat b (right ear) in the Kirishima International Concert Hall are demonstrated in Fig. 10.43. In this measurement, an omnidirectional dodecahedron loudspeaker with 12 full-range drivers was placed on the stage 1.5 m above the floor for a sound source. The total amplitude of reflections A at a seat close to the stage is usually smaller than that at seat far from the stage.

Another powerful signal to be radiated from the loudspeaker to measure the impulse binaural responses is the pulse signal generated by inverse Fourier transformation [10.78].

Reverberation Time

After the impulse response is obtained, the reverberation time is measured by *Schroeder's* method [10.79,80]. The integrated decay curve as a function of time may be obtained by squaring and integrating the impulse response of the sound field in a room, such that

$$\langle s^2(t)\rangle = \mathrm{K}\int_{t+T}^{t} h^2(x)\,\mathrm{d}x \qquad (10.16)$$

Fig. 10.44 Integrated decay curves obtained from the impulse responses at the two ear entrances, at seat **(a)** in the Kirishima International Concert Hall

Amazon
EX1010 Page 392

where the time T should be chosen sufficiently longer than the reverberation time.

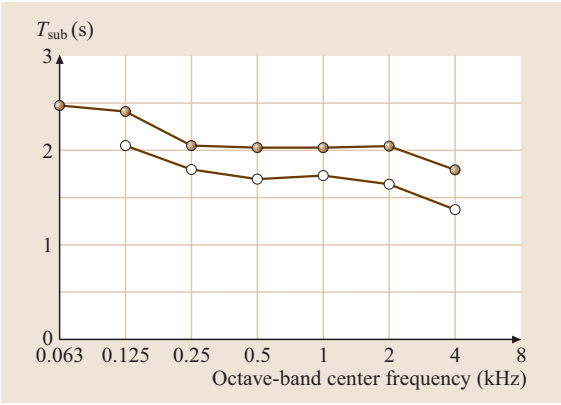


Fig. 10.45 Reverberation time measured in the Kirishima International Concert Hall. ●: measured values without audience; ○: estimated with full audience

For the 500 Hz octave band, examples of the measured decay curve and the decay rate of both left and right ears at seating position ***a*** are shown in Fig. 10.47. The reverberation times measured are both 2.07 s. The measured reverberation times with octave band filters in the Kirishima International Concert Hall (without audience) are plotted as filled circles in Fig. 10.45. The empty circles are estimated values of the reverberation time for a full audience. It is worth noticing that *Jordan* [10.81] showed that the values of the early decay time (EDT) measured over the first 10 dB of decay are close to values of the reverberation time averaged with the interval of −5 to −35 dB.

The total amplitude of reflection A, defined by (10.5), is obtained as its square

$$A^2 = \frac{\int_{\infty}^{\varepsilon} h^2(x)\,\mathrm{d}x}{\int_{\varepsilon}^{0} h^2(x)\,\mathrm{d}x}\,, \qquad (10.17)$$

where ε signifies a small delay time just large enough to cover the duration of the direct sound.

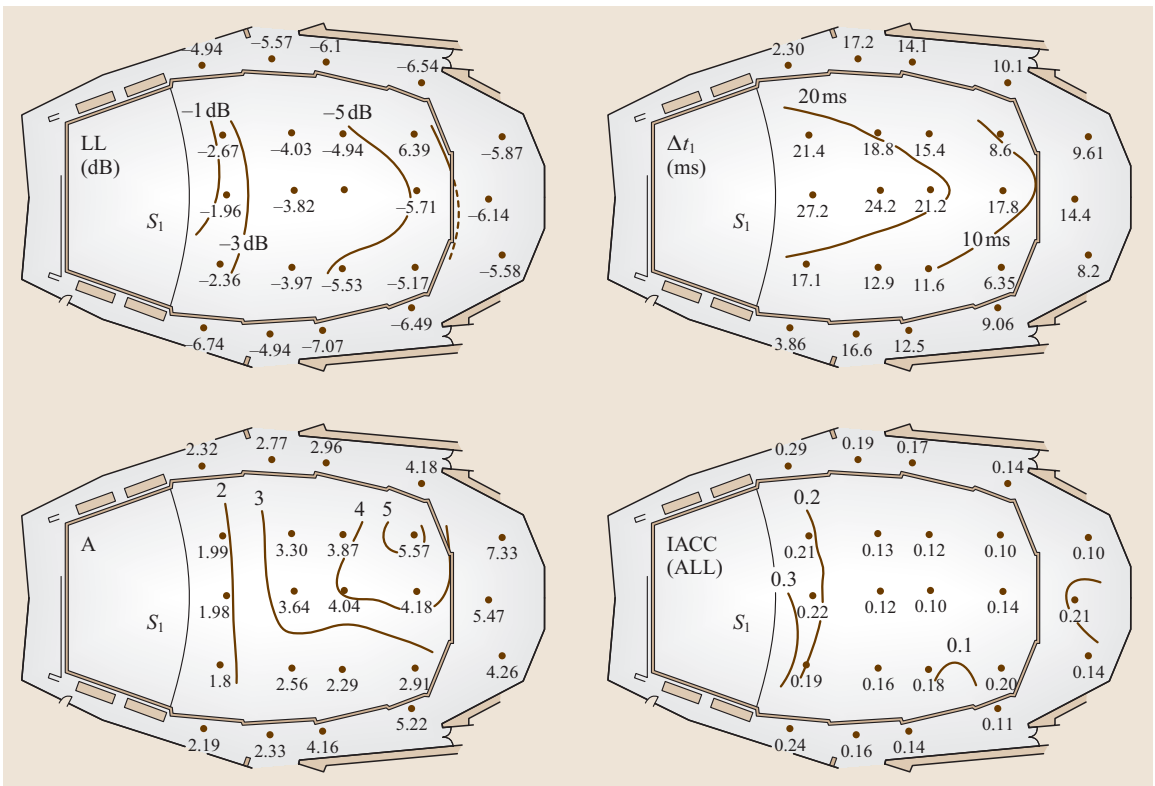


Fig. 10.46a–d Orthogonal factors measured at each seat in the Kirishima International Concert Hall, other than the reverberation time, which is almost constant throughout the hall: **(a)** listening level; **(b)** Δt_1; **(c)** A value, the total amplitude of reflections; **(d)** IACC

Amazon
EX1010 Page 393

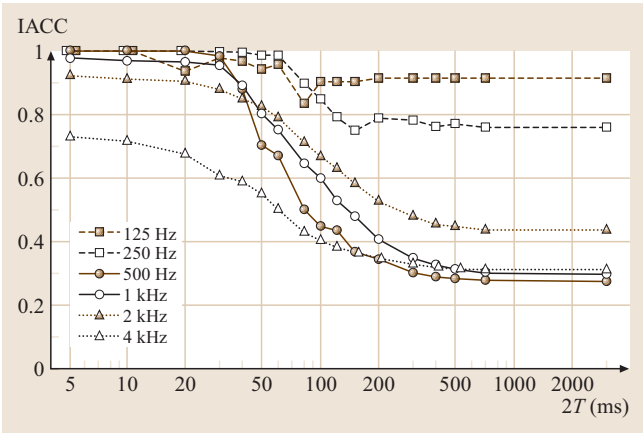


Fig. 10.47 Measured IACC as a function of the integration interval $2T$ of the impulse responses for each octave band range. The value of IACC converged for $2T > 200$ ms (After [10.82])

Measurement of Acoustic Factors at Each Seat in a Concert Hall

In Sect. 10.3.1 we discussed the seat selection system, designed for the purpose of enhancing individual satisfaction. To begin with, four orthogonal factors are measured at each seat in a concert hall [10.67, 68]. Measured values of the listening level (LL), the total amplitude of reflection (A), the initial time delay gap (Δt_1) between the direct sound and the first reflection excluding the reflection from the floor, and the IACC at each seat in the Kirishima International Concert Hall

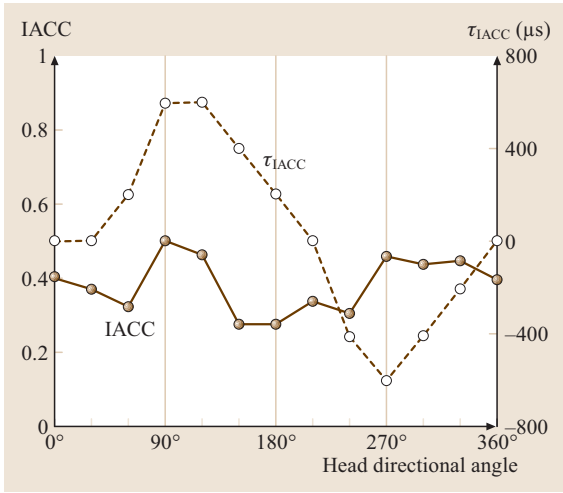


Fig. 10.48 Measured IACC and τ_{IACC} as a function of head direction relative to the sound source in a narrow hotel atrium (After [10.83])

are shown in Fig. 10.46. The reverberation times at all the seats had almost the same value, about 2.05 s for the 500 Hz band.

Even though the final scheme of the concert hall was changed in terms of the width of the hall (one meter wider) from the scheme at the design stage, values of each physical factor measured as shown in Fig. 10.46 are not very different from the values calculated (Fig. 10.22).

Recommended Method for IACC Measurement

There are two purposes for measuring IACC, as needed for subjective evaluations and acoustic comparison of existing halls:

1. In order to evaluate the subjective quality of the sound field in an existing hall, the IACF (with values of IACC, τ_{IACC} and W_{IACC} defined in Fig. 10.4 as well as LL) together with the other three factors Δt_1, T_{sub} and A are measured. Without any octave band filtering, measurements must be performed after passage of the music or the speech signal through an A-weighting network, under identical conditions with subjective judgment.
2. In order to compare values of the IACC as well as T_{sub} for the sound field in existing halls, measurements with octave band filtering are performed. With a fixed sound source on the stage, the IACC is defined by a long integration interval, which includes the effects of the direct sound and all reflections, including reverberation, without any temporal subdivisions.

A typical example of measuring the IACC as a function of the integration interval, which was performed in Symphony Hall, Boston, is shown in Fig. 10.47 [10.82]. It is remarkable that the measured values of IACC almost converged for $2T \approx 200$ ms, and the values are not so different for longer intervals.

If a room is used for performing dance, ice-skating or a party, then the listeners face in various directions. In this case, the values of IACC and τ_{IACC} are measured as a function of the direction of the head. The measured results with the 500 Hz octave band noise in an oblong atrium of a hotel at the distance 10 m from the source position are demonstrated in Fig. 10.48 [10.83]. When the listener is facing the sound source, then IACC = 0.41, and $\tau_{\mathrm{IACC}} = 0$, and thus no image shift occurs. These values are nearly unchanged for head directional angles less than 30° when the listener is facing the lateral side at 90°, then the IACC is greater than 0.50, and τ_{IACC} is about 600 μs, due to the interaural delay time.

Amazon
EX1010 Page 394

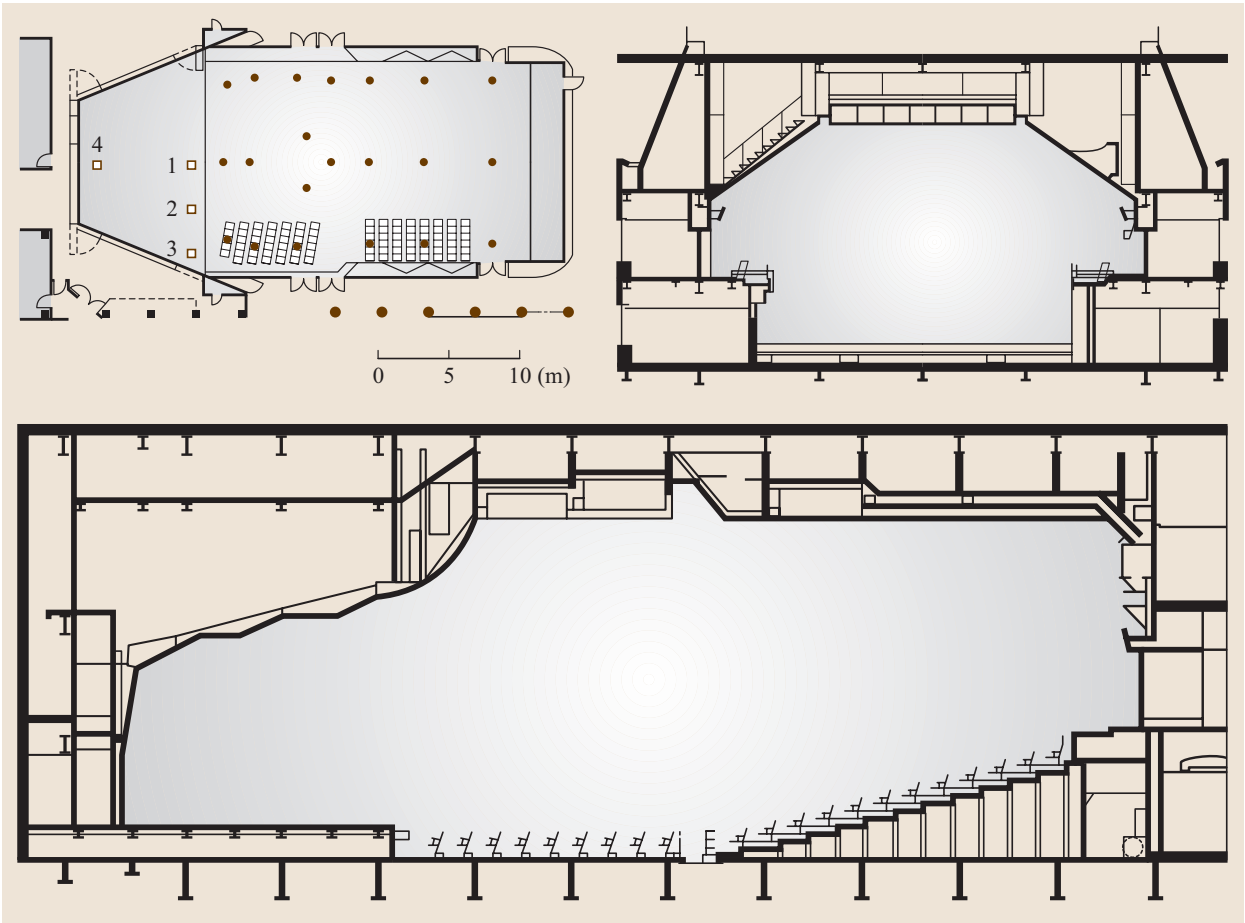


Fig. 10.49 *Left panel* plan; *right* and *bottom panel* cross sections of the Uhara Hall, Kobe. Four source positions, 1, 2, 3 and 4 on the stage, which were switched in the paired-comparison test of subjective preference without moving subjects from seat to seat. There were 21 listening positions including neighboring seats

10.4.2 Subjective Preference Test in an Existing Hall

The subjective preference judgments for different source locations on the stage at Uhara Hall, Kobe, were performed by a paired-comparison test at each set of seats. The relationship between the resulting scale value of subjective preference and the physical factors obtained by calculation, using architectural plan drawings, was examined by factor analysis [10.84]. Calculated scale values of subjective preference were reconfirmed for the Uhara Hall (Fig. 10.49). The physical factors at each set of seats for four source locations on the stage were calculated. In the simulation, the directional characteristics of the four loudspeakers used in preference tests were not taken into consideration for the sake of convenience. The simulation calculation was performed up to the third order of reflection. Due to a floor structure with a fair amount of acoustic transparency, the floor reflection was not taken into account for the calculation, and part of the diffuser ceiling was regarded as a nonreflective plane for the sake of convenience. In the calculation of the IACC, the listeners faced toward the center of the stage, so that the IACC was not always a maximum at the interaural time delay $\tau = 0$.

The hall contains 650 seats with a volume of 4870 m^3. Four identical loudspeakers with the same characteristics were placed 0.8 m above the stage floor,

Amazon
EX1010 Page 395

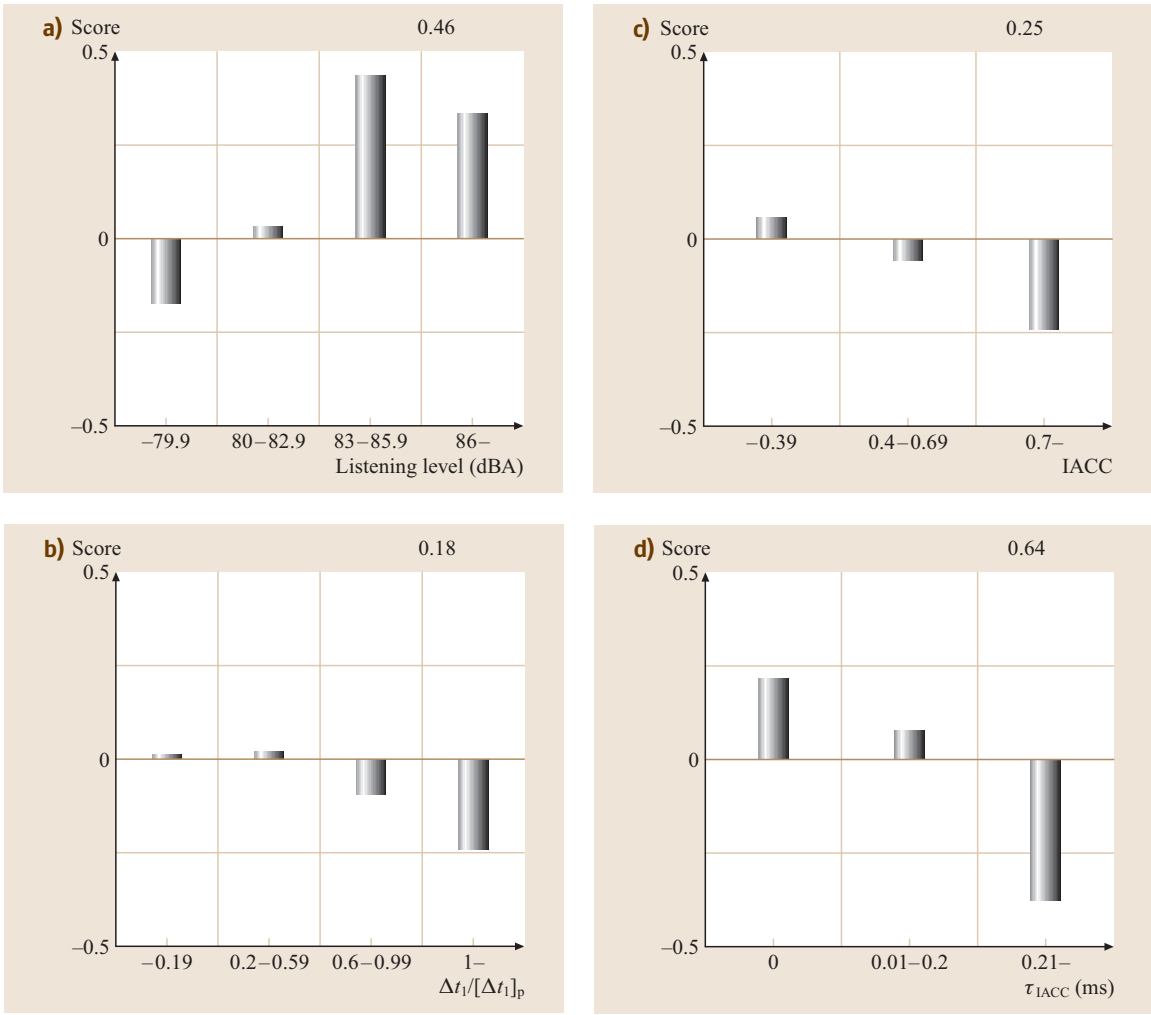


Fig. 10.50a–d Scores for each category of four physical factors obtained by the factor analyses. The number indicated at the upper left part of each figure signifies the partial correlation coefficient between the score and each factor. **(a)** Listening level; **(b)** normalized initial time delay gap between the direct sound and the first reflection; **(c)** IACC; **(d)** interaural time delay of the IACC, τ_{IACC}, found as the most significant factor in this investigation with loudspeaker reproductions on the stage. Tendencies obtained here are similar to those of the scale value shown in Fig. 10.7, which were obtained from the simulated sound field

and sixty-four listeners, divided into 21 groups, were seated in the specified set of seats. Without moving from seat to seat and excluding the effects of other physical factors such as visual and tactual senses on judgments, subjective preference tests by the paired-comparison method were conducted, switching only the loudspeakers on the stage. As a source signal, music motif B was selected in the tests. Scale values of preference were obtained by applying the law of comparative judgment and were reconfirmed by the goodness of the fit [10.85, 86]. The session was repeated five times, exchanging seats, and thus data for 14–16 subjects in total were obtained for each set of seats.

Results of Multiple-Dimensional Analyses

In order to examine the relationship between scale values of subjective preference and physical factors obtained

Amazon
EX1013 Page 396

by simulation of an architectural scheme, the data were analyzed by factor analysis [10.79, 80, 87].

Of the four orthogonal factors, the reverberation time was almost constant for the source location and the seat location throughout the hall, and thus was not involved in the analysis. As previously discussed, as a condition for calculating the scale value of preference, the maximum value of the interaural cross-correlation function must be maintained at $\tau_{IACC} = 0$ to ensure frontal localization of the sound source. However, the IACC was not always maintained at $\tau = 0$ due to the loudspeaker locations, because the subjects were facing the center of stage. In this analysis, therefore, the effect of the interaural time delay of the IACC was added as an additional factor. Thus, the outside variable to be predicted with factor analysis was the scale value obtained by subjective judgments, and the explanatory factors were: (1) the listening level, (2) the initial time delay gap, (3) the IACC, and (4) the interaural time delay (τ_{IACC}).

Scores for Each Factor

The scores for each category of the factors obtained from the factor analysis are shown in Fig. 10.50. As shown in Fig. 10.50a, the scores for the listening level indicate a peak at the subcategory of 83–85.9 dB, with decreasing scores moving away from the preferred listening level. For the IACC, the preference score increases with a decrease in the IACC (Fig. 10.50c). It is worth noting that the scores for the aforementioned two factors are in good agreement with preference scale values obtained from preference judgments for a simulated sound field (Fig. 10.7a and 10.7d). The scores of the initial time delay gap normalized to the optimum value ($\Delta t_1/[\Delta t_1]_p$) peaked at smaller values (Fig. 10.50b) than the most preferred value of the initial time delay gap obtained from the simulated sound fields (Fig. 10.7b). It is considered that, due to the limited range of the Δt_1 in the existing concert hall and the limited data for the short range of the Δt_1, the effects of the Δt_1 of the sound fields was rather minor in this investigation. Concerning τ_{IACC}, as shown in Fig. 10.50d, the score decreases monotonically as the delay is increased. This may be caused by an image shift without balancing of the sound field.

Measured and Calculated Subjective Preference Values

The relationship between the scale value obtained by subjective judgments and the total score at each center of three or four seats is shown in Fig. 10.51. The scale values of preference are well predicted with the total score for four loudspeaker locations ($r = 0.70$, $p < 0.01$). In some cases there is a certain degree of

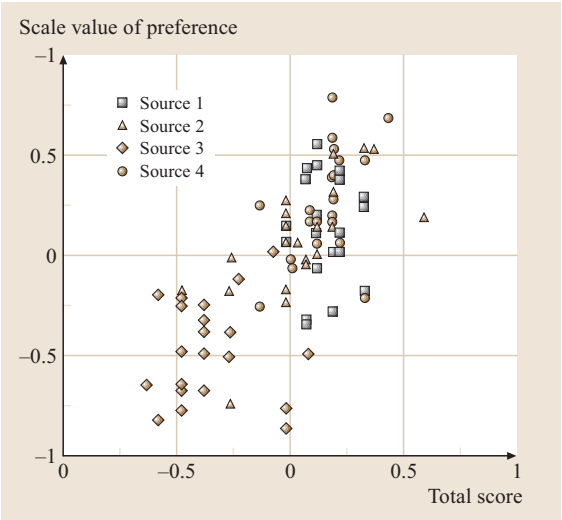


Fig. 10.51 Relationship between the scale value of subjective preference obtained by the paired-comparison test in the existing hall and the total score calculated by using the scores shown in Fig. 10.50. The correlation coefficient was $r = 0.70$ ($p < 0.01$)

apparent coherence between physical factors, for example, the calculated listening level and the IACC for sound fields in existing concert halls. However, these factors are theoretically orthogonal, and therefore the preference scores obtained were in good agreement with the calculated preference scale values obtained by the simulation.

So far the subjective preference of source locations on the stage has been examined at each set of seats. The rear source position (#4) on the stage is more preferred than that of the other source locations. The side source position (#3) indicates a low preference, due to the interaural time delay. The initial time delay gap resulted in a small influence on the total score because of its limited range.

10.4.3 Conclusions

Results of the analysis demonstrate that the theory of calculating subjective preference by the use of orthogonal parameters obtained in the laboratory is supported by experiments in a real hall. This may hold only when the maximum value of the interaural cross-correlation is maintained at $\tau = 0$. However, this condition is usually realized by introducing certain diffusing elements on the sidewalls in a real concert hall when the listeners face a performer.

Amazon
EX1010 Page 397

References

10.1 Y. Ando: *Architectural Acoustics, Blending Sound Sources, Sound Fields, and Listeners* (AIP/Springer, New York 1998)

10.2 W.C. Sabine: *Reverberation (The American Architect and the Engineering Record, 1900), Prefaced by L.L. Beranek: Collected papers on acoustics* (Peninsula, Los Altos 1992)

10.3 H. Haas: Über den Einfluss eines Einfachechos auf die Hörsamkeit von Sprache, Acustica **1**, 49–58 (1951)

10.4 L.L. Beranek: *Music, Acoustics and Architecture* (Wiley, New York 1962)

10.5 P. Damaske: Subjektive Untersuchungen von Schallfeldern, Acustica **19**, 199–213 (1967/68)

10.6 M.V. Keet: *The influence of early lateral reflections on the spatial impression* (Proc. 6th Int. Congress of Acoustics, Tokyo 1968), Tech. Dig., paper E-2-4

10.7 A.H. Marshall: Acoustical determinants for the architectural design of concert halls, Architect. Sci. Rev. (Australia) **11**, 81–87 (1968)

10.8 M. Barron: The subjective effects of first reflections in concert halls – The need for lateral reflections, J. Sound Vibr. **15**, 475–494 (1971)

10.9 P. Damaske, Y. Ando: Interaural crosscorrelation for multichannel loudspeaker reproduction, Acustica **27**, 232–238 (1972)

10.10 M.R. Schroeder, D. Gottlob, K.F. Siebrasse: Comparative study of European concert halls: Correlation of subjective preference with geometric and acoustic parameters, J. Acoust. Soc. Am. **65**, 958–963 (1974)

10.11 Y. Ando: Subjective preference in relation to objective parameters of music sound fields with a single echo, J. Acoust. Soc. Am. **62**, 1436–1441 (1977)

10.12 Y. Ando: Calculation of subjective preference at each seat in a concert hall, J. Acoust. Soc. Am. **74**, 873–887 (1983)

10.13 Y. Ando: *Concert Hall Acoustics* (Springer, Berlin, Heidelberg 1985)

10.14 A. Cocchi, A. Farina, L. Rocco: Reliability of scale-model research: A concert hall case, Appl. Acoust. **30**, 1–13 (1990)

10.15 S. Sato, Y. Mori, Y. Ando: The subjective evaluation of source locations on the stage by listeners, music and concert hall acoustics. In: *Conf. Proc. MCHA 1995*, ed. by Y. Ando, D. Noson (Academic, London 1997) pp. 117–123, Chap. 12

10.16 T. Hotehama, S. Sato, Y. Ando: Dissimilarity judgments in relation to temporal and spatial factors for the sound fields in an existing hall, J. Sound Vibr. **258**, 429–441 (2002)

10.17 H. Sakai, P.K. Singh, Y. Ando: Inter-individual differences in subjective preference judgments of sound fields. In: *Music and Concert Hall Acoustics, Conf. Proc. MCHA 1995*, ed. by Y. Ando, D. Noson (Academic, London 1997) pp. 125–130, Chap 13

10.18 M. Sakurai, Y. Korenaga, Y. Ando: A sound simulation system for seat selection. In: *Music and Concert Hall Acoustics, Conf. Proc. MCHA 1995*, ed. by Y. Ando, D. Noson (Academic, London 1997) pp. 51–59, Chap. 6

10.19 Y. Ando: Evoked potentials relating to the subjective preference of sound fields, Acustica **76**, 292–296 (1992)

10.20 S. Sato, K. Nishio, Y. Ando: Propagation of alpha waves corresponding to subjective preference from the right hemisphere to the left with change in the IACC of a sound field, J. Temporal Des. Architect. Environ. **3**, 60–69 (2003)

10.21 Y. Soeta, S. Nakagawa, M. Tonoike, Y. Ando: Magnetoencephalographic responses corresponding to individual subjective preference of sound fields, J. Sound Vibr. **258**, 419–428 (2002)

10.22 Y. Soeta, S. Nakagawa, M. Tonoike, Y. Ando: Spatial analysis of magnetoencephalographic alpha waves in relation to subjective preference of a sound field, J. Temporal Des. Architect. Environ. **3**, 28–35 (2003)

10.23 L.A. Jeffress: A place theory of sound localization, J. Comp. Physiol. Psychol. **41**, 35–39 (1948)

10.24 J.C.R. Licklider: A duplex theory of pitch perception, Experientia **7**, 128–134 (1951)

10.25 Y. Ando, K. Yamamoto, H. Nagamastu, S.H. Kang: Auditory brainstem response (ABR) in relation to the horizontal angle of sound incidence, Acoust. Lett. **15**, 57–64 (1991)

10.26 H.E. Secker-Walker, C.L. Searle: Time domain analysis of auditory-nerve-fiber firing rates, J. Acoust. Soc. Am. **88**, 1427–1436 (1990)

10.27 P.A. Cariani, B. Delgutte: Neural correlates of the pitch of complex tones. I. Pitch and pitch salience, J. Neurophysiol. **76**, 1698–1716 (1996)

10.28 P.A. Cariani, B. Delgutte: Neural correlates of the pitch of complex tones. II. Pitch shift, pitch ambiguity, phase-invariance, pitch circularity, and the dominance region for pitch, J. Neurophysiol. **76**, 1717–1734 (1996)

10.29 M. Inoue, Y. Ando, T. Taguti: The frequency range applicable to pitch identification based upon the auto-correlation function model, J. Sound Vibr. **241**, 105–116 (2001)

10.30 S. Sato, T. Kitamura, H. Sakai, Y. Ando: The loudness of "complex noise" in relation to the factors extracted from the autocorrelation function, J. Sound Vibr. **241**, 97–103 (2001)

10.31 K. Saifuddin, T. Matsushima, Y. Ando: Duration sensation when Listening to pure tone and complex tone, J. Temporal Des. Architect. Environ. **2**, 42–47 (2002)

10.32 Y. Ando, H. Sakai, S. Sato: Formulae describing subjective attributes for sound fields based on

Amazon
EX1010 Page 398

a model of the auditory-brain system, J. Sound Vibr. **232**, 101–127 (2000)
10.33 Y. Ando: A theory of primary sensations measuring environmental noise, J. Sound Vibr. **241**, 3–18 (2001)
10.34 Y. Ando, Y. Kurihara: Nonlinear response in evaluating the subjective diffuseness of sound field, J. Acoust. Soc. Am. **80**, 833–836 (1986)
10.35 Y. Ando, S.H. Kang, H. Nagamatsu: On the auditory-evoked potentials in relation to the IACC of sound field, J. Acoust. Soc. Jpn. (E) **8**, 183–190 (1987)
10.36 Y. Ando, S. Sato, H. Sakai: Fundamental subjective attributes of sound fields based on the model of auditory – brain system. In: *Computational Acoustics in Architecture*, ed. by J.J. Sendra (WIT, Southampton 1999)
10.37 Y. Ando, R. Pompoli: Factors to be measured of environmental noise and its subjective responses based on the model of auditory-brain system, J. Temporal Des. Architect. Environ. **2**, 2–12 (2002)
10.38 S. Sato, Y. Ando, V. Mellert: Cues for localization in the median plane extracted from the autocorrelation function, J. Sound Vibr. **241**, 53–56 (2001)
10.39 Y. Ando, T. Okano, Y. Takezoe: The running autocorrelation function of different music signals relating to preferred temporal parameters of sound fields, J. Acoust. Soc. Am. **86**, 644–649 (1989)
10.40 Y. Ando, K. Kageyama: Subjective preference of sound with a single early reflection, Acustica **37**, 111–117 (1977)
10.41 K. Kato, Y. Ando: A study of the blending of vocal music with the sound field by different singing styles, J. Sound Vibr. **258**, 463–472 (2002)
10.42 K. Kato, K. Fujii, K. Kawai, Y. Ando, T. Yano: *Blending vocal music with the sound field – the effective duration of autocorrelation function of Western professional singing voices with different vowels and pitches, Proc. Int. Symp. Musical Acoust., ISMA* (Acoustical Society of Japan, Kyoto 2004) pp. 37–40
10.43 Y. Ando, M. Sakamoto: Superposition of geometries of surface for desired directional reflections in a concert hall, J. Acoust. Soc. Am. **84**, 1734–1740 (1988)
10.44 Y. Ando: Investigations on cerebral hemisphere activities related to subjective preference of the sound field, published for 1983 – 2003, J. Temporal Design Architect. Environ. **3**, 2–27 (2003)
10.45 S. Sato, K. Nishio, Y. Ando: Propagation of alpha waves corresponding to subjective preference from the right hemisphere to the left with change in the IACC of a sound field, J. Temporal Des. Architect. Environ. **3**, 60–69 (2003)
10.46 K. Mouri, K. Akiyama, Y. Ando: Preliminary study on recommended time duration of source signals to be analyzed, in relation to its effective duration of autocorrelation function, J. Sound Vibr. **241**, 87–95 (2001)
10.47 T. Taguti, Y. Ando: Characteristics of the short-term autocorrelation function of sound signals in piano performances. In: *Music and Concert Hall Acoustics, Conf. Proc. MCHA 1995*, ed. by Y. Ando, D. Noson (Academic, London 1997) pp. 233–238, Chap. 23
10.48 Y. Ando, S.H. Kang, Morita: On the relationship between auditory-evoked potentials and subjective preference for sound field, J. Acoust. Soc. Jpn. (E) **8**, 197–204 (1987)
10.49 Y. Ando, S.H. Kang, H. Nagamatsu: On the auditory-evoked potential in relation to the IACC of sound field, J. Acoust. Soc. Jpn. (E) **8**, 183–190 (1987)
10.50 Y. Ando, C. Chen: On the analysis of autocorrelation function of α-waves on the left and right cerebral hemispheres in relation to the delay time of single sound reflection, J. Architect. Planning Environ. Eng., Architectural Institute of Japan (AIJ) **488**, 67–73 (1996), (in Japanese)
10.51 C. Chen, Y. Ando: On the relationship between the autocorrelation function of the α-waves on the left and right cerebral hemispheres and subjective preference for the reverberation time of music sound field, J. Architect. Planning Environ. Eng., Architectural Institute of Japan (AIJ) **489**, 73–80 (1996), (in Japanese)
10.52 Y. Soeta, S. Nakagawa, M. Tonoike, Y. Ando: Magnetoencephalographic responses corresponding to individual subjective preference of sound fields, J. Sound Vibr. **258**, 419–428 (2002)
10.53 Y. Soeta, S. Nakagawa, M. Tonoike, Y. Ando: Spatial analysis of magnetoencephalographic alpha waves in relation to subjective preference of a sound field, J. Temporal Des. Architect. Environ. **3**, 28–35 (2003)
10.54 D. Kimura: The asymmetry of the human brain, Sci. Am. **228**, 70–78 (1973)
10.55 R.W. Sperry: Lateral specialization in the surgically separated hemispheres. In: *The Neurosciences: Third study program*, ed. by F.O. Schmitt, F.C. Worden (MIT, Cambridge 1974), Chap. 1
10.56 J.H. Holland: *Adaptation in Natural and Artificial Systems* (Univ. Michigan Press, Ann Arbor 1975)
10.57 S. Sato, K. Otori, A. Takizawa, H. Sakai, Y. Ando, H. Kawamura: Applying genetic algorithms to the optimum design of a concert hall, J. Sound Vibr. **258**, 517–526 (2002)
10.58 S. Sato, T. Hayashi, A. Takizawa, A. Tani, H. Kawamura, Y. Ando: Acoustic design of theatres applying genetic algorithms, J. Temporal Des. Architect. Environ. **4**, 41–51 (2004)
10.59 H. Sakai, P. K. Singh, Y. Ando: Inter-individual differences in subjective preference judgments of sound fields. In: *Music and Concert Hall Acoustics, Conf. Proc. MCHA 1995*, ed. by Y. Ando, D. Noson (Academic, London 1997), Chap. 13
10.60 F. Maki: Sound and figure: concert hall design. In: *Music and Concert Hall Acoustics, Conf. Proc. MCHA 1995*, ed. by Y. Ando, D. Noson (Academic, London 1997), Chap. 1

Amazon
EX1010 Page 399

10.61 Y. Ikeda: Designing a contemporary classic concert hall using computer graphics. In: *Music and Concert Hall Acoustics, Conf. Proc. MCHA 1995*, ed. by Y. Ando, D. Noson (Academic, London 1997), Chap. 2

10.62 I. Nakayama: Preferred time delay of a single reflection for performers, Acustica **54**, 217–221 (1984)

10.63 I. Nakayama, T. Uehara: Preferred direction of a single reflection for a performer, Acustica **65**, 205–208 (1988)

10.64 J. Meyer: *Influence of Communication on Stage on the Musical Quality* (Proc. 15th Int. Congress Acoustics, Trondheim 1995) pp. 573–576

10.65 Y. Ando, B. P. Johnson, T. Bosworth: Theory of planning physical environments incorporating spatial and temporal values, Memoir of Graduate School Science and Technology **14-A**, 67–92 (1996)

10.66 Y. Ando: On the temporal design of environments, J. Temporal Des. Architect. Environ. **4**, 2–14 (2004)

10.67 Y. Ando, S. Sato, T. Nakajima, M. Sakurai: Acoustic design of a concert hall applying the theory of subjective preference, and the acoustic measurement after construction, Acustica Acta Acustica. **83**, 635–643 (1997)

10.68 T. Nakajima, Y. Ando: Calculation and measurement of acoustic factors at each seat in the Kirishima International Concert Hall. In: *Music and Concert Hall Acoustics, Conf. Proc. MCHA 1995*, ed. by Y. Ando, D. Noson (Academic, London 1997), Chap. 5

10.69 M.R. Schroeder: *Number Theory in Science and Communication* (Springer, Berlin, Heidelberg 1984)

10.70 P.M. Morse: *Vibration and Sound* (McGraw-Hill, New York 1948)

10.71 Y. Ando, P.K. Singh: Global subjective evaluations for design of sound fields and individual subjective preference for seat selection. In: *Music and Concert Hall Acoustics, Conf. Proc. MCHA 1995*, ed. by Y. Ando, D. Noson (Academic, London 1997), Chap. 4

10.72 A.H. Marshall, D. Gottlob, H. Alrutz: Acoustical conditions preferred for ensemble, J. Acoust. Soc. Am. **64**, 1437–1442 (1978)

10.73 A.C. Gade: Investigations of musicians' room acoustic conditions in concert halls. Part I: Methods and laboratory experiments, Acustica **69**, 193–203 (1989)

10.74 D. Noson, S. Sato, H. Sakai, Y. Ando: Singer responses to sound fields with a simulated reflection, J. Sound Vibr. **232**, 39–51 (2000)

10.75 D. Noson, S. Sato, H. Sakai, Y. Ando: Melisma singing and preferred stage acoustics for singers, J. Sound Vibr. **258**, 473–485 (2002)

10.76 S. Sato, S. Ohta, Y. Ando: Subjective preference of cellists for the delay time of a single reflection in a performance, J. Sound Vibr. **232**, 27–37 (2000)

10.77 H.P. Seraphim: Über die Wahrnehmbarkeit mehrerer Rückwürfe von Sprachschall, Acustica **11**, 80–91 (1961)

10.78 N. Aoshima: Computer-generated pulse signal applied for sound measurement, J. Acoust. Soc. Am. **69**, 1484–1488 (1981)

10.79 C. Hayashi: Multidimensional quantification I., Proc. Jpn. Acad. **30**, 61–65 (1954)

10.80 C. Hayashi: Multidimensional quantification II., Proc. Jpn. Acad. **30**, 165–169 (1954)

10.81 V.L. Jordan: Acoustical criteria for auditoriums and their relation to model techniques, J. Acoust. Soc. Am. **47**, 408–412 (1969)

10.82 T. Hidaka: Personal communication (1996)

10.83 Y. Kobayasi, H. Tokuhiro, M. Owaki, K. Okuno, S. Yamada, Y. Ando: Acoustical design and characteristics of the atrium for music performance in a hotel. In: *Music and Concert Hall Acoustics, Conf. Proc. MCHA 1995*, ed. by Y. Ando, D. Noson (Academic, London 1997), Chap. 27

10.84 S. Sato, Y. Mori, Y. Ando: The subjective evaluation of source locations on the stage by listeners. In: *Music and Concert Hall Acoustics, Conf. Proc. MCHA 1995*, ed. by Y. Ando, D. Noson (Academic, London 1997), Chap. 12

10.85 L.L. Thurstone: A law of comparative judgment, Psychol. Rev **34**, 273–289 (1951)

10.86 F. Mosteller: Remarks on the method of paired comparison, III. Psychometrika **16**, 207–218 (1951)

10.87 C. Hayashi: On the prediction of phenomena from qualitative data and the quantification of qualitative data from the mathematico-statistical point of view, Ann. Inst. Statist. Math., 69–98 (1952)

Amazon
EX1010 Page 400

11. Building Acoustics

This chapter summarizes and explains key concepts of building acoustics. These issues include the behavior of sound waves in rooms, the most commonly used rating systems for sound and sound control in buildings, the most common noise sources found in buildings, practical noise control methods for these sources, and the specific topic of office acoustics. Common noise issues for multi-dwelling units can be derived from most of the sections of this chapter. Books can be and have been written on each of these topics, so the purpose of this chapter is to summarize this information and provide appropriate resources for further exploration of each topic.

11.1 **Room Acoustics** 387
11.1.1 Room Modes 388
11.1.2 Sound Fields in Rooms 389
11.1.3 Sound Absorption 390
11.1.4 Reverberation 394
11.1.5 Effects of Room Shapes 394
11.1.6 Sound Insulation 395

11.2 **General Noise Reduction Methods** 400
11.2.1 Space Planning 400
11.2.2 Enclosures 400
11.2.3 Barriers 402
11.2.4 Mufflers 402
11.2.5 Absorptive Treatment 402
11.2.6 Direct Impact and Vibration Isolation 402
11.2.7 Active Noise Control 402
11.2.8 Masking 403

11.3 **Noise Ratings for Steady Background Sound Levels** 403

11.4 **Noise Sources in Buildings** 405
11.4.1 HVAC Systems 405
11.4.2 Plumbing Systems 406
11.4.3 Electrical Systems 406
11.4.4 Exterior Sources 406

11.5 **Noise Control Methods for Building Systems** 407
11.5.1 Walls, Floor/Ceilings, Window and Door Assemblies 407
11.5.2 HVAC Systems 412
11.5.3 Plumbing Systems 415
11.5.4 Electrical Systems 416
11.5.5 Exterior Sources 417

11.6 **Acoustical Privacy in Buildings** 419
11.6.1 Office Acoustics Concerns 419
11.6.2 Metrics for Speech Privacy 419
11.6.3 Fully Enclosed Offices 422
11.6.4 Open-Plan Offices 422

11.7 **Relevant Standards** 424

References 425

11.1 Room Acoustics

When a sound wave in a room encounters a boundary surface, some of its energy is reflected back into the room, as illustrated in Fig. 11.1. The physical laws regarding reflected sound energy are analogous to those for the laws of optics. Just as light bounces off a mirror at the same angle as its angle of incidence, sound waves have equal angles of incidence and reflection. Acoustically reflective surfaces are typically smooth and hard.

Some common room acoustics problems caused by reflection are echoes and room resonance. Echoes result from the limitations of our hearing mechanisms to process sounds. When the difference in arrival times between two sounds is less than 60 ms, we hear the combination of the two sounds as a single sound. However, when this difference exceeds 60 ms, we hear the two distinct sounds (Fig. 11.2). When these two sounds are generated by the same source, this effect (which is called an echo) can cause difficulty in understanding speech, especially when arrival times differ by more than 100 ms. These kinds of delays occur when a person hears a sound wave coming directly from a source and another coming from a reflecting surface. Given that the speed of sound in air is roughly 300 m per second, the 100 ms delay translates to a distance of roughly 30 m. There-

Amazon
EX1010 Page 401

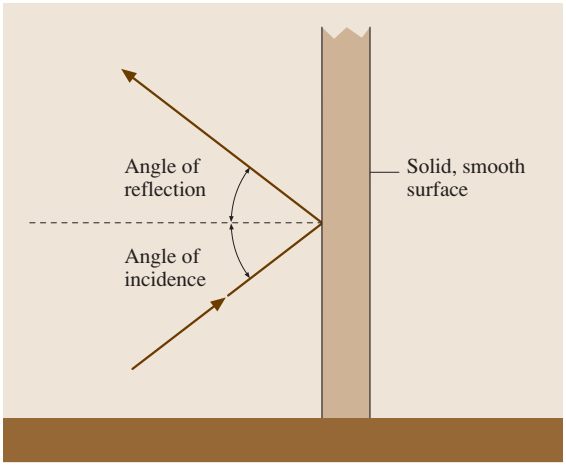


Fig. 11.1 Reflection of a sound wave off a hard, smooth surface

fore, a difference in sound travel path of more than 30 m between a sound wave traveling directly from a source to a listener and a sound wave traveling from a source to a reflecting surface and then to a listener causes an echo.

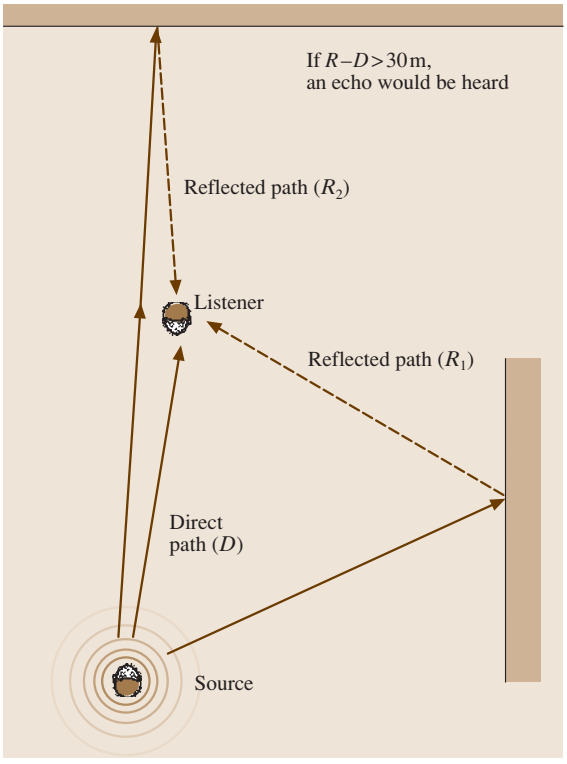


Fig. 11.2 Generation of an echo

When parallel reflective surfaces are tall and more than 10 m from each other, a rapid succession of mid-frequency echoes can occur, known as flutter echo, resulting in a flapping sound similar to that generated by birds or bats. When these surfaces are fairly close to each other, as in a narrow hallway or stairwell, flutter echo sounds more like a high-pitched buzzing since the smaller spacing accommodates higher frequencies (shorter wavelengths).

Echoes are normally perceived as discrete reflections that can be clearly heard and identified, but many reflections off all surfaces within a room can combine to produce the phenomenon known as reverberation. Reverberation can raise the sound level in a room and can also reduce speech intelligibility, but it is desirable for certain types of music. More discussion on reverberation and its control can be found later in this chapter.

11.1.1 Room Modes

Room modes occur at specific frequencies when two reflective walls are parallel to each other. Since the surfaces reflect the sound, their mirror images reflect off each wall to set up a stationary pressure pattern in a room. This phenomenon is called a single-dimensional (or axial) standing wave, as shown in Fig. 11.3, and it is the simplest form of room modes.

Axial standing waves occur at frequencies described by the equation below:

$$f_n = nc/2d\,, \tag{11.1}$$

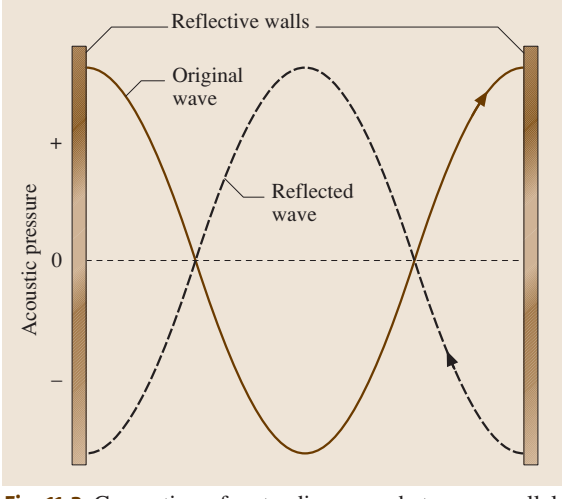


Fig. 11.3 Generation of a standing wave between parallel, reflective surfaces

Amazon
EX1010 Page 402

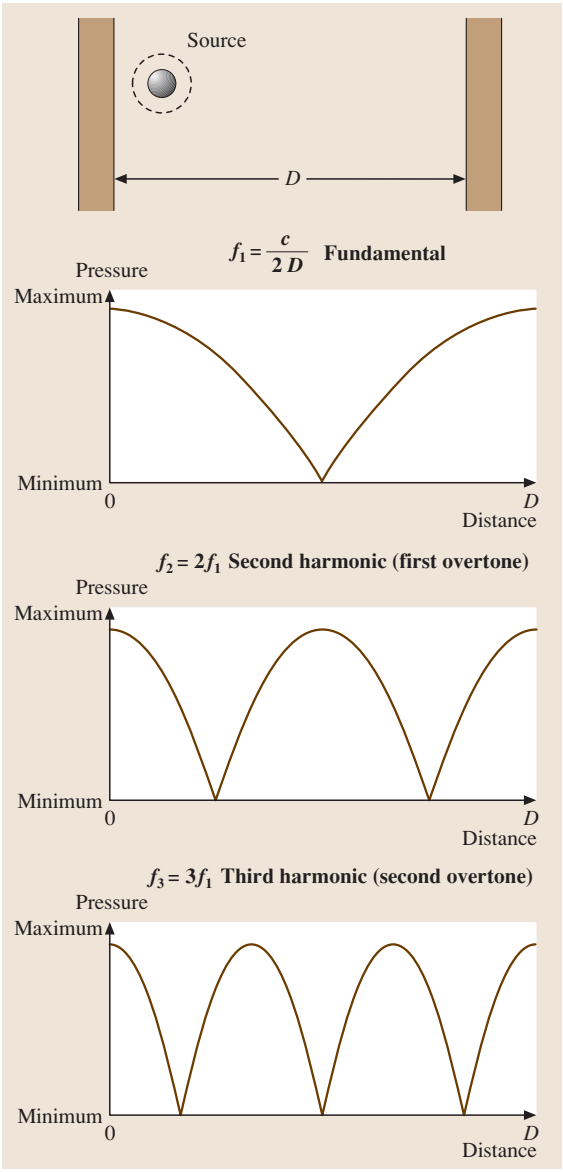


Fig. 11.4 Pressure patterns of the lowest axial standing wave modes in a room with parallel reflective surfaces

where $n = 1, 2, 3, \ldots$, c is the speed of sound, and d is the distance between the parallel reflective surfaces. This means that axial standing wave room modes occur at integer multiples of specific 1/2-wavelengths of sound, as is shown in Fig. 11.4. Standing waves can become more complex in two and three dimensions, where they are known as tangential and oblique modes, respectively.

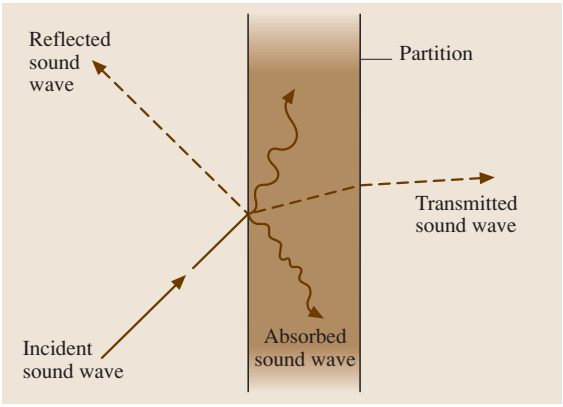


Fig. 11.5 The interaction of a sound wave with a partition

A design problem with standing waves is that they generate uneven sound distribution patterns. Some areas will have higher levels of sound (because a standing wave is reinforcing the pressure at those locations) and some areas will have lower levels of sound (because the standing wave is canceling much of the pressure at those locations), but only at specific frequencies.

The topic of building acoustics stresses the importance of controlling sound. When one talks about controlling sound, it is often assumed that one is referring to the reduction of sound. However, there are cases (e.g., auditorium or concert hall design) in which we want to preserve the sound energy but we would like to control its spatial spreading characteristics. The primary ways to reduce sound are through absorption and insulation. Using absorption on an auditorium's side walls may eliminate unwanted reflections but may also eliminate the possibility of some people hearing sound coming from the stage. We therefore must clarify how we plan to control the sound. Redirection and diffusion can have favorable acoustic results for even sound distribution in large rooms.

Discussions about noise control usually refer to the reduction of sound (since noise is defined as unwanted sound). Figure 11.5 shows what happens to a sound wave that interacts with a room's surface. Part is absorbed, part is redirected, and the rest is transmitted through the surface.

11.1.2 Sound Fields in Rooms

Several different fields, or acoustic environments, exist in all rooms. The size of these fields depends on the dimensions of the room, the reflective qualities of the room's surfaces, and the frequency of interest. The

Amazon
EX1010 Page 403

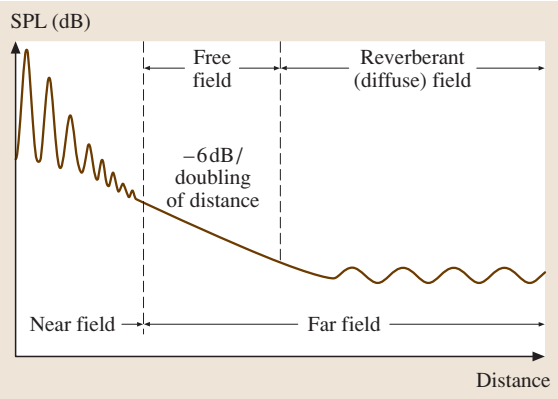


Fig. 11.6 Sound fields in rooms

near field is the region within 1/4-wavelength (of the lowest frequency of interest) of a sound source or large reflective surface. Sound pressure levels can fluctuate dramatically in the near field of a source and sound pressures cancel and enhance each other near large reflective surfaces, so sound pressure level measurements should be avoided in near fields.

The far field is the region beyond the near field. It is contrasted with the near field to designate the region that is appropriate for recording sound pressure level measurements from a sound source. As one moves out of the near field and into the far field, sound pressure levels drop off at a rate of 6 dB per doubling of distance, for a point source, in accordance with the inverse square law that is simplified in the following equation:

$$\mathrm{SPL}_2 = \mathrm{SPL}_1 - [20 \times \log(d_2/d_1)] \,, \qquad (11.2)$$

where SPL_1 is the sound pressure level at the location closer to the sound source, SPL_2 is the sound pressure level at the location farther from the sound source, d_1 is the distance from the source at which SPL_1 is measured, and d_2 is the distance from the source at which SPL_2 is measured.

The region in which (11.2) is valid is known as the free field. Free-field conditions exist in large open outdoor spaces or in rooms having highly absorptive surfaces, in which there are no obstructions in the sound travel path between the source and listener. The free field is sometimes referred to as the direct field when source measurements are taking place that only consider the sound wave traveling from the source to the listener with no influence by reflected sound coming from room surfaces.

As sound pressure levels decay from sources within a room, they eventually drop to a relatively constant level which is determined by the amount of reflected sound within a room. This lower limit is known as the reverberant or diffuse field. The size of the reverberant field depends on the size of the room and the size and characteristics of its reflective surfaces. Within the reverberant field, sound pressures are similar independent of location. Figure 11.6 puts all of the fields described above into perspective.

11.1.3 Sound Absorption

Absorption converts sound energy into heat energy. It is useful for reducing sound levels *within* rooms but not *between* rooms. Each material with which a sound wave interacts absorbs some sound. The most common measurement of that is the absorption coefficient, typically denoted by the Greek letter α. The absorption coefficient is a ratio of absorbed to incident sound energy. If a material does not absorb any sound incident upon it, its absorption coefficient is 0. In other words, a material with an absorption coefficient of 0 reflects all sound incident upon it. In practice, all materials absorb some sound, so this is a theoretical limit. If a material absorbs all sound incident upon it, its absorption coefficient is 1. As with the lower limit for absorption coefficients, all materials reflect some sound, so this is also a theoretical limit. Therefore, absorption coefficients range between 0 and 1.

Absorption coefficients vary with frequency. Typical absorptive materials are porous and characterized by absorption coefficients that increase with frequency. They therefore have limited effectiveness for lower frequencies, especially below 250 Hz. There are absorbers that have been designed to absorb these lower frequencies, and these will be discussed shortly. However, for typical cases, it is convenient to use a single number (incorporating multiple frequency components) to describe the absorption characteristics of a material. This value has been defined by the American Society for Testing and Materials (ASTM) in Standard C 423 as the noise reduction coefficient (NRC). The NRC is the arithmetic (as opposed to the logarithmic) average of a material's absorption coefficients at 250, 500, 1000, and 2000 Hz, rounded to the closest 0.05.

Table 11.1 lists absorption coefficients and NRC values for common materials. Note that the values listed in Table 11.1 are for general reference purposes only, and specific values should be based on manufacturers specifications. Also note that absorption coefficients and NRC values have no units associated with them. In general, materials with NRC values less than 0.20 are considered

Amazon
EX1010 Page 404

Table 11.1 Absorption coefficients and NRC values for common materials

Material	125 Hz	250 Hz	500 Hz	1000 Hz	2000 Hz	4000 Hz	NRC
Painted drywall	0.10	0.08	0.05	0.03	0.03	0.03	0.05
Plaster	0.02	0.03	0.04	0.05	0.04	0.03	0.05
Smooth concrete	0.10	0.05	0.06	0.07	0.09	0.08	0.05
Coarse concrete	0.36	0.44	0.31	0.29	0.39	0.25	0.35
Smooth brick	0.03	0.03	0.03	0.04	0.05	0.07	0.05
Glass	0.05	0.03	0.02	0.02	0.03	0.02	0.05
Plywood	0.58	0.22	0.07	0.04	0.03	0.07	0.10
Metal blinds	0.06	0.05	0.07	0.15	0.13	0.17	0.10
Thick panel	0.25	0.47	0.71	0.79	0.81	0.78	0.70
Light drapery	0.03	0.04	0.11	0.17	0.24	0.35	0.15
Heavy drapery	0.14	0.35	0.55	0.72	0.70	0.65	0.60
Helmholtz resonator	0.20	0.95	0.85	0.49	0.53	0.50	0.70
Ceramic tile	0.01	0.01	0.01	0.01	0.02	0.02	0.00
Linoleum	0.02	0.03	0.03	0.03	0.03	0.02	0.05
Carpet	0.05	0.05	0.10	0.20	0.30	0.40	0.15
Carpet on concrete	0.05	0.10	0.15	0.30	0.50	0.55	0.25
Carpet on rubber	0.05	0.15	0.13	0.40	0.50	0.60	0.30
Upholstered seats	0.19	0.37	0.56	0.67	0.61	0.59	0.55
Occupied seats	0.39	0.57	0.80	0.94	0.92	0.87	0.80
Water surface	0.01	0.01	0.01	0.01	0.02	0.03	0.00
Soil	0.15	0.25	0.40	0.55	0.60	0.60	0.45
Grass	0.11	0.26	0.60	0.69	0.92	0.99	0.60
Cellulose spray (1″)	0.08	0.29	0.75	0.98	0.93	0.76	0.75

to be reflective while those with NRC values greater than 0.40 are considered to be absorptive. When significant sound energy must be absorbed, as may be the case for eliminating echoes or standing waves, materials having higher absorption coefficients are usually recommended.

A few cautionary notes apply. NRC values are convenient to use for rating the absorption characteristics of a material. However, they should only be used when the sound sources of interest are within the 200–2000 Hz range. For sources outside of this range, and especially below this range, materials effective for the specific frequency of interest must be used. Also note that some manufacturers specify NRC and absorption coefficient values that are greater than 1.0. Methods used to measure absorption coefficients can artificially raise their values above 1.0; yet such values inaccurately imply that more energy is absorbed by a material than is incident upon it, which is a physical impossibility. Therefore, any published absorption coefficient or NRC values greater than 1.0 should be not be considered as greater than 1.0.

Another absorption metric gaining increasing application is the sound absorption average (SAA). The SAA is a single number rating that is the average, rounded off to the nearest 0.01, of the sound absorption coefficients of a material for the twelve one-third octave bands from 200 through 2500 Hz. Although the SAA replaces the NRC rating, as directed by the ASTM C 423 since the year 2000, most product literature still uses NRC values.

The method by which these materials are mounted affects their sound absorption effectiveness, especially for low frequencies (below 500 Hz). Figure 11.7 shows

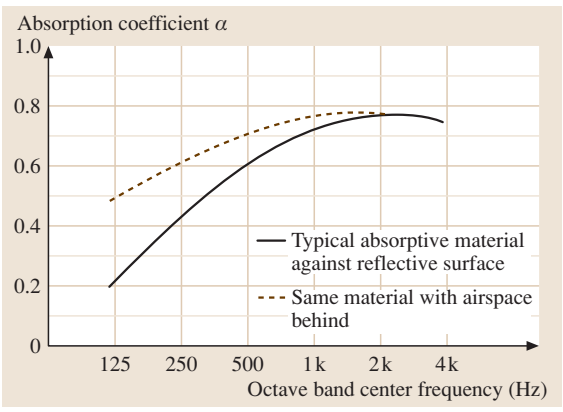


Fig. 11.7 The general effect of an air space between absorptive material and its mounting surface

Amazon
EX1010 Page 405

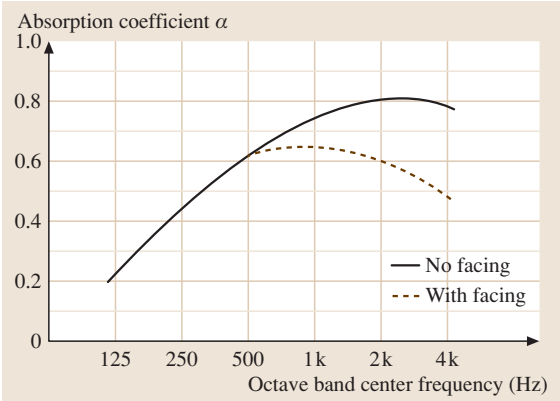


Fig. 11.8 The general effect of non-acoustically transparent facings on absorption

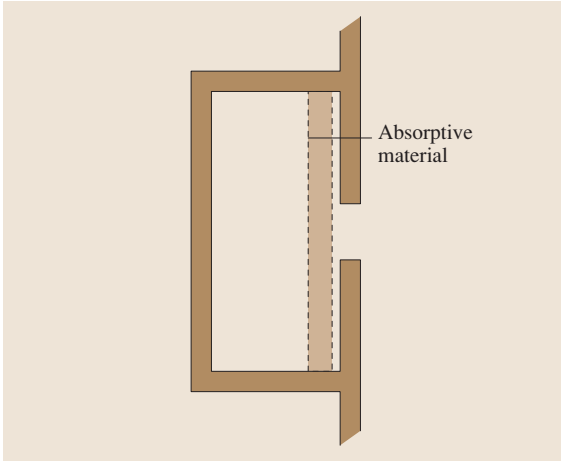


Fig. 11.10 Cross section of a Helmholtz resonator concrete masonry unit. The absorptive material helps to spread the absorptive properties over a larger frequency range than would otherwise occur

the effect of air spaces between an absorptive material and a mounting surface.

Facings on absorptive materials can degrade their absorptive properties, especially for higher frequencies (above 2000 Hz). Acoustically transparent facings, such as grill cloth and open-weave fabrics, will have little effect on absorption properties, but facing materials that are not acoustically transparent, such as perforated metal and wood slats, can produce the kind of effects shown in Fig. 11.8.

Of critical importance with these facings is the open area ratio. Since there are so many perforated metal designs, it is best to check with the manufacturer for the most appropriate opening ratio and design for the situation. Figure 11.9, however, offers some guidelines for wood-slat ceiling designs.

As Table 11.1 shows, the absorption coefficients of most porous materials increase with increasing frequency. This means that they are not as effective at low frequencies as at higher ones. If absorption is required for frequencies below 250 Hz, special materials must be used. Each of these materials has an air space behind its light or open surface to provide the extra absorption. Two common materials used for this purpose are Helmholtz resonators and diaphragmatic absorbers. Helmholtz resonators have narrow openings that lead to the outside on one end and into a larger air cavity on the other, as is shown in Fig. 11.10.

As viewed by an incoming sound wave, the air in the narrow neck functions as a mass and the air in the larger cavity functions as a spring. A mass on a spring will resonate at a frequency appropriate to that mass

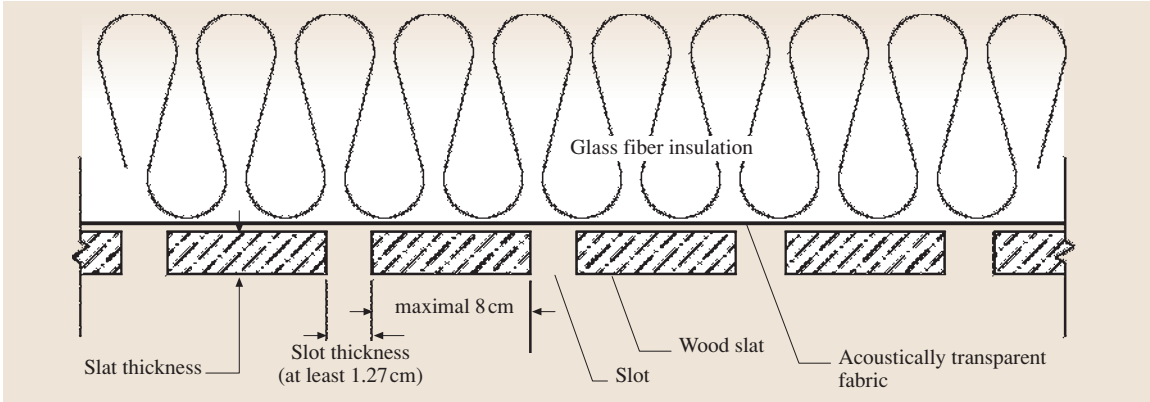


Fig. 11.9 General design guidelines for absorptive wood-slat ceilings

Amazon
EX1010 Page 406

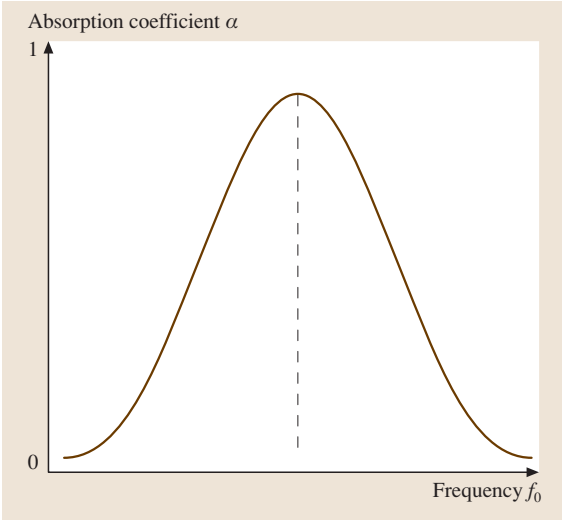


Fig. 11.11 General absorption characteristics of Helmholtz resonators not filled with absorptive material

and spring stiffness. Thus, at and near the resonant frequency of such an acoustic chamber, sound will be absorbed from an incoming sound wave, as is shown in Fig. 11.11.

Such devices incorporated in wall constructions are usually resonant below 250 Hz, depending on the dimensions of the neck and size of the cavity. There are commercially available products that incorporate this design into concrete masonry units. When viewing these products installed as partitions, the wall surfaces have slots in them, as are shown in Fig. 11.12. Table 11.1 has a listing for these products which shows their superior absorption in a narrow low-frequency range. The porous and coarse nature of the surface provides modest absorption at higher frequencies also.

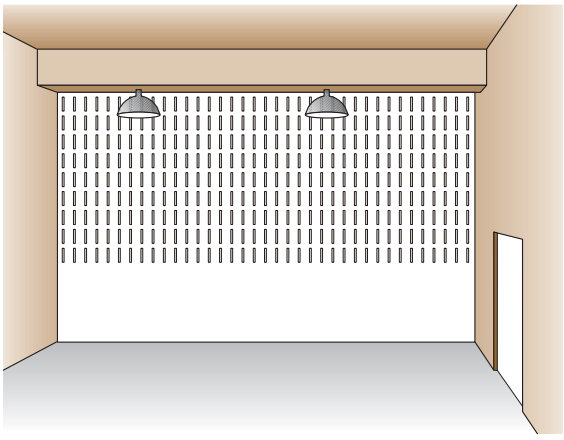


Fig. 11.12 Wall built from Helmholtz resonator concrete masonry units

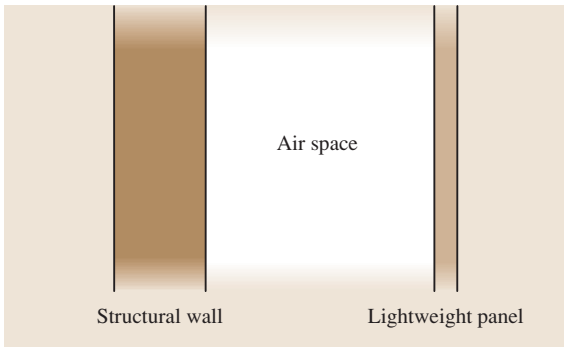


Fig. 11.13 Cross section of a generalized diaphragmatic absorber

Diaphragmatic absorbers work according to similar principles to Helmholtz resonators, except they are comprised of an air space behind a lightweight wall, as shown in Fig. 11.13.

Reverberant Field Noise Reduction

Adding absorptive materials to a room's surfaces, in addition to reducing or eliminating echoes and standing waves, can reduce the overall reverberant field noise level within a room. The mathematical basis for this is to determine the total absorption for all of a room's surfaces using the following equation:

$$A = \sum_{i=1}^{n} \alpha_i S_i = \alpha_1 S_1 + \alpha_2 S_2 + \ldots + \alpha_n S_n \,, \quad (11.3)$$

where α_1, α_2, etc., are the absorption coefficients of each surface material in the room while S_1, S_2, etc. are the surface areas corresponding to the surfaces having the same subscript value as those for the absorption coefficients. The total absorption (A) is in units of sabins, for which one sabin is defined as the total absorption provided by a one square foot piece of material having an absorption coefficient of 1.

The reverberant field noise reduction is defined as

$$\mathrm{NR} = 10 \times \log(A_2/A_1) \,, \quad (11.4)$$

where A_1 is the total absorption within a room before absorptive treatment is applied and A_2 is the total absorption within that same room after absorptive treatment is applied. The practical limits of NR are 12–15 dBA with typical cases yielding 6–8 dBA of noise reduction

Amazon
EX1010 Page 407

within a room from the proper use of absorptive materials. Bear in mind that this will not reduce sound pressure levels close to a source but will only reduce reflected sound pressure levels, which limits the effectiveness of the noise reduction to locations in a room's reverberant field.

11.1.4 Reverberation

Absorption is useful in reducing or eliminating unwanted reflections off surfaces. The standing waves discussed in Sect. 11.1.1 can be eliminated by covering one of the parallel surfaces with absorptive material. Absorption can also be used to eliminate echoes. The rear walls of auditoriums are prime candidates for absorptive materials since rear walls have the greatest potential to cause echoes. The most common use of absorption, however, is to control reverberation.

Reverberation is the build up of sound within a room resulting from repeated sound wave reflections off all of its surfaces. Reverberation can increase sound levels within a room by up to 15 dBA, as well as distort speech intelligibility. Reverberation is desirable for rooms in which music is being played, especially classical and cathedral-style music, to add a pleasant persistence to the sounds. Therefore, there are different reverberation characteristics that would be appropriate for different room uses.

Reverberation is described by a parameter known as the reverberation time (denoted RT_{60}). RT_{60} can be defined in two ways – physically and mathematically. Physically, RT_{60} is the time (in seconds) that it takes for a sound source to reduce in sound pressure level (within a room) by a factor of 60 dB after that sound source has been silenced. Mathematically, in what is known as the sabine equation, RT_{60} is directly proportional to the volume of a room and inversely proportional to the absorption of the materials in the room, as follows:

$$RT_{60} = 0.161 \cdot V/A \,, \tag{11.5}$$

where V is the room volume in cubic meters and A is the total absorption of the room's surfaces in metric sabins.

This means that RT_{60} increases as the size of a room increases and as the absorption of the room's surfaces decreases. Conversely, RT_{60} decreases as the size of a room decreases and as the absorption of the room's surfaces increases. There are then two principal ways to control RT_{60}: (1) by changing a room's size and (2) by changing the amount of absorption on its surfaces. Although it is possible to reduce a large room's volume by dividing the space with walls, it is more practical to adjust RT_{60} by adding sound absorptive materials.

Table 11.2 Optimum mid-frequency RT_{60} values for various occupied facilities

Type of facility	Optimum mid-frequency RT_{60} (s)
Broadcast studio	0.5
Classroom	1.0
Lecture/conference room	1.0
Movie/drama theater	1.0
Multipurpose auditorium	1.3 to 1.5
Contemporary church	1.4 to 1.6
Rock concert hall	1.5
Opera house	1.4 to 1.6
Symphony hall	1.8 to 2.0
Cathedral	3.0 or higher

Since the absorption performance of materials varies with frequency, so does RT_{60}. Table 11.2 offers generally accepted ranges of RT_{60} for different uses in the mid-frequency (500–1000 Hz) range. As you can see from the table, lower RT_{60} values are desirable for rooms used mainly for human speech and higher RT_{60} values are desirable for rooms used mainly for music. The optimum mid-frequency RT_{60} for a fully occupied room is different for various types of music. Because contemporary orchestral repertoires emphasize late classical and romantic music, the optimum mid-frequency RT_{60} for a fully occupied concert hall is usually stated as 1.8–2.0 s.

Optimum RT_{60} values generally increase by 10% of the values in Table 11.2 for each halving of frequency below 500 Hz and decrease by 10% of the values in Table 11.2 for each doubling of frequency above 1000 Hz. A room with a low (less than 0.8 s) RT_{60} is called a *dead* room and a room with a high (greater than 1.7 s) RT_{60} is called a *live* room. Multipurpose facilities should have RT_{60} values between the live and dead range limits.

Note that the sabine equation is based on the assumption that the absorptive properties of the surface materials are spread evenly throughout the room. When this is clearly not the case, other (more complex) RT_{60} calculation methods would be more appropriate.

11.1.5 Effects of Room Shapes

Although absorption is necessary in many circumstances, eliminating reflections is not always useful. This

Amazon
EX1010 Page 408

is of key importance in rooms where an audience is listening to a performance or lecture. In this type of room, it is desirable that all audience members hear the sound not only clearly, but without preference to seating location. Without an electronic sound system, this can only be accomplished by reflections off side walls and ceilings. Discrete echoes can be eliminated by avoiding smooth, flat reflective surfaces and by having irregular and convex surfaces to diffuse the sound evenly throughout the audience. For smaller rooms such as recording studios that require diffusion, commercially available sound-diffusing panels called quadratic residue diffusers are available. These panels can also be used for larger spaces, as well as irregularly shaped surfaces.

Concave reflective surfaces focus sound in certain areas and defocus sound from others, causing hot spots where sound is concentrated and dead spots where sound cannot be heard. Concave reflective surfaces should be avoided for this reason. If aesthetics dictate the need for a concave surface, it would be best to install an absorptive or diffusive surface (as needed) and cover it with acoustically transparent fabric in the concave shape.

Reflective rear walls in auditoriums are notorious for generating echoes because of their associated large sound travel path differences. For this reason, reflective surfaces should be avoided for rear walls. Reflective surfaces are beneficial, especially for concert halls, when they are close to the stage and along side walls. Reflective surfaces close to the stage assist in several ways, by sending sound into the audience rather than allowing it to be lost behind the stage and by enhancing the sound through lateral reflections off side walls to spread the sound more evenly throughout an audience. Another benefit of reflective surfaces near the stage is that they permit the performers to hear each other, something that is critical to concert performances. These so-called early reflections are usually generated by shells on the stage or by hanging reflective panels.

11.1.6 Sound Insulation

The description of the insulation of sound is similar in many ways to the description of the absorption of sound. As with absorption, there is a transmission coefficient that ranges from the ideal limits of 0 to 1. The transmission coefficient, denoted by the Greek letter τ, is the unitless ratio of transmitted to incident sound energy. Unlike the absorption coefficient, however, the limit of $\tau = 1$ is possible in practice since a transmission coefficient of 1 implies that all of the sound energy is transmitted through a partition. This would be the case

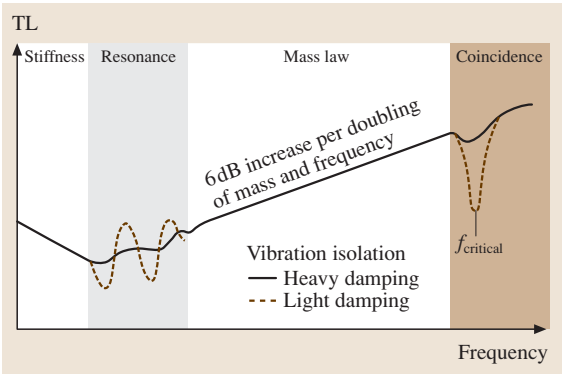


Fig. 11.14 General characteristics of the transmission loss spectrum

for an open window or door, where the sound energy has no obstruction to its path. The other extreme of $\tau = 0$ (implying no sound transmission), however, is not a practical value since some sound will always transmit through a partition.

Unlike absorption, the principal descriptor for sound insulation is a decibel level based on the transmission coefficient. This value is known as the transmission loss (TL), and is based on the following equation:

$$\mathrm{TL} = 10 \cdot \log(1/\tau)\,. \tag{11.6}$$

The transmission loss can be loosely defined as the amount of sound reduced by a partition between a sound source and a listener. The complete sound reduction of a partition between two rooms also takes into account the absorptive characteristics of the listener's room, as follows:

$$\mathrm{SPL_S} - \mathrm{SPL_L} = \mathrm{TL} + 10 \cdot \log(A_\mathrm{L}/S)\,, \tag{11.7}$$

where $\mathrm{SPL_S}$ is the average sound pressure level in the room enclosing the sound source, $\mathrm{SPL_L}$ is the average sound pressure level in the adjacent listener's room, A_L is the total absorption in the listener's room, TL is the transmission loss of the partition between the two rooms, and S is the surface area of the partition between the two rooms. Note that TL is the quantity that is typically reported in manufacturers' literature since it is measured in a laboratory independent of the installation.

Since the logarithm of 1 is 0, the condition in which the transmission coefficient is 1 translates to a TL of 0 dB. This concurs with the notion that an open air space in a wall allows the free passage of sound. Although an open air space itself would have a TL value of 0 dB associated with it, a wall with an open air space in it

Amazon
EX1010 Page 409

Table 11.3 Critical frequencies for common building materials

Material	Thickness (cm)	Critical frequency (Hz)
Concrete	8	100
Plywood	1.2	1700
Gypsum wall board	1.2	3100
Steel or aluminum	0.3	4100
Lead	1.2	4400
Glass	0.3	4900
Plexiglass	0.3	9800

would have a TL value greater than 0 (up to 10) dB, depending on the size of the opening and the location with respect to the wall. The practical upper limit of TL is roughly 70 dB.

As for absorption, TL is frequency dependent. Typical partitions have TL values that increase with increasing frequency, as is shown in Fig. 11.14, with the exception of a dip in TL around a bending wave resonance frequency, known as the critical frequency. This effect is known as the coincidence dip. The extent of this dip depends on the vibrational damping of the partition and the frequency at which it occurs depends on the density and thickness of the material.

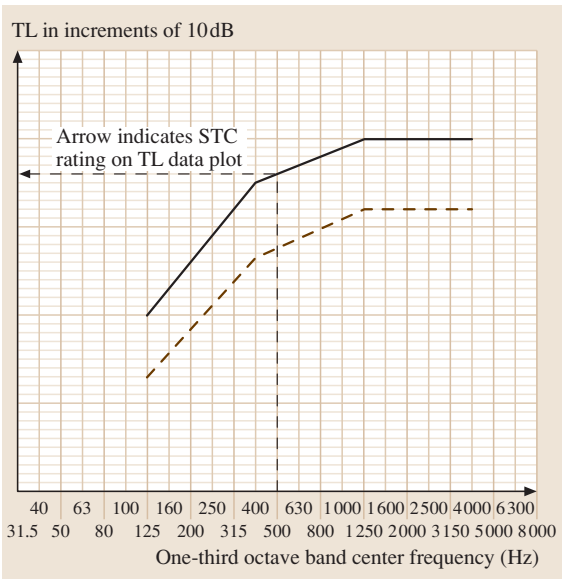


Fig. 11.15 The standard STC calculation curve, from ASTM E 413. STC values are derived by plotting the TL spectrum on this curve and determining the highest curve shape that meets the criteria of: (1) the sum of the differences between individual TL values and the *solid line* is less than 32 dB and (2) no individual 1/3-octave band TL value is more than 8 dB below the *solid line*. The TL value at 500 Hz corresponding to this spectrum is the STC value

Table 11.3 lists critical frequencies for common building materials. Critical frequencies generally decrease at the same rate as the material thickness increases. Therefore, a doubling in material thickness translates to cutting the critical frequency in half for the same homogeneous material. Coincidence effects can be minimized by using multilayered partitions with different materials and different material thicknesses combined into a single partition.

There is a single-number rating for TL that takes the entire frequency spectrum into account, established by ASTM standard E413. This value, known as the sound transmission class (STC), is not derived by the simple averaging method used for NRC values. Instead, the TL frequency spectrum is matched to a standard curve within the limits imposed by the ASTM standard. Figure 11.15 shows how STC is calculated from the TL spectrum. Note that STC values have no units associated with them, but they are based on decibels. Similar to NRC, STC is useful to describe the sound insulation efficiency of a partition over the human speech frequency range of roughly 500–2000 Hz. If sound insulation outside of that frequency range (especially for frequencies below 250 Hz) is required, the TL values relevant to the frequency range of interest must be used.

Table 11.4 lists TL and STC values for common partitions. As with Table 11.1, these values are for general reference purposes only, and specific values should be based on manufacturers' specifications. Table 11.5 gives some meaning to the numbers by listing speech privacy ratings for different ranges of STC values.

As with any construction system, the actual in-field performance seldom matches the theoretical or laboratory STC rating for the construction. This is most often caused by flanking paths, poor construction practices, and/or lack of sealing cracks, gaps and openings. The noise isolation class (NIC) is the metric that considers these conditions. NIC is determined using the same method and template as is used for determining STC (shown on Fig. 11.15), using measured field data instead of using controlled laboratory data. The NIC value is typically 5–10 points less than the STC rating of a given partition design.

STC does not effectively consider the transmission of impact noise on floors from foot traffic as it may affect floors below. For this purpose the impact insulation class (IIC) was established by ASTM standard

Amazon
EX1010 Page 410

Table 11.4 Transmission loss and STC values for common partitions

Partition	125 Hz	250 Hz	500 Hz	1000 Hz	2000 Hz	4000 Hz	STC
1/2 inch drywall on both sides of wooden studs	17	31	33	40	38	36	33
1/2 inch drywall on wooden studs with 2 inches of insulation	15	30	34	44	46	41	37
Double layer of 1/2 inch drywall on wooden studs	25	34	41	51	48	50	41
1/2 inch drywall on staggered wooden studs	23	28	39	46	54	44	39
1/2 inch drywall on staggered wooden studs with 2 inches of insulation	29	38	45	52	58	50	48
1/2 inch drywall on metal studs	22	27	43	47	37	46	39
1/2 inch drywall on metal studs with 2 inches of insulation	26	41	52	54	45	51	45
8 inch thick concrete masonry units	36	44	50	54	58	56	53
Open-plane office partition	10	12	12	12	12	11	12
4 inch thick brick wall	32	34	40	47	55	61	45
1/2 inch drywall inside/1 inch stucco outside on wooden studs	21	33	41	46	47	51	42
Single-paned 1/8 inch thick glass	18	21	26	31	33	22	26
1/2 inch thick laminated glass	31	34	38	40	37	46	40
Double-paned 1/8 inch thick glass with 2 inch air gap	13	25	35	44	49	43	37
Hollow wooden door, 1 3/4 inch thick	14	19	23	18	17	21	19
Solid wooden door, 1 3/4 inch thick	29	31	31	31	39	43	34
Hollow metal door, 1 3/4 inch thick	24	23	29	31	24	40	28
Filled metal door, 1 3/4 inch thick	26	34	40	48	44	52	43
Wood joist floor/ceiling with 1/2 inch plywood subfloor and 1/2 inch drywall	23	32	36	45	49	56	37
8 inch thick concrete slab floor	32	38	47	52	57	63	50
Wood plank shingled roof	29	33	37	44	55	63	43
Wood plank shingled roof with 1/2 inch drywall ceiling, 4 inches of insulation	35	42	49	62	67	79	53
Corrugated steel roof with 1 inch of sprayed cellulose	17	22	26	30	35	41	30

E 989. The IIC stresses the low-frequency range, as is shown in Fig. 11.16, but note that IIC does not address very low (below 100 Hz) frequencies, which may be associated with resonances of a building's structural components.

One other single-number rating worth noting here is the outdoor–indoor transmission class (OITC), established in ASTM E 1332. The OITC is a single-number rating for the effectiveness of a building façade in reducing noise to interior spaces. The calculation of OITC is based on an A-weighted source spectrum of typical transportation (aircraft, rail, and traffic) sources in the 80–4000 Hz range and the façade's transmission loss spectrum in the same frequency range.

Non-Homogeneous Partitions

Up to this point we have been discussing homogeneous partitions. Actual designs, however, include walls composed of different materials, such as those with windows and doors. Each of these wall components has different associated TL characteristics. Wall components having lower TL characteristics than the rest of the wall can significantly degrade a wall's sound reduction effectiveness. This can be calculated using the composite

Amazon
EX1010 Page 411

Table 11.5 Speech privacy associated with STC ratings*

STC range	Sound privacy
0 to 20	No privacy (voices heard clearly between rooms)
20 to 40	Some privacy (voices heard in low** background noise)
40 to 55	Adequate privacy (only raised voices heard in low background noise)
55 to 65	Complete privacy (only high level noise heard in low background noise)
70	Practical limit

* assuming no significant flanking paths or openings in walls
** in the 35 dBA range

Table 11.6 Transmission loss reduction as a function of air opening*

Wall area having air opening (%)	Resultant wall TL (dB)	Resultant reduction in TL (dB)
0.01	39	6
0.1	30	15
0.5	23	22
1	20	25
5	13	32
10	10	35
20	7	38
50	3	42
75	1	44
100	0	45

* based on original wall TL of 45 dB

transmission coefficient, which is defined as:

$$\tau_{\text{comp}} = \left(\sum_{i=1}^{n} \tau_i S_i\right) / S$$
$$= (\tau_1 S_1 + \tau_2 S_2 + \ldots + \tau_n S_n)/S\,, \qquad (11.8)$$

where τ_1, τ_2, etc., are the transmission coefficients of each wall component while S_1, S_2, etc. are the surface areas corresponding to the surfaces having the same subscript value as those for the transmission coefficients, and S is the surface area of the entire partition. The composite transmission coefficient that is calculated using (11.8) can then be replaced in (11.6) to yield the composite transmission loss for the partition.

Air gaps (e.g., around doors, windows or penetrations) are notorious for compromising the sound reduction effectiveness of walls. Table 11.6 shows the TL degradation caused by varying sizes of air gaps in a wall originally rated at a TL of 45 dB. As the table shows, an air gap just one tenth of one percent the size of a wall can lower the TL rating from 45 to 30 dB. Figure 11.17 offers a graphical method for making this determination, not only for openings but also for doors and windows that have lower TL values than the walls in which they are installed. This emphasizes the importance of sealing walls, avoiding air gaps, and placing airtight seals around doors.

A rule that governs most of the TL spectrum of homogeneous partitions, known as the mass law, states that TL increases at a rate of 6 dB with each doubling of mass and with each doubling of frequency (shown in Fig. 11.14). This rule can make it impractical to solve sound privacy issues with homogeneous partitions. For example, if a 1/2 meter-thick concrete wall does not provide enough sound insulation for a specific situation,

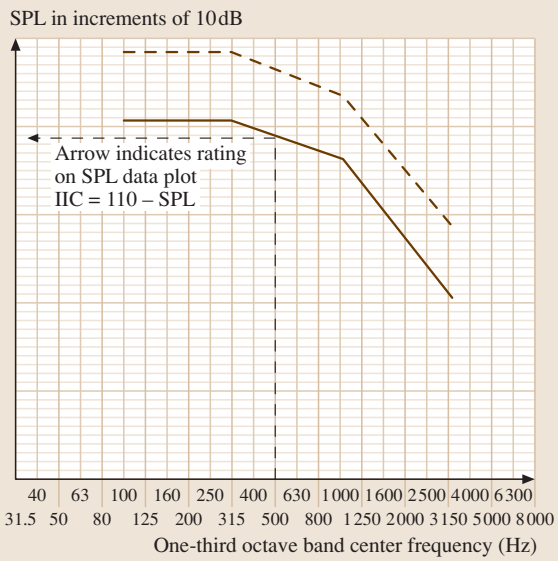


Fig. 11.16 The standard IIC calculation curve, from ASTM E 989. IIC values are derived by plotting the SPL spectrum (from a tapping machine specified in ASTM E 492) on this curve and determining the lowest curve shape that meets the criteria of: (1) the sum of the differences between individual SPL values and the *solid line* is less than 32 dB and (2) no individual 1/3-octave band TL value is more than 8 dB above the *solid line*. The SPL value at 500 Hz corresponding to this spectrum, subtracted from 110, is the IIC value

Amazon
EX1010 Page 412

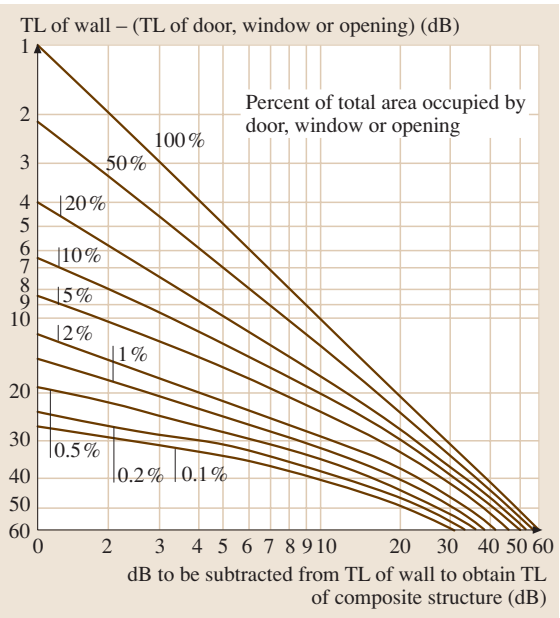


Fig. 11.17 Chart for determining the reduction in TL wall rating by the installation of a door, window, or opening

doubling the thickness of that wall to 1 meter would only offer an additional 6 dB of sound reduction. A more practical way of avoiding this kind of issue is by using multilayered partitions.

Multilayered partitions are comprised of layers of different materials. Each time sound passes through a different material, its level is reduced. Therefore, this method can be used to reduce costs, weight and space restrictions while providing adequate sound reduction. A sharp change in density of material is most effective in raising TL. Air spaces between wall sections and materials are effective by setting up such environments and also breaking any rigid connections between sides of a partition. A rigid connection can provide a vibration channel for sound to pass through with little reduction. For example, the noise reduction effectiveness of a studded wall filled with fiber insulation between studs can be short-circuited because sound may travel unimpeded

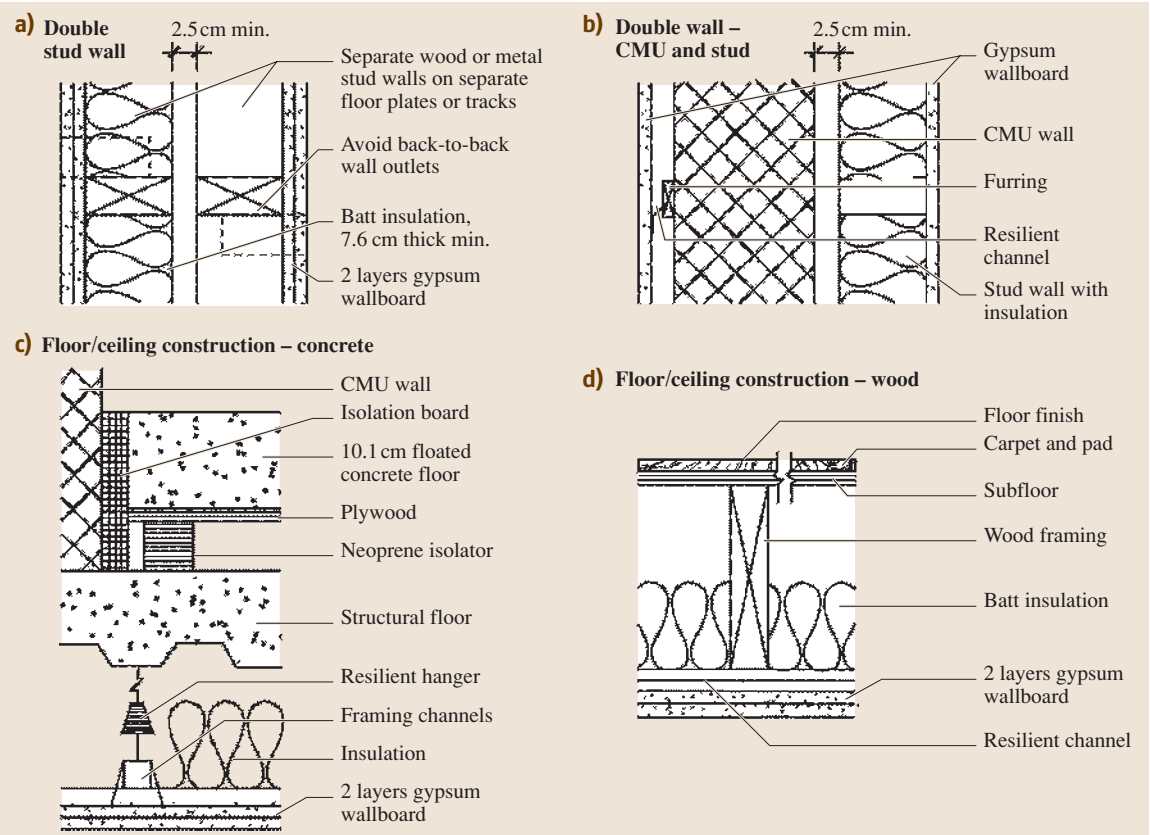


Fig. 11.18 Examples of multilayered partition and floor/ceiling designs that result in high TL

Amazon
EX1010 Page 413

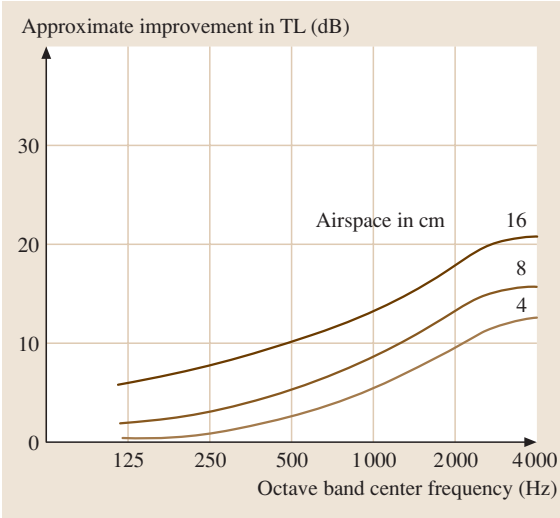


Fig. 11.19 General TL improvement that can be expected from air spaces in partitions

through the studs to the other side of the wall. Figure 11.18 shows examples of multilayered partitions that are effective for sound insulation.

Figure 11.19 shows the TL benefit of different air spaces in partitions. In general, the TL of a partition increases at a rate of 5 dB with each doubling of air space (within a partition) beginning with an air space of 5 cm.

As is mentioned above, transmission loss generally increases with frequency. If significant sound reduction is required for frequencies below 250 Hz, it is most practical to use multilayered partitions with air spaces and staggered studs or resilient channels between components. Resilient channels are shaped metal bars (the S shape is common) or resilient clips that connect two wall components. Only one side of their shape touches each side of the wall, and they effectively reduce vibrational energy from traveling through them. Resilient clips resemble isolation hangers, which are discussed later in this chapter. Another option for greater transmission loss at low frequencies is massive concrete slabs.

11.2 General Noise Reduction Methods

Noise can be controlled at its source, in the path between the source and the listener, or at the listener. Table 11.7 summarizes the general options available. If the noise can be controlled sufficiently well at its source, it is unnecessary to consider the path or listener locations. Likewise, if the noise can be controlled sufficiently well in the path between the source and listener, it is unnecessary to consider the listener's location for noise control measures.

The options for noise control at the source are generally self-explanatory. Most often, due to economic or logistic issues, noise control options are limited to the path between the source and the listener. Given many misconceptions about these options, it is useful to discuss some of them further.

11.2.1 Space Planning

The most effective noise control method for buildings is space planning. This is true both for room layout within a building and for the placement of the building itself with respect to exterior noise sources. Inherently noisy spaces adjacent to spaces inherently requiring quiet should be avoided as much as possible. The noisiest indoor spaces tend to be mechanical rooms, restrooms, and elevator shafts.

For placement with respect to loud exterior sources, buildings should be as far as possible from noisy streets or rail lines, taking advantage of shielding from other buildings and topographical features. If building placement near noisy outdoor sources is unavoidable, special attention should be paid to the design of the façade(s) facing the noisy sources, avoiding operable windows, doors, and penetrations.

Another aspect to consider for outdoor sound is the potential effect of a building's noise sources on the surrounding community. Rooftop mechanical units are the most common noise sources that may need to be insulated from community intrusions, especially when municipal codes are involved. The community noise aspect of a building is often considered in the building's permitting process.

11.2.2 Enclosures

Enclosures can be effective at reducing noise levels as long as they are properly designed. The following points should be considered when designing noise enclosures (also illustrated in Fig. 11.20a–d).

1. The enclosure must completely surround the noise source, with no air gaps. As mentioned earlier in

Amazon
EX1010 Page 414

Table 11.7 Generalized noise reduction options

Control at the source	Control in the path	Control at the listener
Maintenance	Enclosure(s)	Relocate listener
Avoid resonance	Barrier(s)	Enclose listener
Relocate source/ space planning	Muffler(s)	Hearing protection
Remove unnecessary sources	Absorptive treatment	Masking
Use quieter model(s)	Vibration isolation	
Redesign source to be quieter	Active noise control	

this chapter, air gaps can significantly compromise the noise reduction effectiveness of partitions. An enclosure with any side open is not an enclosure but a barrier, and the noise reduction effectiveness of barriers is limited by diffraction to 15 dBA, independent of the barrier material (as long as the material would provide at least 20 dBA of noise reduction on its own). Enclosures, on the other hand, can provide up to 70 dBA of reduction.

2. The enclosure must be isolated from floors or any structural members of a building. An enclosure covering the sides and top of a noise source but not the bottom (since the source is sitting on the floor or ground) can compromise its effectiveness for several reasons. First, the chances of the sides of the enclosure perfectly sealing to the ground are slim, and therefore, air gaps would result. Second, vibrations will be carried along the ground or floor since the source is in direct contact with it. The only way to reduce these vibrations is to vibrationally isolate the source from the ground or floor using tuned springs (appropriate for the source), pads, or a floating floor.
3. The enclosure should be constructed using nonporous materials. Sound absorptive material can be effective in reducing noise when it is used as part of a multilayered enclosure (on the inside); however, absorptive material by itself is not effective in reducing noise.

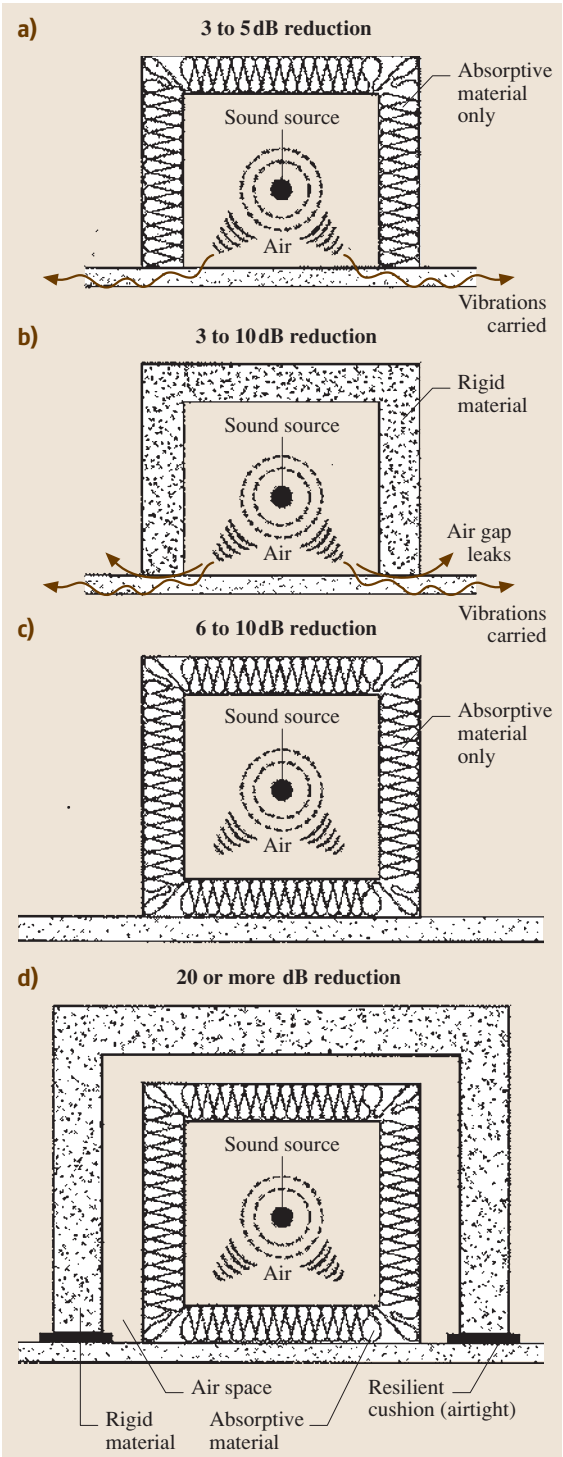


Fig. 11.20a–d Noise reduction effectiveness of enclosures sitting on a solid surface **(a)** enclosing the source on five sides with absorptive material only, **(b)** enclosing the source on five sides with one layer of rigid, nonporous material, **(c)** completely enclosing the source with absorptive material only, and **(d)** surrounding the source in an isolated, multilayered enclosure

Amazon
EX1010 Page 415

4. The enclosure designer must consider that some sources require ventilation. This cannot translate to leaving an opening in the enclosure without compromising the noise control effectiveness of the enclosure. Ventilation systems must be developed that minimize noise transmission.
5. The enclosure should be constructed using multilayered construction for maximum efficiency. As is mentioned earlier in this chapter, doubling the mass of an enclosure would add 6 dB to its noise reduction effectiveness. This can easily lead to excessive weight for an effective homogeneous enclosure. As for single partitions, multilayered enclosures can add more than 20 dB of effectiveness (under similar space requirements) to massive enclosures with a fraction of the weight.

11.2.3 Barriers

A barrier is contrasted from an enclosure by being open to the air on at least one side. Because of diffraction, noise barriers are limited to 15 dBA of noise reduction capability, independent of the material. This limited effectiveness is compromised even more if there are reflective ceilings above the barrier because sound reflected off the ceiling minimizes the barrier's effectiveness. Therefore, wherever noise barriers are used indoors, an absorptive ceiling should be installed above them. It is also important to have no air spaces within or under the barriers, since this will compromise their already limited effectiveness.

The noise reduction effectiveness of barriers is typically rated by the insertion loss (denoted by IL). The IL is the reduction in sound pressure level, at a specific location, resulting from the installation of a barrier. The IL is then the difference between conditions with and without a barrier.

To provide any insertion loss, a barrier must break the line of sight between the sound source and listener. In other words, if you can see a sound source on the other side of a barrier, that barrier is providing no sound reduction (from that source) for you. Breaking this line of sight typically provides a minimum of 3–5 dBA of insertion loss, with insertion loss increasing as one goes further into the shadow zone of the barrier.

Bear in mind that a row of trees is ineffective for outdoor noise control. Only solid walls or earth berms breaking the line of sight between the noise source and building occupants will produce any meaningful noise reduction.

11.2.4 Mufflers

Mufflers are devices that are inserted in the path of ductwork or piping with the specific intention of reducing sound traveling through that conduit. The effectiveness of mufflers is typically rated using insertion loss. Mufflers must be designed for each purpose to preserve the required static or back pressure characteristics of the equipment and to reduce noise in the appropriate frequency range(s). For that reason, each muffler is unique to its installation.

11.2.5 Absorptive Treatment

Absorptive treatment within a room can reduce reverberation and, in this process, reduce noise levels by up to 10 dBA. Bear in mind, though, that absorptive treatment is only effective for reducing reverberation within a room and not for reducing transmission of sound between rooms.

11.2.6 Direct Impact and Vibration Isolation

Mechanical equipment can generate vibration that can travel through a building's structural members to affect remote locations within a building. It is therefore prudent to isolate any heavy equipment from any structural members of buildings. This can be accomplished by mounting the equipment on springs, pads, and/or inertia blocks; however, the selection of specific isolating devices (especially springs) should be performed by a specialist trained in vibration analysis. The main reason for this is that each vibration isolation device is tuned to a specific frequency range. If this is not matched properly with the treated equipment, the devices can amplify the vibration and cause more of a problem than would have occurred without any treatment.

Mechanical equipment and, to a lesser degree, footfalls generate direct impacts that should also be addressed by properly isolating floors from building structures.

11.2.7 Active Noise Control

Passive noise control involves all of the noise control methods discussed above, in which the sound field is not directly altered. Active noise control involves electronically altering the character of the sound wave to reduce its level. In this case, a microphone measures the noise and a processor generates a mirror image of

Amazon
EX1010 Page 416

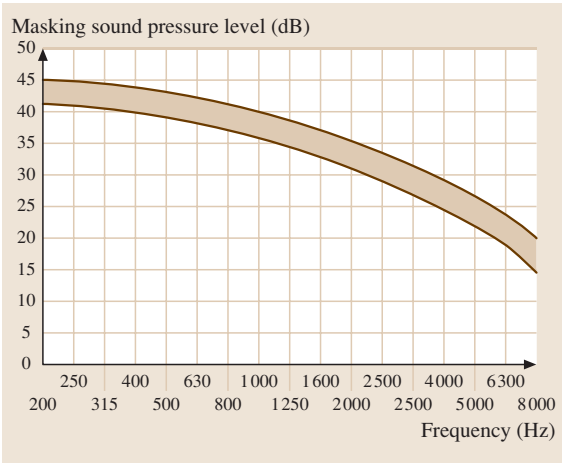


Fig. 11.21 Typical characteristics of effective masking systems (frequency response range in *shaded area*)

(180° out of phase from) that source. This mirror image is then reproduced by a loudspeaker in the path of the original sound. This new sound cancels enough of the original signal to reduce levels by up to 40 dB under the appropriate conditions. Although this is a very powerful noise control tool, active noise control is only practical in local environments and for tones below 500 Hz. Ventilation ducts provide ideal environments for active noise control systems because they are enclosed environments and their noise is often dominated by low frequency tones (associated with the fan characteristics).

11.2.8 Masking

As long as background sound levels are low in a building, one way of easing a noise problem is to add a more pleasing sound to the environment to make the noise less noticeable. This is especially desirable in open-plan offices where people can clearly hear activities in other offices and areas (since their offices are not completely enclosed). Any desirable sound can provide masking, but most often electronic masking systems are used, comprised of loudspeakers placed between

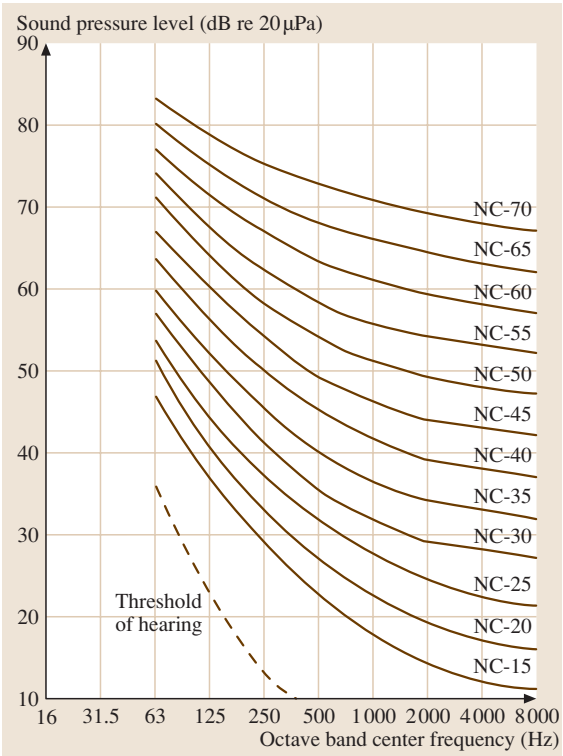


Fig. 11.22 NC curves

dropped ceilings and structural ceilings. These loudspeakers are connected to signal processors that are set to generate sounds similar to those generated by typical heating, ventilating and air conditioning (HVAC) systems. Although many people think of masking system sounds as white noise, which has an equal amount of energy in all audible frequencies, a typical masking system frequency response is more like that shown in Fig. 11.21, where less emphasis is placed on higher frequencies. Whatever the response, it is advisable to have an electronic masking system installed by a contractor with experience in this area. If the system is set at too high a level or with a harsh frequency response, the resulting environment may be more unpleasant with the masking system than without.

11.3 Noise Ratings for Steady Background Sound Levels

There are two standardized methods for rating the background sound levels inside rooms. Each of these methods is referenced in ANSI standard S12.2 and the *American Society of Heating, Refrigerating and Air-Conditioning Engineers (ASHRAE) Handbook*. These are the balanced noise criterion (NCB) and the room criterion (RC)

Amazon
EX1010 Page 417

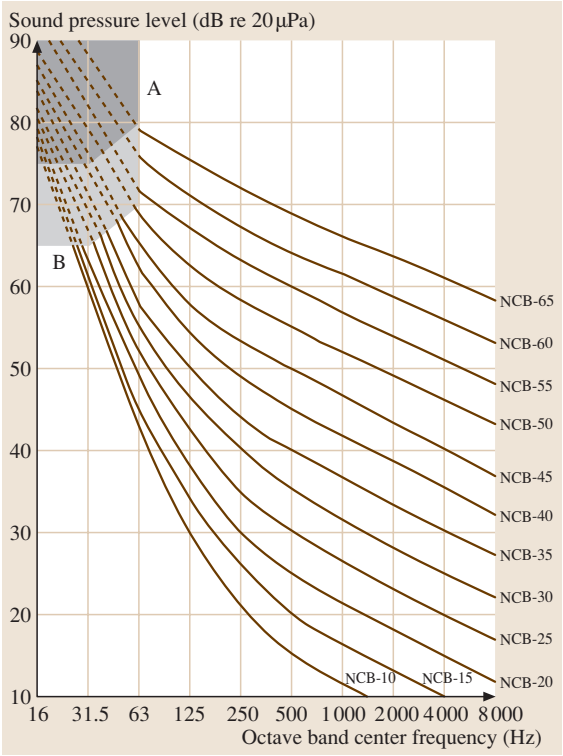


Fig. 11.23 NCB curves. Sound in the *region labeled A* can cause perceptible noise-induced vibration such as rattling of doors, windows, or fixtures. Sound in the *region labeled B* may generate lower levels of these noise-induced vibrations

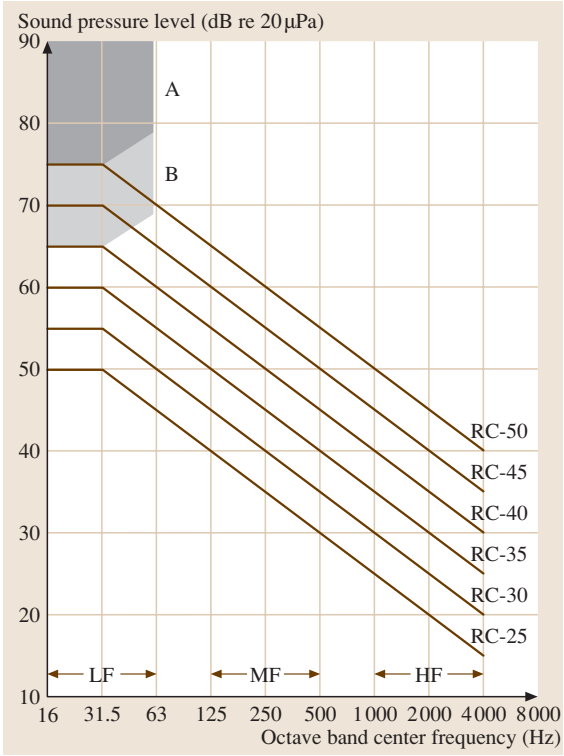


Fig. 11.24 RC curves. The *A and B regions* have the same meanings as the NCB curves in Fig. 11.23. The LF, MF, and HF regions are designated as low-frequency (rumble), medium-frequency (roar), and high-frequency (hiss) ranges, respectively

curves. The NCB curves are updated versions of the widely used noise criterion (NC) curves, different in that they are extended down to the 16 and 31.5 Hz octave bands. Figure 11.22 shows the NC curves and Fig. 11.23 shows the NCB curves.

Table 11.8 Recommended background noise criteria for common spaces

Category of space	Specific uses	NC, NCB or RC(N) range	dBA limit
Sensitive listening spaces	Broadcast and recording studios, concert halls	15 to 20	25 dBA
Performance spaces	Theaters, churches, video and teleconferencing	20 to 25	30 dBA
Presentation spaces	Large conference rooms, small auditoriums, movie theaters, courtrooms, meeting and banquet rooms, executive offices	25 to 30	35 dBA
Private spaces	Offices, small conference rooms, classrooms, private residences, hospitals, hotels, libraries	30 to 35	40 dBA
Public spaces	Restaurants, lobbies, open-plan offices, clinics	35 to 40	45 dBA
Service and support spaces	Computer equipment rooms, public circulation areas, arenas, convention centers	40 to 45	50 dBA

Amazon
EX1010 Page 418

As for the room criterion (RC) method, the NCB method was developed to better consider low-frequency noise generated by HVAC systems. In each case, standardized curves are used in conjunction with measured noise levels in a room to yield a single-number rating for HVAC noise. The NC and NCB rating values result from plotting the measured octave band sound pressure level spectrum on each chart and noting the lowest standard curve that is not exceeded by the measured values. This single number is then rated against design guidelines established in the two references above. Determining the RC rating is more complicated, based on the 1000 Hz value of the standard RC curve (in Fig. 11.24) that matches the arithmetic average of the 500, 1000, and 2000 Hz values of the SPL room spectrum. The quality of the sound is also rated by the RC method, based on the deviations of the measured SPL spectrum from the standard RC curve. A *neutral* spectrum, designated by *N* and used in most RC specifications, implies that levels below 500 Hz do not exceed an RC curve by more than 5 dB and levels above 1000 Hz do not exceed an RC curve by more than 3 dB. When deviations greater than these exist, the RC rating is given the designation of the frequency range (from Fig. 11.24) in which the greatest deviations occur. The levels in the octave bands below 500 Hz are much lower for RC curves than those for the NCB curves. The purpose of this lower limit is to consider fluctuations or surges at the ventilation outlets better. These fluctuations are not considered for NCB ratings.

Table 11.8 lists generally recommended NC, NCB and RC(N) ranges for common spaces.

11.4 Noise Sources in Buildings

The most common noise sources in buildings, other than the inhabitants, are related to HVAC systems, plumbing systems, electrical systems, and exterior sources. Figure 11.25 shows the most common paths for intrusive noise in buildings.

Although there is legislation that often deals with noise disturbances directly related to people as sources, these other sources are typically unregulated and their associated noise levels are governed by the desires of developers, builders, and occupants.

11.4.1 HVAC Systems

Noise sources associated with HVAC systems can be separated into two general categories – mechanical equipment and duct-borne/airflow noise.

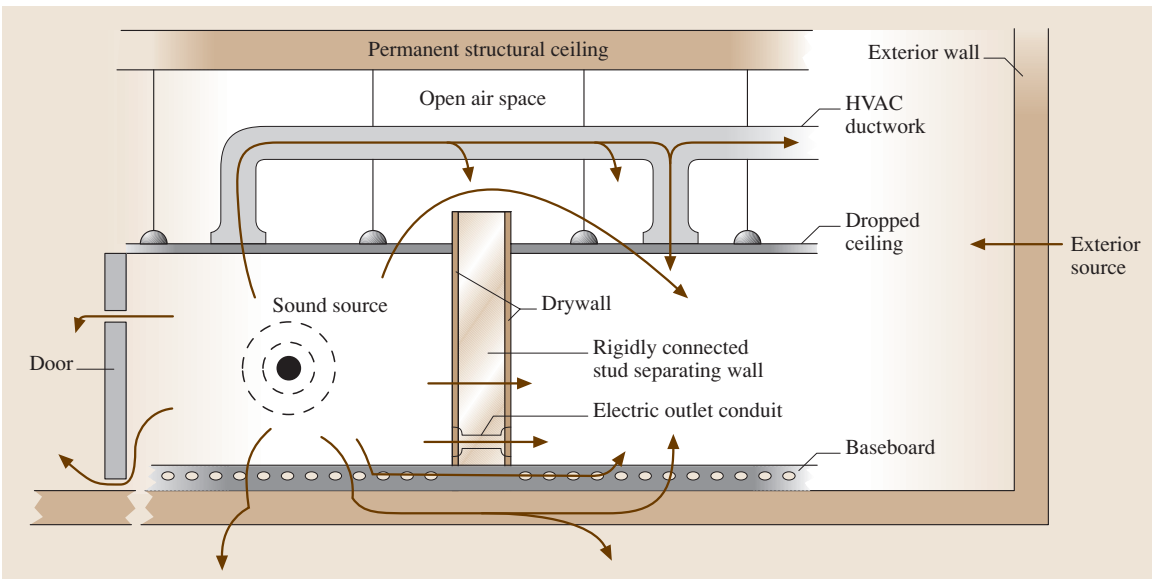


Fig. 11.25 Common noise leaks occur through these nine paths

Amazon
EX1010 Page 419

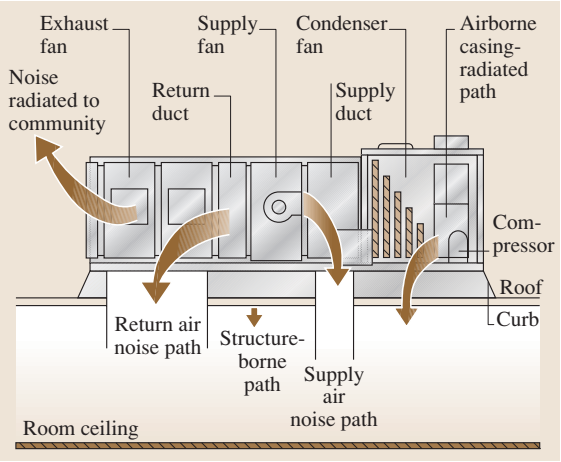


Fig. 11.26 Common noise paths for a typical rooftop HVAC unit

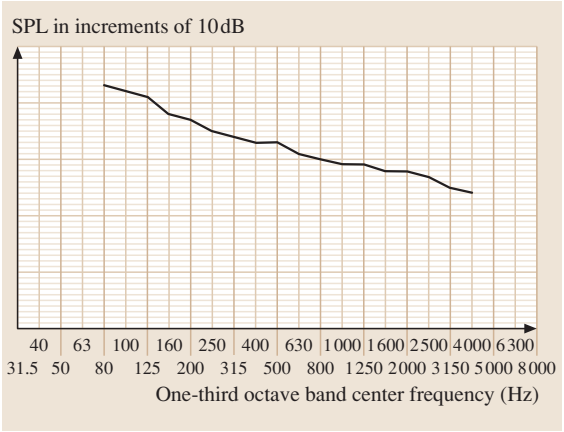


Fig. 11.27 Average transportation noise spectrum shape (adapted from data in ASTM E 1332)

Mechanical Equipment

Common mechanical equipment associated with HVAC systems includes pumps, compressors, chillers, generators, and air handlers. Rotating components of these pieces of equipment, such as gears and fans, generate most of the noise that causes concerns in buildings. Rotating mechanical equipment typically generate tones, their frequencies being associated with their rotational speeds. When mechanical equipment is housed in rooms within buildings, its associated noise can affect rooms throughout a building. When mechanical equipment is placed on rooftops or slabs outside buildings, its associated noise can also affect the surrounding communities. Figure 11.26 shows noise sources and paths for a typical rooftop HVAC unit.

Mechanical equipment not only generates noise in buildings, but also generates vibrations that can propagate throughout a building's structural members if not properly isolated. These vibrations can excite building members far from the sources and cause remote building components to rattle and generate their own noise.

Duct-Borne/Airflow Noise

Air is typically carried throughout a building using a system of ductwork. Ducts carry the tones generated by fans and they cause additional noise by inducing turbulence in the airflow. Some of this noise is carried through the ductwork to rooms in buildings (out of grilles in each room) and some of it is radiated directly from the duct walls (known as breakout noise).

11.4.2 Plumbing Systems

The most common plumbing system noise sources are water flowing through pipes and noise radiating from the walls of pipes.

11.4.3 Electrical Systems

The most common electrical system noise sources are transformers and noise radiated from associated conduit (by carrying vibrations that excite walls).

11.4.4 Exterior Sources

The most common exterior noise sources that affect building inhabitants are those associated with transportation (such as vehicular traffic, rail, and aircraft), industrial operations, and mechanical equipment from nearby buildings or mounted outside the same building. Figure 11.27 shows an average spectrum shape for transportation noise sources used by ASTM E 1332. This shows the concentration of sound in the low frequency (below 500 Hz) range, emphasizing the need for exterior-wall noise control design measures that effectively address low frequencies.

Amazon
EX1010 Page 420

11.5 Noise Control Methods for Building Systems

The principles discussed in Sect. 11.2 can be put into practice using the general design concepts listed in this section. Specific dimensions and sound ratings have intentionally been omitted from the drawings in this section because these drawings stress the design principles rather than specific installations. These design concepts can be used to develop specific designs for each project.

11.5.1 Walls, Floor/Ceilings, Window and Door Assemblies

A key issue with all of these designs is to stop the path of sound and vibration through rigid connections between building components. Generous use of air spaces and resilient materials is the most effective method for this to occur. Another key issue is avoiding openings in and around partitions (for the reasons stated in Sect. 11.1.6). All openings must therefore be completely sealed. These two themes will be repeated in most of the designs listed in this section.

Walls

The most effective wall system for noise reduction is a double-wall system, in which wall sections (including studs) are separated by an air space. The larger the depth of the air space, the more effective the wall will be in controlling sound. Double walls can be especially effective for controlling low-frequency sound, as long as the walls are properly sealed and isolated from the building structure.

Figure 11.28 shows the general concept of a double-studded wall that is effective for noise control. Although metal studs are shown in the drawing, wooden studs would provide comparable results in this design because of the air gap. Figure 11.29 shows a full floor-to-structural-ceiling double-wall construction concept.

Note that the wall must be sealed with a non-hardening material at its perimeter to avoid any sound leakage through air gaps (since a hardening material may crack and leave gaps). Figure 11.30 shows a double-wall concept using a concrete masonry unit (CMU) and studded component.

All of these double-wall designs will provide STC values in excess of 55; however, if low-frequency noise

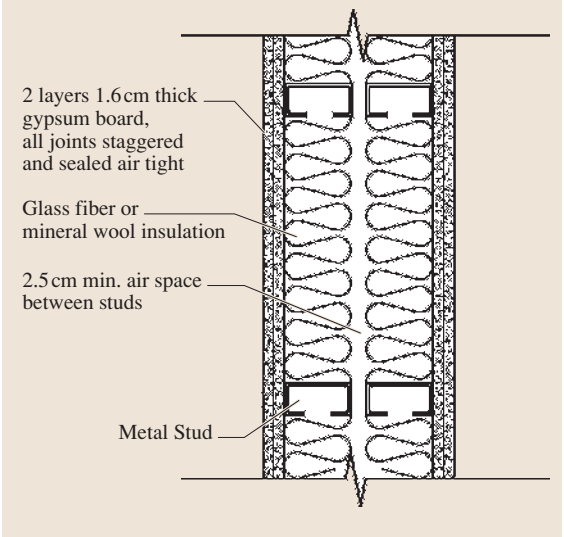


Fig. 11.28 Cross section of a double-wall design

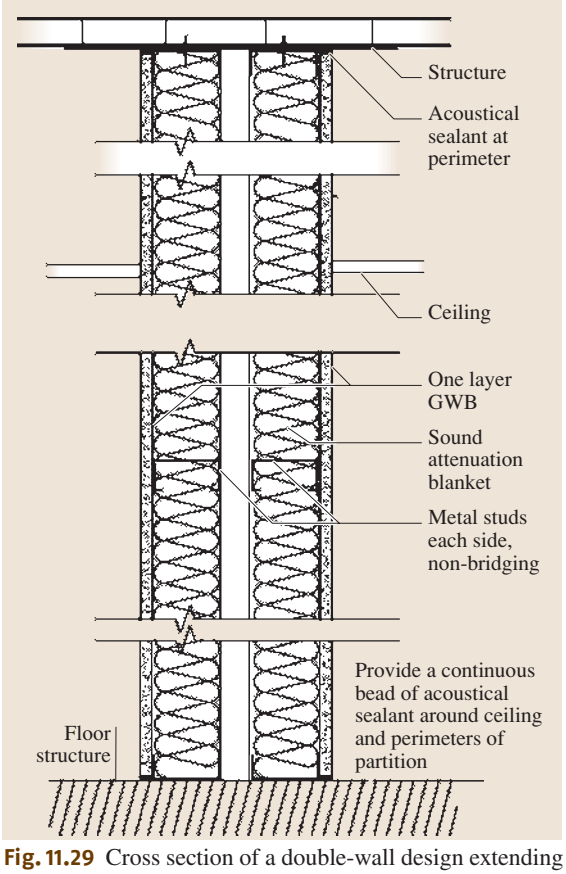


Fig. 11.29 Cross section of a double-wall design extending from floor to structural ceiling

Amazon
EX1010 Page 421

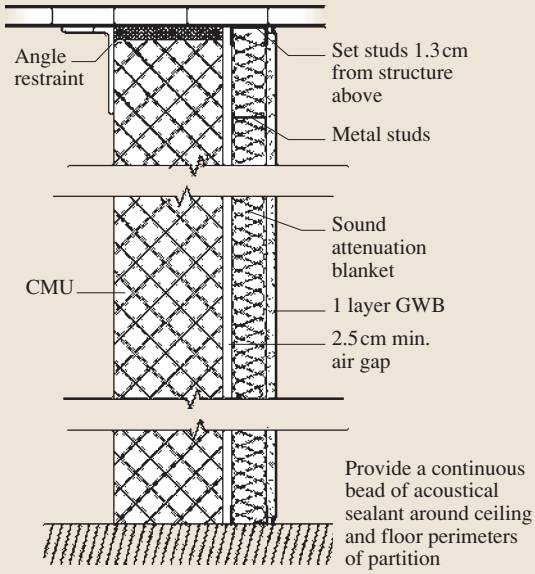


Fig. 11.30 Cross section of a floor to structural ceiling double-wall design with a CMU wall

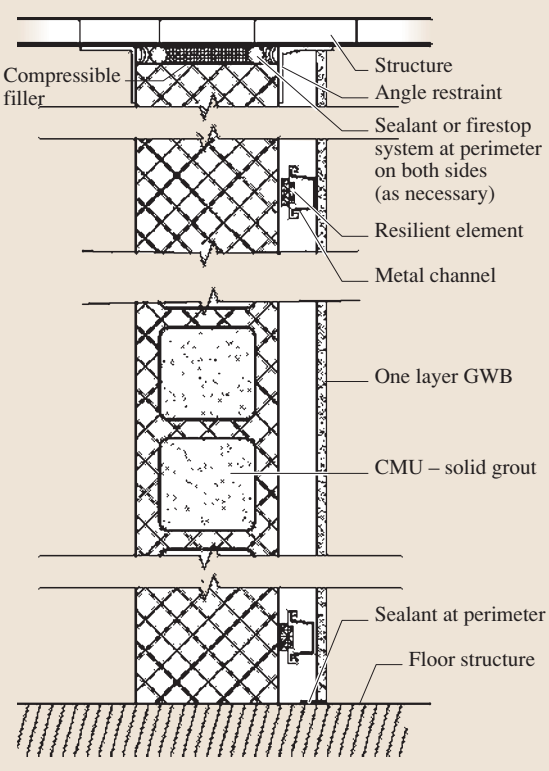


Fig. 11.31 Cross section of alternate construction to a double-wall design in Fig. 11.30

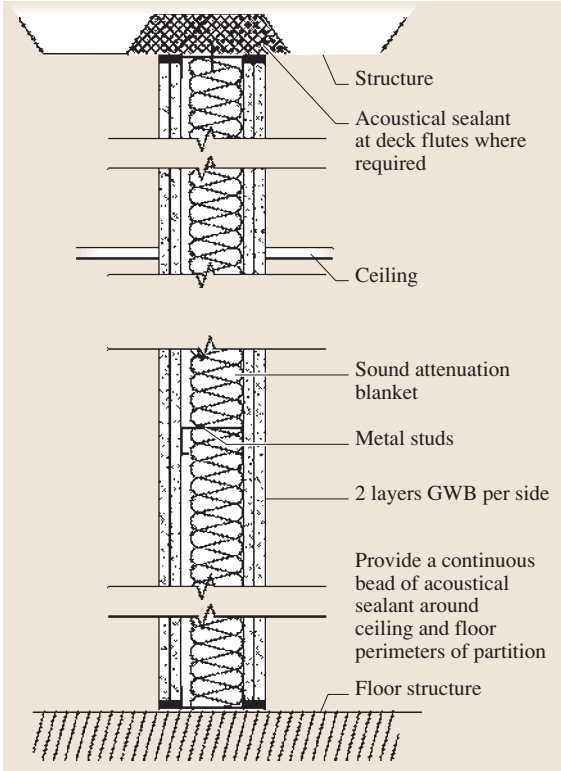


Fig. 11.32 Cross section of a single-studded sound insulating wall meeting a fluted metal structural deck

control is an issue, the STC rating does not address that and larger air spaces between wall components will increase the low-frequency noise control effectiveness.

Double-wall constructions are often impractical because of space restrictions. In these cases, an alternative to the CMU construction in Fig. 11.30 would be that shown in Fig. 11.31, in which the air space is replaced by a resilient element.

When working with gypsum board, Fig. 11.32 shows a design concept that will provide an STC of at least 50 as long as it is sealed properly. Note that a fluted structural deck may provide air gaps at the top of the wall that would need to be sealed to preserve the noise reduction effectiveness of the system.

When a room needs to be isolated from the building structure (which would be the case when structure-borne vibrations cause unwanted noise and vibration in certain rooms in which sensitive activities are tak-

Amazon
EX1010 Page 422

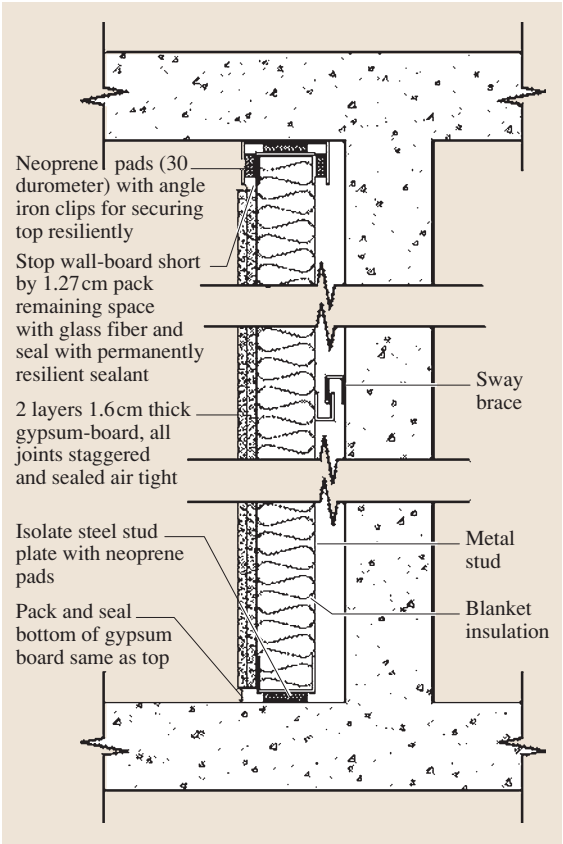


Fig. 11.33 Cross section of a resiliently mounted wall on a concrete building structure

ing place), Fig. 11.33 shows the conceptual design for a resiliently mounted wall. Figure 11.34 shows appropriate designs for intersections of double-studded walls.

A common path for sound leaks between rooms in buildings with large windows as facades is the connection between walls and those windows. Figures 11.35 and 11.36 show designs that effectively minimize sound transmission between rooms having this situation, Fig. 11.35 with a permanent installation and Fig. 11.36 with a curtain wall design.

Floor/Ceilings

Noise control design for floor/ceiling assemblies typically involves a significant amount of vibration isolation to minimize the transmission of footfall and other impact noise between floors. The design concepts that minimize vibration between floors can also be used to minimize sound transmission between floors.

The most common noise control design for floors is the floating floor system, in which a layer of resilient material is placed between the floor structure and the subflooring. More complicated measures are required for effective control of the high vibration and noise levels that can be associated with mechanical equipment in buildings. Figures 11.37–11.43 offer design concepts for resiliently mounted ceilings for mechanical rooms or other noisy spaces. Figure 11.44 shows a sound isolating design for a metal roof deck and Fig. 11.45 shows a sound isolating design for a concrete roof deck.

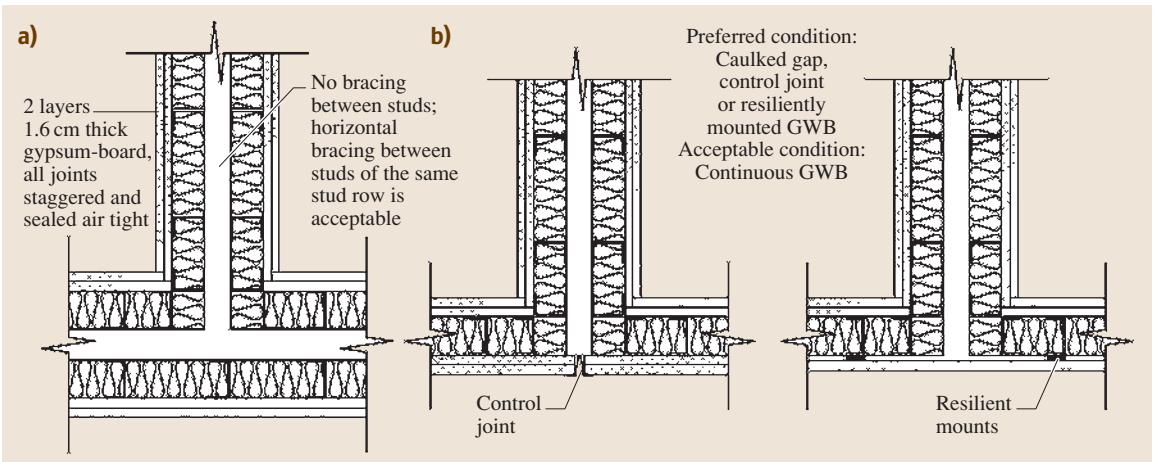


Fig. 11.34 Cross section of effective double-stud wall junction designs

Amazon
EX1010 Page 423

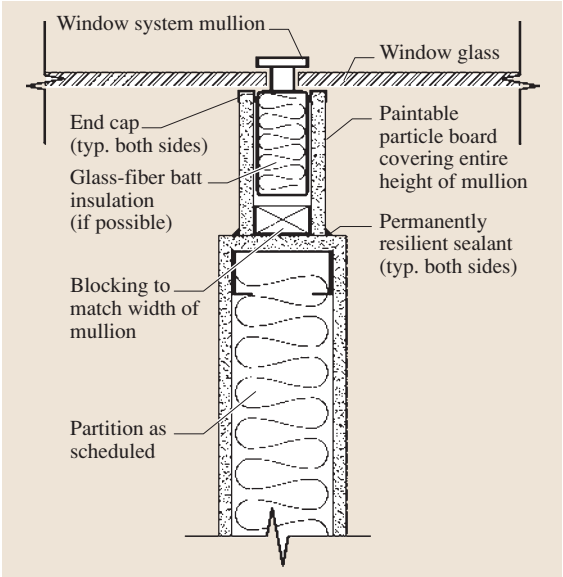


Fig. 11.35 Cross section of an effective mullion/partition junction

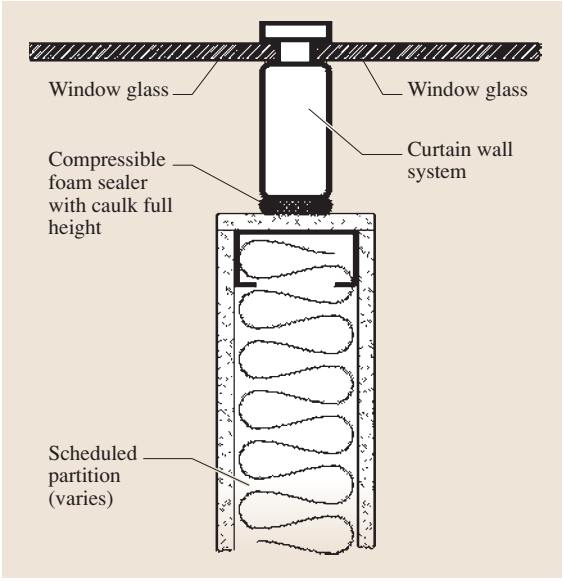


Fig. 11.36 Cross section of an effective mullion/partition junction with a curtain wall system

Windows and Doors

Windows and doors often have the lowest TL ratings of a wall system and are therefore often the sources of noise leaks through partitions. In addition to their lower TL ratings than the main wall, installation with air gaps

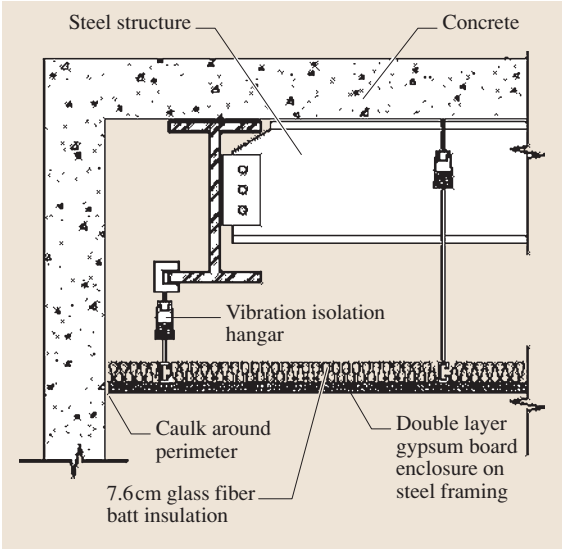


Fig. 11.37 Cross section of a resiliently mounted gypsum-board ceiling

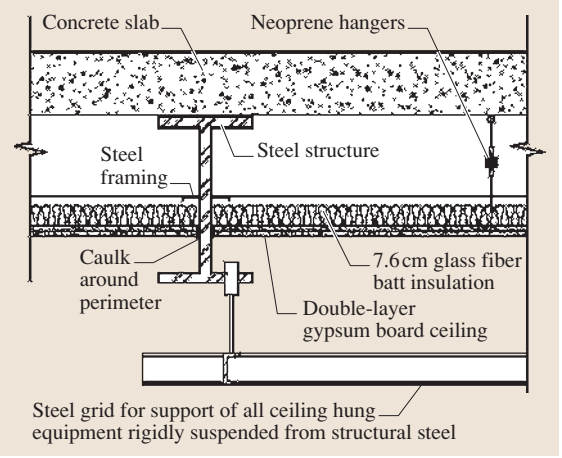


Fig. 11.38 Cross section of a sound insulating gypsum board ceiling framed from I-beams

around them can significantly compromise their noise control effectiveness.

Many window manufacturers provide models that offer significant sound insulation and each of these manufacturers offers its own acoustical test data and design parameters. As for walls, larger air spaces between double-paned designs will provide better sound insulation than single-paned windows of the same thickness. For those wishing to manufacture custom sound-insulating windows, Fig. 11.46 shows some design

Amazon
EX1010 Page 424

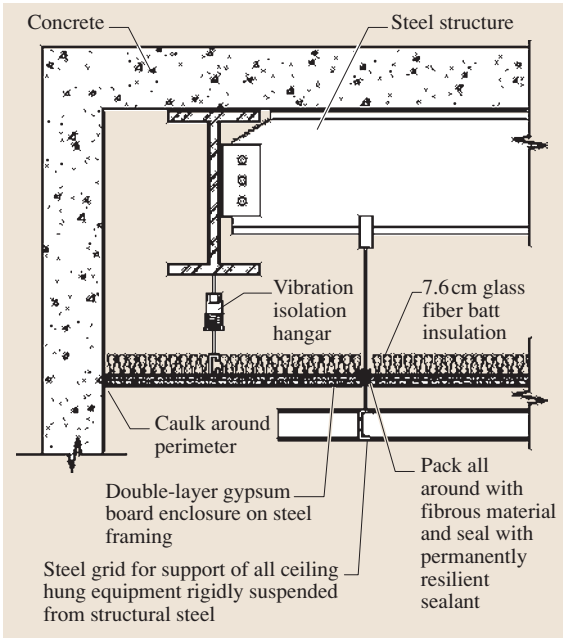


Fig. 11.39 Cross section of an effective sound insulating ceiling for mechanical rooms

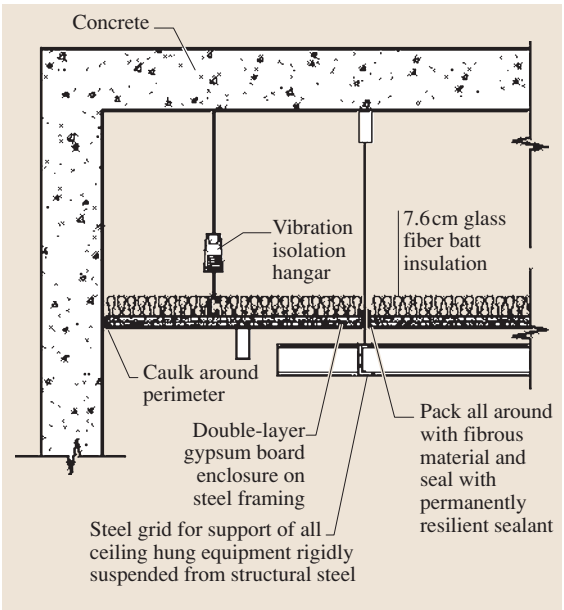


Fig. 11.40 Cross section of a ceiling resiliently mounted from a concrete slab

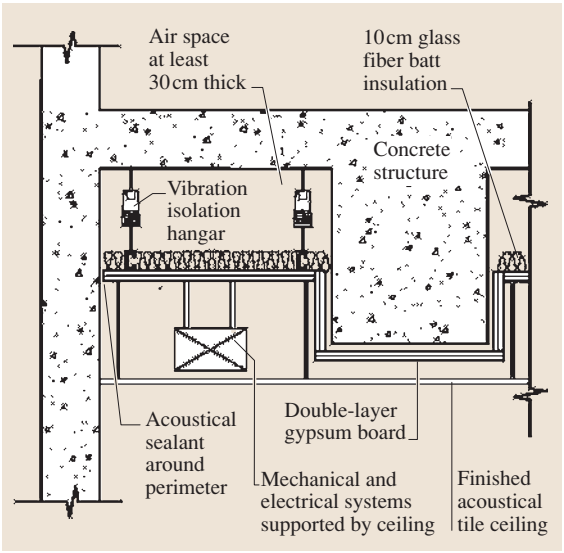


Fig. 11.41 Cross section of a resilient ceiling supporting mechanical and electrical system equipment

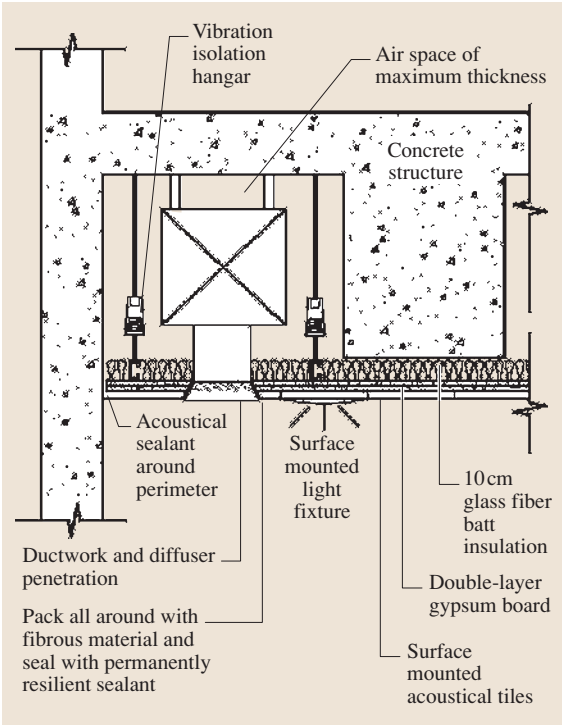


Fig. 11.42 Cross section of a resilient ceiling with HVAC equipment

Amazon
EX1010 Page 425

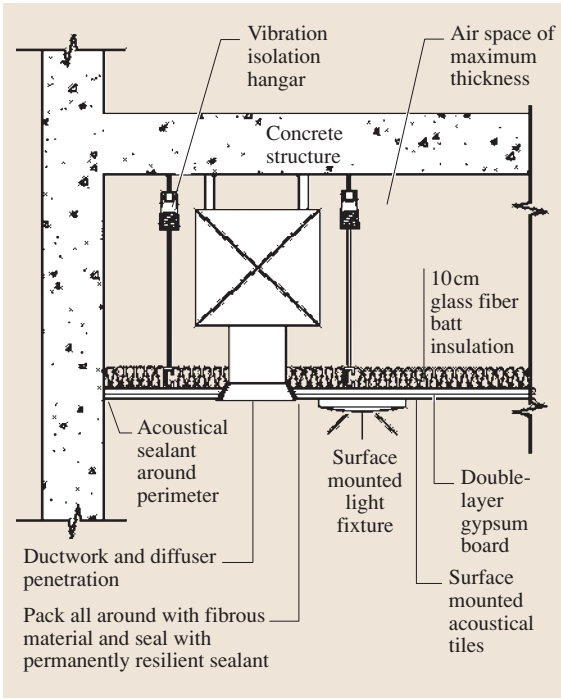


Fig. 11.43 Cross section of an alternative resilient ceiling design

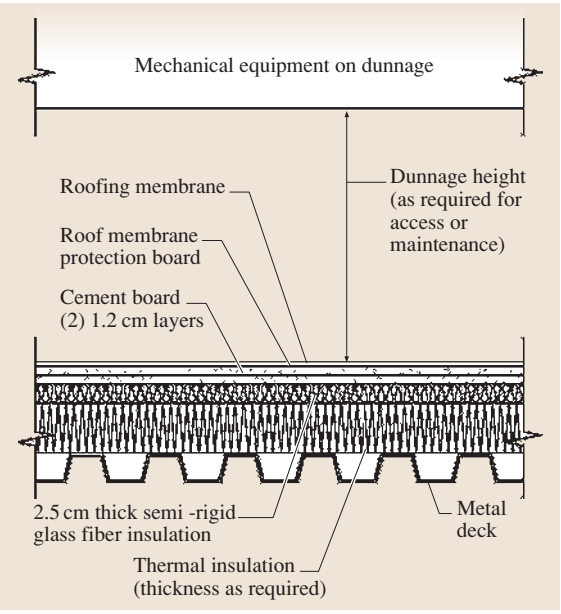


Fig. 11.44 Cross section of a sound isolating sandwich design for a metal roof deck

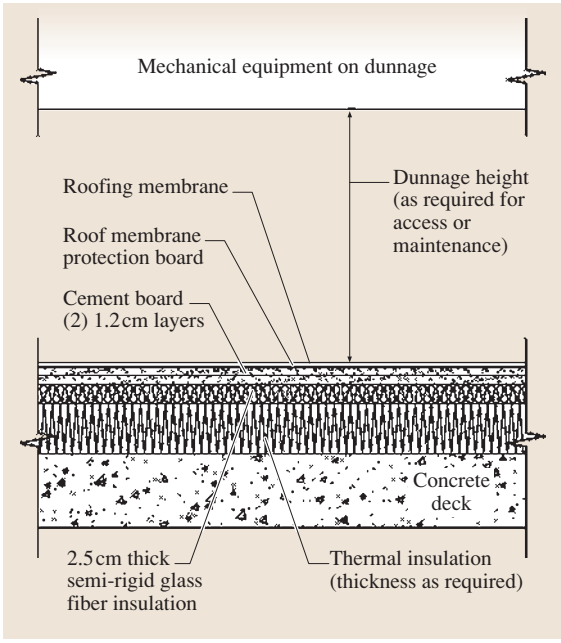


Fig. 11.45 Cross section of a sound isolating sandwich design for a concrete roof deck

guidelines for high-TL interior windows and Fig. 11.47 shows design guidelines for high-TL exterior windows.

As for windows there are many door manufacturers that provide sound insulation data for their prefabricated products. In general, solid-core doors are more effective than hollow-core doors for noise reduction. To maximize the effectiveness of these doors, they should be gasketed around their perimeters and they should either have drop seals or rubber skirts on their undersides, which should contact solid floor thresholds.

11.5.2 HVAC Systems

ASHRAE publishes thorough discussions on HVAC noise sources and their control in their *Fundamentals and Applications Handbooks*. The basic principles to bear in mind for minimizing HVAC noise are minimizing airflow turbulence and isolating vibrations, each of which is able to carry noise far from the source to remote locations in buildings.

Airflow Turbulence

Airflow turbulence noise can be minimized by

- lowering flow rates as much as possible,

Amazon
EX1010 Page 426

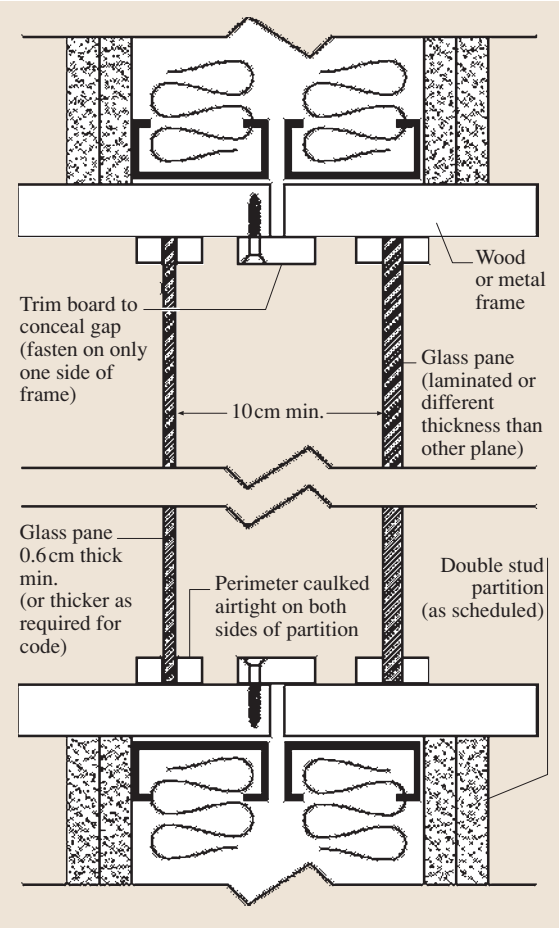


Fig. 11.46 Cross section of a high-TL interior window in a double-wall design

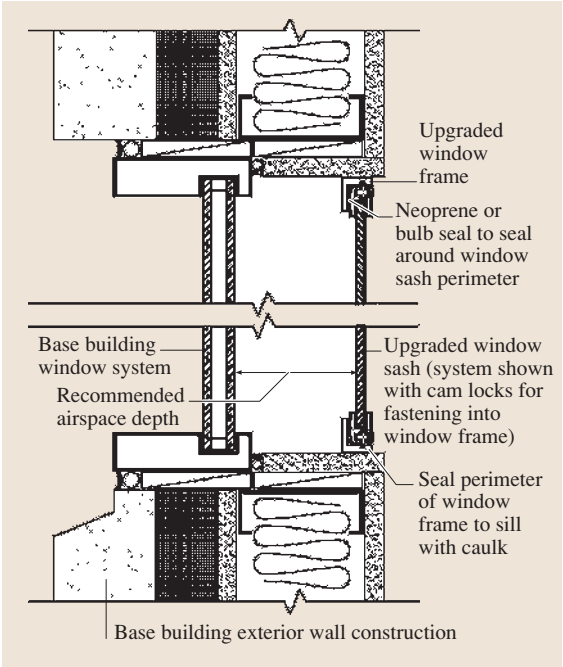


Fig. 11.47 Cross section of an upgraded exterior window for high-TL design

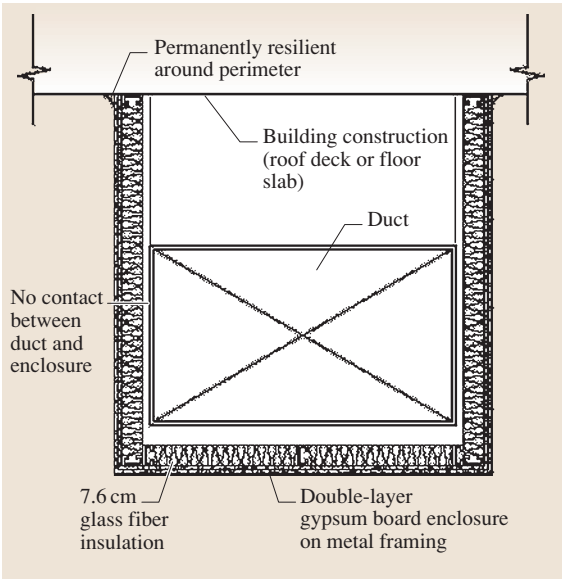


Fig. 11.48 Cross section of a double-layer gypsum-board duct enclosure

- distributing the flow as evenly as possible throughout the ducted system,
- providing long ducted passages and transitions that avoid sharp changes in direction or discontinuities in cross-sectional area,
- installing properly designed silencers and absorptive lining in the flow path that do not unduly compromise the efficiency of the HVAC system,
- wrapping ductwork with lagging materials, and
- enclosing ductwork and HVAC equipment.

Figures 11.48 through 11.50 offer effective noise control designs for duct and hanging HVAC equipment enclosures.

Another issue to consider with ductwork is sound leaks through wall and ceiling duct penetrations. If these penetrations are not sealed properly, they will diminish the noise reduction effectiveness of the wall or ceiling

Amazon
EX1010 Page 427

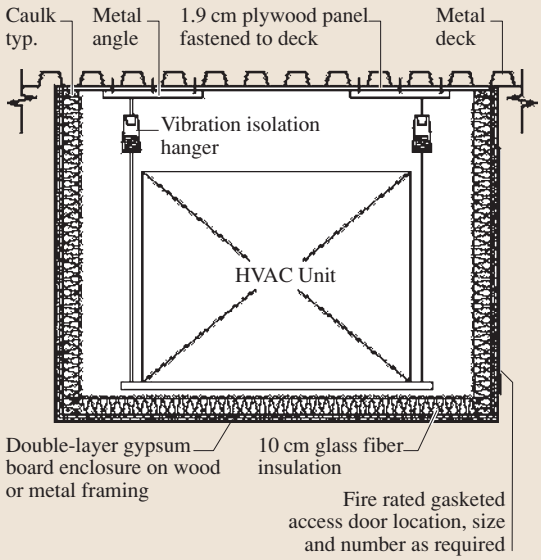


Fig. 11.49 Cross section of a duct enclosure resiliently mounted to a metal deck

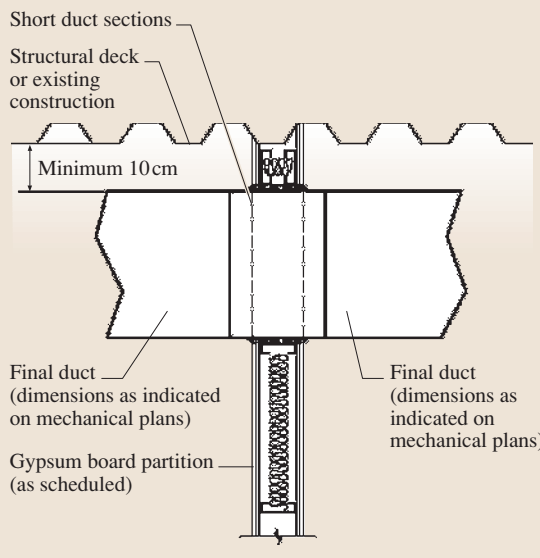


Fig. 11.51 Cross section of a duct penetrating a gypsum-board partition near a deck

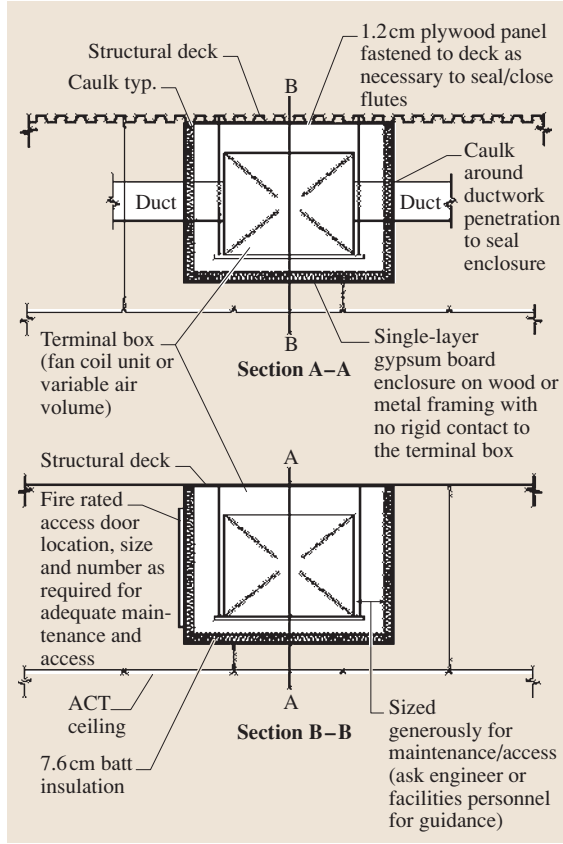


Fig. 11.50 Sections of a ducted terminal box enclosure mounted to a structural deck

that they are penetrating. Figure 11.51 shows an effective design for a single duct penetrating a wall and Fig. 11.52 shows an effective design for multiple duct penetrations. Figure 11.53 shows design considerations for the placement of a duct silencer near a wall penetration.

Vibration Isolation

Springs and pads are the most common tools used to minimize the transfer of vibration from HVAC units to the building structure. The key here is to eliminate any rigid connections between the units and the structure. Figure 11.54 shows a typical spring isolator properly mounted to reduce this transfer of vibrations effectively.

These benefits, however, will become short-circuited if improper or misaligned isolators are installed. Figure 11.55 shows improperly loaded spring isolators supporting a piece of equipment, one being overcompressed and the other being undercompressed.

Figure 11.56 shows an example of a spring isolating pipe hanger that is misaligned. The rigid connections established by this misalignment compromise the effectiveness of the system.

Figure11.57 shows a common design in which pipe supports are rigidly attached to a floor. Figure 11.58

Amazon
EX1010 Page 428

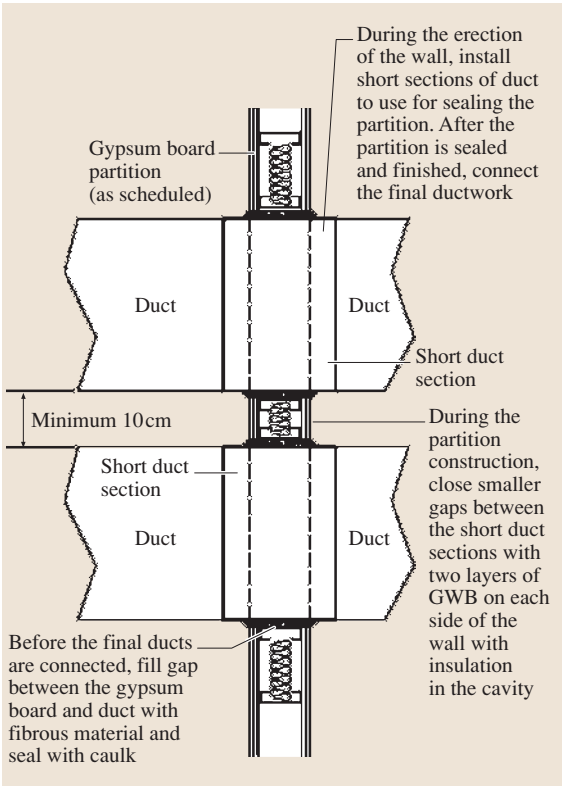


Fig. 11.52 Cross section of sealed multiple duct penetrations in a partition

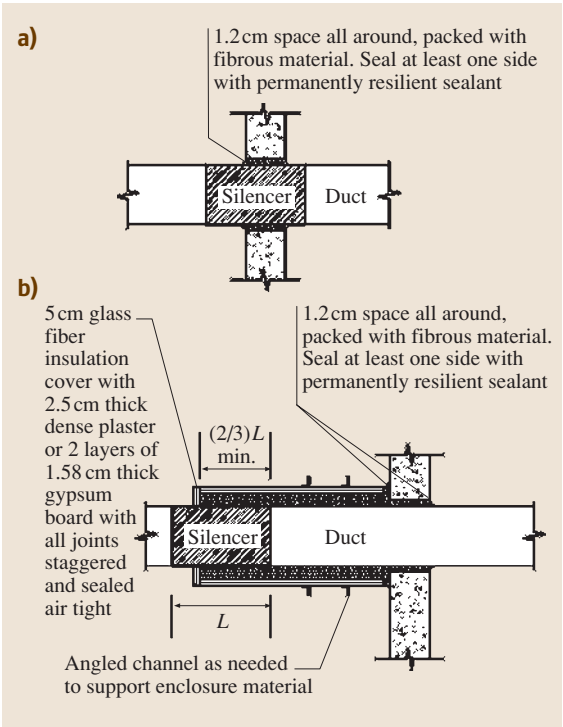


Fig. 11.53a,b Cross section of a duct penetration with appropriate silencer locations. **(a)** preferred location; **(b)** alternate location

shows an effective design to reduce the transfer of vibrations between the piping and the floor using neoprene pads and spring hangers. Note that any spring hangers must be appropriately sized for each situation. When lateral restraints are required for large equipment, Fig. 11.59 offers a general design for effective vibration isolation.

Enclosures for Floor-Based Equipment

When barriers and source treatments do not provide enough noise control, the only practical noise control option for many floor-based units may be a full enclosure. Key issues for enclosures of HVAC equipment are access (for maintenance) and ventilation. A practical design for indoor environments is shown in Fig. 11.60, in which a heavy curtain system (which can be drawn along tracks for access) surrounds the equipment. There are hoods built into the sliding curtains to provide the necessary ventilation for the equipment.

Exterior enclosures are discussed in Sect. 11.5.5 below.

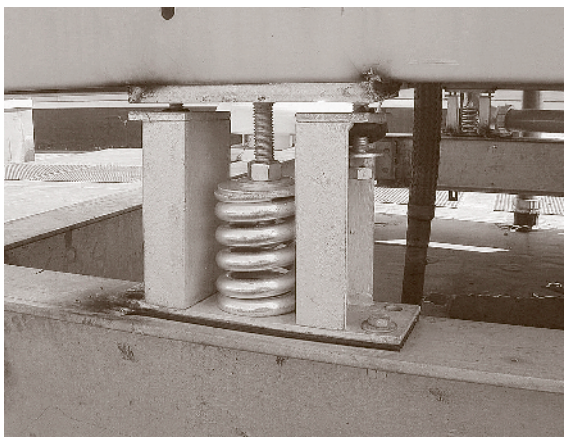


Fig. 11.54 A properly mounted spring isolator

11.5.3 Plumbing Systems

As for HVAC systems, the most common plumbing-system noise issues are related to reducing flow turbulence and vibration isolation. For plumbing sys-

Amazon
EX1010 Page 429

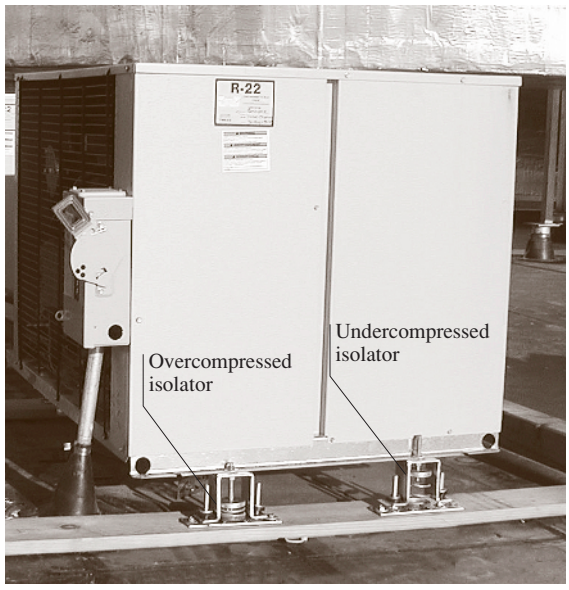


Fig. 11.55 Examples of misaligned and misloaded spring isolators

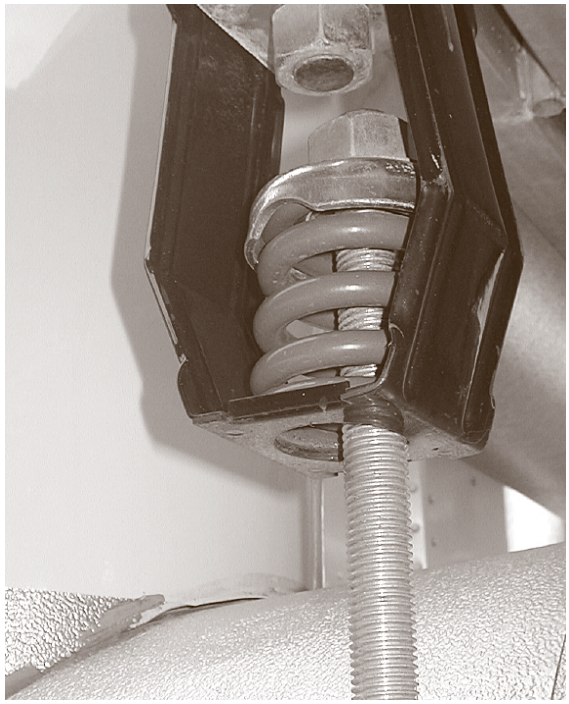


Fig. 11.56 A misaligned isolating pipe hanger. Note that the post is touching the support, thus short-circuiting the isolating effect of the hanger

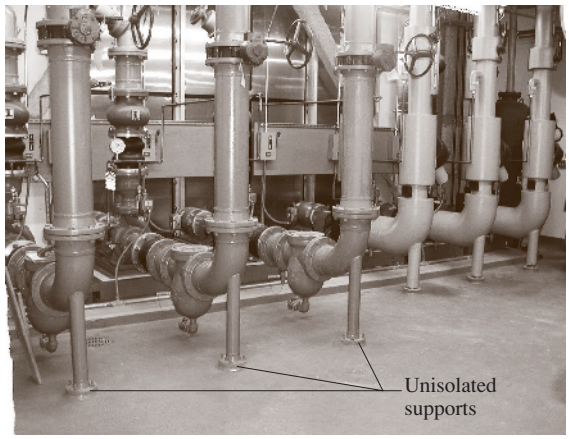


Fig. 11.57 Pipe supports rigidly attached to a structural floor. This can channel vibrations through the building structure

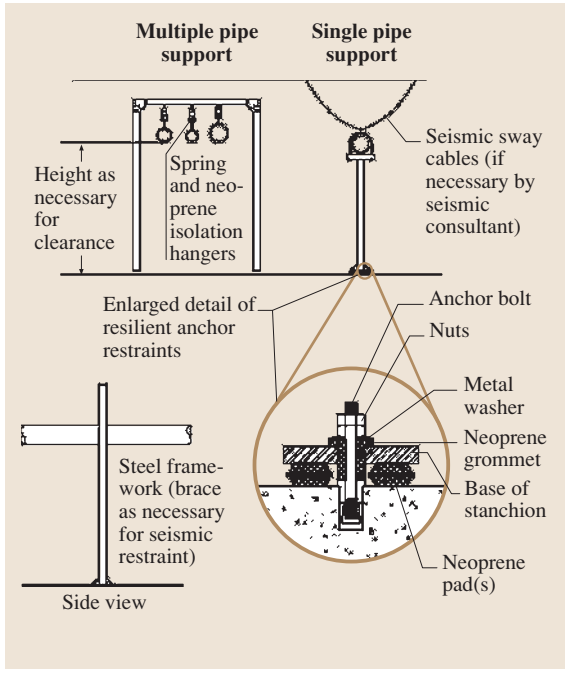


Fig. 11.58 Pipe floor supports with resilient anchors

tems we are dealing with liquid flow rather than air flow and pipe noise and vibration isolation rather than duct noise and vibration isolation. As for ducted systems, pipes can be wrapped with lagging materials to reduce breakout noise radiated from the pipe walls. Figures 11.61 and 11.62 show the general design principles to bear in mind for pipe penetrations through common

Amazon
EX1010 Page 430

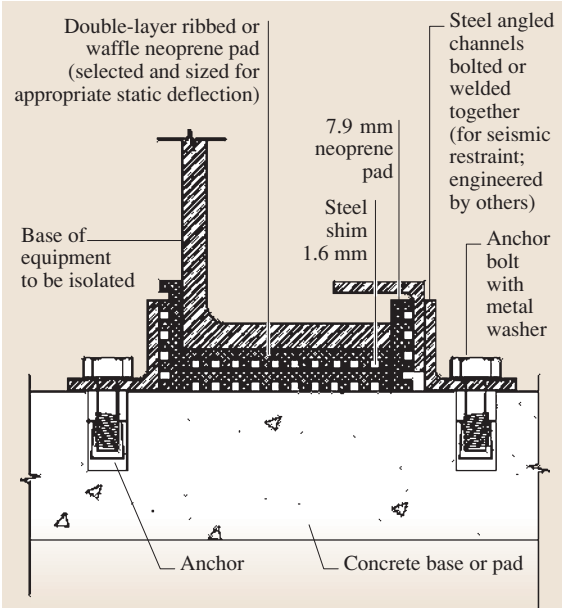


Fig. 11.59 Cross section of a lateral restraint for an equipment base on neoprene pads

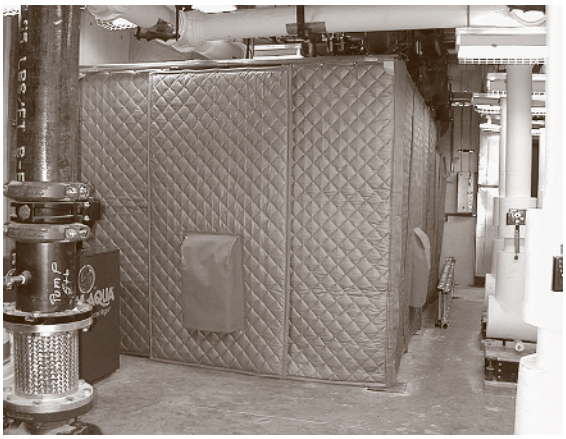


Fig. 11.60 A heavy curtain enclosure system for floor-based equipment

walls and Fig. 11.63 shows these principles in practice in an installation.

11.5.4 Electrical Systems

Electrical system noise control issues typically deal with transformer noise control and the vibration channel set up by rigid conduit between noise and vibration sources and noise-sensitive spaces. When transformers cause

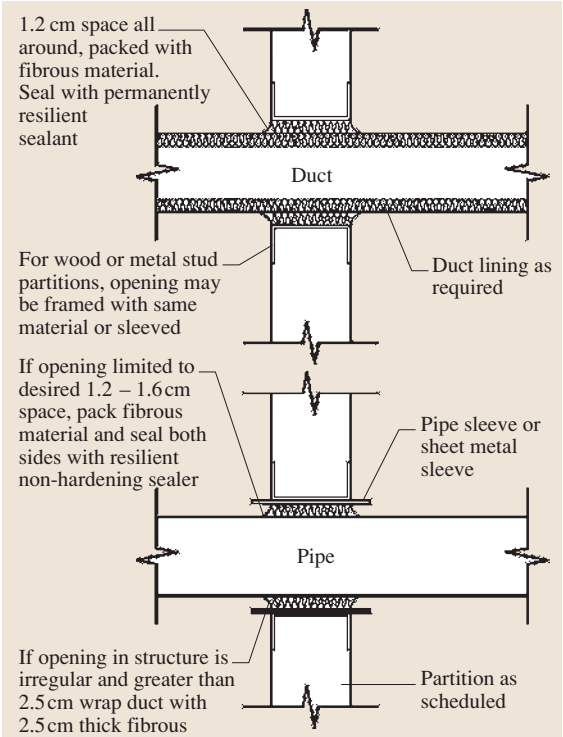


Fig. 11.61 Cross sections of sealed wall penetrations with a duct and a pipe

noise issues, they are most commonly addressed by enclosing the transformers. Conduit issues can be addressed by using a flexible conduit that is not stretched. Figure 11.64 shows an example of stretched electrical conduit, which provides a clear vibration channel from the source to remote locations.

An air space between an electrical box and other equipment will break any vibration channel that would otherwise have been established, as is shown in Fig. 11.65.

11.5.5 Exterior Sources

Environmental noise sources, such as transportation or industrial sources, can only be controlled in buildings by using exterior-wall designs that effectively reduce noise in the frequency ranges of those sources. Exterior noise sources, such as rooftop mechanical equipment or mechanical equipment in lots beside buildings (associated with the operations of the building in question) can be controlled by appropriately designed enclosure systems.

Amazon
EX1010 Page 431